Mineralogical and textural variation in modern estuarine sands: implications for sandstone reservoir quality

Thesis submitted in accordance with the requirements of the University of Liverpool for the degree of Doctor in Philosophy by

Joshua Griffiths

December 2017

To Val, my mum,
and to Paul, my dad,
we've come a long way from
"This is the bear who fell in the bin"

Tempus Fugit Memento Mori

TABLE OF CONTENTS

LIST OF FIGURES

LIST OF TABLES

ABSTRACT

Mineralogical and textural variation in modern estuarine sands: implications for sandstone reservoir quality

Joshua Griffiths

The spatial and temporal variability of primary depositional mineralogy and sediment texture (e.g. detrital clay coat coverage and matrix abundance) in sandstones are poorly-understood, and therefore empirical models often fail to accurately predict reservoir quality in ancient and deeply-buried petroleum-bearing sandstones. To address this challenge, surface sediment (< 2 cm) samples and one-metre cores were collected from the Ravenglass Estuary, NW England, and detailed ground surveys were made of the variety of marginal-marine depositional environments. Samples were analysed using a suite of X-ray diffraction approaches, SEM-EDS, laser particle size analysis and statistical techniques. The spatial distribution of quartz, feldspar, carbonates and clay minerals (chlorite, illite and kaolinite) in surface sediment of the Ravenglass Estuary, UK, have here been mapped at an unprecedented high-resolution, at a scale similar to many oil and gas reservoirs. Furthermore, clay mineral, clay coat and Fe-sulphide distribution patterns in near-surface sediment (< 1 m below the sediment surface) have been analysed to establish whether post-depositional processes e.g. bioturbation and mechanical infiltration, may over-print surface distribution patterns. Results show that estuarine composition is largely controlled by provenance; both the character of bedrock and drift-sediment in the drainage basin. Quartz, feldspar, clay mineral, carbonate and clay coat distribution patterns, are primarily controlled by the grain size of specific minerals (e.g. rigid versus brittle grains), estuarine hydrodynamics, and processes active in the top few centimetres of the primary deposition environment. Surface mineral distribution patterns are not over-printed by post-depositional processes such as bioturbation or mechanical infiltration. The distribution of smectite and pyrite is primarily controlled by geochemical conditions in the primary depositional environment, which are strongly influenced by topographic relief, bioturbation type and intensity, and extent of groundwater-flushing. Results of this study show that the abundance of quartz, feldspar, carbonates and clay minerals, and the extent of detrital clay coat coverage on sand grains, are predictable as a function of depositional environment (lithofacies) and mean grain size. However, the relative abundance of specific clay minerals (chlorite, illite and kaolinite) is much more sensitive to local specific hydrodynamic conditions e.g. wave-direction.

This integrated study may be used, by analogy, to better predict sandstone reservoir quality during oil and gas exploration, field appraisal and in planning well locations in ancient and deeply-buried marginal-marine sandstones. Based upon findings of this research and typical burial diagenetic pathways, reservoir quality in analogous ancient and deeply buried sandstone reservoirs is likely to vary accordingly. Outer estuarine sediment is likely to be extensively quartz cemented (and so have low porosity and low permeability), due to insufficient volumes of clay-grade material to create porosity preserving continuous clay coats. Mud-flats and mixed-flats at the margin of the inner estuary and central basin are likely to express low porosity and low permeability due to pore-filling clays that block pore-throats. In contrast, low amplitude dunes and tidal-bars in the central basin and inner estuary may contain sufficient quantities of clay grade material to form continuous clay coats that are porosity-preserving. Furthermore, low amplitude dunes and tidal-bars in the central basin and inner estuary are relatively chlorite-enriched and are often intensely bioturbated. Increased bioturbation is likely to inhibit Fe-sulphide development (reduce Fe-sequestration) permitting the chloritization of none Fe-bearing precursor minerals such as kaolinite. Reservoir quality is therefore likely to be greatest in low amplitude dunes and tidal-bars in the central basin and inner zones in marginal-marine sandstones.

ACKNOWLEDGEMENTS

First I would like to thank my mum and dad, who recognised the value of education and ensured that I was given the best possible start to life; without your support, love and friendship, I would not be in the fortunate position I am today. I would also like to thank my big bro and little sis, who have provided me with the laughter, inspiration and motivation to keep moving forward with a smile on my face. I am forever grateful for the love and encouragement received from my Grandad Jim and Grandma Kitty.

Special thanks go to Prof. Richard H. Worden for taking me under his wing, and for being an incredible supervisor and friend. I look forward to many more pints in the Belvedere for years to come, hopefully, without any more head injuries or lost passports.

I would wholeheartedly like to thank Luke Wooldridge for his support and friendship, I couldn't have asked for a better teammate to share this experience with; what an amazing four years it has been! I would also like to acknowledge the support and guidance of James Utley for is XRD wisdom and Rob Duller for his questionable dance-moves; both have helped shape this PhD enormously. I would like to thank all past and present office comrades for many hours (probably days) of counter-strike; fire in the hole!

I want to express my sincere gratitude to the sponsors of this research: BP, Woodside, Chevron, Petrobras, Statoil, ENI, and Shell. Without industry backing, this PhD would not have been possible.

Thank you to all of the company representatives that have truly made this PhD such a fruitful, enjoyable and exciting experience. Special thanks go to James Churchill, Peter Armitage, Nigel Clark, Simon Shoulders, Annabel Dale, Christian Brostrøm, Allard Martinius, Riccardo Pessina, Claudio Geloni and Andrea Ortenzi, who have provided an enormous amount of encouragement, industry training and support throughout my PhD. I will cherish our memories together, from Jägerbombs in Bumper, Liverpool to an exquisite meal in Røst, Trondheim.

1. INTRODUCTION

Rising global prosperity has led to increasing demand for energy. Despite global efforts to reduce fossil-fuel usage, oil and gas account for over half of the world's energy demand. The economic viability of an oil and gas reservoir is governed by multiple variables, such as socio-economic and political factors (e.g. modern conflicts), market forces (e.g. supply and demand) and geological constraints (e.g. flow-rate and hydrocarbons initially in place). The extraction of hydrocarbons from sedimentary rocks has led to extensive research in predicting the quality (porosity and permeability) of sandstone reservoirs (Taylor et al., 2010). However, despite recent efforts, predicting the permeability (control on flow-rate) and porosity (control on size of reserve) of many petroleum reservoirs remains challenging (Taylor et al., 2010). Sandstone porosity typically decreases with increasing burial depth, although anomalously high-porosity sandstones may deviate from the normal porosity-depth trends. For example, compaction and cementation of deeply-buried sandstones may be reduced due to reservoir overpressure and grain-coating chlorite, respectively (Stricker and Jones, 2016). Available statistical correlations typically fail to accurately predict reservoir quality, at least partly due to the spatial and temporal variability of sandstone composition being poorly-understood (Ajdukiewicz and Lander, 2010).

Three studies are reported in this thesis with the primary overall focus of better predicting textural and compositional variation, and thus sandstone reservoir quality in marginal-marine sandstones. The aim of the first study (Chapter 2) was to understand the fundamental processes in operation in the present day, that control clay mineral distribution in the surface sediment (< 2 cm below the sediment surface) of the Ravenglass Estuary, UK (Fig. 1.1). The aim of the second study (Chapter 3) was to better understand the distribution of clay minerals, iron-sulphides (e.g. pyrite) and detrital clay coats in near-surface sediment (< 1 m below the sediment surface) in the Ravenglass Estuary. The aim of the third study (Chapter 4) was to better understand the controls on the distribution of quartz, feldspar, clay minerals (both matrix and lithics) and carbonates in surface sediment of the Ravenglass Estuary.

The objectives of this chapter are to:

(i) Introduce the dominant minerals present in sandstones and to highlight the importance of sediment texture and composition on reservoir quality,
(ii) Discuss why a modern-analogue approach has been adopted,
(iii) Highlight the research aims and methods,
(iv) Discuss the layout of the thesis,
(v) Summarize key research questions.

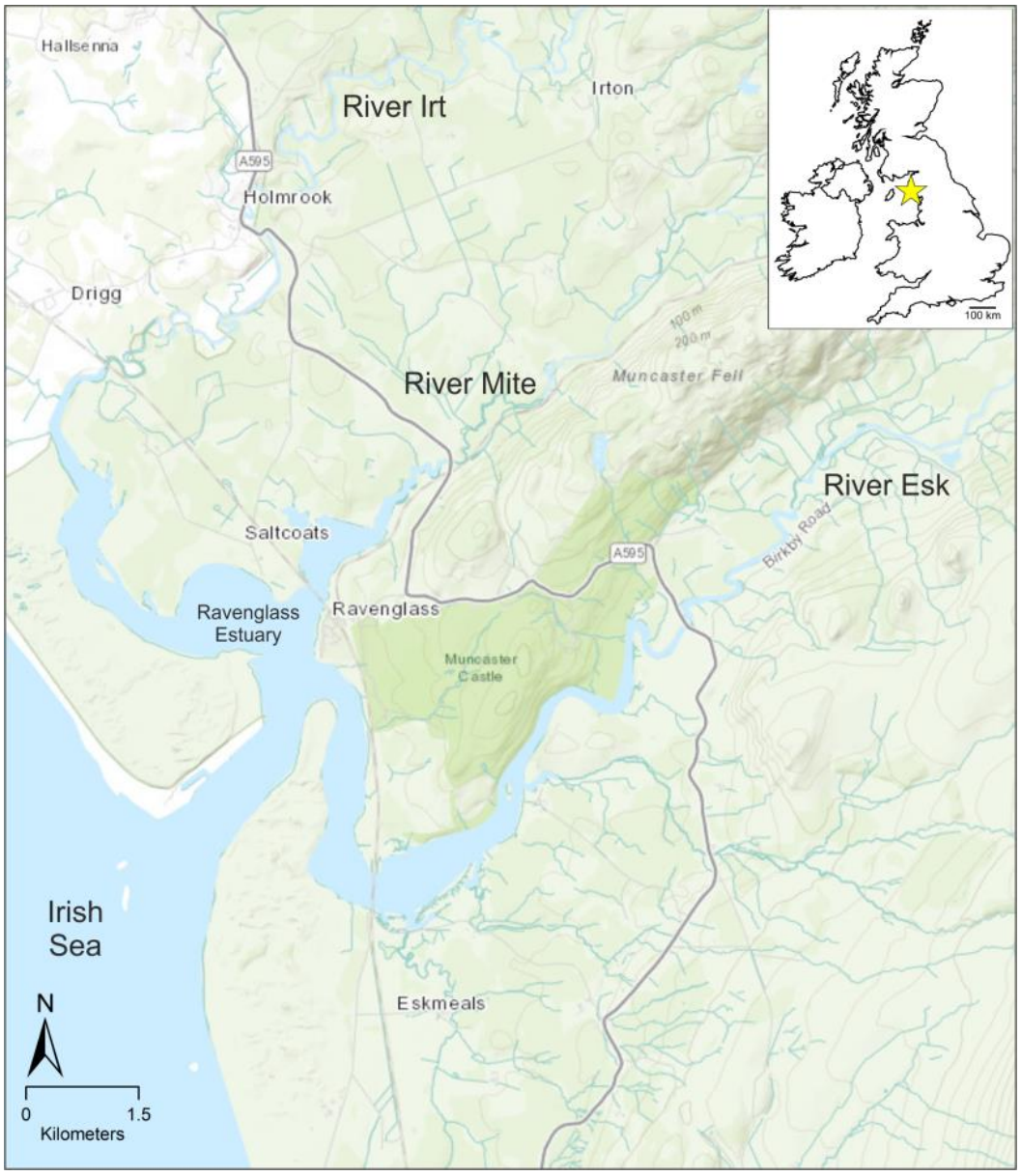

Figure 1-1 – Location of the Ravenglass Estuary, UK.

1.1 BACKGROUND

In this section, the type and importance of common clay minerals (chlorite, illite, kaolinite and smectite), framework-grain minerals (quartz, feldspar, lithics and carbonate), and iron-sulphides (e.g. pyrite) in sandstone reservoirs are discussed.

1.1.1. Clay minerals: type, occurrence and implications for sandstone reservoir quality

The term "clay mineral", referring to hydrous aluminosilicates (phyllosilicates), and the term "clay", referring to sediment particles that are smaller than 2 μm in size are carefully discriminated in this study. Clay minerals have a sheet-like structure in which individual building blocks (tetrahedra or octahedra) are linked to form planar layers by sharing oxygen ions between Si or to a lesser extent Al and Fe $^{3+}$ ions (Worden and Morad, 2003) (Fig. 1.2). Individual tetrahedra are comprised of the close packing of four O ions, with Si^{4+} ion or, to a lesser extent, an Al^{3+} ion or Fe^{3+} filling the spaces between them (Moore and Reynolds, 1997; Worden and Morad, 2003). The octahedra result from the close packing of six anions, predominantly, oxygen but also include some hydroxyl (OH) ions. Spaces between the tetrahedra and octahedra are mainly occupied by Si and Al, however, other cations such as iron, calcium, magnesium and potassium may be required to achieve charge balance depending on elemental substitutions elsewhere in the other octahedra and tetrahedra (Worden and Morad, 2003). Clay minerals are classified based on the types of ions occupying the octahedral and tetrahedral sites, the order these sheets are stacked, the strength of bond between sheets, and the presence of cations and or water between sheets. The term trioctahedral is used for clay minerals that contain ions that are divalent (Mg^{2+}, Fe^{2+}), since three ions are needed to provide six positive charges (Worden and Morad, 2003). If the ions are trivalent (Al^{3+}, Fe^{3+}), clay minerals are classified as being dioctahedral, because only two ions are needed to provide six positive charges (Worden and Morad, 2003). There is limited substitution of divalent ions in trioctahedral clay minerals, and trivalent ions in dioctahedral clay minerals; thus, Al^{3+}- and Fe^{3+}-rich clay minerals are dioctahedral, whereas Mg^{2+}- and Fe^{2+}-rich clay minerals are trioctahedral.

Chlorite: Chlorite is from the Greek, *chloros*, green, and gives the colour to the green schist facies (Moore and Reynolds, 1997). Chlorite is a 2:1:1 mineral with an interlayer sheet of cations octahedrally coordinated by hydroxyls (Fig. 1.2). The most common octahedral cations in chlorite are Mg^{2+}, Fe^{2+}, Al^{3+} and Fe^{3+}. A general formula for chlorite is $(Mg, Al, Fe)_{12}[(Si, Al)_8O_{20}]\ (OH)_{16}$ (Worden and Morad, 2003). Fe-rich diagenetic chlorite (chamosite) and Mg-rich diagenetic varieties (clinochlore) can occur as grain-coats on

detrital sand grains (Dowey et al., 2012), and may also be found in both metamorphic and igneous rocks, often due to intense hydrothermal alteration e.g. pseudomorphs after biotite alteration (Moseley, 1978; Young et al., 1986). Grain-coating chlorite in deeply-buried sandstone reservoirs can lead to anomalously high-porosity, by preserving open pore networks through the inhibition of authigenic quartz cement growth (Dowey et al., 2012; Ehrenberg, 1993; Pittman et al., 1992; Saïag et al., 2016; Skarpeid et al., 2017; Stricker and Jones, 2016). The fraction of the sand grain-surface covered by clay coating (extent and completeness of the clay coat) is a dominant control on the ability of grain coats to inhibit quartz cementation (Ajdukiewicz and Larese, 2012; Billault et al., 2003; Lander et al., 2008). In contrast, an over-abundance of chlorite may fill-pore spaces and blocks pore throats, and thus decreases porosity and permeability (Islam, 2009; Pay et al., 2000).

Illite: The name illite in this study is used for the clay-size, mica-like mineral commonly associated with clastic-sediments, following the definition of Grim et al. (1937); although, illite is generally considered to have more Si, Mg, and H_2O but less tetrahedral Al and less interlayer K than muscovite (Moore and Reynolds, 1997).

Illite is a K-rich dioctahedral 2:1 clay mineral comprised of one octahedral later, situated between two tetrahedral layers (Fig. 1.2), with K tightly bound between each octahedra-tetrahedra-octahedra unit. The general formula for illite is $K_yAl_4(Si_{8-y},Al_Y)O_{20}(OH)_4$, where y is typically significantly less than 2 (Velde, 1985). Illite occurs as flakes, filaments or hair-like crystals, and can occur as various polytypes that reflect different stacking patterns of individual layers (Moore and Reynolds, 1997). Analyses of the ratio between the intensity of the 5Å and 10Å peaks from X-ray diffractograms (Esquevin Index), can differentiate illite chemistry (Al-rich from Fe-Mg-rich illite) (Esquevin, 1969). High Esquevin Indices (Al-rich illites) are characteristic of chemically-weathered rocks (Chamley, 1989) that have lost divalent cations (Fe and Mg) from the octahedral sites, whereas low Esquevin Indices correspond to mechanically weathered rocks (Chamley, 1989). In addition, measurement of the full width at half-maximum (FWHM) of the 10Å (001) illite peak from X-ray diffractograms provides an illite crystallinity index ($2^0\theta$), also known as the Kübler Index (Kübler, 1964). Broad basal reflections (high FWHM values) represents poorly-crystalline illite, associated with highly-degraded, low growth-temperature, low-structural-order illite (Chamley, 1989; Kübler, 1964). In contrast, narrow basal-reflections (low FWHM values) represent highly-crystalline illite, associated with relatively unaltered, high growth-temperature, high-structural-order illite (Chamley, 1989; Kübler, 1964).

Mixed chlorite and illite grain coats (analogous to chlorite grain coats) may preserve porosity through the inhibition of quartz cement in deeply-buried sandstone reservoirs, as observed in

the Heron and Skua fields (Stricker et al., 2016) and Jurassic Garn formation (Storvoll et al., 2002). However, illite is more commonly associated with reservoir quality degradation, since hair-like, fibrous-filaments of illite effectively bridge and block pore throats, significantly reducing permeability (Lander and Bonnell, 2010) e.g. pore-filling illite in the Bohai Bay Basin, East China (Yuan et al., 2015). In addition, the presence of illite can promote chemical compaction (increase in quartz-cementation, as well as assisting pressure dissolution), leading to pore-space reduction, and decreased permeability (Worden and Morad, 2003). Illite may also react with CO_2, (e.g. during enhanced oil recovery, alteration or oxidation of oil and/or carbon capture and geological storage practise), which may lead to iron being released from Fe-rich illite/mica and formation of siderite (if there is an additional presence of carbonate minerals) (Gunter et al., 2004). Siderite is important, as the presence of kaolinite and siderite may lead to the formation of authigenic chlorite at burial temperatures of around 120 °C (Worden and Morad, 2003).

Kaolinite: Kaolin series represent 1:1 clay minerals, comprised of one tetrahedral layer linked to one octahedral layers by O-H-O bonds, with no interlayer cations (Worden and Morad, 2003) (Fig. 1.2). The chemical formula of kaolin is $Al_2Si_2O_5(OH)_4$. Low temperature forms of kaolin are called kaolinite, whereas high temperature forms are dickite and nacrite. In reservoir sandstones, kaolinite is characterised by a stacked, booklet texture formed from pseudohexagonal plates, whereas dickite tends to form small rhombic crystals (Worden and Morad, 2003).

Booklets of kaolinite block pore-throats and typically diminish permeability, degrading reservoir quality, for example, Jurassic Ravenscar and Brent Group sandstones (Kantorowicz, 1984). Furthermore, kaolinite booklets have been reported to be mobile during petroleum production, and often ‘gather’ in pore throats toward the well-bore, significantly lowering production rates (Cerda, 1987). In contrast, kaolinite-rich sandstones have also been reported to provide sufficient micro-porosity to produce gas, such as the Tirrawarra Sandstone Reservoir, Southern Cooper Basin, Australia (Rezaee and Lemon, 1996).

Smectite: Smectite is a term used for a group of 2:1 minerals with one octahedral layer sandwiched between two tetrahedral layers, with a general chemical formula consisting of $(0.5Ca, Na)_{0.7}(Al, Mg, Fe)_4(Si, Al)_8O_{20}(OH)_4\, nH_2O$ (Worden and Morad, 2003). Octahedral sites are dominated by divalent metals (Fe^{2+}, Mg, Ca) in trioctahedral smectite, whereas, octahedral sites are dominated by trivalent metals (Fe^{3+}, Al) in dioctahedral smectite (Worden and Morad, 2003) (Fig. 1.2). Interlayer cations (Fe^{2+}, Fe^{3+}, Mg^{2+}, Ca^{2+}, Na^{+}) are

variably hydrated, and thus smectites are classified by their ability to swell when exposed to organic solvents, which may be absorbed by the cations present in the interlayer space.

Dioctahedral smectite typically transforms to illite during burial diagenesis with an additional source of K^+ (e.g. through K-feldspar dissolution), and trioctahedral smectite may transform to chlorite via mixed-clay intermediates during progressive diagenesis (McKinley et al., 2003; Worden and Morad, 2003). Smectites may supply material for other diagenetic processes which may reduce reservoir quality, such as illitization, quartz cementation and zeolite growth (Boles and Franks, 1979). Smectite clay minerals are highly detrimental to reservoir quality, since they typically contain much ineffective microporosity (McKinley et al., 2003). In addition, smectites are also expandable clay minerals, which readily absorb and incorporate water and organic material, and thus alter the wetting state of a sandstone, potentially rendering it oil-wet (McKinley et al., 2003).

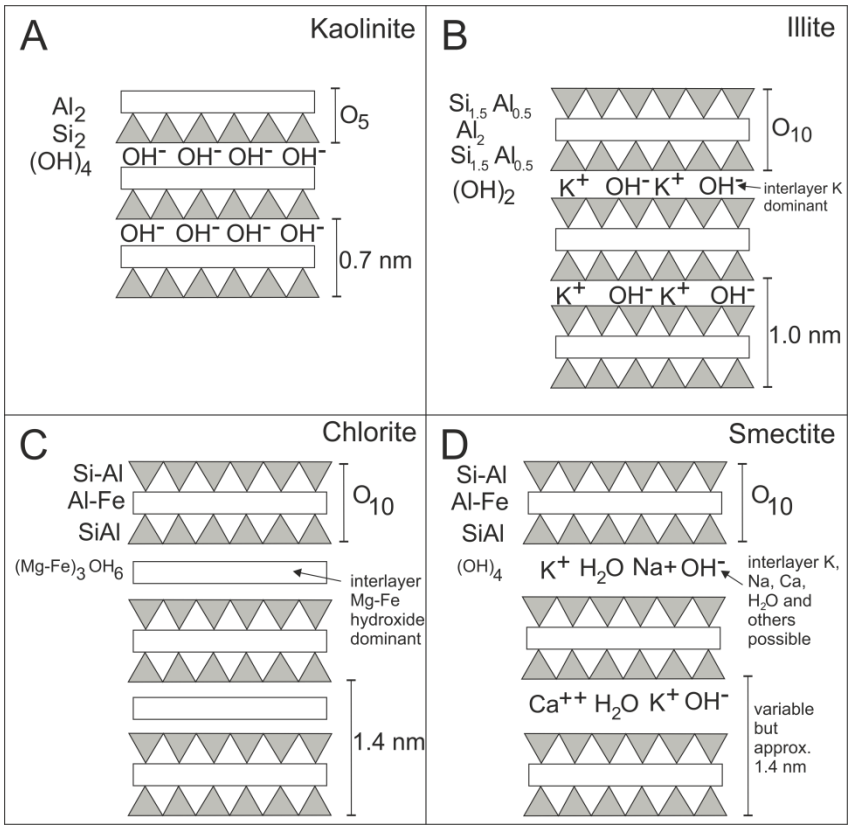

Figure 1-2 – Schematic diagram showing the structure of common clay minerals in sandstone reservoirs, modified after Worden and Morad (2003), (A) kaolinite, (B) illite, (C) chlorite, and (D) dioctahedral smectite. Triangles represent tetrahedral layers, whereas bars represent octahedral layers.

1.1.2 Detrital clay coats and burial-diagenetic grain coats: origin and implications for sandstone reservoir quality

Chlorite and mixed-mineralogy (e.g. illite/chlorite) grain-coats may preserve anomalously high-porosity in deeply-buried sandstones reservoirs, through the inhibition of authigenic quartz cement (Dowey et al., 2012). Such diagenetic clay coats are reported to originate from the thermally-driven recrystallization of low-temperature, precursor (prior to burial) detrital clay coats, and/or through *in situ* growth from the authigenic alteration of precursor (detrital) and early-diagenetic minerals, which interact with pore fluids during burial (Ajdukiewicz and Larese, 2012; Worden and Morad, 2003). Thus it is critical to understand the distribution of precursor, detrital clay coats, to better understand the distribution of diagenetic, porosity-preserving grain coatings. The clay coat mineralogy and the fraction of the sand grain-surface covered by clay coating (extent and completeness of the clay coat) are reported to be the dominant controls on the ability of grain coats to inhibit quartz cementation (Ajdukiewicz and Larese, 2012; Billault et al., 2003; Lander et al., 2008). As such, it is advantageous to understand primary deposition patterns of specific clay minerals, as well as the occurrence and completeness of detrital clay coats.

1.1.3 Quartz, feldspar, carbonate and iron-sulphide: type, occurrence and implications for sandstone reservoir quality

In this section, the common mineral types found in sandstones reservoirs are discussed, as is the influence of eogenetic, mesogenetic and natural and anthropogenic-induced diagenesis, in relation to sandstone reservoir quality.

Quartz: Quartz (SiO_2) is one of the most common rock-forming minerals, and is one of the main components of granites, sandstones and many metamorphic rocks (MacKenzie and Adams, 1994). The relative abundance of rigid-grains (e.g. detrital quartz) in comparison to ductile grains (e.g. clay minerals) controls the degree of mechanical compaction of sandstones, which is the dominant porosity reducing mechanisms during burial from 0 to 2.5 to 3 km (Ramm, 1992). In addition to detrital quartz grains, quartz may occur as authigenic quartz cement, which typically forms in sandstones at temperatures in excess of 70 to 80 °C; excessive quartz cementation occurring at a temperature range of 80 to 100 °C (Worden and Burley, 2003). Quartz cementation may be promoted by the presence of clay minerals (e.g. illite). Furthermore, micro-quartz cement may originate from the dissolution and subsequent precipitation of siliceous micro-organisms such as sponge-spicules and diatoms. Micro-quartz grain coats (analogous to clay coats) may preserve porosity in deeply-buried sandstones, inhibiting authigenic quartz cement, as reported in the Upper Jurassic sandstones

in the Central Graben area of the North Sea (Aase et al., 1996). Despite many years of controversy, a recent publication by (Worden et al., 2017 in press) provides convincing evidence that quartz cementation is inhibited by oil emplacement into the shallow marine, Upper Jurassic sandstones, Norwegian North Sea.

Feldspar: Feldspars are common rock forming minerals present in the Earth's crust (MacKenzie and Adams, 1994). Feldspars may be split into two end-members, alkali feldspars (K-feldspar) and plagioclase feldspars. Alkali feldspars have a composition which ranges from orthoclase ($KAlSi_3O_8$) and albite ($NaAlSi_3O_8$). Plagioclase composition ranges from albite ($NaAlSi_3O_8$) and anorthite ($CaAl_2Si_2O_8$), and has multiple species in-between the two end-members (i.e. oligoclase, andesine, labradorite and bytownite). Plagioclase feldspars typically contain a minor amount (< 5 %) of K-feldspar; alkali feldspars typically contain a minor amount (< 5 %) of calcium (MacKenzie and Adams, 1994).

Feldspars may significantly influence the mechanical and chemical properties of sandstones, as well as providing reaction agents which buffer diagenetic reactions during burial diagenesis. It is noteworthy that plagioclase usually exceeds potassium feldspar in abundance in most sandstones (Bloch and Helmold, 1995).

Since feldspar minerals fracture at lower differential stress than quartz grains, feldspathic sandstones typically have a lower mechanical strength (Griffiths et al., 2016). Furthermore, preferentially feldspar fracturing may lead to localized broadening of the grain-size distribution, resulting in more efficient grain packing, causing significantly reduced porosity and permeability (Griffiths et al., 2016).

The origin and effect of abundant feldspar-dissolution and formation of kaolin cement in sandstone reservoirs have been topics of long-standing interest and controversy (Ehrenberg and Jakobsen, 2001). Feldspar dissolution is common in shallow-marine sandstones (Bjorlykke, 1998; Morad et al., 2010), since marginal and shallow marine sediments (unlike more distal shelf facies and turbidites) are commonly subject to extensive meteoric water-flushing. Meteoric water flushing (also known as subsurface weathering) may occur at depths < 100 m, but typically occurs at depths < 10 m (Bjorlykke, 1998). During burial, K-feldspar dissolution typically occurs over depth ranges of 1.5 to 4.5 km (50 to 150 °C) in sandstones (Wilkinson et al., 2001), and is typically extensive at depth > 2.5 km (Worden and Burley, 2003). In addition, feldspar dissolution may occur through the presence of CO_2 (Ehrenberg and Jakobsen, 2001), which may be generated by the alteration/oxidation of oil, during enhanced oil recovery techniques, and/or through carbon capture and geological storage. Furthermore, during telogenesis (uplift) feldspar minerals are usually transformed to

clay minerals, due to meteoric water-flushing, such as the Kimmeridge Clay Formation, Gullfaks field, northern North Sea (Bjorkum et al., 1990).

Anomalously high-porosity in deeply-buried sandstones has been commonly attributed to secondary porosity as a result of feldspar dissolution (Burley, 1986; Dutton and Loucks, 2010; Surdam et al., 1984; Wilkinson et al., 1997), which occurs through the total- or part-removal of dissolution products (detrital grains, matrix or diagenetic-cements) from the sandstone (Schmidt and McDonald, 1979). In contrast, other studies such as Yuan et al. (2015), have suggested that since most sedimentary rock-forming minerals are low-solubility (e.g. feldspars), the dissolution and flushing of sandstones is unlikely to occur in sufficient quantities to significantly enhance porosity. Furthermore, dissolved material may simply precipitate locally, and occlude pores with the formation of new diagenetic-minerals which may reduce permeability, such as illite, or K-feldspar overgrowths, as reported in the Brent Group, Gulffaks Field, northern North Sea (Ehrenberg and Jakobsen, 2001).

The influence of feldspar on chemical properties of a sandstone and subsequent diagenetic reactions is largely dependent on whether the feldspar is K-feldspar or plagioclase feldspar. Small amounts of carbonate and clay minerals cements may be formed through the albitization of plagioclase, with the supply Ca^{2+} and Al^{3+} (Morad et al., 2010). Whereas, the albitization of K-feldspar may enhance illite formation by supplying K^{+} (Morad et al., 2010). Furthermore, K-feldspar and kaolinite are universally unstable together at temperatures greater than about 70 °C (Worden and Burley, 2003); thus the co-deposition of kaolinite with K-feldspar often leads to the formation of illite and quartz during deeper burial, as observed in the Garn formation, Norwegian North-Sea (Chuhan et al., 2001).

Carbonate: Calcite ($CaCO_3$) and dolomite ($CaMg(CO_3)_2$) are the primary constituents of carbonate rocks. Aragonite (also $CaCO_3$) is common in many shallow marine carbonates, however it is metastable and is often dissolved and recrystallized to calcite (MacKenzie and Adams, 1994). Shallow marine sandstones are commonly cemented with nodules or discrete layers of eogenetic calcite (reducing porosity and permeability), resulting from the dissolution and precipitation of shell detritus (Hendry et al., 1996; Morad et al., 2010; Wilkinson, 1991; Worden and Burley, 2003). In contrast, a minor amount of early-carbonate cement precipitation may reduce early-compaction by reducing the stresses at grain contacts and strengthening the grain framework (Bjorlykke, 2010). Thus, a small-amount of carbonate cement may in fact help preserve porosity, through the resistance of mechanical compaction (Morris et al., 2006).

The three major carbonate cements which form during eodiagenesis and mesodiagenesis are calcite, dolomite and siderite ($FeCO_3$) (Worden and Burley, 2003). During diagenesis (at

burial temperatures of around 120 °C) kaolinite and siderite may react to form authigenic chlorite (Worden and Morad, 2003). Unlike diagenetic clay mineral formation, carbonate cement can occur in sandstones void of precursor carbonate material, due to the 'mass influx transfer' of highly soluble carbonate material (e.g. Ca^{2+} and Mg^{2+}) from neighbouring carbonate-rich facies (typically from low-permeability to high permeability rocks) (Worden and Burley, 2003). As a result, it is important to understand neighbouring relationships between carbonate-rich facies and potential reservoir formations.

Iron-sulphide: Iron availability is essential for the formation of burial-diagenetic, porosity-preserving, Fe-bearing clay minerals, such as berthierine, odinite and Fe-chlorite. Iron-sulphides originate from the bacterial reduction of aqueous sulphate derived from marine-inundation (Daneshvar and Worden, 2017). Iron-sulphides (e.g. pyrite, marcasite and pyrrhotite) in modern marginal-marine sediments are common, in comparison to brackish and freshwater systems which have lower concentrations of dissolved sulphate ions than marine pore waters (Morad et al., 2010). Pyrite growth leads to the sequestration of iron in the sediment. As a result there is less iron available for the formation of burial-diagenetic berthierine, odinite and Fe-chlorite, which might have otherwise preserved porosity in deeply-buried sandstones. As a result, understanding the primary distribution of Fe-sulphides in modern sediments is critical in order to better understand the potential ingredients available for the formation of burial-diagenetic clay minerals.

1.2 RESEARCH OUTLINE, AIMS, OBJECTIVES AND QUESTIONS

In this section, the motivation for adopting a modern analogue approach is discussed, in addition to the research rationale of each chapter and the specific research questions which shall be addressed.

1.2.1 Adopting a modern analogue approach

Four methods are available to better understand the distribution of sandstone composition and texture (e.g. detrital clay coat coverage) in clastic reservoirs. First, studying core from oil and gas fields provides an insight into the distribution of sandstone composition and texture; however, core datasets are often spatially-limited, contain high-levels of uncertainty on the diagenetic history, and the exact initial depositional environment is often unknown. Second, outcrop studies may provide useful analogues, however, exposed bedrock typically suffers from weathering-related alterations, and thus mineralogy and sediment texture is poorly-preserved, or removed. Third, experimental-studies can provide very insightful information, however, up-scaling and extrapolation to the highly-complex real-world remains challenging.

Thus, fourth, a modern-analogue approach has been adopted as the preferred method of study. Modern analogues do not suffer from spatial-limitations, the exact depositional-environment is known, and a thorough understanding on the transport processes and provenance can be obtained.

Clay mineral distribution patterns in the primary depositional sediment are likely to control the distribution of diagenetic clay-minerals since, even during the long time-scale of burial diagenesis, the main components of clay minerals (for chlorite: Fe-, Al- and Si-oxides) are effectively water-insoluble. Therefore clay mineral (and especially chlorite) diagenesis during burial can be assumed to be an isochemical process (closed-system), and not the result of mass influx of materials into sandstones during diagenesis. A study of modern environments is thus an appropriate way of developing an understanding, by analogy, on the distribution of clay minerals in sandstone reservoirs (Worden et al., in press; Worden and Morad, 2003). It is acknowledged, that modern-analogues also come with challenges. The biggest challenge in utilising modern-analogues is the ability to forward-model dataset to simulate burial diagenesis (e.g. compaction and diagenetic mineral-alteration). However, with an understanding of the burial-history of sandstone reservoirs (e.g. time and temperature) predictions of potential mineral-alterations can be made by using well-established burial-diagenetic pathways, such as Figure 1.3.

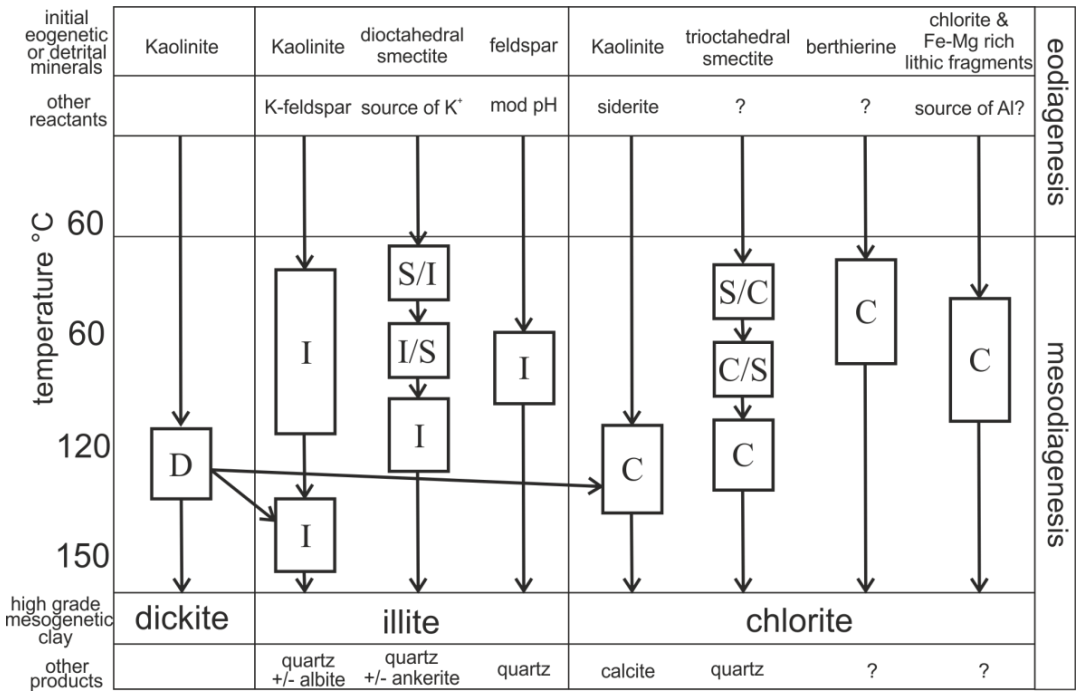

Figure 1-3 – Common mesogenetic pathways for clay minerals in sandstones, edited from Worden and Morad (2003). Where D is dickite, S is smectite, I is illite and C is chlorite. Randomly stratified mixed-layer clay minerals are named accordingly: S/I is mixed-layer smectite-illite dominated by smectite; I/S is the same mineral mixture dominated by illite.

1.2.2 Ravenglass Estuary, UK

Following the recent post-glacial transgression, estuaries are common at the present day; some estuaries are actively undergoing transgression, whereas others may be transitioning to deltas (Davis and Dalrymple, 2011). The primary control on the nature and distribution of facies in estuaries, is estuarine type i.e. the relative influence of waves and tides (Dalrymple et al., 1992). Dalrymple et al. (1992) provided a comprehensive study comparing the nature and organization of facies in tapered wave-dominated and tide-dominated estuaries (end-members). Many estuaries, such as the Ravenglass Estuary (Fig. 1.1), deviate from the idealized models presented by Dalrymple et al. (1992); however, mainly due to the typical paucity of data associated with reservoir studies, reconstruction analyses are often forced to abide too closely to previously published end-member, wave- or tide-dominated models (Davis and Dalrymple, 2011). Thus, mixed-energy estuarine systems such as the Ravenglass Estuary (Fig. 1.1) are likely underreported in the stratigraphic record. To address this challenge, this study provides an additional lithofacies scheme (chapter 3) which has been constructed based upon diagnostic host-sediment properties (e.g. grain size) and sedimentary structures which are unique to specific and known depositional environments.

The Ravenglass Estuary, in northwest England (Fig. 1.1) was chosen for its accessibility, because its overall surface area is similar to that of many oil and gas fields, and because the two main fluvial arms, that feed the estuary, drain different bedrock types, giving a potential insight into provenance controls on mineral distribution (Fig. 1.4). In addition, recent work has been undertaken on detrital clay coat coverage in the surface sediment of the Ravenglass Estuary (Wooldridge et al., 2017a; Wooldridge et al., 2017b). Furthermore, the Ravenglass area has previously benefitted from substantial geological and geomorphological research due to the location of the nuclear reprocessing plant at Sellafield (20 km away), and the low level nuclear waste repository at Drigg (immediately to the north of the River Irt).

The Ravenglass Estuary encompasses the tidal reaches of the Rivers Esk, Irt and Mite, and occupies an area of 5.6 km^2, of which ~86% is intertidal (Bousher, 1999; Lloyd et al., 2013; Wooldridge et al., 2017b). The development of two coastal-spits, around 3,000 BP (Bousher, 1999), created a single estuarine complex following the coalescence of the previously-separate and westward flowing Rivers Irt, Mite and Esk. The estuary is macro-tidal (> 7 m tidal range) and is predominantly fed by the river Esk and river Irt. The Ravenglass Estuary is here defined as a 'dual-funnelled', mixed-energy estuary. The Rivers Irt, Mite and Esk drain a variety of bedrock lithologies and drift deposits. Upland catchment areas are composed of Devonian Eskdale Granite, Ordovician Borrowdale Volcanic Group, and Cambrian Skiddaw Group rocks (Fig. 1.4). These Palaeozoic rocks juxtapose the low lying

coastal plains of the Triassic Sherwood Sandstone Group, with the Lake District boundary fault separating the Palaeozoic from the Mesozoic rocks. The Skiddaw Group includes weakly-metamorphosed, fine-grained sedimentary rocks (Merritt and Auton, 2000). In addition to bedrock, the west Cumbria region of the UK was affected by glaciation during the Quaternary, on at least three occasions (McDougall, 2001; Moseley, 1978), which has led to the deposition of a suite of drift-deposits. Merritt and Auton (2000) reported that the upper group of Quaternary sediments within the area around Sellafield and Ravenglass include estuarine, alluvial, organic and aeolian sequences sitting on top of the final glacial deposits. However, much of the glacial deposit has been removed from the land surface following the last glaciations (Merritt and Auton, 2000).

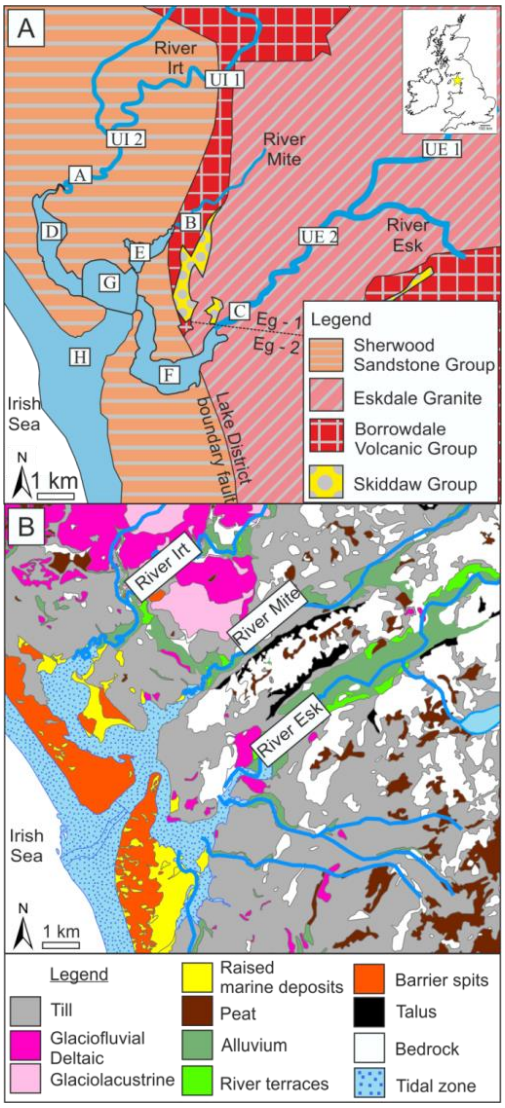

Figure 1-4 - Geological setting of the Ravenglass Estuary, UK, (A) bedrock geology, note, Eskdale Granite – 1 (Eg-1) and Eskdale Granite – 2 (Eg-2) are distinguished, and (B) Quaternary drift-deposits. Estuarine zones are labelled accordingly; UI, upper-Irt; UE, upper-Esk; A, lower-Irt; B lower-Mite; C lower-Esk; D, inner-Irt; E, inner-Mite; F, inner, Esk; G, central-basin; and H, outer-estuary.

1.2.3 Estuarine clay mineral distribution: modern analogue for ancient sandstone reservoir quality prediction (chapter 2 rationale)

Clay minerals may both enhance or degrade porosity and permeability in sandstones as a function of clay mineral type, abundance and location in pore network (Worden and Morad, 2003). Thus, the ability to predict precursor (detrital) clay-mineral distribution patterns would be of great benefit in reservoir quality studies during oil and gas exploration, field appraisal, in planning well locations and in planning production strategies.

The primary objective of this part of the study is to better understand the distribution of clay minerals in a modern marginal-marine setting (in this case an estuary). Modern clay mineral distribution patterns can improve reservoir quality predictive capabilities, since primary clay mineral distribution patterns control the type and occurrence of clay minerals in ancient sandstones, based on the assumption of isochemical burial-diagenesis (Worden and Morad, 2003). Thus, results of this study will enable the prediction, by analogy, of clay mineral type, abundance and distribution in ancient, deeply-buried, marginal-marine sandstones (and thus reservoir quality).

Clay mineral type and abundance in sedimentary basins is reported to be controlled primarily by a combination of climate (weathering intensity) and provenance (sediment supplied) (Chamley, 1989; Eberl et al., 1984; Rateev et al., 2008). Previously recognised and suggested controls on clay mineral distribution patterns include; the landward displacement of marine sediment (Chamley, 1989; Hathaway, 1972; Meade, 1969; Postma, 1967); provenance (Biddle and Miles, 1972; Feuillet and Fleischer, 1980; Hathaway, 1972; Rudert and Müller, 1981); differential settling due to salinity or clay mineral stability (Edzwald and O'Mella, 1975; Whitehouse et al., 1960); the physical sorting of clay minerals by size (Gibbs, 1977); local hydrodynamics (Feuillet and Fleischer, 1980); and both early physicochemical (Griffin and Ingram, 1955; Grim and Johns, 1954; Nelson, 1960; Powers, 1957), and biologically-mediated diagenesis (McIlroy et al., 2003; Needham et al., 2006; Needham et al., 2004; Needham et al., 2005; Wooldridge et al., 2017a; Worden et al., 2006).

A detailed modern-analogue study of the clay mineral distribution patterns in the Ravenglass Estuary, UK was thus designed to better understand whether clay mineral proportions are controlled by, or a combination of the following mechanisms (i) provenance; the distribution of various potential sources of clay-mineral, (ii) estuarine hydrodynamics and redistribution of material and/or (iii) early-diagenesis; continued chemical and/or biological alteration of sedimentary minerals in the estuary.

1.2.4 Clay coats, clay minerals, pyrite and estuarine facies: modern shallow-core analogue for ancient deeply-buried sandstones (chapter 3 rationale)

Clay-coated sand-grains can preserve anomalously-high porosity in deeply-buried petroleum reservoirs. The ability of grain coats to preserve porosity is primarily controlled by the clay mineralogy and the extent and completeness of the clay coat (Ajdukiewicz and Larese, 2012). Clay coats in sandstones are reportedly derived from the *in situ* growth from the authigenic alteration of precursor (detrital) and early-diagenetic minerals, and/or due to the thermally-driven recrystallization of precursor detrital clay coats. Near-surface pyrite formation reduces iron availability which is required for the formation of diagenetic Fe-chlorite grain coatings from precursor clay minerals, such as kaolinite, which do not contain iron.

The primary aim of this part of the study is to better understand the distribution of detrital clay coats, clay minerals and iron-sulphides in near-surface (< 1 m) sediment in the Ravenglass Estuary, UK.

Three mechanisms are have been invoked to explain the origin and distribution precursor clay coats in sediment: macro- and micro-biological activity (McIlroy et al., 2003; Needham et al., 2006; Needham et al., 2004; Needham et al., 2005; Worden et al., 2006), mechanical infiltration (Matlack et al., 1989; Wilson, 1992), and inheritance (Wilson, 1992). Surface clay mineral distribution patterns have been explained by the landward displacement of marine sediment (Chamley, 1989; Hathaway, 1972; Meade, 1969; Postma, 1967); provenance (Biddle and Miles, 1972; Feuillet and Fleischer, 1980; Hathaway, 1972; Rudert and Müller, 1981); differential settling due to salinity or clay mineral stability (Edzwald and O'Mella, 1975; Whitehouse et al., 1960); the physical sorting of clay minerals by size (Gibbs, 1977); local hydrodynamics (Feuillet and Fleischer, 1980); and both early physicochemical (Griffin and Ingram, 1955; Grim and Johns, 1954; Nelson, 1960; Powers, 1957), and biologically-mediated diagenesis (McIlroy et al., 2003; Needham et al., 2006; Needham et al., 2004; Needham et al., 2005; Worden et al., 2006).

This study provides the first opportunity to compare both surface (< 2 cm) (Wooldridge et al., 2017b) and near-surface (< 1 m) clay mineral and clay coat distribution patterns. By comparing surface (< 2 cm) clay coat and clay mineral distribution patterns to the near-surface (< 1 m) it is possible to account for processes which may influence surface clay coat and clay mineral distribution patterns at depths greater than 2 cm i.e. mechanical-infiltration and bioturbation. A shallow-subsurface study also permits the study of the distribution of pyrite (Fe-sulphide) which requires reducing-conditions to form.

1.2.5 Compositional variation in modern estuarine sands: predicting major controls on sandstone reservoir quality (chapter 4 rationale)

Primary sediment composition and early diagenetic reactions determine the burial diagenetic reactions and rock properties (reservoir quality) as a function of depth (Bjorlykke, 1998). Primary clastic composition of sedimentary rocks is reported to be related to provenance, weathering and erosion in the hinterland, transport processes and to the depositional environment (Bjorlykke, 1998). However, statistical correlations commonly fail to accurately predict reservoir quality, partly due to the spatial and temporal variability of sandstone composition being poorly-understood (Ajdukiewicz and Lander, 2010). Thus, the aim of this part of the study is to map the spatial distribution of quartz, feldspar, carbonates and clay minerals on a scale similar to many oil and gas reservoirs, to aid reservoir quality prediction.

Variations in sandstone composition may be explained by variations in the primary depositional sediment or differences in diagenetic alterations during burial. Depositional sand composition is reported to be controlled by i) relative proportions of different provenance components (Dickinson and Suczek, 1979), including sediment received from aeolian dust fallout (Khalaf and Ala, 1980), ii) hydrodynamic sorting processes (Odom et al., 1976) and/or iii) varying degree of mineral alteration during sand transport to the site of final deposition (Johnsson and Meade, 1990). For example, the vertical (stratified) differences in plagioclase content in the Stratfjord Formation, Gullfaks Field, are reported to reflect differences in sand provenance (Dalland et al., 1995).

A study undertaken by Odom et al. (1976) revealed that feldspar distribution and abundance in four quartz-rich cratonic sandstones, of different ages (Cambrian, Ordovician, Pennsylvanian-Permian and Jurassic) was controlled primarily by grain-size, which reflects transport processes and depositional environment, which may all lead to different degrees of sediment abrasion (thus, extent of grain size reduction). Odom et al. (1976) reported that in the Cambrian to Ordovician sandstones of the upper Mississippi Valley, and Palaeozoic Weber Sandstone, feldspar tends to be concentrated in the < 125 μm fraction of the sediment or in some cases that coarse silt fraction. Odom et al. (1976) hypothesised that 125 μm represents a threshold below which feldspar tends to be less susceptible to further size reduction by abrasion. Field and Pilkey (1969) have also shown that feldspar in shelf and beach sands off North Carolina is concentrated in the fine and very fine sand fractions, as a result of abrasion. Consequently, many studies of ancient sandstone often cite this work to explain feldspar distribution patterns. However, there remains no high-resolution study which analyses mineral distribution patterns on scale similar to many oil and gas fields, and

with statistical analysis which shows whether there are significant differences in mineral abundances between individual depositional environments e.g. foreshore sediment versus inner-estuarine tidal-bars. Consequently, studies which focus on sandstones reservoirs, perhaps too often rely upon a small number of studies, such as Odom et al. (1976) and Dickinson and Suczek (1979), to predict the variations in sandstone composition. For example, other geological processes, such as glacial comminution, may lead to both quartz and feldspar being concentrated in the silt fraction (Stevens, 1991).

The study addresses the control on the type and abundance of minerals in the modern Ravenglass Estuary, as well as understanding the fundamental controls on quartz, plagioclase, K-feldspar, carbonate and clay mineral distribution within a modern estuarine setting. Mineral distribution patterns are then compared to variables, which are observed or predictable in sandstone reservoirs, such as host-sediment properties (e.g. grain size and sorting), estuarine zone and depositional environment.

1.2.6 Summary of research questions

The three main chapters of this thesis may be distilled down into seven specific research questions, which will be addressed in specific chapters, as well as in the final discussion chapter of this thesis.

1. What is the composition of sediment in the Ravenglass Estuary?
2. What are the fundamental controls on estuarine sediment composition in Ravenglass?
3. How are quartz, feldspar, carbonate, clay minerals and Fe-sulphides distributed in sediment in the Ravenglass Estuary?
4. What are the fundamental controls on mineral distribution patterns in the Ravenglass Estuary?
5. How are detrital clay coats distributed in the Ravenglass Estuary?
6. What are the fundamental controls on detrital clay coat distribution patterns in the Ravenglass Estuary?
7. Can primary sediment composition and/or detrital clay coat coverage be predicted as a function of host-sediment properties (e.g. grain size, sorting, and bioturbation intensity), depositional environment, and/or estuarine zone?

1.3 METHODS

1.3.1 Identification of depositional-environments and estuarine zones

In order to determine whether mineral and clay coat distribution patterns are predictable as a function of depositional environment and lithofacies, it was first necessary to map environments of deposition. Aerial imagery and detailed ground-surveys were used to define a suite of estuarine sub-environments, which included coastal-spits; gravel-bed; mud-flat; mixed-flat; sand-flat; tidal bars and dunes; tidal-inlet; backshore; foreshore; and pro-ebb delta deposits. Throughout this thesis, tidal flats have been categorized following the classification scheme proposed by Brockamp and Zuther (2004); sand-flat is > 90 % sand, a mixed-flat has 50 to 90% sand, and a mud-flat has 15 to 50 % sand. Furthermore, the Ravenglass Estuary has been split into zones, primarily to test whether provenance exerts a control on mineral type and abundance in the three fluvial arms (Irt, Esk and Mite). The Ravenglass Estuary was split into eight estuarine zones (Fig. 1.4), which may be grouped into four categories, based upon the dominant physical processes active in each zone. The following divisions are used, 1) fluvial (river) zone, freshwater-dominated in the Esk (zone A), Mite (zone B) and the Irt (zone C), 2) a brackish, inner river- and tide-dominated Irt, (zone D), Mite (zone E), and Esk (zone F), 3) a mixed-energy (fluvial-, tide- and wave-influenced), heterogeneous central zone (zone G) with near-seawater salinity, which contains extensive mud-flat and mixed-flat (Saltcoats tidal flat), and 4) an outer zone (zone H), dominated by seawater with wave and/or tidal currents, which are dissipated by barrier-spits.

1.3.2 Detailed ground-surveys (grain size and bioturbation)

In order to characterise the whole estuary at high resolution, surface sediment grain size was determined with a hand-lens and a grain-size comparison-card at 3,151 sites across the estuary. Macrobiological activity (*Arenicola marina*, more commonly known as lugworms) has been previously reported to form clay coats, as well incite early-diagenesis (creation of new clay minerals) (McIlroy et al., 2003; Needham et al., 2006; Needham et al., 2004; Needham et al., 2005; Worden et al., 2006). Therefore, the distribution of *Arenicola marina* was determined at 3,182 sites by counting the number of *Arenicola marina* faecal castings per square metre, using a 1 m^2 quadrat. A quadrat was thrown randomly i.e. blindly thrown behind the individual doing the measurement to ensure an absence of bias.

1.3.3 Surface (< 2 cm) sample collection

Sediment for laboratory analysis was collected at low-tide along pre-defined transects at 185 sites to give an approximately uniform distribution of samples, as well as 21 fluvial sample-

locations, and four upper-fluvial sediment samples. The entire sample collection was analysed for grain size, sorting, clay fraction weight, and fine-fraction (< 2 μm) clay mineralogy (chapter 2). A total of 191 samples were analysed to quantify the coarse-fraction mineralogy (chapter 3). To prevent sample degradation prior to LPSA and XRD analyses, all samples were placed in air-tight plastic-jars in the field prior to being stored in a refrigeration unit at ~ 2°C.

1.3.4 Shallow-core (< 1 m) collection, sampling and description

Twenty-three cores were collected along predefined transects in order to capture surface-sediment heterogeneity for each depositional-environment. Core collection was achieved by using a jackhammer-driven window sampler following the method detailed by Dowey et al. (2017). Each sediment core was collected in a polythene liner to avoid oxidation and sample degradation. Cores were placed within a rigid plastic tube for protection during storage and transport. Each sediment core was dissected and photographed, wet and dry, to capture ichnofabrics (bioturbation traces), redox boundaries and key sedimentary structures. Core subsamples collected for X-ray diffraction analysis were extracted and placed in an air-tight, screw-top plastic jar, and refrigerated (at ~ 2 °C) to avoid degradation. Sediment samples collected for the qualitative analysis of detrital clay coat coverage were sub-sampled and prepared following the same procedure detailed by Wooldridge et al. (2017b). Grain size was measured in the laboratory using a hand-lens every 5 cm (in relatively homogenous facies), and at a sub-centimetre scale (in very thinly-bedded sediment (< 3 cm)). The Campbell (1967) classification was used to assign bed-thickness. The classification between wavy flaser bedding and wavy bedded heterolithics are defined after Reineck and Wunderlich (1968). Bioturbation Index (BI) was recorded using the classification scheme proposed by Taylor and Goldring (1993) to test the strength of the relationship between detrital clay coat coverage and bioturbation intensity.

1.3.5 Quantification of grain size and sorting (Laser Particle Size Analysis)

Mean grain size, sorting and sand abundance was determined for sediment samples using a Beckman Coulter Laser Particle Size Analysis (LPSA) in unison with GRADISTAT (Blott and Pye, 2001). Grain size sorting (σg) values follow the classification outlined by Folk and Ward (1957); high values are indicative of poorly-sorted sediment.

1.3.6 Qualitative analyses of detrital-clay coat coverage (Scanning Electron Microscopy)

Qualitative estimation of detrital clay coat coverage was achieved by the method proposed by Wooldridge et al. (2017b). Following detailed assessment of Scanning Electron Microscopy (SEM) images (n = ~ 200 sand grains per sample), detrital- clay coat coverage was categorized into five classes: class 1, complete absence of attached clay; class 2, 1 to 5 % coverage is observed on < 50 % of the sand grains; class 3, all grains have at least 5 to 15% clay coat coverage; class 4, all grains have clay coats, with the majority of grains having 15 to 30 % clay coat coverage; and, class 5, > 30 % clay coat coverage (extensive) is observed on all grains (Wooldridge et al., 2017b).

1.3.7 Mineral identification and quantification (X-ray diffraction)

Clay fractions (< 2 μm) and silt- and sand-fractions (2 μm to 2 mm) of estuarine-sediment samples and quaternary-drift deposits were physically separated prior to X-ray diffraction (XRD) analysis. The clay fraction was separated, and recombined with the silt- and sand-fraction in order to accurately identify and quantify the type and abundance clay minerals, through improved detection limits. An ultrasonic bath followed by centrifuge settling at 5,000 rpm for 10 minutes to isolate the clay fraction (< 2 μm), which was subsequently dried at 60°C for 24 hours and weighed to calculate the percentage of clay-size material. The clay fraction was then crushed into a fine loose powder using a pestle and mortar ready for XRD analysis.

To analyse the silt- and sand-fractions (2 μm to 2 mm), a representative 5 g subsample was taken from the silt- and sand-fractions (2 μm to 2 mm) and placed in an agate McCrone mill with 12 mL of distilled water and finely crushed for 10 minutes. The resultant slurry was washed into a petri dish using distilled water, and then dried at 60 °C, prior to being crushed into a fine loose powder using an agate pestle and mortar ready for XRD analysis. A PANalytical X'Pert Pro MPD X-ray Diffractometer was used to quantify the mineralogy of fine-fraction (< 2 μm) and silt- and sand-fraction (2 μm to 2 mm). To assess the presence of expandable clay minerals, samples were glycolated for 24 h and re-scanned over a range of 3.9 to 13.0°2θ (Moore and Reynolds, 1997). XRD results were then combined to study the mineralogy of the whole sample (material < 2 mm).

The Esquevin Index has been calculated (using clay fraction XRD-data) to differentiate Al-rich from Fe-Mg-rich illite. Esquevin Index is calculated by analysing the ratio between the 5Å and 10Å peak heights on X-ray diffractograms (Esquevin, 1969). The following classification boundaries are used in this study, after Esquevin (1969); biotite, < 0.15 (most

Fe-Mg-rich); biotite + muscovite, 0.15-0.3; phengite, 0.3-0.4; muscovite, >0.4 (most Fe-Mg-depleted). To establish illite crystallinity index ($2^0\theta$), also known as the *Kübler* Index (Kübler, 1964), the full width at half-maximum (FWHM) of the 10Å (001) illite peak was measured on the X-ray diffractogram (using clay fraction XRD-data). The following boundaries are used, after Kübler (1964); epizone (highest temperature): < 0.25; anchizone: 0.25-0.42, diagenesis (lowest temperature): >0.42.

In addition, gravity-settling (as above) and sieving, followed by X-ray diffraction analyses, was undertaken to determine the mineralogy of different size-fractions of a single central-basin (mixed-flat) sample. The following grain-size classes were analysed; < 0.2 µm (fine clay); 0.2 µm to 2 µm (coarse clay); 2 µm to 32 µm (fine silt); 32 µm to 62 µm (coarse silt); 62 µm to 125 µm (very fine sand); and 125 µm to 250 µm (fine sand).

1.3.8 Textural and mineralogical analyses (SEM-EDS; QEMSCAN®)

The QEMSCAN® system is comprised of a scanning electron microscope (SEM) coupled with Energy Dispersive Spectrometers (EDS). Data is processed to provide information about the micron-scale texture and chemical and mineralogical composition, as detailed by Armitage et al. (2010). Data was collected with a step size of 2 µm to ensure both the fine fraction (< 2 µm) and silt- and sand-fraction (> 2 µm) was analysed. A limitation of quantifying mineral abundances of material < 2 µm is that any mixtures of clay minerals may show a mixed or inconclusive signal, due to the activation volume of the beam being ~ 4 µm across. Thus, for mineral quantification, XRD was the preferred technique. Therefore, the primary purpose of using an SEM-EDS (QEMSCAN®) was to achieve textural and mineralogical analysis, to assess whether clay minerals (chlorite, illite and kaolinite) occur as, or form part of clast and/or occur as part of the fine fraction (< 2 µm).

1.3.9 Spatial mapping of mineralogy (ArcGIS)

All mineral distribution maps were made in ArcGIS using an inverse distance weighted (IDW) interpolation technique to avoid the creation of ridges or valleys of extreme and unrepresentative values (Watson and Philip, 1985). An interpolation barrier (polyline drawn in ArcGIS) along the long axis of Drigg and Eskmeals spits, to ensure interpolated values, either side of the spits (i.e. in the estuary and on the coast), did not influence one another despite their relative spatial proximity.

1.3.10 Statistical analyses (R Studio)

All statistical analyses were performed in R statistical software (R Core Team, 2016), using the following symbols to highlight statistical significance; marginally-significant (+ or †) when $p < 0.1$; significant (*) when $p < 0.05$; very-significant (**) when $p < 0.01$; and extremely significant (***) when $p < 0.001$.

Pearson's' correlation coefficients were calculated to describe the strength of the relationship between continuous variables e.g. grain size, sorting, clay fraction, bioturbation intensity, mineral abundance and depth. Spearman's correlation coefficients were calculated to describe the strength of the relationship between categorical variables e.g. bioturbation index and detrital clay coat coverage.

An Analysis Of Variance (ANOVA) test was used to assess whether there is a statistically significant difference in continuous variables (e.g. clay mineral, pyrite abundance and clay fraction) as a function of estuarine lithofacies, depositional environments and estuarine zones. Following ANOVA, a post-hoc Tukey's honestly significant difference (HSD) test was employed to highlight where the identified significant differences between a given variable (e.g. clay mineral abundance) and individual lithofacies, depositional environments or estuarine zones could be found.

A Kruskal-Wallis H test was used to assess whether there is a statistically significant difference in categorical variables e.g. bioturbation index and detrital clay coat coverage, as a function of estuarine lithofacies, depositional environments and estuarine zones. Following Kruskal-Wallis H test, a post-hoc Dunn test was used to highlight where the identified significant differences between a given variable (e.g. detrital clay coat coverage) and individual lithofacies, depositional environments or estuarine zones could be found. The Benjamini-Hochberg method (False Discovery Rate) was applied to correct the *p-values* after performing multiple comparisons (Benjamini and Hochberg, 1995).

1.4 ORGANISATION OF THE THESIS

This thesis is presented in a paper-style format and thus the three main chapters have either been submitted, or are intended to be submitted to international journals (namely, Sedimentology, American Association of Petroleum Geologists and Journal of Sedimentary Research). The outline of each chapter, publication status, and work contribution from other authors are listed in this section.

1.4.1 Estuarine clay mineral distribution: modern analogue for ancient sandstone reservoir quality prediction (Chapter two)

Publication status: Submitted to Sedimentology (in review)

Outline: This chapter is a study of clay mineral distribution patterns in the surface sediment (< 2 cm) of the Ravenglass Estuary, UK. The study assesses the fundamental controls on clay mineral distribution patterns, in order to better predict precursor clay mineral distribution in ancient and deeply-buried sandstone reservoirs.

Work contribution and responsibilities:

Joshua Griffiths: Planning and undertaking detailed ground-surveys, to define a suite of sub-environments (including recording bioturbation intensity) and the collection of surface (< 2 cm) sediment samples. Laser Particle Size Analysis to establish grain size. Sample preparation (separation of clay-size material) required prior to XRD-analyses. X-ray diffraction analyses to reveal mineral proportions, as well as illite chemistry and crystallinity in bedrock, drift and surface-sediment samples. Spatial mapping and statistical analyses of mineral distribution patterns. Secured £125,000 funding from Woodside following detailed-discussions at the Geological Society of London conference.

Richard H. Worden: Primary PhD supervisor. Responsible for raising industry funding for the project and defining fieldwork site (Ravenglass Estuary, UK). Provided in-depth discussions and detailed manuscript review.

Luke J. Wooldridge: Planning and undertaking detailed ground-surveys, to define a suite of sub-environments (including recording bioturbation intensity) and the collection of surface (< 2 cm) sediment samples. In-depth discussions and detailed manuscript review.

James E. P. Utley: X-ray diffraction sample preparation and analysis. In-depth discussions and detailed manuscript review.

Robert. A. Duller: Discussions and detailed manuscript review.

Rhiannon L. Edge: Support in statistical analyses and detailed manuscript review.

In addition, thanks go to Joanna Jeffreys and Robert Wilcox for their assistance in collecting lugworm population density data.

1.4.2 Clay coats, clay minerals, pyrite and estuarine facies: modern shallow-core analogue for ancient deeply-buried sandstones (Chapter Three)

Publication status: In preparation for submission to Journal of Sedimentary Research

Outline: This chapter is a study of clay coat, clay mineral, and pyrite distribution in the near-surface (< 1 m) in the Ravenglass Estuary, UK; to better predict textural variation and compositional distribution of precursor sediment in marginal-marine sandstone reservoirs. In addition, this paper allowed for the detailed comparison between published surface (< 2 cm) clay coat distribution patterns (Wooldridge et al., 2017a) and those observed in the near-surface (this study), to account for possible post-depositional controls (e.g. infiltration, and bioturbation).

Work contribution and responsibilities:

Joshua Griffiths: Planning and undertaking detailed ground-surveys, defining a suite of sub-environments and core collection. Core preparation, description and construction of a detailed lithofacies scheme. Sample preparation (separation of clay-size material) required prior to XRD-analyses. X-ray diffraction analyses to reveal mineral proportions, as well as illite chemistry and crystallinity in bedrock, drift and surface-sediment samples. Statistical analyses of mineral and clay coat distribution patterns. Spatial mapping and statistical analyses of mineral distribution patterns. Secured £125,000 funding from Woodside following detailed-discussions at the Geological Society of London conference.

Richard H. Worden: Primary PhD supervisor and field assistant. Responsible for raising industry funding for the project and defining fieldwork site (Ravenglass Estuary, UK). Field assistant and provided in-depth discussions and detailed manuscript review.

Luke J. Wooldridge: Planning and undertaking detailed ground-surveys, defining a suite of sub-environments (including recording bioturbation intensity) and core collection. Core preparation and description, and qualitative analysis of detrital clay coat coverage using Scanning Electron Microscopy (SEM) images.

James E. P. Utley: Field assistant. X-ray diffraction sample preparation and analysis. In-depth discussions and detailed manuscript review.

Robert. A. Duller: Field assistant and detailed manuscript review.

In addition, thanks go to Jack Walker for his assistance in X-ray diffraction analysis sample-preparation.

1.4.3 Compositional variation in modern estuarine sands: predicting major controls on sandstone reservoir quality (Chapter Four)

Publication status: in preparation for submission to American Association of Petroleum Geologists

Outline: This chapter is a study of the distribution of quartz, feldspar, carbonate and clay minerals in surface sediment of the Ravenglass Estuary, since sandstone composition exerts a strong control on reservoir quality. This study aims to better predict specific estuarine depositional environments, which may be likely to form porosity-preserving or pore-occluding cements using detailed statistical analysis and spatial mapping.

Work contribution and responsibilities:

Joshua Griffiths: Planning and undertaking detailed ground-surveys, to define a suite of sub-environments and the collection of surface (< 2 cm) sediment samples. Laser Particle Size Analysis to establish grain size. Sample preparation (separation of clay-size material) required prior to XRD-analyses. X-ray diffraction analyses to reveal mineral proportions in drift and surface-sediment samples. Spatial mapping and statistical analyses of mineral distribution patterns. Interpretation of mineral distribution patterns, and the primary author of both text and figures. Detailed Scanning Electron Microscopy (SEM-EDS) and Energy Dispersive Spectrometers (EDS) analyses, to identify the nature of clay minerals (e.g. grain coating, pore filling, and clasts). Secured £125,000 funding from Woodside following detailed-discussions at the Geological Society of London conference.

Richard H. Worden: Primary PhD supervisor. Responsible for raising industry funding for the project and defining fieldwork site (Ravenglass Estuary, UK). Provided in-depth discussions and detailed manuscript review.

Luke J. Wooldridge: Planning and undertaking detailed ground-surveys, to define a suite of sub-environments and the collection of surface (< 2 cm) sediment samples. In-depth discussions and detailed manuscript review.

James E. P. Utley: X-ray diffraction and QEMSCAN® sample preparation and analysis. In-depth discussions and detailed manuscript review.

2. ESTUARINE CLAY MINERAL DISTRIBUTION: MODERN ANALOGUE FOR ANCIENT SANDSTONE RESERVOIR QUALITY PREDICTION

2.1 ABSTRACT

The ability to predict clay mineral distribution patterns would be of great benefit in reservoir quality studies during oil and gas exploration, field appraisal and in planning well locations, since clay minerals may both enhance or degrade porosity and permeability. To address the absence of relevant modern analogue datasets, here a high sample-resolution analogue approach was adopted using the Ravenglass marginal-marine system, in NW England, UK. The aim of the study is to establish the dominant controls on clay mineral distribution patterns in modern estuarine sands. Extensive geomorphic mapping, grain size analysis and data collection on bioturbation intensity (as defined by lugworm faecal cast count per square meter) were followed by X-ray diffraction analysis of clay separates and statistical analyses. Local drift deposits were also analysed as well as dominant rock types in the hinterland to the estuary and local littoral sediments. The estuary sediment is dominated by illite (typically Fe-Mg-rich illite) with subordinate chlorite and kaolinite, although the rivers supply sediment with less illite and significantly more chlorite than found in the estuary. Separation of an estuary sediment sample into different grain sizes revealed chlorite is most abundant in the coarse sediment fraction (sand), whereas illite and kaolinite are most abundant in the finest sediment fraction (silt and clay). Fluvial-supplied sediment has been locally diluted by sediment derived from glaciogenic drift deposits on the margins of the estuary. Detailed, high-resolution maps reveal that the estuarine sediment has a heterogeneous distribution of illite, chlorite and kaolinite. Chlorite is most concentrated in coarse grained depositional environments within the estuary and concentrated on the northern foreshore and backshore. There is no relationship between bioturbation intensity and clay mineral distribution patterns. The clay mineral distribution pattern in the estuary has been strongly influenced by sediment supply, and subsequently modified by hydrodynamic processes within the inner, central and outer estuarine zones.

2.2 INTRODUCTION

It is well known that clay minerals can have a major impact on the properties of sandstone reservoirs. Specific clay minerals have different effects on reservoir properties; for example, pore-filling illite is bad for reservoir quality (especially permeability), while grain-coating chlorite can be good for reservoir quality. For example, grain-coating chlorite can inhibit the

growth of typically ubiquitous pore-filling quartz cement in deeply buried (>80 to 100 ºC) sandstones (Ehrenberg, 1993; Skarpeid et al., 2017; Stricker et al., 2016). Note that the term "clay mineral", referring to aluminium-rich sheet silicate minerals (phyllosilicates), is carefully discriminated from the term "clay", referring to sediment particles that are smaller than 2 μm in size. Volumes of sediment, modern or ancient (as sedimentary rock), are rarely homogeneous; instead they typically display significant heterogeneities in terms of total clay content, primary grain mineralogy, grain size and grain sorting, and varying degrees of bioturbation, soil development and infiltration. It can also be anticipated that specific clay minerals are not homogeneously distributed throughout modern and ancient sand bodies, in terms of either the total amount of clay minerals or the relative abundance of specific types of clay minerals at any specific site.

The sandstone community and energy industry have started using modern analogues to help develop predictive models of reservoir quality, with some focus on understanding carbonate cement distribution, especially in aquifers, marginal marine settings and in arid intracontinental soils (Arakel, 1986; McBride et al., 1995; McBride and Parea, 2001). New focus on the use of clastic depositional analogues to help with reservoir quality prediction has arisen with an imperative to understand the origin and distribution of primary (detrital) grain coating clay minerals, that serve to inhibit quartz cement and thus preserve porosity, in deeply buried sandstone reservoirs (Dowey et al., 2017; Wooldridge et al., 2017a; Wooldridge et al., 2017b). Marginal marine environments are of specific interest for reservoir quality since grain-coating chlorite (Fe-Mg-rich clay) has been found to be especially common in sandstones from such environments (Dowey et al., 2012). However there is no mechanism to predict chlorite distribution in the subsurface, to help reduce exploration and reservoir development uncertainty. With reference to modern marginal marine environments, while it is possible to start to predict the distribution of clay grade material (Dalrymple et al., 1992; Dowey et al., 2017; Wooldridge et al., 2017a; Wooldridge et al., 2017b), it is not possible to identify areas of enrichment of one specific clay mineral (e.g. chlorite) relative to other clay minerals. Fundamentally, there is a lack of knowledge and understanding on how specific clay minerals are distributed in most modern sedimentary environments and in ancient, deeply buried sandstone reservoirs. Therefore, there is a need to map clay mineral distribution patterns, and understand the dominant controls on clay mineral distribution, at a scale relevant to oil and gas reservoirs, before modern clastic sedimentary systems can be used as analogues.

Even during the long time-scale of burial diagenesis, the main components of clay minerals (for chlorite: Fe-, Al- and Si-oxides) are effectively water-insoluble, and therefore clay

mineral (and especially chlorite) diagenesis during burial can be assumed to be an isochemical process (closed-system) (Worden and Morad, 2003). Chlorite, and other clay mineral presence, is thus not the result of mass influx of materials into sandstones during diagenesis, rather it represents either primary chlorite presence or the diagenetic transformation of precursor components that were initially present in the primary sediment. A study of modern environments is thus an appropriate way of developing an understanding (by analogy) of the distribution of chlorite in sandstones since the distribution of chlorite, or the key components of chlorite (Fe-, Al- and Si-oxides) in the original sediment, which controls where chlorite will be found in the sandstone after burial diagenesis (Wooldridge et al., 2017a; Worden and Morad, 2003).

The primary objective of this study is to better understand the distribution of clay minerals in a modern marginal-marine setting (in this case an estuary), which will enable the prediction of clay mineral type, abundance and distribution in ancient, deeply-buried, marginal-marine sandstones (thus, reservoir quality). It is here speculated that there are three dominant discrete controls on clay mineralogy in marginal marine settings, although note that all three may operate to different degrees at the same time. First, clay mineral distribution patterns may be controlled by provenance, and reflect the relative contribution of different potential sources of clay-mineral (i.e. different bedrock types, drift deposits, offshore sediment). Second, hydrodynamic processes in the estuary may control the redistribution of clay minerals (possibly from one or multiple sources), and thus the relative abundance of a specific clay mineral may be associated with certain depositional-environments. Third, there may be continued weathering and alteration of pre-existing clay minerals and/or sedimentary grains (e.g. feldspars or lithics) in the estuary via a combination of physical, chemical and/or biological processes that serve to alter the minerals that were delivered and possibly sort by hydrodynamics during sediment transport and deposition.

It is noteworthy that, across the sediment below the world's ocean, clay minerals are not uniformly distributed. The type and relative abundance of clay minerals found in modern oceanic and marginal-marine settings has been reported to be governed primarily by a combination of climate (weathering intensity) and the type of sediment supplied (provenance) (Chamley, 1989; Eberl et al., 1984; Rateev et al., 2008). Chlorite and illite have been reported to be most abundant in high-latitude marine environments adjacent to land masses, subject to relatively cold climatic-conditions that favour mechanical weathering (Chamley, 1989; Eberl et al., 1984; Rateev et al., 2008; Windom, 1976). Kaolinite is reported to be most abundant in low-latitude marine environments adjacent to land masses with warm and humid conditions that permit intense chemical weathering (Chamley, 1989;

Eberl et al., 1984; Rateev et al., 2008; Windom, 1976). Smectite is generally typical of weathering from semi-arid continental sources, subject to only the early stages of chemical weathering conditions (Salem et al., 2000).

Estuarine clay mineral assemblages have been reported to be similar to those in the near-offshore (Hathaway, 1972; Meade, 1969; Postma, 1967), leading to a conclusion that landward displacement of marine sediment, during marine-transgression, can explain some clay mineral distribution patterns (Chamley, 1989). It has been reported that provenance plays a critical role in determining the clay mineral assemblage in marginal marine settings (Chamley, 1989). For example, Rudert and Müller (1981) suggested that the relatively homogenous clay mineral assemblages reported within south-eastern estuaries from the North Sea, from Denmark (Varde Å) to the Netherlands (Rhine-Meuse), reflects the minor variability of north-western European climatic conditions and soil composition. In contrast, a diverse estuarine clay mineral assemblages reported from British and North American estuaries was interpreted to reflect the heterogeneous composition of continental rocks and soils in the hinterlands of each estuary (Biddle and Miles, 1972; Hathaway, 1972).

Hydrodynamic processes in the estuary control the redistribution of the sediment fed in to the estuary. The competing physical forces of inward river flow, wave energy transmitted from the open ocean and twice-daily tidal emptying and filling will combine to move sediment into specific sub-environments such as salt marshes, mud flats, tidal bars, channels and the local foreshore (Dalrymple et al., 1992). Not all clay minerals necessarily have the same mean grain size, shape and/or density, so that different clay minerals may be preferentially associated with different sub-environments. It is also noteworthy that not all clay minerals are necessarily clay grade (clay minerals may be > 2 μm in size); clay minerals may exist in lithic silt or sand grains, as discrete silt or sand grade grains, as well as in the finest grain size fraction (clay grade) of any sediment. Once suspended, clays and clay minerals that have been fed into an estuary may undergo flocculation into larger aggregates, which subsequently preferentially settle out of the water column. Laboratory studies undertaken by Whitehouse et al. (1960) reported that, in relatively slow moving (or static) and brackish waters (1.8 % salinity), kaolinite settles prior to illite. However Edzwald and O'Mella (1975) and Gibbs (1977) suggested that results from Whitehouse et al. (1960) have been wrongly extrapolated from the laboratory to the natural environment. Edzwald and O'Mella (1975) instead suggested that suspended illite is more stable (slower aggregation or flocculation rate) than kaolinite, and is thus deposited downstream relative to kaolinite. In contrast, Gibbs (1977) proposed that clay mineral distribution patterns are due to physical sorting by size irrespective of mineralogy. It was suggested that mixing of fluvial and marine

waters with distinctly different clay mineral suites, combined with estuarine circulation patterns, can explain clay mineral distribution patterns in the James River Estuary, Virginia, USA (Feuillet and Fleischer, 1980).

On top of provenance- and hydrodynamic-sorting controls on the proportions of clay minerals in marginal marine sediment, it has further been suggested that early diagenesis can alter the clay mineralogy of sediment, in the environment, very soon after deposition. It is possible that this early diagenesis is simply a continuation of the physical and chemical alteration (weathering) processes that started in the hinterland and continued when the sediment was in transit. However, marginal marine, and especially estuarine environments tend to be geochemically active given that they tend to accumulate organic matter and contain sediment that is sufficiently physically stable so as to develop active micro- and macro-biological communities (Berner and Berner, 2012). Both physicochemical (Griffin and Ingram, 1955; Grim and Johns, 1954; Nelson, 1960; Powers, 1957), and biologically-mediated (McIlroy et al., 2003; Needham et al., 2006; Needham et al., 2004; Needham et al., 2005; Worden et al., 2006) early-diagenetic mineral-alteration processes have been reported in deposited estuarine sediment. Large scale studies of the Amazon concluded that rapid alteration of clay minerals and biogenic silica occurred in deltaic sediment (Aller and Michalopoulos, 1999; Michalopoulos and Aller, 1995; Michalopoulos and Aller, 2004; Michalopoulos et al., 2000).

A detailed study of the clay mineralogy of a modern estuary was thus designed to establish whether clay mineral proportions are controlled by (i) the distribution of various potential sources of clay-mineral, (ii) estuarine hydrodynamics and redistribution of material and/or (iii) continued chemical and/or biological alteration of sedimentary minerals in the estuary. To achieve this, it is necessary to understand what clay minerals are being fed into the estuary from all the various sources. It is also necessary to establish the average, or overall, clay mineral assemblage of the estuary and to determine how the clay minerals are distributed if they are not homogenous. The Ravenglass Estuary, in NW England (Fig. 2.1), has been selected for a high spatial resolution study of the surface (< 2 cm) clay mineral distribution, along with a study of the clay mineralogy of the various provenance sources, followed by statistical analysis. The Ravenglass Estuary was chosen for its accessibility, because it has an overall surface area is similar to many oil and gas fields, and because the two main fluvial arms, that feed the estuary, drain different bedrock types (Fig. 2.1); thus, the Ravenglass Estuary is an ideal natural laboratory to test the effects of provenance on estuarine clay mineralogy.

2.3 STUDY AREA: RAVENGLASS ESTUARY

The Ravenglass Estuary, in north-west England (Fig. 2.1), sits near the small town of Ravenglass located on the west coast of Cumbria. The Ravenglass Estuary, which encompasses the tidal reaches of the Rivers Esk, Irt and Mite, occupies an area of 5.6 km^2, of which ~86% is intertidal (Bousher, 1999; Lloyd et al., 2013; Wooldridge et al., 2017b). It has been suggested (Bousher, 1999) that the Drigg and Eskmeals barrier-spits developed at around 3,000 BP, causing the coalescence of the previously-separate and westward flowing Rivers Irt, Mite and Esk, into a singular complex estuary with one main channel out to the Irish Sea. The dominant fluvial arms, the Rivers Esk and Irt, are separated by Muncaster Fell. The estuary is macro-tidal (> 7 m tidal range) and is fed by two dominant arms; the River Esk drains a southern hydrological basin and the River Irt drains a northern hydrological basin (Fig. 2.1). The estuary is separated from the Irish Sea by the northern Drigg and southern Eskmeals barrier-spits. The Ravenglass Estuary is here thus defined as a 'dual-funnelled', mixed-energy estuary.

The northern part of the UK (including Cumbria) is presently undergoing limited isostatic recovery following the last glacial maximum (Bousher, 1999). The west Cumbria region of the UK was affected by glaciation during the Quaternary, on at least three occasions. The last glaciation occurred in the late Devensian, at about 28 to 13 ka (McDougall, 2001; Moseley, 1978). The Ravenglass area has benefitted from substantial geological and geomorphological research due to the location of the nuclear reprocessing plant at Sellafield (20 km away), and the low level nuclear waste repository at Drigg (immediately to the north of the River Irt). Much of the glacial deposit has been removed from the land surface following the last glaciations (Merritt and Auton, 2000). Merritt and Auton (2000) reported that the upper group of Quaternary sediments within the area around Sellafield and Ravenglass include estuarine, alluvial, organic and aeolian sequences sitting on top of the final glacial deposits. The estuarine sediments have a maximum thickness of about 10 to 15 meters in this area (Bousher, 1999).

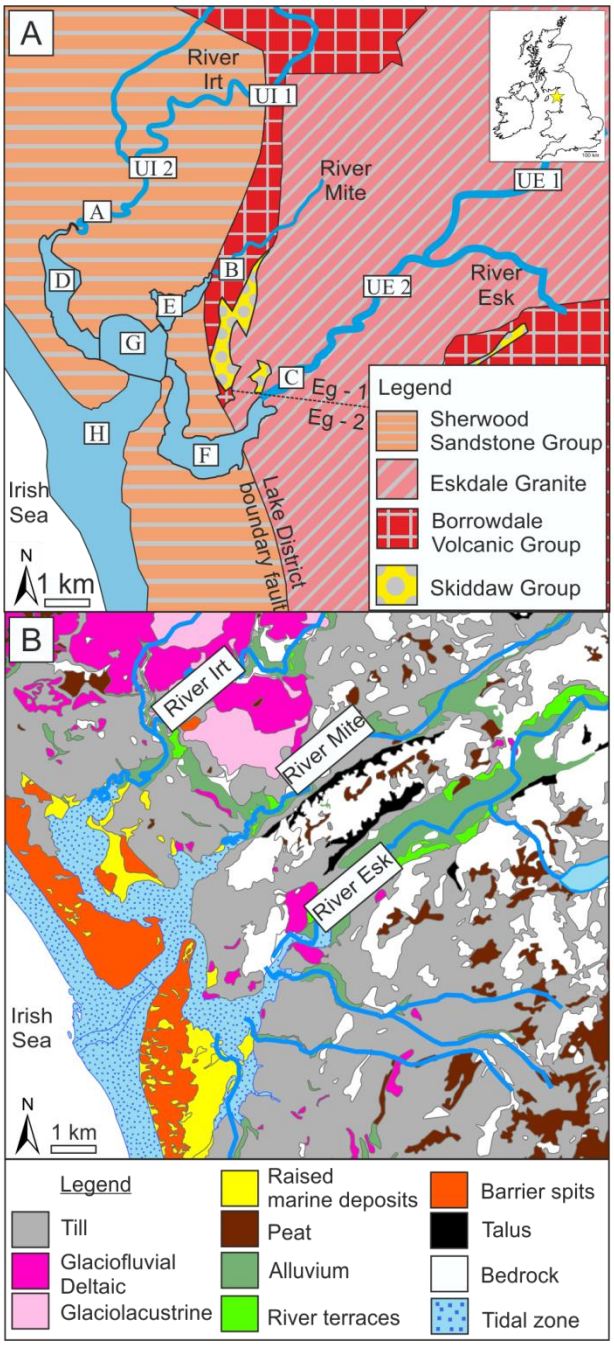

Figure 2-1 – Geological setting of the Ravenglass Estuary, UK, (A) bedrock geology, note, Eskdale Granite – 1 (Eg-1) and Eskdale Granite – 2 (Eg-2) are distinguished, and (B) Quaternary drift-deposits. Upper-fluvial sediment sampling locations, and estuarine zones are labelled accordingly; UI, upper-Irt; UE, upper-Esk; A, lower-Irt; B lower-Mite; C lower-Esk; D, inner-Irt; E, inner-Mite; F, inner, Esk; G, central-basin; and H, outer-estuary.

2.3.1 Geological setting and sediment source areas

The Rivers Irt, Mite and Esk drain a variety of bedrock lithologies and drift deposits (Fig. 2.1; Table 2.1). Upland catchment areas are composed of Devonian Eskdale Granite, Ordovician Borrowdale Volcanic Group, and Cambrian Skiddaw Group rocks (Fig. 2.1A).

These Palaeozoic rocks juxtapose the low lying coastal plains of the Triassic Sherwood Sandstone Group, with the Lake District boundary fault separating the Palaeozoic from the Mesozoic rocks. The Skiddaw Group includes weakly-metamorphosed, fine-grained sedimentary rocks (Merritt and Auton, 2000). The Borrowdale Volcanic Group is dominated by subduction-related, K-rich, calc-alkaline andesite that forms the central component of the Lake District massif (Quirke et al., 2015). The Borrowdale Volcanic Group was subject to regional, sub-greenschist facies metamorphism at about 395 Ma, during the Caledonian Orogeny (Quirke et al., 2015). The Eskdale Granite is part of the Lake District Batholith, at the western-margin of the Lake District massif; the southern part is granodioritic, while the northern part is coarse-grained granite (Young et al., 1986). In both granite types, chloritization of mafic silicates and plagioclase-alteration are widespread (Moseley, 1978; Quirke et al., 2015; Young et al., 1986). The Lower Triassic Sherwood Sandstone Group rocks are predominantly composed of fluviatile sandstones, locally known as the St Bees sandstone (Quirke et al., 2015). The Ravenglass Estuary is thus predominantly fed by the southern River Esk which drains an area dominated by Eskdale Granite and the northern River Irt which drain a combination of Borrowdale Volcanic Group andesites and Triassic Sherwood Sandstone Group sedimentary rocks.

Glacial till is exposed as knolls in all zones (inner, central and outer) within the estuary. These Quaternary sediments (Fig. 2.1B) in the Ravenglass Estuary area contain distinctive clasts of the underlying bedrocks, allowing detailed lithostratigraphical division, as well as revealing complex ice-movement patterns (Merritt and Auton, 2000). Fluctuations in relative sea-level during the Holocene were caused by glacioeustatic sea-level change and spatially-variable glacioisostatic rebound following deglaciation. These sea-level fluctuations led to the deposition of a suite of tills, glaciofluvial and glaciolacustrine deposits (Fig. 2.1B), locally known as the Seascale Glacigenic Formation (predominantly the Ravenglass Till member) and the overlying Gosforth Glacigenic Formation (Lloyd et al., 2013; Merritt and Auton, 2000).

Table 2.1- Mineralogical descriptions of hinterland bedrock and drift-deposits in the Ravenglass Estuary drainage basin.

Lithology	Mineralogical description
Fishgarth Wood Till Member (part of the Gosforth Glaciogenic Formation)	Holocene glacial till. The matrix-supported sandy-silty-clay diamicton also includes clasts of Borrowdale Volcanic Group lithologies, granite, granophyre, olive brown siltstone and sandstone (Merritt and Auton, 2000).
Ravenglass Till (part of the Seaforth Glaciogenic Formation)	Holocene glacial till. Dispersed clasts (up to boulder size) of Borrowdale Volcanic Group lithologies, granite, granophyre, siltstones, with minor concentrations of sandstones, ironstones and shell fragments are present (Merritt and Auton, 2000).
St. Bees Sandstone (part of the Sherwood Sandstone Group)	Lower Triassic sandstone. Feldspathic or subarkose, with dominant quartz and K-feldspar, albite, muscovite, biotite grains and minor Fe oxides (Quirke et al., 2015). Borrowdale Volcanic Group lithic fragments occur toward the base of the formation (Strong et al., 1994). Diagenetic phases include dolomite, quartz overgrowths and calcite authigenesis (Strong et al., 1994).
Eskdale granite – 1	Coarse-grained Devonian granite. Typical for the Eskdale Granite, plagioclase feldspars are more altered than alkali feldspars (Simpson, 1934). Plagioclase phenocrysts have relatively unaltered Na-rich rims with pervasively altered cores, forming fine-grained aluminous clay-minerals alteration products (Quirke et al., 2015). Biotite crystals with incipient alteration to chlorite (Fe/Mg 2.5) are abundant. Opaque Fe-oxides (predominantly ilmenite) occur as inclusions within the main silicates as well as groundmass phases, and as < 0.15 mm grains (Quirke et al., 2015).
Eskdale granite – 2	Devonian Granodiorite. Both plagioclase and alkali feldspars are more altered than those found within Eskdale granite – 1. Micas are Fe-rich and Al-poor, and classified as phengite. Intergrowths of white-mica and relatively Mg-enriched chlorite (Fe/Mg 0.6) are reportedly pseudomorphs after biotite or hornblende (Quirke et al., 2015; Simpson, 1934)
Borrowdale Volcanic Group	Ordovician Andesitic extrusive igneous rocks. Fine-grained groundmass shows ophitic textures between euhedral altered Na- and K-rich feldspars and patchy chlorite or biotite. Primary plagioclase phenocrysts have been partly altered to muscovite. Relatively Fe-enriched chlorite (Fe/Mg 1.8) crystals (~1 mm diameter) are reported to be pseudomorphs after pyroxene (Quirke et al., 2015).
Skiddaw Group	Cambrian metamorphic rocks. Lower grade rocks are reported to be dominated by illite, chlorite, and interlayered illite-smectite, whereas the higher grade rocks are dominated by muscovite and chlorite, and commonly interlayered paragonite-muscovite (Young et al., 1986). Aluminous K-mica with low phengite content dominate the rock and are characteristic of the Skiddaw Group (Stone and Merriman, 2004)

2.3.2 Morphology and hydrodynamics

The geological and topographic constraints on the width of the arms of the estuary and gradients of the lower parts of the river catchments (Figs. 2.1 and 2.2) constrain the area of the estuary to 5.6 km^2; typical of estuaries within northern and western Britain (Pye and Blott, 2014). Due to frictional effects commonly associated with shallow estuaries (Fig. 2.2), tidal-cycles at Ravenglass are strongly asymmetric, resulting in prolonged, outward ebb tidal-flows in comparison to the inward flood tidal-flows (Kelly et al., 1991). The rivers flowing into the estuary have average flow-rates of 3.4 m^3 s^{-1} for the Irt, 4.2 m^3 s^{-1} for the Esk and 0.4 m^3 s^{-1} for the Mite (Bousher, 1999). The maximum discharge measured for the lower Esk arm of the estuary during the ebb is only slightly lower at 4.99 m^3 s^{-1} than the flood at 5.41 m^3 s^{-1}; interpreted to result from quick-ebb drainage due to the estuary being short in length (Kelly et al., 1991).

Longitudinal salinity gradients (from the tidal limit to the open-sea) reported by Assinder et al. (1985) and Daneshvar (2015) and are shown in Figure 2.2. Stations A and D are reported as freshwater (Assinder et al., 1985; Daneshvar, 2015). Water-sampling stations B (River Irt) and E (River Esk) were reported to be fresh-water dominated, with only minor marine-dilution of the fresh-water, creating brackish-waters conditions for approximately 2.5 hrs at high-tide (Assinder et al., 1985; Daneshvar, 2015). Water-sampling stations C (Saltcoats) and F (River Esk bridge viaduct) were reported to be seawater-dominated (i.e. approaching seawater salinity), with only minor freshwater-incursions during low-tide (Assinder et al., 1985; Daneshvar, 2015).

Anthropogenic impact on the estuary is here considered to be minor since the surrounding area is sparsely populated, although the construction of the bridge has resulted in constriction and sheltering of the river Mite (Fig. 2.2). Cartographic evidence also suggests that fringing salt marsh has at least partially developed as a consequence of the railway viaduct construction (Carr and Blackley, 1986).

The Ravenglass Estuary has been divided zones, which may be grouped into four categories (Figs. 2.1A), based upon the dominant physical processes active in each zone; 1) fluvial (river) zone, freshwater-dominated in the Esk (zone A), Mite (zone B) and the Irt (zone C), 2) a brackish, inner river- and tide-dominated Irt, (zone D), Mite (zone E), and Esk (zone F), 3) a relatively mixed-energy (fluvial-, tide- and wave-influenced), heterogeneous central zone (zone G) with near-seawater salinity, which contains extensive mud-flat and mixed-flat (Saltcoats tidal flat), and 4) an outer zone (zone H), dominated by seawater with wave and/or tidal currents, which are dissipated by barrier-spits.

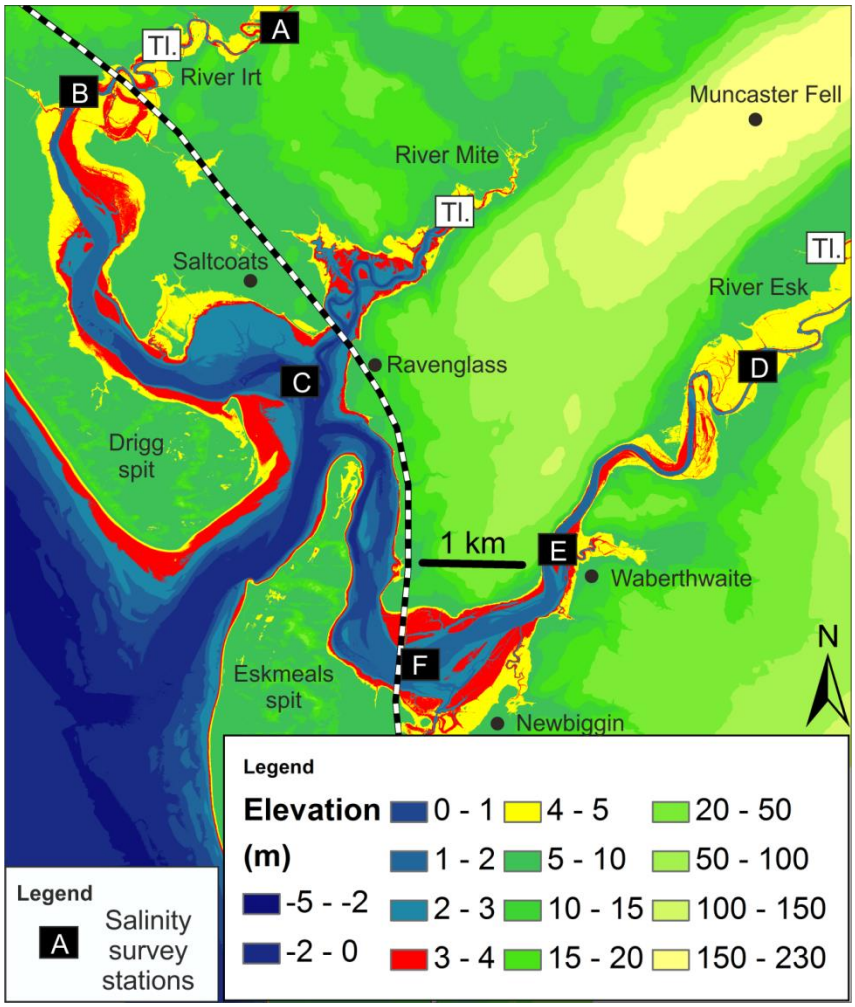

Figure 2-2 – Estuarine bathymetry and hinterland elevation (m OD) derived from Lidar Imagery (UK Environmental Agency, 2015). Stations in which salinity has previously (Assinder et al., 1985; Daneshvar, 2015) been measured are labelled (A-F). Tidal limits (Tl.) are marked, after Kelly et al. (1991).

2.4 SAMPLES AND METHODS

In order to study the clay mineral distribution, it was necessary to determine the surface sedimentology by defining all depositional environments throughout the estuary, describing surface sediment characteristics, collecting surface samples (< 2 cm) and then analysing them by X-ray diffraction (XRD) preceded by sample separation into different grain size fraction.

2.4.1 Field mapping and sample collection

Aerial photographs (e.g. Fig. 2.3) and detailed ground-surveys were used to define a suite of sub-environments: gravel-bed; tidal flats, tidal bars and dunes; tidal-inlet; backshore; foreshore; and pro-ebb delta. Tidal-flats have been further subdivided and categorised based on the percentage of sand; calculated using subsequent Laser Particle Size Analysis (LPSA)

of surface sediments samples (Fig. 2.3) (see later). The tidal-flat classification scheme of Brockamp and Zuther (2004) was employed whereby a sand-flat is > 90 % sand, a mixed-flat has 50 to 90% sand, and a mud-flat has 15 to 50 % sand

Sediment for laboratory analysis was collected at low-tide along pre-defined transects at 185 sites to give an approximately uniform distribution of samples (Fig. 2.3). Sediment was also collected from 21 fluvial sample-locations; four upper-fluvial samples are marked on Figure 2.1. All sediment samples were placed in air-tight, screw-top, plastic jars in the field before storing them in a refrigeration unit at ~ 2°C. This procedure prevented sample degradation prior to LPSA and XRD analyses.

Grain size and sorting were determined for all collected sediment samples by LPSA analyses using a Beckman Coulter Laser Particle Size Analysis, in unison with GRADISTAT (Blott and Pye, 2001). This revealed the mean grain size, grain-size sorting and sand-percentage at each surface sediment site (Fig. 2.3). In this chapter, the grain-size sorting (σg) scale presented by Folk and Ward (1957) is used, where high-values are indicative of poorly-sorted sediment. Additionally, in order to characterise the whole estuary at high resolution, surface sediment grain size was determined with a hand-lens at 3,151 sites across the estuary using a grain size comparison card.

In order to assess the macrobiological activity in the sediment throughout the estuary, the abundance of *Arenicola marina* (lugworms) was determined at 3,182 sites by counting the number of *Arenicola marina* faecal castings per square metre, using a 1 m^2 quadrat. The quadrat was thrown randomly i.e. blindly thrown behind the individual doing the measurement to ensure an absence of bias.

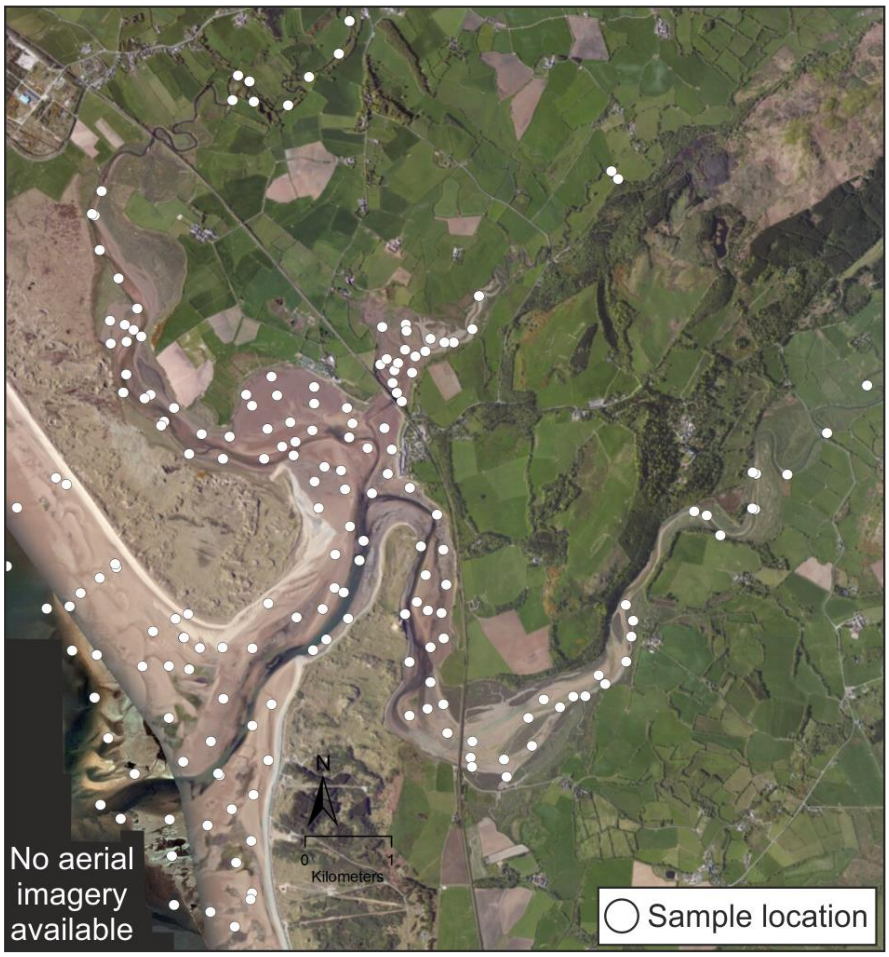

Figure 2-3 – Distribution of surface-sediment samples (< 2 cm) used for XRD and LPSA analyses.

2.4.2 Clay mineral separation, identification and quantification

Surface-sediment clay fractions (< 2 µm) from the estuary were determined by physical-separation prior to XRD analysis. Samples were physically separated in an ultrasonic bath, followed by centrifuge settling at 5,000 rpm for 10 minutes to isolate the clay fraction (< 2 µm). The wet-separated clay fractions were then dried at 60°C for 24 hours and weighed to calculate the percentage of clay-size material within each surface sample.

The clay mineralogy of all the estuary sediment samples was determined by X-ray diffraction analysis of randomly-orientated powders using a PANalytical X'Pert Pro MPD X-ray Diffractometer (Fig. 2.4). To assess the presence of expandable clay minerals, samples were glycolated for 24 h and re-scanned over a range of 3.9 to 13.0°2θ (Moore and Reynolds, 1997). An array of grain-size separates; < 0.2 µm (fine clay); 0.2 µm to 2 µm (coarse clay); 2 µm to 32 µm (fine silt); 32 µm to 62 µm (coarse silt); 62 µm to 125 µm (very fine sand); and 125 µm to 250 µm (fine sand), using a combination of gravity-settling (as above) and sieving, was used to reveal the X-ray diffraction mineralogy of different size-

fraction separates. Relative abundances of chlorite (chlorite/ (chlorite + illite + kaolinite)), kaolinite (kaolinite/ (chlorite + illite + kaolinite)), and illite (illite/ (chlorite + illite + kaolinite)) were derived to assess the relative abundance of each clay mineral at each sample location. In this study, the name illite is used for the clay-size, mica-like mineral commonly associated with clastic-sediments, following the definition of Grim et al. (1937).

The Esquevin Index (revealing illite chemistry) has been calculated by analysing the ratio between the intensity of the 5Å and 10Å peaks i.e. the ratio between the (002) and (001) peak heights (Esquevin, 1969), on X-ray diffractograms (Fig. 2.4). High Esquevin Indices indicate Al-rich illites (with muscovite representing the highest Esquevin Index end-member), reported to correspond to chemically-weathered rocks that have lost divalent cations (Fe and Mg) from the octahedral sites (Chamley, 1989). In contrast, low Esquevin Index values represent relatively Fe-Mg-rich illite (with biotite representing the lowest Esquevin Index end-member), which is considered to be characteristic of physically eroded, unweathered rocks (Chamley, 1989). The following classification boundaries have here been used, after Esquevin (1969); biotite, < 0.15; biotite + muscovite, 0.15-0.3; phengite, 0.3-0.4; muscovite, >0.4.

The illite crystallinity index ($2^0\theta$), also known as the Kübler Index (Kübler, 1964), was determined by measuring the full width at half-maximum peak height (FWHM) of the 10Å (001) illite peak on X-ray diffractograms (Fig. 2.4). Illite crystallinity has been reported to be inversely proportional to the temperature at which the illite (mica) formed: high illite-crystallinity indices (wide basal-reflections, high FWHM) indicate poorly-crystalline, highly-degraded, low growth-temperature, low-structural-order illite; whereas low-illite crystallinity indices (narrow basal-reflections, low FWHM) indicate highly-crystalline, relatively unaltered, high growth-temperature, high-structural-order illite (Chamley, 1989; Kübler, 1964). The following boundaries are here used, after Kübler (1964); epizone (highest temperature): < 0.25; anchizone: 0.25-0.42, diagenesis (lowest temperature): >0.42.

A key assumption made when utilising illite crystallinity values and Esquevin Indices to infer provenance of sediments (Borchers et al., 2011; Bout-Roumazeilles et al., 2013; Du Chatelet et al., 2016; Gingele et al., 2001; Oliveira et al., 2002), is that that illite crystallinity and chemistry values remain unchanged between supply, transport and deposition, i.e. there is no subsequent alteration of illite crystallinity or chemistry within the sedimentary environment.

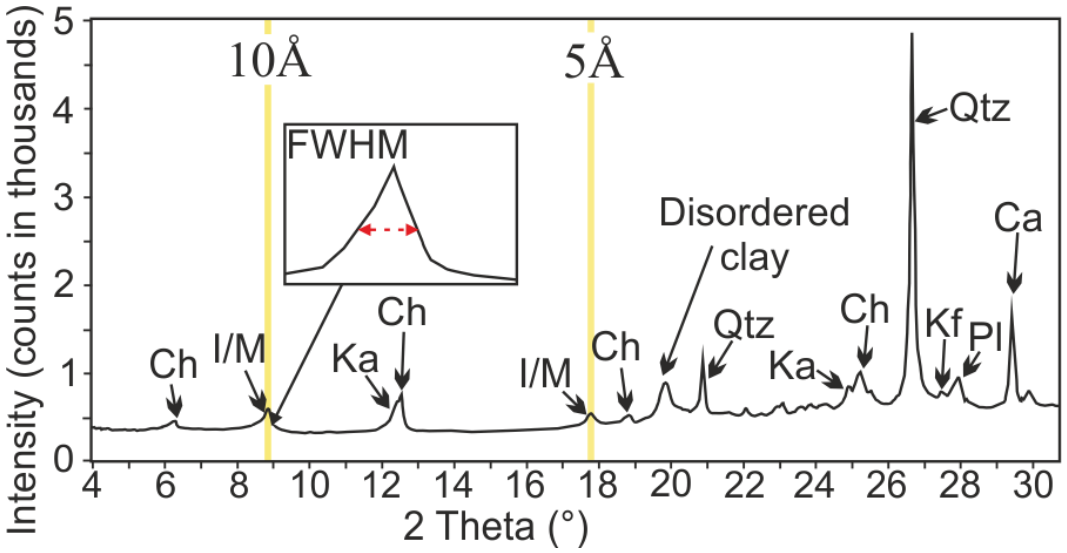

Figure 2-4 – Example, X-ray diffractogram used to quantity clay mineral abundance. Illite crystallinity is measured on the 10Å illite peak, using the full width at half maximum (FWHM). Esquevin Index is derived by comparing the relative peak heights of the 5Å and 10Å illite peaks.

2.4.3 Bedrock and drift analyses

In order to compare estuary sediment to the drift deposits (Fig. 2.1B), clay fractions (< 2 µm) from both the Seascale and the Gosforth Glacigenic Formations were determined by physical-separation prior to XRD analysis. Samples were physically separated in an ultrasonic bath, followed by centrifuge settling at 5,000 rpm for 10 minutes to isolate the clay fraction. The wet-separated clay fractions were then dried at 60°C for 24 hours and weighed to calculate the percentage of clay-size material within each surface drift sample. All drift samples were then analysed by PANalytical X'Pert Pro MPD X-ray Diffractometer using the same approaches as listed for the estuary sediment samples.

Although substantial work has been previously undertaken for the bedrock in the hydrological basins that supply the Ravenglass Estuary, several samples of the Triassic Sherwood Sandstone, Borrowdale Volcanic Group and Eskdale Granite were collected, in order to allow for mineralogical analysis and direct comparison to the clay minerals in the estuary sediment samples. Samples of Sherwood Sandstone from St Bees Head, Eskdale Granite from Devoke Water, and Borrowdale Volcanic Group from just west of Lake Wastwater, were all treated to produce clay mineral separates that are comparable to the modern sediment samples. Fresh, unweathered rock sub-samples were collected at each site using a hammer and chisel. Loose material was removed from the sub-sample using mild

detergent and tap water before being dried at 60°C. A steel disc mill was used for two seconds to crush the subsample to < 1 mm particle sizes. A representative 5 g subsample was taken from the part-crushed material, and placed in an agate McCrone mill with 12 mL of distilled water and finely crushed for 10 minutes. The resultant slurry was washed into a petri dish using distilled water, and then dried at 60 °C. The dried material was crushed into a fine loose powder using an agate pestle and mortar ready for XRD analysis using the same approaches as listed for the estuary sediment samples.

2.4.4 Spatial mapping and statistical analysis

All spatial-distribution maps were made in ArcGIS using an inverse distance weighted (IDW) interpolation technique, in order to avoid the creation of ridges or valleys of extreme and unrepresentative values (Watson and Philip, 1985). The insertion of an interpolation barrier, using a polyline drawn through the long axis of Drigg and Eskmeals spits, ensured interpolated values, either side of the spits (i.e. in the estuary and on the coast), did not influence one another despite their relative spatial proximity. Spatial maps have been plotted using a geometrical class-interval, in order to avoid divorcing the statistical distribution of data from its geographic context.

Pearson's correlation coefficients were calculated to describe the strength of the relationship between relative clay mineral abundance and host-sediment properties (mean grain size, grain size sorting, clay fraction, sand percentage and bioturbation-intensity), as well as elevation (m OD). Statistical significance is highlighted using the following symbols; marginally-significant (†) when $p < 0.1$, significant (*) when $p < 0.05$, very-significant (**) when $p < 0.01$, extremely significant (***) when $p < 0.001$. An Analysis Of Variance (ANOVA) approach was used to assess whether there is a statistical difference ($p < 0.05$) in relative clay mineral abundance (chlorite, kaolinite and illite) and illite type and illite crystallinity (Esquevin Index and FWHM) between estuarine zones (fluvial, inner, central and outer), as well as depositional environments (De1 to De9). Following ANOVA, post-hoc Tukey's honestly significant difference (HSD) test was employed to highlight where the identified significant differences in relative abundance could be found. All statistical analyses were performed in R statistical software (R Core Team, 2016).

2.5 RESULTS

The output of the surveys of surface-characteristics, grain size, grain size sorting, abundance of clay fraction, lugworm density together with the X-ray diffraction results of the analysis

of estuary sediment, fluvial sediment, drift deposits and bed rock samples will be presented here.

2.5.1 Estuary sediment characteristics

During the detailed field studies, nine discrete depositional environments were defined: gravel-beds (De 1), tidal flats (De2 to De4), tidal bars and dunes (De5), tidal-inlet deposits (De6), backshore deposits (De7), foreshore deposits (De8) and pro-ebb delta deposits (De9). The tidal flats were subdivided into mud-flats (De2); mixed-flats (De3); sand-flats (De4) using subsequent LPSA analysis and the Brockamp and Zuther (2004) method of classification. The general appearance of the nine depositional environments is illustrated in Figure 2.5. The mapped distribution of the nine discrete depositional-environments in the Ravenglass Estuary is displayed in Figure 2.6. The average characteristics of the nine depositional environments, in terms of grain size, grain size sorting, clay fraction and degree of lugworm bioturbation, are presented in Table 2.2. The estuary has also been subdivided into discrete zones (Fig. 2.1). The average characteristics of the eight estuary zones, in terms of grain size, grain sorting, clay fraction and degree of lugworm bioturbation, are presented in Table 2.3. The following text describes the appearance and character of the various deposition environments in the defined estuary zones.

The mapped distribution of grain size, grain sorting, clay fraction and degree of lugworm bioturbation, are presented Figure 2.7. Grain size, grain size sorting and clay fraction vary as a function of depositional environment and estuarine zone are represented in Figure 2.8.

Inner and central estuarine zones (zones D to G on Fig. 2.1) are fringed by upper-tier well-vegetated salt marsh, which transition into moderately to sparsely vegetated and intensely bioturbated (*Corophium volutator*, also known as sand shrimp, which form < 5 cm deep U-shaped burrows) middle- and lower-tier salt marsh (Fig. 2.5). Salt marsh grades into poorly-sorted (2.0 to 4.0 σg) clay- and silt-dominated (< 62 μm) mud-flats (Fig. 2.8; Table 2.2), which are densely bioturbated by *Corophium volutator* but have a relatively sparse lugworm population (Fig 2.7D).

Mud flats (Fig. 2.5D) within the inner and central (zones D to G on Fig. 2.1) grade into poorly-sorted (2.0 to 4.0 σg) and very-fine grained (62 to 125 μm) mixed-flats (Fig. 2.8; Table 2.2). Mixed-flats are highly-heterogeneous; substrates vary between lower-plane beds (including fluidised mud and sand) and sinuous to linguoid current ripples, typically draped in mud; bioturbation intensity (*Arenicola marina)* ranges from 0 to 115 castings per square metre (Figs. 2.5E and 2.7D), with a mean of 4 castings per square metre (Fig. 2.8; Table 2.2).

The inner and central zones have a wide range of mean grain size and grain sorting values (Fig. 2.8; Table 2.2).

In proximity to the ebb-channel, within the inner and central estuary (zones D to G on Fig. 2.1), there is a gradational change from mixed-flats to moderately-well to moderately-sorted (1.41 to 2.00 σg) fine- to medium-grained (125 to 350 μm) sand flats with sinuous to linguoid current ripples; mud-drapes are common (Figs. 2.5A, 2.5B, 2.6, 2.7A-C). *Arenicola marina* is the dominant macrofauna in intertidal sand flats, with highly variable bioturbation intensity ranging from 0 to 48 castings per square metre (Fig. 2.7D), with a mean of ~7 castings per square metre (Table 2.2). The lower inner Esk Estuary (zone F on Fig. 2.1) hosts gravel beds (partly colonised by mussels) which extend between the railway crossing and Ravenglass village (Fig. 2.6), directly adjacent to glacial-till deposits (Fig. 2.5L).

Fine-medium grained (125 to 350 μm) and moderately well sorted to moderately sorted (1.41 to 2.00 σg) tidal-dunes (in both the inner and central estuary; zones D to G on Fig. 2.1) and tidal-bars (inner estuary only; zones D to F on Fig. 2.1), generated by flood tidal-currents, are proximal to the channel-axis (Fig. 2.5C, Table 2.2). Bioturbation intensity (*Arenicola marina)* is relatively low and ranges from 0 to 8 castings per square metre (Fig. 2.7D), with a mean of ~ 1 casting per square metre (Table 2.2). The transition from mixed-flat to sand-flat in the central basin (zone G on Fig. 2.1) broadly reflects elevation; sand flats are typically < 2 m OD (Fig. 2.2).

The outer estuary (zone H on Fig. 2.1) is comprised of the tidal inlet (the narrow-inlet that dissects Eskmeals and Drigg barrier-spits), foreshore (De8: defined as the section of beach between the backshore and the mean-low-water line) and backshore deposits (De7: tidally-inundated only during spring-tide and/or storm-events) (Fig. 2.6). Bioturbation is typically absent in the outer estuary (Table 2.2) with exception isolated patches in the tidal inlet (Fig. 2.7D, Table 2.2). The abundance of clay fraction in the outer estuary (Fig 2.7C, Table 2.2) is minor (< 0.5 %). Tidal inlet sediment is typically moderately-well sorted (1.41 to 1.62 σg), and medium grained (250 to 500 μm). Wind-blown sands (backshore deposits) grade into tidal inlet substrates which contain both wave-ripples, 3D-dunes, and with increasing proximity to the ebb-channel upper-phase plan beds (Figs. 2.5G-I, 2.6, 2.7A-C). Sediment upon the southern foreshore and in pro-ebb delta deposits are typically finer (125 to 250 μm) than deposits upon the northern foreshore and backshore (250 to 500 μm) (Fig. 2.7A). Sorting ranges from moderately-well (1.41 to 1.62 σg) to well-sorted (1.27 to 1.41 σg) within foreshore and backshore deposits (Fig. 2.7A). The upper-foreshore (here defined as > 2 m OD) is typically structureless, whereas wave-formed ripples (typically draped by shelly-debris) occur upon the lower-foreshore (< 2 m OD). However, sedimentary structures in the

outer estuary are highly-dependent upon tidal-, wave-, and wind-conditions that were active during the time of sampling.

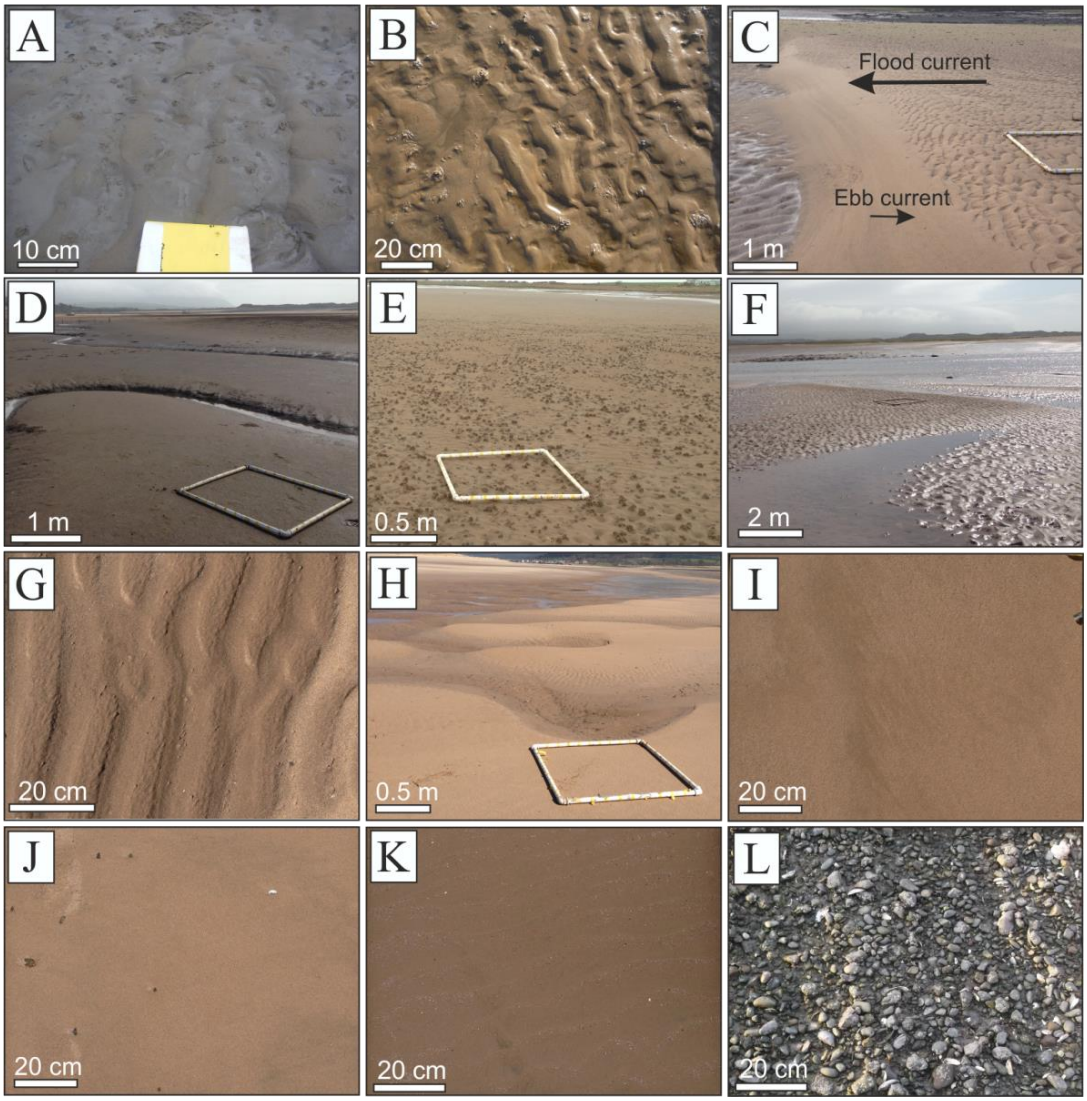

Figure 2-5 – Compilation of surface photographs taken throughout the Ravenglass Estuary. A-B) inner estuarine sand-flats with mud-drapes, C) inner estuary flood-dominated tidal-bar, D) central basin mud-flat, E) central basin, highly-bioturbated (*Arenicola marina*), mixed-flat, F) central-basin low amplitude dunes, G) upper-foreshore/tidal-inlet wave-formed ripples, H) tidal-inlet, migratory 3D dunes, I) tidal-inlet upper-phase plane bed, proximal to the ebb-channel, J) wind-blown, upper-foreshore sediment, K) lower-foreshore wave-ripples, with subtle shell-debris lag deposits, and L) gravel-bed, exposed in the inner-Esk.

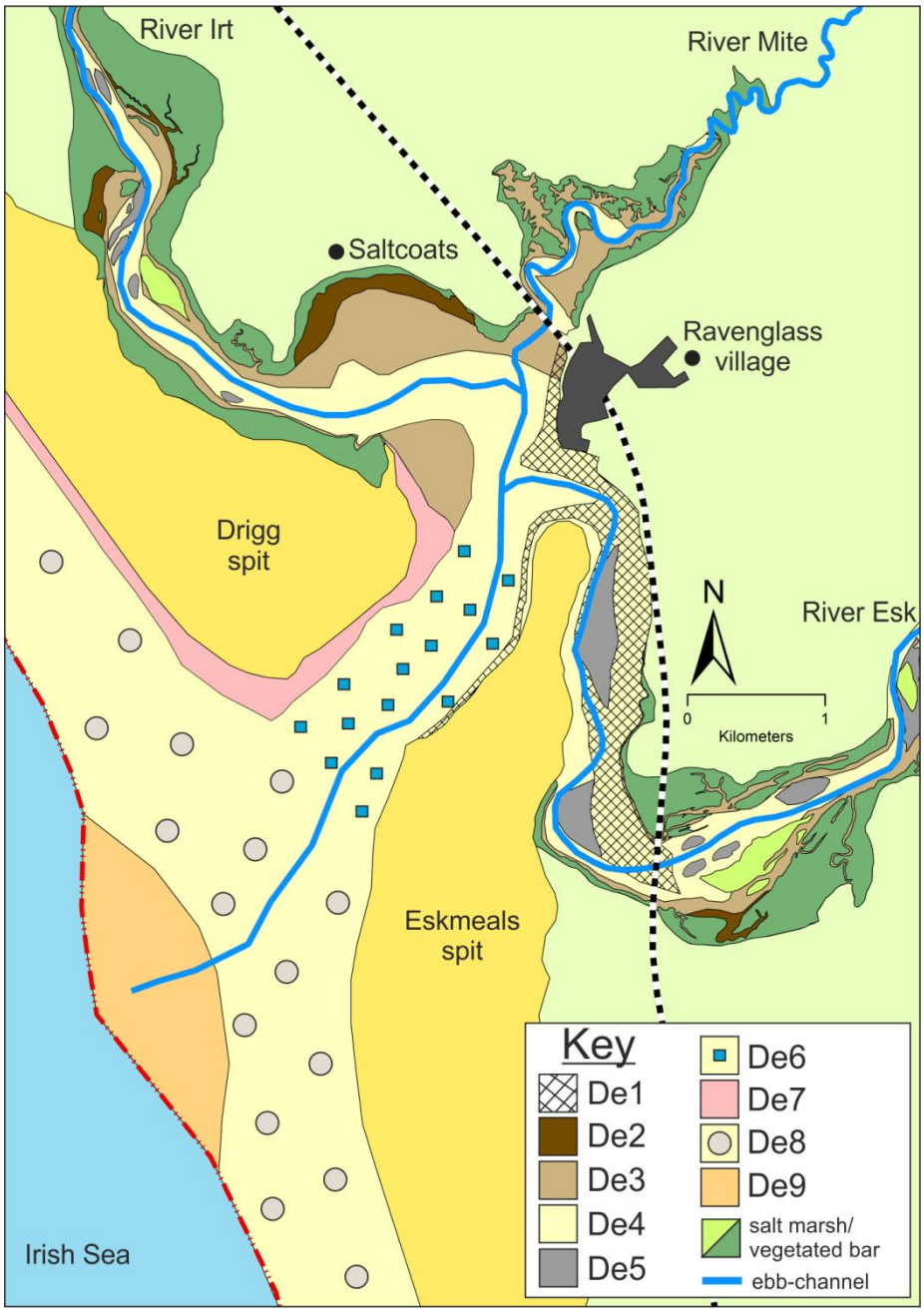

Figure 2-6 – Distribution of estuarine depositional-environments in the Ravenglass Estuary. Depositional environments, are labelled accordingly; De1, gravel-bed; De2, mud-flat; De3, mixed-flat; De4, sand-flat; De5, tidal bars and dunes; De6, tidal-inlet; De7, backshore; De8, foreshore; and De9, pro-ebb delta.

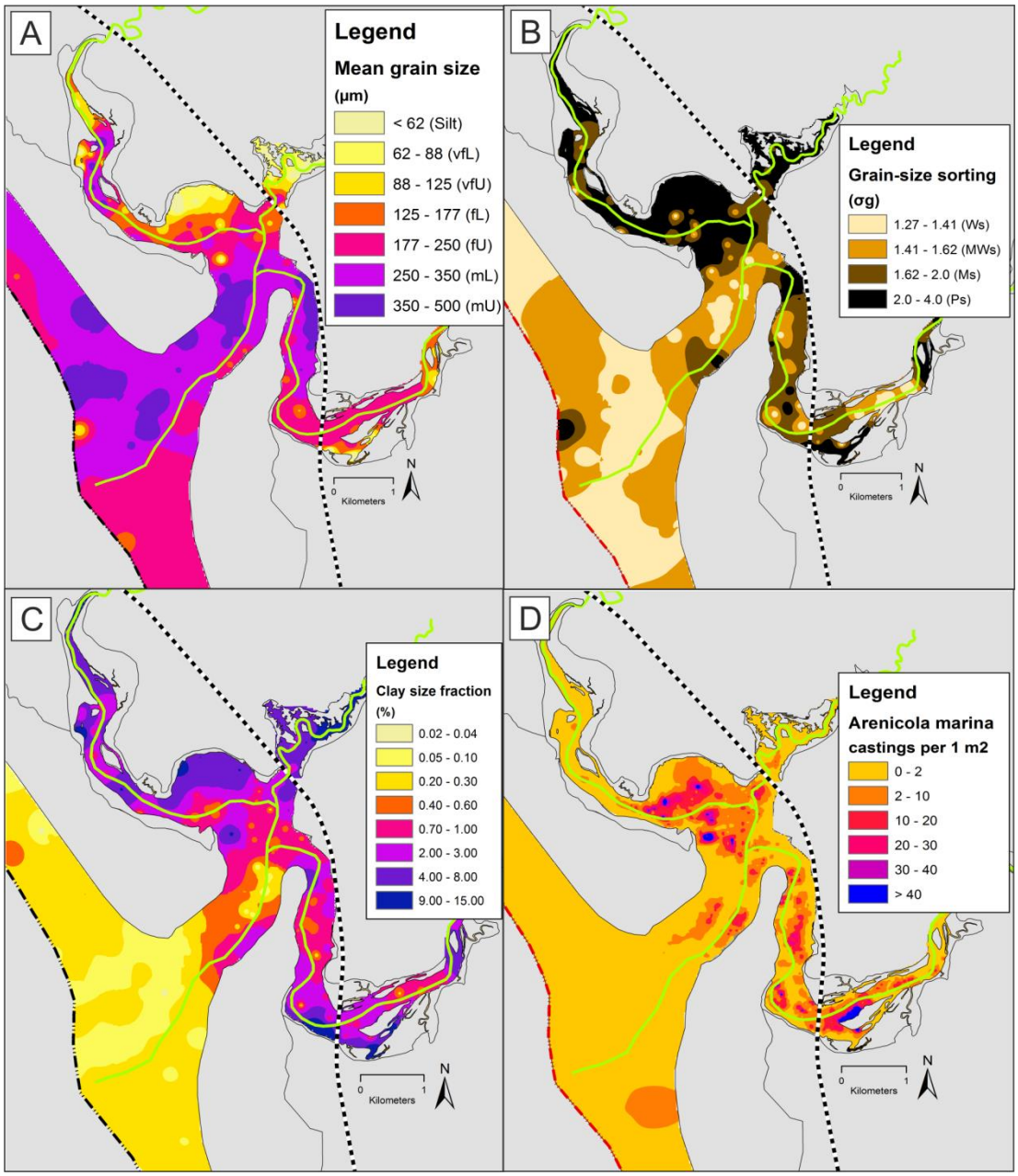

Figure 2-7 – Distribution of host-sediment properties, (A) mean grain size, (B) grain size sorting, (C) clay fraction (%), and (D) lugworm (*Arenicola marina*) bioturbation intensity.

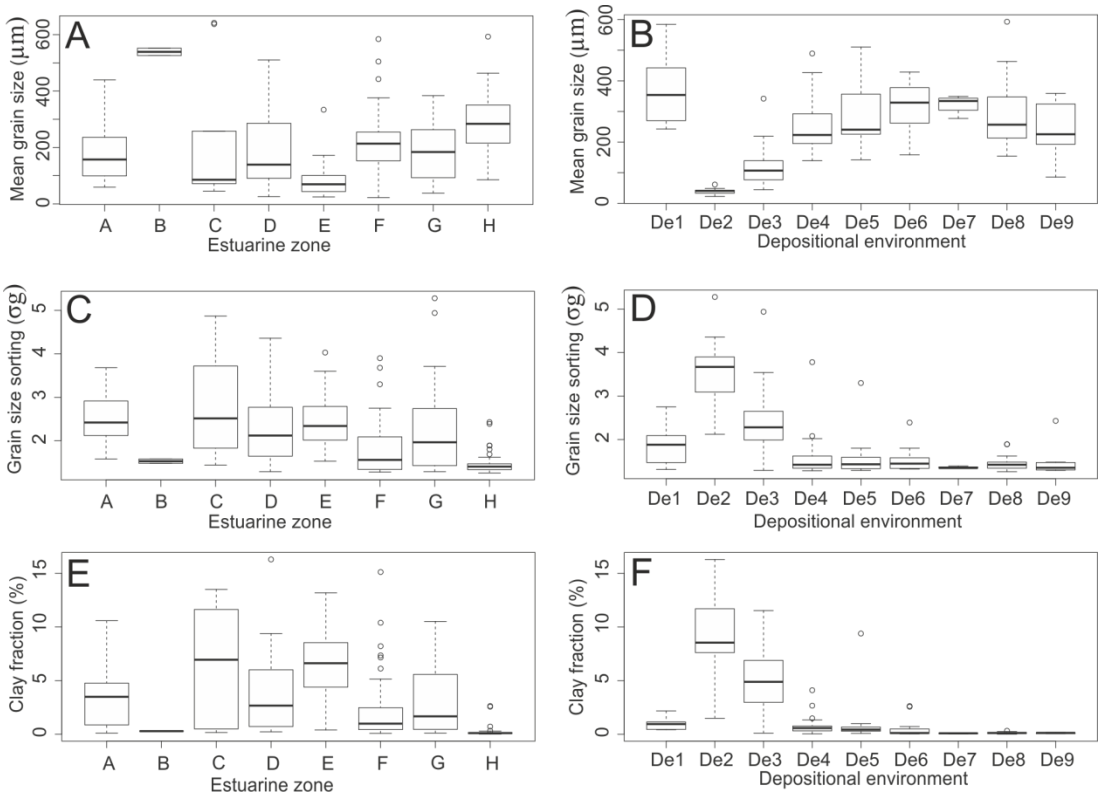

Figure 2-8 – Mean grain size (A-B), grain size sorting (C-D) and clay fraction (E-F) as a function of estuarine zone (zone A, lower-Irt; zone B lower-Mite; zone C lower-Esk; zone D, inner-Irt; zone E, inner-Mite; zone F, inner, Esk; zone G, central-basin; and zone H, outer-estuary), and depositional environment (De1, gravel-bed; De2, mud-flat; De3, mixed-flat; De4, sand-flat; De5, tidal bars and dunes; De6, tidal-inlet; De7, backshore; De8, foreshore; and De9, pro-ebb delta).

Table 2.2 - Summary of the main characteristics of the nine depositional environments and their clay mineralogy attributes. Depositional environments, are labelled accordingly; De1, gravel-bed; De2, mud-flat; De3, mixed-flat; De4, sand-flat; De5, tidal bars and dunes; De6, tidal-inlet; De7, backshore; De8, foreshore; and De9, pro-ebb delta.

Depositional environment (code)	n	Mean grain size (mm)	Grain size sorting (σg)	Clay fraction (%)	Mean bioturbation (casts/m2)	Illite index	stdev	Chlorite index	stdev	Kaolinite index	stdev	Esquevin index (5Å/10Å)	stdev	Illite crystallinity (FWHM)	stdev
De1	10	371	1.86	0.99	1.30	0.607	0.012	0.180	0.009	0.213	0.006	0.278	0.017	0.247	0.019
De2	13	39	3.54	9.47	0.46	0.614	0.014	0.178	0.008	0.208	0.009	0.279	0.020	0.231	0.016
De3	44	115	2.37	5.05	4.07	0.607	0.015	0.183	0.008	0.210	0.012	0.293	0.027	0.238	0.024
De4	23	253	1.59	0.83	6.57	0.600	0.031	0.186	0.018	0.214	0.018	0.307	0.040	0.259	0.022
De5	14	283	1.59	1.08	1.14	0.596	0.023	0.185	0.013	0.220	0.015	0.319	0.044	0.271	0.026
De6	12	312	1.53	0.58	2.17	0.593	0.022	0.201	0.018	0.206	0.015	0.314	0.031	0.272	0.033
De7	4	324	1.36	0.08	0.00	0.564	0.025	0.234	0.013	0.202	0.014	0.349	0.035	0.270	0.029
De8	41	291	1.44	0.13	0.27	0.600	0.027	0.202	0.016	0.199	0.020	0.345	0.036	0.301	0.044
De9	10	239	1.48	0.12	0.10	0.613	0.021	0.188	0.017	0.200	0.011	0.336	0.044	0.294	0.053
weighted average		225	1.90	2.36	2.36	0.602		0.190		0.208		0.313		0.265	

2.5.2 Estuarine clay mineral assemblage

On average, across the 171 samples of the main Ravenglass Estuary, the clay mineral assemblage (excluding clays present in sediment > 2 μm in size e.g. chlorite lithics) is dominated by illite (average illite index ~ 0.602), with subordinate quantities of chlorite (average chlorite index ~ 0.190) and kaolinite (average kaolinite index ~ 0.208) (Table 2.2). The estuarine illite is relatively Fe-Mg-rich (average Esquevin index, 0.315) and well-crystalline (average illite crystallinity index, 0.265) (Table 2.3).

The average illite, chlorite and kaolinite indices, illite crystallinity and Esquevin Indices have been derived for the nine depositional environments (Table 2.2; Fig. 2.1), and for each estuarine zone (Table 2.3, Fig. 2.6) to help understand the relationship between position in the estuary and clay mineralogy. Box-and-whisker plots display the range and standard deviations as well as the median values for individual depositional environments (Fig. 2.9) and estuarine zones (Fig. 2.10). To further understand the relationship between the different types of illite, in terms of crystallinity and chemistry, and position in the estuary, illite crystallinity and Esquevin Index values have been compared by estuary zone (Fig. 2.11).

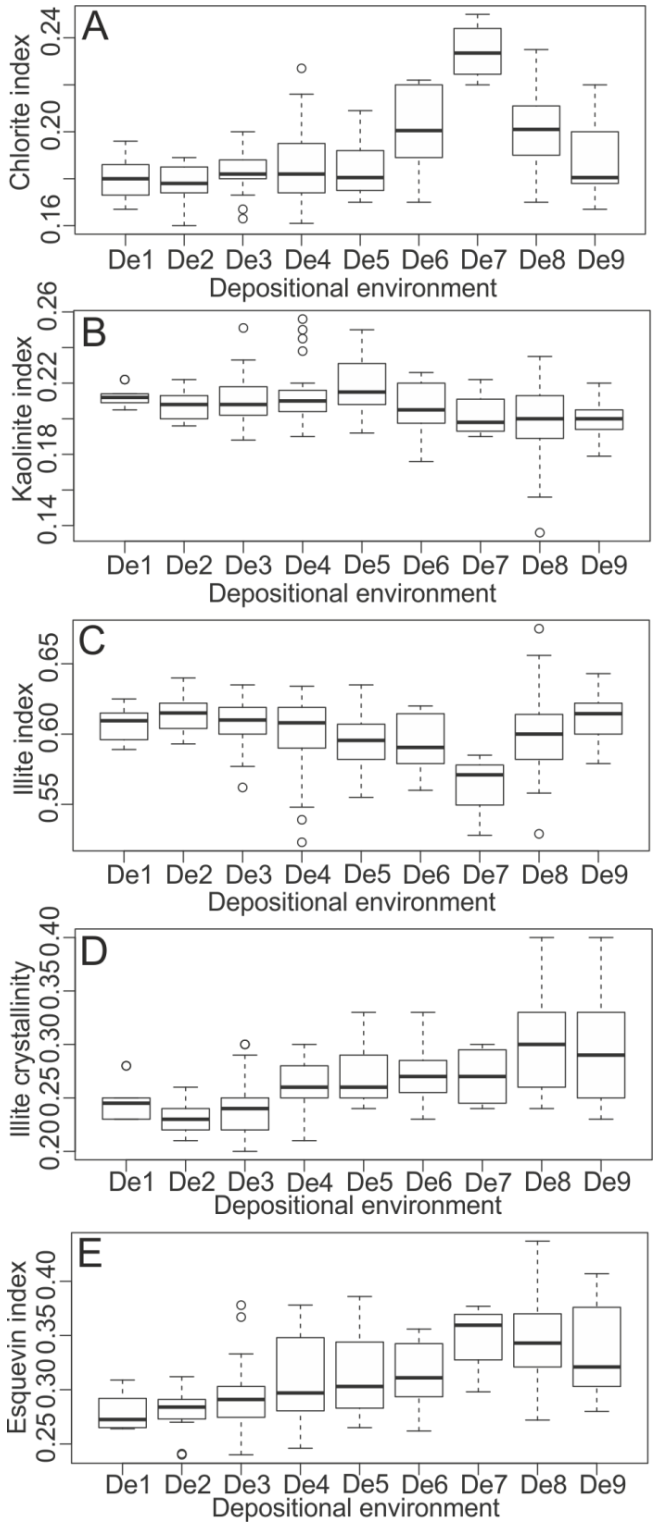

Figure 2-9– Clay mineral abundance as a function of depositional environment, (A) chlorite index, (B) kaolinite index, (C) illite index, (D) illite crystallinity, and (E) Esquevin index. Depositional environments, are labelled accordingly; De1, gravel-bed; De2, mud-flat; De3, mixed-flat; De4, sand-flat; De5, tidal bars and dunes; De6, tidal-inlet; De7, backshore; De8, foreshore; and De9, pro-ebb delta.

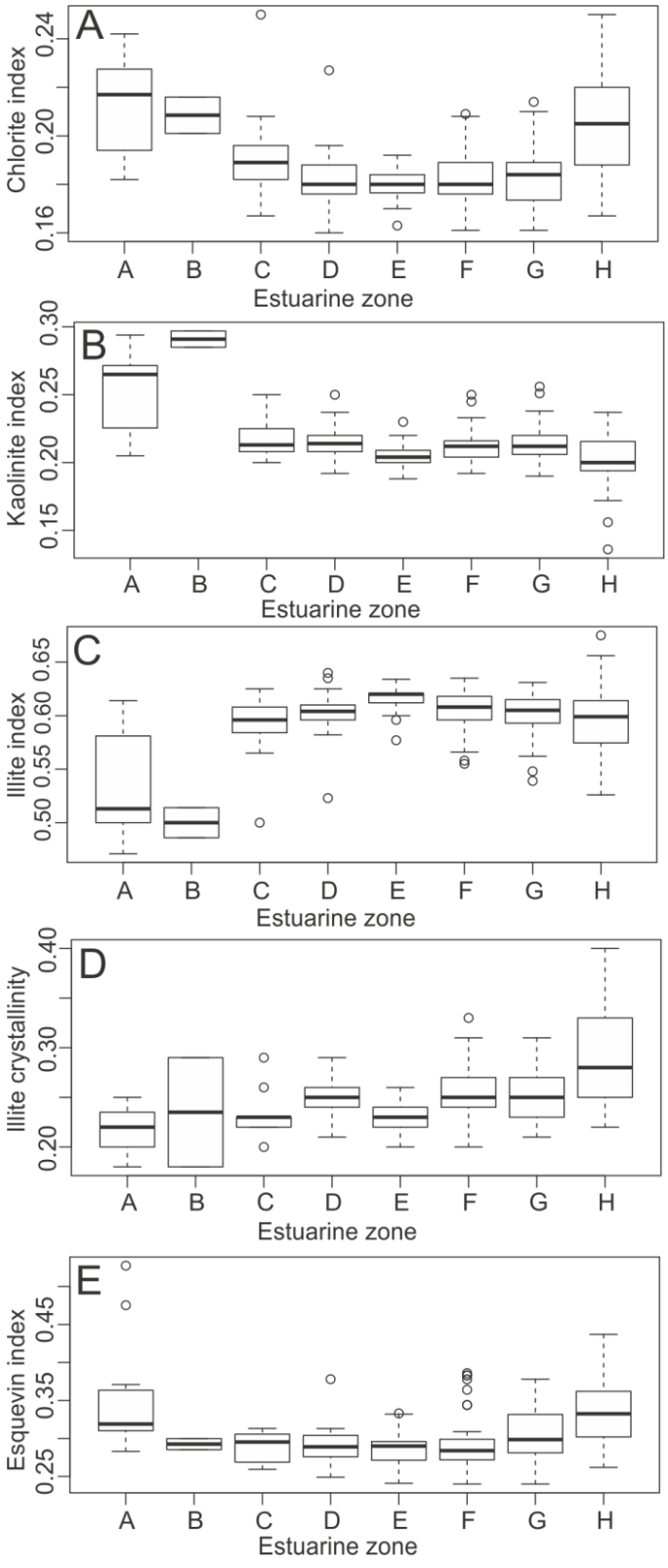

Figure 2-10 – Clay mineral abundance as a function of estuarine zone, (A) chlorite index, (B) kaolinite index, (C) illite index, (D) illite crystallinity, and (E) Esquevin index. Estuarine zones are labelled accordingly; A, lower-Irt; B lower-Mite; C lower-Esk; D, inner-Irt; E, inner-Mite; F, inner, Esk; G, central-basin; and H, outer-estuary.

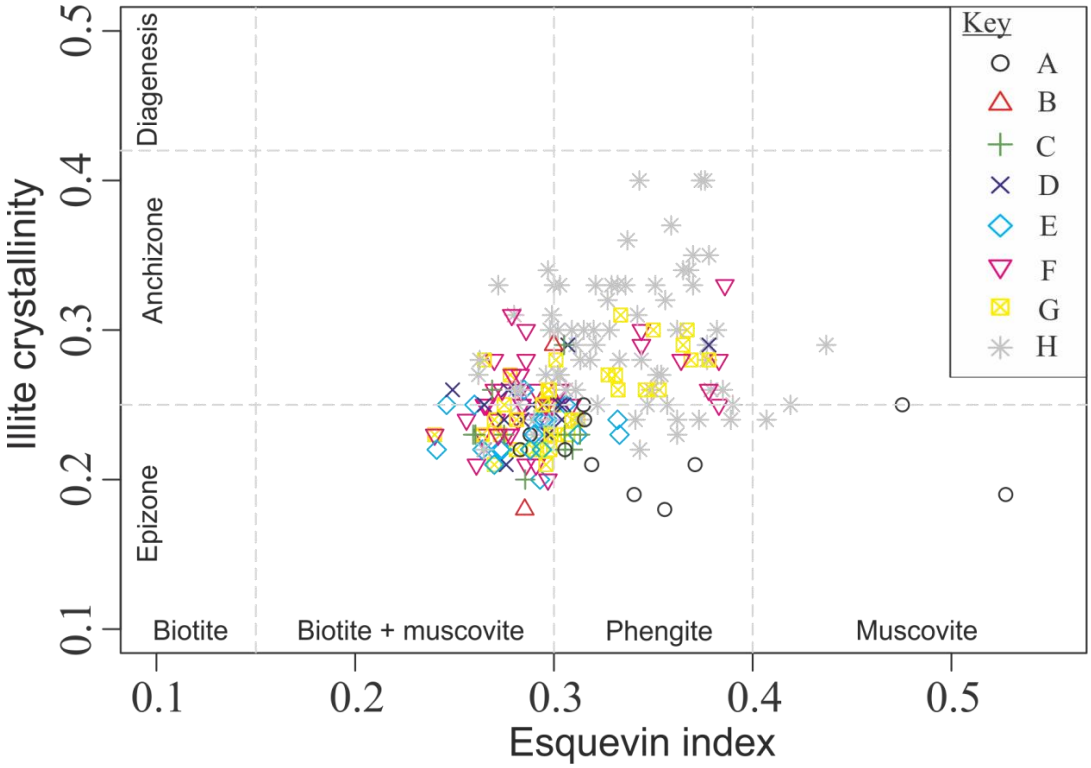

Figure 2-11 – Variation in Esquevin index and illite crystallinity as a function of estuarine-zone. Estuarine zones are labelled accordingly; A, lower-Irt; B lower-Mite; C lower-Esk; D, inner-Irt; E, inner-Mite; F, inner, Esk; G, central-basin; and H, outer-estuary.

Table 2.3 - Summary of the main characteristics of the eight defined estuary zones and their clay mineralogy attributes. Estuarine zones are labelled accordingly; A, lower-Irt; B lower-Mite; C lower-Esk; D, inner-Irt; E, inner-Mite; F, inner, Esk; G, central-basin; and H, outer-estuary.

Estuary zone	n	Mean grain size (mm)	Grain size sorting (σg)	Clay fraction (%)	Mean bioturbation (casts/m2)	Illite index	stdev	Chlorite index	stdev	Kaolinite index	stdev	Esquevin index (5Å/10Å)	stdev	Illite crystallinity (FWHM)	stdev
A	11	190	2.53	3.44	0.00	0.537	0.052	0.211	0.022	0.252	0.031	0.354	0.078	0.217	0.024
B	2	539	1.53	0.29	0.00	0.500	0.020	0.208	0.011	0.291	0.008	0.293	0.010	0.235	0.078
C	10	213	2.79	6.76	0.00	0.589	0.036	0.193	0.023	0.218	0.016	0.289	0.021	0.234	0.025
D	19	202	2.30	3.85	0.32	0.602	0.024	0.183	0.014	0.215	0.013	0.292	0.028	0.249	0.021
E	19	90	2.47	6.74	0.26	0.615	0.014	0.180	0.007	0.205	0.010	0.287	0.025	0.231	0.016
F	37	222	1.86	2.41	2.35	0.605	0.019	0.183	0.011	0.212	0.012	0.296	0.039	0.255	0.029
G	35	184	2.31	3.13	9.79	0.602	0.022	0.184	0.012	0.215	0.015	0.307	0.034	0.252	0.027
H	75	291	1.45	0.19	0.56	0.594	0.029	0.204	0.020	0.202	0.018	0.334	0.039	0.289	0.044
weighted average		228	1.96	2.50	2.32	0.596		0.192		0.212		0.313		0.261	

2.5.3 Mapped estuarine clay mineral distribution

The relative proportions of the three clay minerals, illite, chlorite and kaolinite, have been mapped out using ArcGIS to visualise their distribution patterns.

Chlorite relative abundance is heterogeneous and displays distinct patterns in the Ravenglass Estuary (Fig. 2.12). Chlorite abundance increases progressively toward the open-sea and is highest in backshore and northern-foreshore sediments (Fig. 2.12). In the inner Esk zone, there are subtle increases in relative chlorite abundance with proximity to the ebb-channel, and in tidal-dunes and tidal-bars (Fig. 2.12). The main ebb-channel, which splits the northern and southern foreshore deposits, is also defined by relative chlorite abundance (Fig. 2.12); there is distinctly more chlorite in the northern than the southern foreshore deposits.

Kaolinite relative abundance is highest in the central and inner estuary, and is depleted within foreshore sediment (Fig. 2.13). In the inner/central estuary, kaolinite relative abundance appears to be somewhat random (i.e., lacking organisation) (Fig. 2.13).

Illite relative abundance is heterogeneous and displays distinct patterns in the Ravenglass Estuary (Fig. 2.14). Relative illite abundance is highest at the margins of the inner and central estuary and in outer estuarine sediment positioned within/proximal to the ebb-channel (Fig. 2.14). Illite relative abundance is lowest in the tidal inlet, northern foreshore/backshore, and within tidal bars and tidal dunes (Fig. 2.14).

Illite crystallinity is heterogeneous and displays distinct patterns in the Ravenglass Estuary (Fig. 2.15). Illite is most crystalline (lowest illite crystallinity) in the inner and central estuary, towards the estuarine margins (Fig. 2.15). Illite crystallinity typically decreases (increased FWHM) toward the open-sea (Fig. 2.15).

Illite composition (derived from the Esquevin Index) is heterogeneous and displays distinct patterns in the Ravenglass Estuary (Fig. 2.16). Mapped Esquevin Indices show illite is relatively-Al rich (Fe-Mg depleted) toward the open sea. Relatively Fe-Mg-enriched illite is located in the inner and central estuary toward the estuarine margin (Fig. 2.16). In the inner estuary, tidal bars and tidal dunes can be differentiated based upon a decrease in both illite crystallinity and Fe-Mg content (Fig. 2.15 to 2.16).

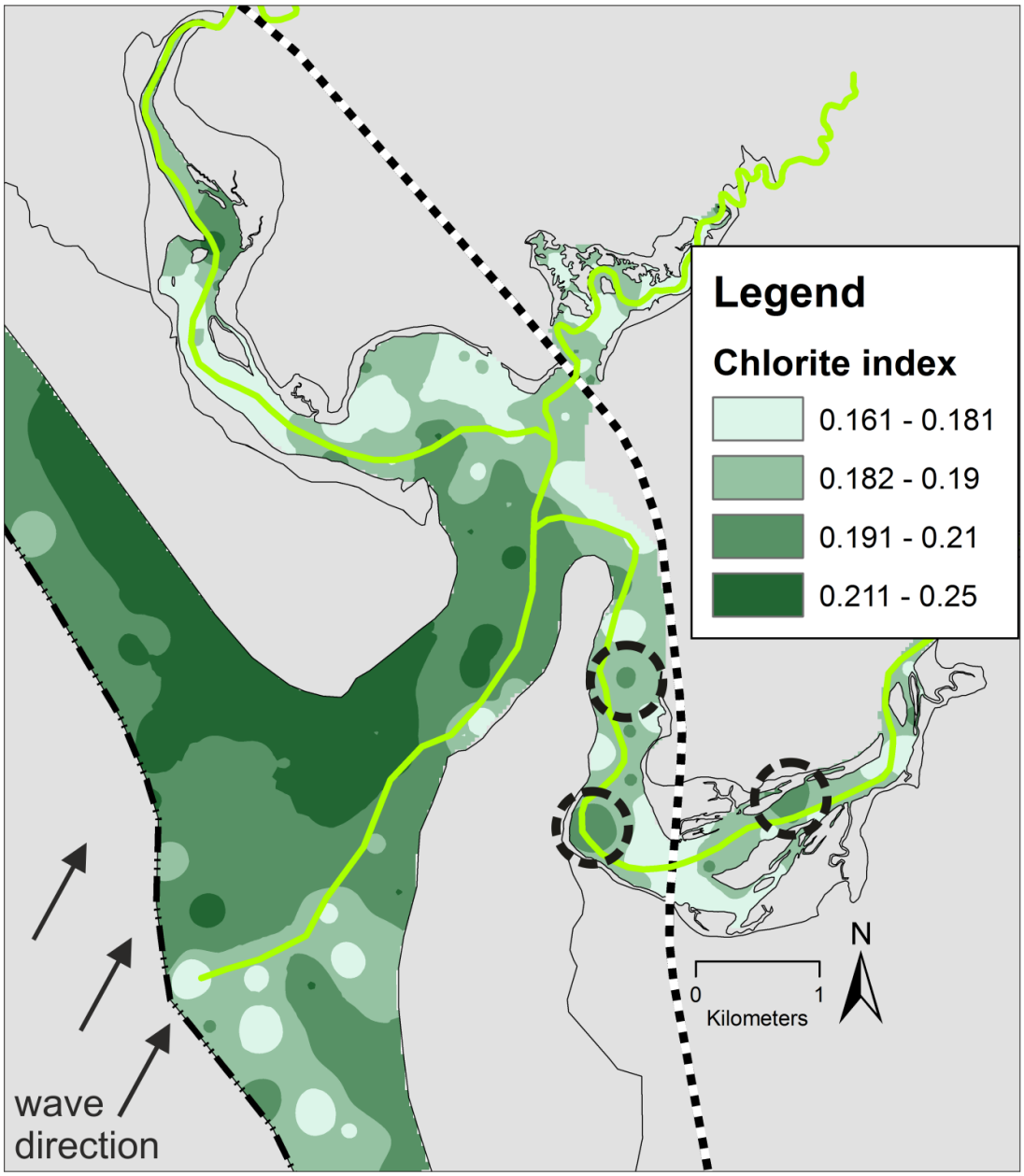

Figure 2-12 – Chlorite distribution within the Ravenglass Estuary. Black dashed-circles highlight relatively chlorite enriched tidal bars and dunes. Black arrows indicate the dominant wave-direction.

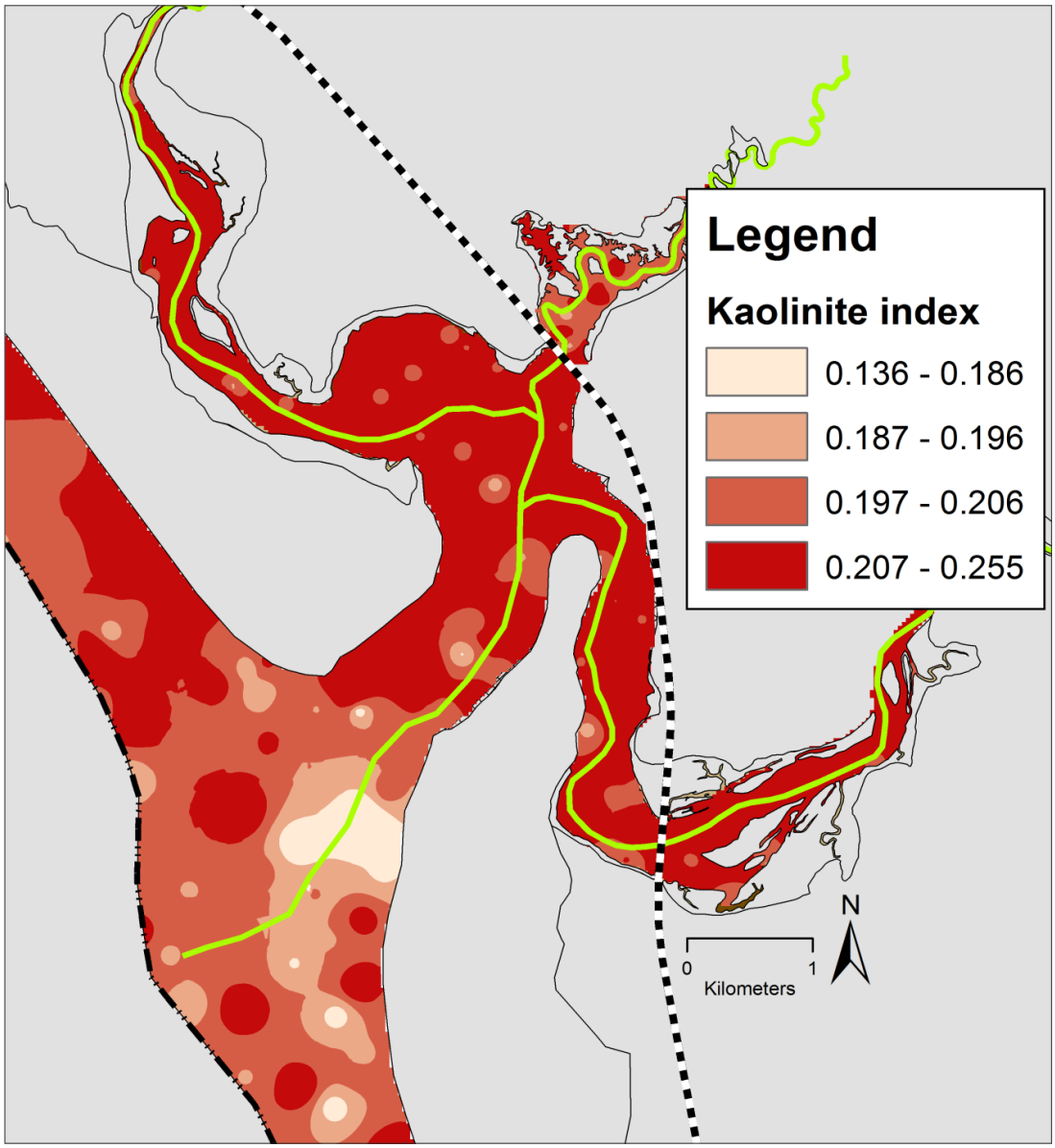

Figure 2-13 – Kaolinite distribution within the Ravenglass Estuary.

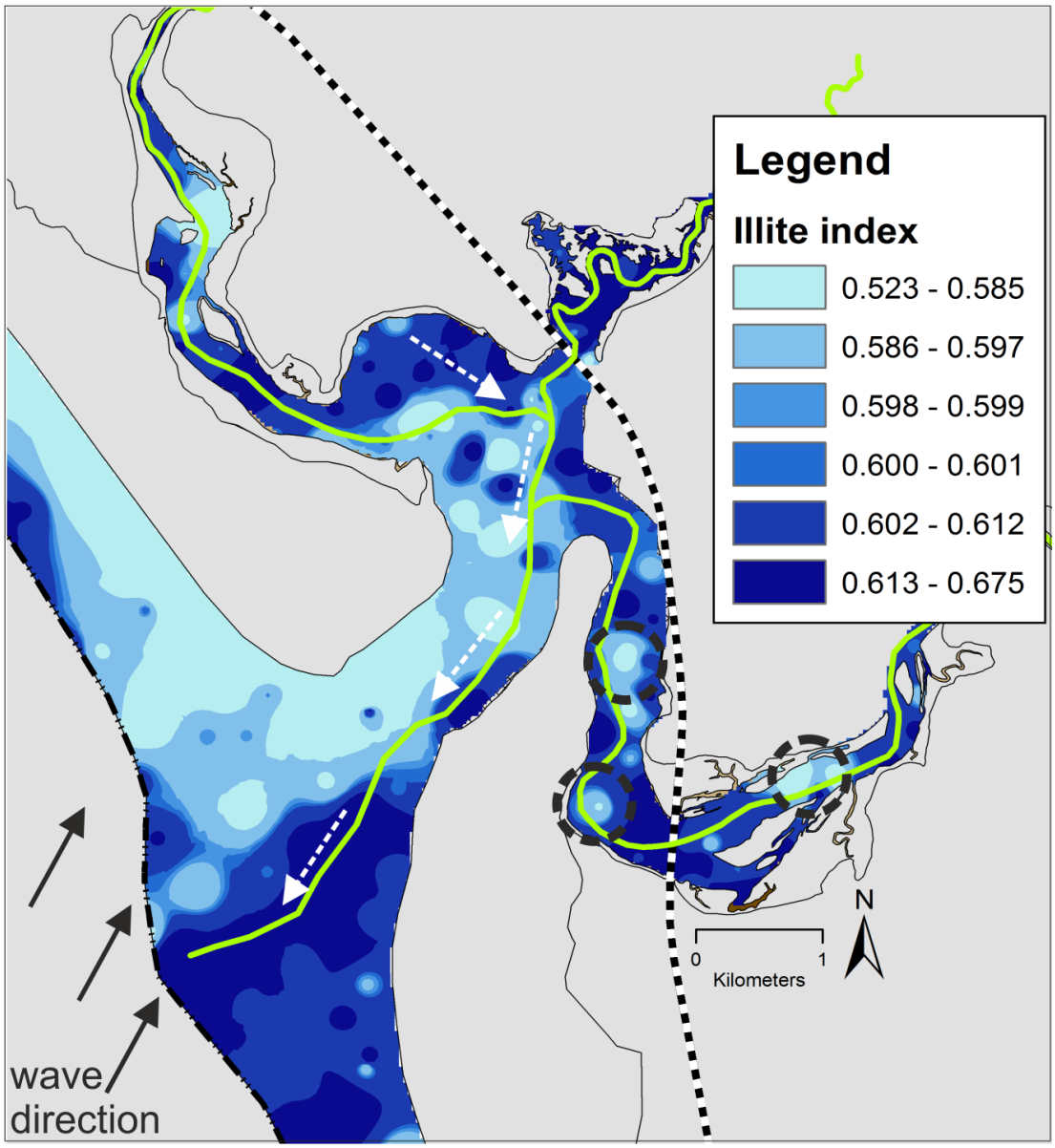

Figure 2-14 – Illite distribution within the Ravenglass Estuary. Black dashed-circles highlight relatively illite depleted tidal bars and dunes. Black arrows indicate the dominant wave-direction. Dashed white arrows highlight the potential importance of connectivity between the illite-enriched central basin and illite-enriched southern-foreshore.

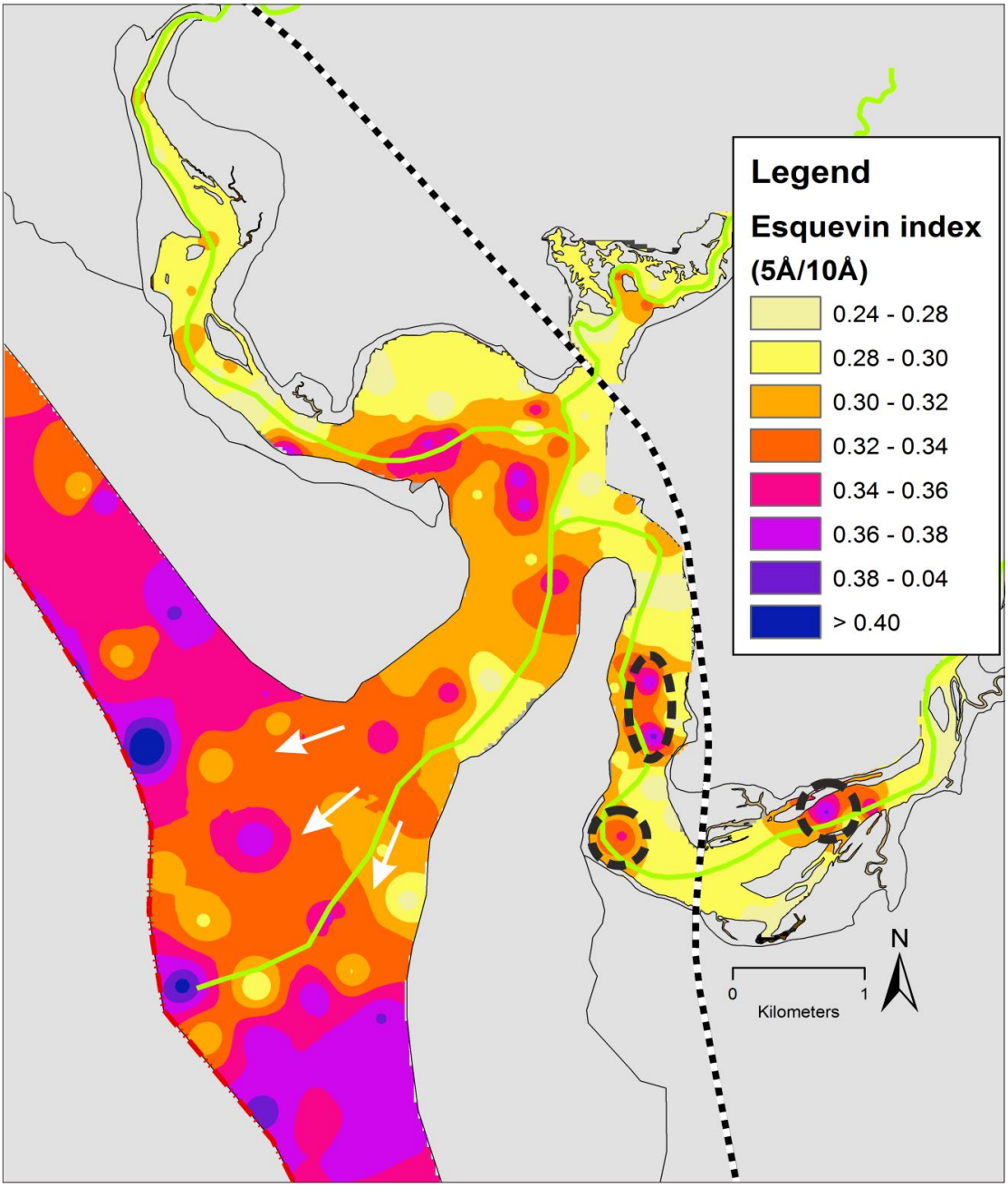

Figure 2-15 – Esquevin index distribution within the Ravenglass Estuary. Black dashed-circles highlight tidal bars and dunes enriched in Al-rich illite. White arrows depict the plume of relatively Fe-Mg enriched illite (inner and central estuarine derived) mixing with the relatively Al-enriched illite upon the foreshore.

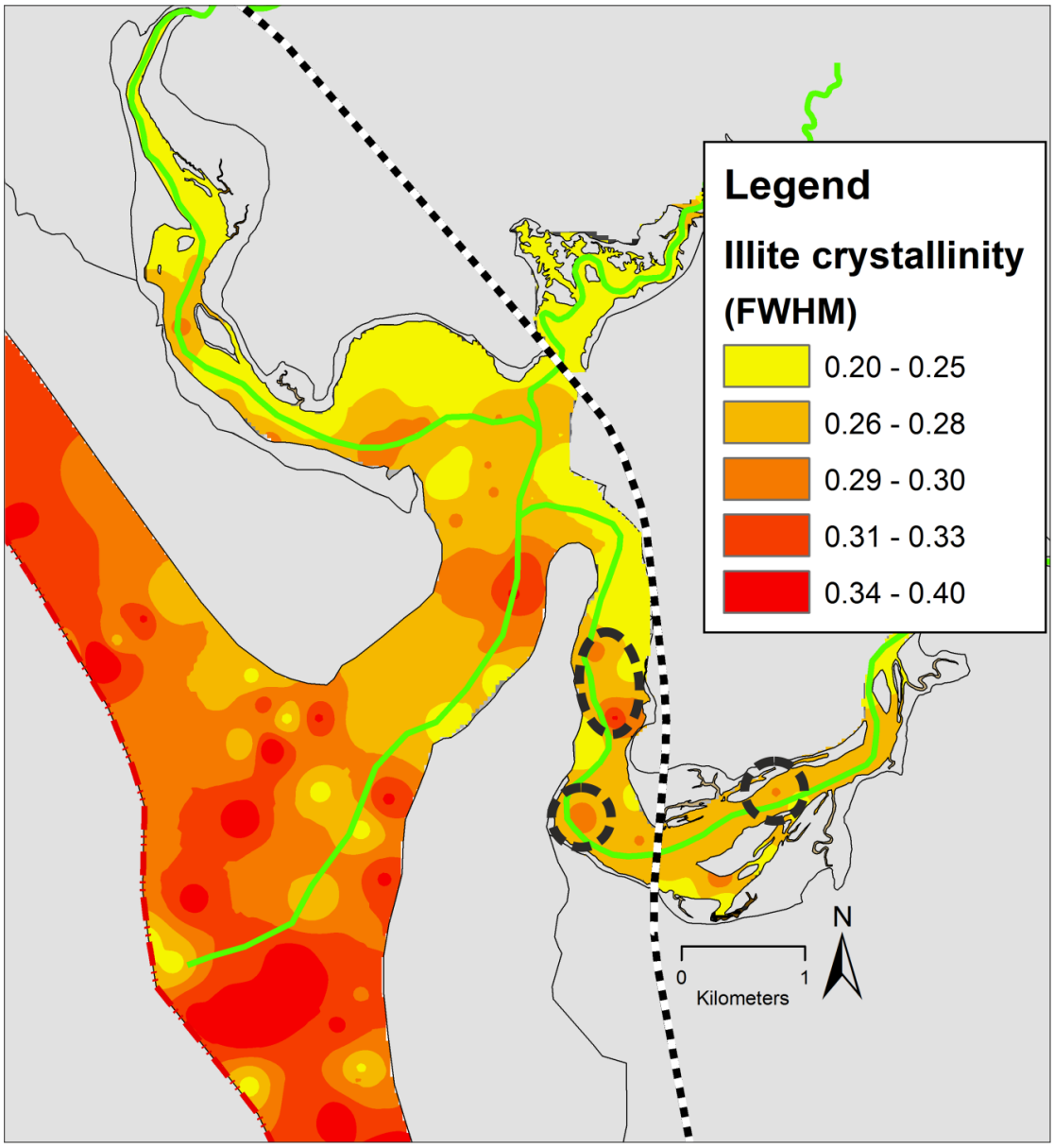

Figure 2-16 – Illite crystallinity distribution within the Ravenglass Estuary. Black dashed-circles highlight tidal bars and dunes enriched in poorly-crystalline illite.

2.5.4 Clay mineral abundance as a function of grain size fraction

A central estuary whole sediment sample, from the Saltcoats mixed-flat, was split into different grain size fractions in order to determine whether different clay minerals preferentially fall with different grades of sediment. Each size separate was analysed by X-ray diffraction analysis. The relative clay mineral proportions have been plotted versus grain size showing that kaolinite and illite abundances increase as grain size decreases, whereas chlorite abundance increases with increasing grain size (Fig. 2.17).

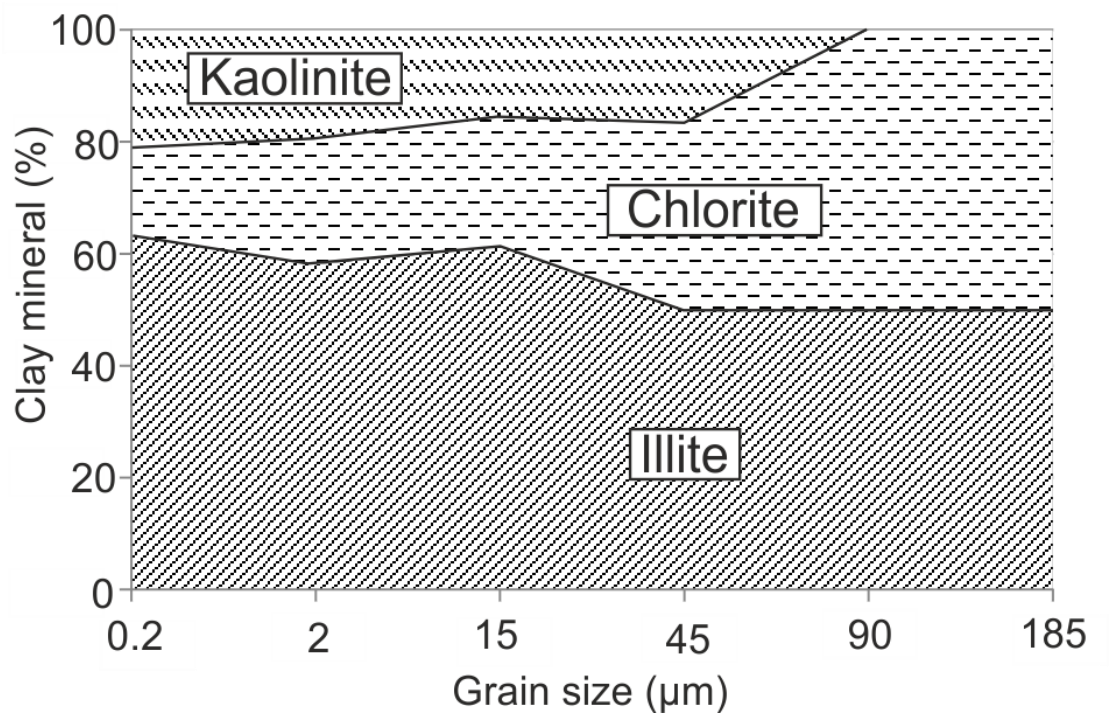

Figure 2-17 – Relative clay mineral abundance as a function of grain-size separates, extracted from a singular central-basin sediment sample.

2.5.5 Mineralogy of bedrock, drift and upper fluvial sediments

The lithology of the Triassic Sherwood Sandstone, the Palaeozoic Borrowdale Volcanic Group and the Palaeozoic Eskdale Granite has been summarised based on previously published studies (Merritt and Auton, 2000; Moseley, 1978; Quirke et al., 2015; Simpson, 1934; Stone and Merriman, 2004; Strong et al., 1994; Young et al., 1986) (Table 2.1). The mineralogy of samples of hinterland bedrocks and drift-deposits was determined using XRD to help understand the clay mineralogy of what is being fed into the estuary. The clay mineralogy and relative quantity of chlorite, kaolinite and illite was determined using the methods described providing. The Esquevin Index of illite could be determined for bedrock samples, but the illite crystallinity could not be determined due to the influence of crystal size of the white mica in rock which has a major influence on the FWHM measurement

(Krumm and Buggisch, 1991). The clay mineralogy of the bedrock and drift deposits is listed in Table 2.4. The mineralogy of upper fluvial sediments was determined by XRD analysis also to help understand the sediment supply budget. The relative abundances of chlorite, kaolinite and illite from four fluvial channel samples (Fig. 2.1) are listed in Table 2.4.

Table 2.4 - Chlorite, kaolinite and illite indices and the illite-Esquevin Index and illite crystallinity (FWHM) in upper-fluvial riverine sediment from the Ravenglass area and bedrock and drift clay mineralogy and Esquevin index data. All data generated within this study except the Esquevin index data from the Skiddaw Slate that is taken from Stone and Merriman (2004).

	Chlorite index	Kaolinite index	Illite index	Illite crystallinity	Esquevin index
River Irt-1	0.39	0.39	0.22	0.20	0.47
River Irt-2	0.24	0.30	0.45	0.19	0.38
River Esk-1	0.58	0.25	0.17	0.23	0.48
River Esk-2	0.57	0.17	0.27	0.26	0.48
Fishgarth Till	0.08	0.31	0.61	0.21	0.43
Ravenglass Till	0.17	0.21	0.62	0.24	0.28
St Bees sandstone	-	-	-	-	0.36
Eskdale granite-1	-	-	-	-	0.16
Eskdale granite-2	-	-	-	-	0.35
Skiddaw slate	-	-	-	-	0.40

2.5.6 Statistical analysis of estuarine clay mineral distribution patterns

Pearson's correlation coefficients have been calculated in order to determine whether there are any statistically significant relationships between the characteristics of estuary zones (e.g. grain size and sorting) and clay mineralogy for both individual estuarine zones and for the entire mapped estuary (Table 2.5). Analysis Of Variance (ANOVA) test results show that there is a statistically significant difference ($p < 0.05$) in relative clay mineral abundance (chlorite, illite and kaolinite) as well as Esquevin Index and illite crystallinity as a function of both estuarine zone, and depositional environment. The multi-comparison, post-hoc Tukey HSD test results show between which estuarine zones (Table 2.6) and depositional environments (Table 2.7) there are statistical differences ($p < 0.05$) in relative clay mineral abundances, Esquevin Index and illite crystallinity values; marginally significant (†, $p < 0.1$) values are also noted.

Table 2.5 - Pearson's correlation coefficient results showing the strength of the relationship between relative clay mineral abundance (chlorite, illite, kaolinite), Esquevin index and illite crystallinity (FWHM), in relation to mean grain size (MGS), grain size sorting (GSS), clay fraction abundance (CF), sand percentage (S), bioturbation intensity (Biot.) and elevation (Elev.). Levels of statistical significant are coded as follows; Marginally-significant (†) when p < 0.1, Significant (*) when p < 0.05, very-significant (**) when p< 0.01, extremely significant (***) when p < 0.001. Grey values representing no significant difference when p > 0.1.

River Irt (A), n = 11						
	MGS	GSS	CF	S	Biot.	Elev.
Chlorite	**0.60***	-0.41	-0.48	0.34	na.	na.
Illite	-0.48	0.28	0.49	-0.39	na.	na.
Kaolinite	0.37	-0.48	-0.48	0.29	na.	na.
FWHM	0.09	-0.08	-0.06	0.06	na.	na.
Esq.I	**0.78****	-0.48	**-0.53†**	0.50	na.	na.

River Esk (C), n = 10						
	MGS	GSS	CF	S	Biot.	Elev.
Chlorite	**0.76****	-0.31	-0.51	**0.58†**	na.	na.
Illite	**-0.63***	0.1	0.35	**-0.56†**	na.	na.
Kaolinite	0.31	0.23	-0.07	0.44	na.	na.
FWHM	0.50	**-0.66***	-0.23	0.41	na.	na.
Esq.I	-0.12	0.36	0.32	-0.04	na.	na.

Inner Irt (D), n = 19						
	MGS	GSS	CF	S	Biot.	Elev.
Chlorite	0.30	-0.22	**-0.44†**	0.22	-0.14	-0.37
Illite	**-0.56****	**0.40†**	**0.59****	**-0.46***	0.19	0.31
Kaolinite	**0.71*****	**-0.48***	**-0.61****	**0.60****	-0.21	-0.25
FWHM	0.36	-0.04	-0.12	0.20	0.01	-0.02
Esq.I	0.32	**-0.52***	-0.29	0.35	-0.25	-0.02

Inner Mite (E), n = 19						
	MGS	GSS	CF	S	Biot.	Elev.
Chlorite	0.04	-0.20	-0.24	0.35	0.36	0.13
Illite	0.07	0.11	0.20	-0.24	-0.34	-0.13
Kaolinite	-0.15	-0.01	-0.10	0.06	0.21	0.08
FWHM	0.11	0.03	-0.32	0.31	0.13	-0.17
Esq.I	-0.04	0.07	0.09	-0.06	0.08	0.30

Inner Esk (F), n = 37						
	MGS	GSS	CF	S	Biot.	Elev.
Chlorite	0.13	-0.12	-0.11	0.15	-0.22	-0.59
Illite	-0.26	0.27	**-0.43****	-0.22	**0.37***	0.26
Kaolinite	**0.29†**	**-0.31†**	**-0.42****	0.22	**-0.38***	-0.26
FWHM	0.17	**-0.50****	**-0.39***	0.17	-0.27	-0.02
Esq.I	0.23	**-0.42***	**-0.49****	**0.35***	-0.10	-0.23

Central basin (G), n = 35						
	MGS	GSS	CF	S	Biot.	Elev.
Chlorite	**0.32†**	-0.16	-0.17	-0.12	-0.11	-0.11
Illite	-0.14	0.06	0.25	0.29	0.25	**0.36†**
Kaolinite	-0.05	0.05	-0.24	**-0.35†**	-0.28	**-0.45***
FWHM	**0.55****	**0.44****	**-0.59*****	**0.33†**	0.11	**-0.47***
Esq.I	0.28	-0.20	**-0.48****	0.02	0.25	**-0.44***

Outer estuary (H), n = 75						
	MGS	GSS	CF	S	Biot.	Elev.
Chlorite	**0.67*****	**-0.30***	**-0.28***	0.08	**-0.29***	**0.49*****
Illite	**-0.56*****	0.11	0.16	-0.05	0.12	**-0.46*****
Kaolinite	0.15	0.15	0.06	0.00	0.12	0.17
FWHM	**-0.22†**	-0.09	0.04	0.04	-0.17	-0.11
Esq.I	-0.12	-0.21	-0.16	0.00	-0.05	**-0.22†**

Inner, central, outer , n = 185						
	MGS	GSS	CF	S	Biot.	Elev.
Chlorite	**0.52*****	**-0.35*****	**-0.39*****	**-0.16†**	**-0.14†**	0.07
Illite	**-0.43*****	**0.20***	**0.32*****	0.12	**0.14†**	-0.11
Kaolinite	0.04	0.11	-0.02	-0.11	-0.05	**0.13†**
FWHM	**0.30*****	**-0.42*****	**-0.47*****	**0.35*****	-0.07	**-0.32*****
Esq.I	**0.20*****	**-0.40*****	**-0.45*****	**0.30*****	0.03	**-0.36*****

Table 2.6 - Matrix comparing clay mineralogy data between the various estuarine zones from Ravenglass. Post-hoc Tukey's HSD test to determine whether there is a statistically-significant variation in clay mineral, Esquevin index, and illite-crystallinity between individual estuarine-zones. The estuarine zones are labelled accordingly; A, lower-Irt; B lower-Mite; C lower-Esk; D, inner-Irt; E, inner-Mite; F, inner, Esk; G, central-basin; and H, outer-estuary. Levels of statistical significant are coded as follows; Marginally-significant (†) when p < 0.1, Significant (*) when p < 0.05, very-significant (**) when p< 0.01, extremely significant (***) when p < 0.001. Grey values representing no significant difference when p > 0.1.

Chlorite Index

	A	B	C	D	E	F	G
A	X						
B	-0.00	X					
C	-0.01	-0.02	X				
D	**-0.03*** **	-0.03	-0.01	X			
E	**-0.03*** **	-0.03	-0.01	-0.00	X		
F	**-0.03*** **	-0.03	-0.01	-0.00	0.00	X	
G	**-0.03*** **	-0.02	-0.01	0.00	0.00	0.00	X
H	-0.03	-0.01	0.01	**0.02*** **	**0.02*** **	**0.02*** **	**0.20*** **

Kaolinite Index

	A	B	C	D	E	F	G
A	X						
B	**0.04***	X					
C	**-0.03*** **	**-0.07*** **	X				
D	**-0.04*** **	**-0.08*** **	0.00	X			
E	**-0.05*** **	**-0.09*** **	-0.01	-0.01	X		
F	**-0.04*** **	**-0.08*** **	-0.01	0.00	0.01	X	
G	**-0.04*** **	**-0.08*** **	0.00	0.00	0.01	0.00	X
H	**-0.05*** **	**-0.09*** **	**-0.02†**	**-0.01***	0.00	**-0.01***	**-0.01***

Illite Index

	A	B	C	D	E	F	G
A	X						
B	-0.04	X					
C	**0.05*** **	**0.09*** **	X				
D	**0.07*** **	**0.10*** **	0.01	X			
E	**0.08*** **	**0.12*** **	0.03	0.01	X		
F	**0.08*** **	**0.15*** **	0.02	0.00	-0.01	X	
G	**0.06*** **	**0.10*** **	0.013	-0.00	-0.01	-0.00	X
H	**0.06*** **	**0.09*** **	0.01	-0.01	**-0.02†**	-0.01	-0.01

Illite Crystallinity

	A	B	C	D	E	F	G
A	X						
B	0.02	X					
C	0.02	0.00	X				
D	0.03	0.01	0.02	X			
E	0.01	-0.01	0.00	-0.02	X		
F	**0.04***	0.02	0.02	0.01	0.02	X	
G	**0.03†**	0.02	0.02	0.00	0.02	0.00	X
H	**0.07*** **	0.05	**0.06*** **	**0.04*** **	**0.06*** **	**0.03*** **	**0.04*** **

Esquevin Index

	A	B	C	D	E	F	G
A	X						
B	0.02	X					
C	0.02	0.00	X				
D	0.03	0.01	0.02	X			
E	0.01	0.00	0.00	0.00	X		
F	**0.04*** **	0.02	0.02	0.01	0.02	X	
G	**0.03*** **	0.02	0.02	0.00	0.02	0.00	X
H	**0.07*** **	0.05	**0.06*** **	**0.04*** **	**0.06*** **	**0.03*** **	**0.04*** **

Table 2.7 - Matrix comparing clay mineralogy data between the various depositional environments from Ravenglass. Post-hoc Tukey's HSD test to determine whether there is a statistically-significant variation in clay mineral, Esquevin index, and illite-crystallinity between individual depositional environments. The depositional environments are labelled accordingly; De1, gravel-bed; De2, mud-flat; De3, mixed-flat; De4, sand-flat; De5, tidal bars and dunes; De6, tidal-inlet; De7, backshore; De8, foreshore; and De9, pro-ebb delta. Levels of statistical significant are coded as follows; Marginally-significant (†) when p < 0.1, Significant (*) when p < 0.05, very-significant (**) when p< 0.01, extremely significant (***) when p < 0.001. Grey values representing no significant difference when p > 0.1.

Chlorite index								
	De1	De2	De3	De4	De5	De6	De7	De8
De1	X							
De2	0.01	X						
De3	0.00	0.01	X					
De4	0.01	0.01	0.00	X				
De5	0.00	0.01	0.00	0.00	X			
De6	**0.02****	**0.02****	**0.02****	**0.01†**	**0.02†**	X		
De7	**0.05*****	**0.06*****	**0.05*****	**0.05*****	**0.05*****	**0.03****	X	
De8	**0.02*****	**0.02*****	**0.02*****	**0.02****	**0.02****	0.00	**-0.03*****	X
De9	0.00	0.01	0.00	0.00	0.00	-0.01	**-0.04*****	-0.01

Kaolinite index								
	De1	De2	De3	De4	De5	De6	De7	De8
De1	X							
De2	-0.01	X						
De3	0.00	0.00	X					
De4	0.00	0.01	0.00	X				
De5	0.01	0.01	0.01	0.01	X			
De6	-0.01	0.00	0.00	-0.01	-0.01	X		
De7	-0.01	-0.01	-0.01	-0.01	-0.01	0.00	X	
De8	-0.01	-0.01	**-0.01***	**-0.02****	**-0.02*****	-0.01	0.00	X
De9	-0.01	-0.01	-0.01	-0.01	**-0.02†**	-0.01	0.00	0.00

Illite index								
	De1	De2	De3	De4	De5	De6	De7	De8
De1	X							
De2	0.01	X						
De3	0.00	-0.01	X					
De4	-0.01	-0.01	-0.02	X				
De5	-0.01	-0.02	-0.01	0.00	X			
De6	-0.01	-0.02	-0.01	-0.01	0.00	X		
De7	**-0.04***	**-0.05****	**-0.04****	**-0.04†**	-0.03	-0.03	X	
De8	-0.01	-0.02	-0.01	0.00	0.00	0.01	**0.04†**	X
De9	-0.01	-0.02	0.01	0.01	0.02	0.02	**0.05****	0.01

Illite crystallinity								
	De1	De2	De3	De4	De5	De6	De7	De8
De1	X							
De2	-0.02	X						
De3	-0.01	0.01	X					
De4	0.01	0.03	0.02	X				
De5	0.02	**0.04†**	**0.03***	0.01	X			
De6	0.02	**0.04†**	**0.03†**	0.01	0.00	X		
De7	0.02	0.04	0.03	0.01	-0.00	-0.00	X	
De8	**0.05*****	**0.07*****	**0.06*****	**0.04*****	**0.03†**	0.03	0.03	X
De9	**0.047***	**0.06*****	**0.06*****	0.03	0.02	0.02	0.02	-0.01

Esquevin index								
	De1	De2	De3	De4	De5	De6	De7	De8
De1	X							
De2	0.00	X						
De3	0.01	0.01	X					
De4	0.03	0.03	0.01	X				
De5	**0.04†**	**0.04†**	0.03	0.01	X			
De6	0.04	0.03	0.02	0.01	-0.01	X		
De7	**0.07****	**0.07****	**0.06***	0.04	0.03	0.03	X	
De8	**0.07*****	**0.07*****	**0.05*****	**0.04*****	0.03	0.03	-0.04	X
De9	**0.06*****	**0.06****	**0.04*****	0.03	0.02	0.02	-0.01	-0.01

2.5.7 Summary of estuarine distribution patterns of clay minerals

For the first time, detailed maps of the distribution of clay minerals of an entire estuary (Figs. 2.12 to 2.16) have been produced. To the author's knowledge, similar high sample-density maps of clay mineral proportions have not been produced for any marine or non-marine modern sedimentary environment. An important output from this work is the observation that clay minerals within the Ravenglass Estuary are not uniformly distributed (Fig. 2.12 to 2.16).

Chlorite is typically most enriched in the coarsest grain fractions of the estuarine sediment (Fig. 2.12), whereas illite (Fig. 2.14) is most abundant in the finest grained fraction. These patterns are confirmed by Pearson's correlation coefficients (Table 2.5) and X-ray diffraction analysis on grain-size separates (Fig. 2.17).

By comparing the clay mineral maps (Fig. 2.12 to 2.16) with host sediment properties (Figs. 2.7 and 2.8) for the inner and central parts of the estuary, and reference to Tables 2.5 and 2.6, it is concluded that illite is most abundant toward the estuarine margins (mixed and mud-flats). In contrast, relatively high-energy, coarse-grained, and well-sorted, inner and central zone facies, i.e. tidal bars and dunes and channel axis, are relatively illite-depleted and relatively enriched in chlorite and kaolinite (Figs 2.12 and 2.13; Tables 2.5 and 2.6). As well as localisation of illite, kaolinite and chlorite as a function of position in the estuary, the types of illite (composition and crystallinity) reveal spatial patterns. The illite at the estuarine margins is predominantly well crystalline (low FWHM value) and Fe-Mg-rich (low Esquevin Index value). The illite in the relatively high-energy, coarse-grained, and well-sorted, inner and central zone facies are relatively enriched in structurally and chemical degraded forms of illite with high FWHM values and high Esquevin Index values (Fig. 2.14 to 2.16).

Outer estuarine sediment is relatively depleted in kaolinite (Fig. 2.13; Table 2.6). Outer estuarine sediment (backshore and upper foreshore) is relatively enriched in chlorite, north of the main channel outlet (Fig. 2.12). In contrast illite is most abundant in the outer estuary in the ebb channel outlet, and the area to the south of the ebb-channel (Fig. 2.14). Outer estuarine sediment contains illite that is relatively poorly-crystalline (high FWHM values) and Al-rich (high Esquevin Index values) (Figs. 2.15 to 2.16). However, there is a plume of relatively Fe-Mg-rich illite (low Esquevin Index values) that is associated with the mouth of the estuary (Fig. 2.15).

2.6 DISCUSSION: CONTROLS ON ESTUARINE CLAY MINERAL DISTRIBUTION

Clay minerals are not homogenously distributed in the Ravenglass Estuary (Fig. 2.12 to 2.16). In order to develop models that can be employed in schemes to help predict sandstone reservoir quality in ancient, deeply buried marginal marine sandstones, it is imperative to determine what has controlled the distribution of clay minerals in the Ravenglass Estuary.

2.6.1 Potential Sources of clay minerals in the Ravenglass Estuary

In order to explain the clay mineralogy of the estuary, it is necessary to consider the clay mineralogy of all potential sources. The suite of clay minerals fed into the Ravenglass Estuary may be derived from a combination of: (i) fluvial drainage of bedrock (Fig. 2.1A; Tables 2.1 and 2.4) (ii) fluvial drainage of Quaternary-drift deposits, including local erosion of Ravenglass Till within and on the margins of the estuary (Fig. 2.1B; Table 2.1), and (iii) marine inundation, with the landward-displacement of littoral-zone sediment.

The clay mineralogy of the upper-fluvial inputs (Table 2.4) is distinctly different to the average clay mineralogy of the estuary as shown by Tables 2.2 and 2.3. The sediment delivered by the River Irt, has relatively high kaolinite and chlorite indices and commensurately low illite index (Table 2.4). The River Irt's illite has high Esquevin Indices representing Fe-Mg-poor mica (Table 2.4). The sediment delivered by the River Esk is even more dominated by chlorite than the River Irt with a low illite index (Table 2.4). Like the River Irt, the River Esk's illite also has a high Esquevin Index (Table 2.4).

Ravenglass Till underlies and surrounds the Ravenglass Estuary (Table 2.1). The till is exposed in localised cliff-sections to the east of the northern part of the upper Esk Estuary (Fig. 2.1), just south of Ravenglass village. The glacial till is dominated by illite (illite index, 0.62) and the illite is both relatively Fe-Mg-rich (Esquevin index, 0.28), and well-crystalline (illite crystallinity, 0.24). The Ravenglass Till has a moderate abundance of kaolinite (kaolinite index, 0.21), and is relatively depleted in chlorite (chlorite index, 0.17).

Littoral-zone grab-samples from below the low water mark could not be collected on the advice of the Ministry of Defence, due to the high risk of unexploded ordinance, as the area has been a testing-ground for large calibre conventional weapons since 1903. However, many samples were collected from the littoral zone between high and low water marks in zone H (Figs. 2.1 and 2.3) with their clay mineral presented in Tables 2.2 and 2.3 and Figures 2.9 to 2.16. It will be subsequently demonstrated that the littoral zone is receiving an

amalgamation of sediment from the estuary, which is supplied by the glacial-till and fluvial discharge from the hinterland.

As established here (Tables 2.2 and 2.3; Figs. 2.9 to 2.16), the clay mineral distribution in the Ravenglass Estuary is heterogeneous. There are three possible influences on clay mineral type and distribution: supply types (provenance), hydrodynamics (transport and deposition) and early diagenesis (post depositional processes).

2.6.2 Provenance control on clay mineral distribution

The estuarine sediment has average illite, chlorite and kaolinite indices of about 0.60, 0.19 and 0.21, respectively, and average Esquevin and illite crystallinity indices of 0.31 and 0.26, respectively (Tables 2.2 and 2.3 and Figures 2.9 to 2.16). However, the variability of these values shows that it is possible that there have been different sources of clay minerals fed into different parts of the estuary.

An initial, simplistic view of sediment in the Ravenglass Estuary could be that the sediment was delivered directly from the mountainous area to the east of the coastline (the English Lake District) via the rivers Irt and Esk.

Upper-fluvial Esk sediment samples (Fig. 2.1) are strongly chlorite-enriched (Table 2.4) and the Upper-fluvial Irt samples are moderately-enriched in chlorite compared to the estuarine sediment (Tables 2.2 to 2.4). The Esk chlorite-enrichment probably reflects the widespread hydrothermal chloritization of biotite and hornblende in the Eskdale Granite (Table 2.1) (Moseley, 1978; Young et al., 1986). The Irt chlorite-enrichment probably reflects the widespread hydrothermal chloritization of biotite and hornblende in the Eskdale Granite, and/or pseudomorphs after pyroxene in the Borrowdale Volcanic Group (Table 2.1) (Quirke et al., 2015).

The upper- and lower-fluvial Irt samples (Fig. 2.1) are significantly enriched in kaolinite (Table 2.4). By analogy to the Esk sediment, it could be expected that the kaolinite was derived from the hinterland bedrock (Borrowdale Volcanic Group and Sherwood Sandstone; Table 2.1) although this is not reported to be enriched in kaolinite. Instead, the kaolinite may have been derived from locally kaolinite-enriched, glaciolacustrine sediment of the Gosforth Glaciogenic Formation (Fig. 2.1; Tables 2.1 and 2.4). Provenance has previously been reported to explain the enrichment of kaolinite in fluvial sediment landward of the Chesapeake Bay (Hathaway, 1972) due to the drainage of kaolinite-enriched Piedmont (Neiheisel and Weaver, 1967).

The upper-fluvial Esk and Irt samples are generally depleted in illite (Table 2.3) compared to the estuarine deposits (Tables 2.2 to 2.4; Fig. 2.10). In contrast to the sediment in the estuary (Tables 2.2 and 2.3), the illite present in the upper-fluvial Esk and Irt samples are relatively Al-rich with much higher Esquevin Indices (mostly greater than 0.40) than the estuarine sediment (Table 2.4). This probably reflects the relatively advanced stage of weathering of micas in the hinterland (Eskdale Granite, Sherwood Sandstone and Borrowdale Volcanic Group; Table 2.1) in contrast to the supply of micas into the estuary. A key point is that the estuarine sediment (Table 2.3) does not closely compare to the supply of sediment being delivered by the rivers (Tables 2.2 to 2.4, Figs. 2.8 to 2.11).

The presence of eroding low cliffs of the Quaternary Ravenglass Till that surround part of the estuary strongly suggests that some of the sediment in the estuary may be supplied by this till. The gravel beds exposed at the surface in the lower Esk estuary appear to be directly formed from the erosion of nearby pebble- and cobble-bearing Ravenglass Till. Glacial till is also exposed as knolls in all zones within the estuary. The relatively well-crystalline and Fe-Mg-rich illite in the Ravenglass Estuary is typical of glacial deposits (such as the Ravenglass Till), which are formed under cold-climatic conditions that result in mechanical weathering that allows the mica (illite) to retain its original high degree of crystallinity and Fe-Mg-rich composition (Chamley, 1989). There is a similarity between the illite-dominated clay mineral assemblage, illite chemistry and illite crystallinity of the Ravenglass Till and the Ravenglass Estuary sediment (Tables 2.1 to 2.4; Figs. 2.8 to 2.11). However, it is likely that there are multiple sources of illite in the drainage basin (Table 2.1) and in the Ravenglass Estuary, given the range in Esquevin Indices (Fig. 2.11) and the range of chlorite enrichments found within the estuary (Fig. 2.12). It thus seems likely that any fluvial supply of sediment, with high Esquevin Indices and relatively enriched in chlorite (Table 2.4), is being heavily diluted by a second sediment source with a distinct clay mineral suite, such as from the eroding Ravenglass Till exposed within, and at the margins of, the Ravenglass Estuary.

2.6.3 Hydrodynamic control on clay mineral distribution

As well as there being several possible sources of the clay minerals in the Ravenglass Estuary, it is also possible that estuarine hydrodynamics has influenced the distribution of clay minerals.

The pair of barrier spits have resulted in the Ravenglass Estuary having the morphological characteristics of a wave-dominated estuary (Dalrymple et al., 1992). Such estuaries usually have high energy outer regions and inner regions that are wave and river dominated

respectively, and a low energy central region. It is likely that typical wave-dominated estuaries will have coarse-grained outer and inner regions separated by a low energy central region. The Ravenglass Estuary, however, does not display a well-defined tripartite zonation (outer, central and inner) in grain size (Figs. 2.7A and 2.8A) or clay fraction (Fig. 2.7C and 2.8E), as typically-observed in end-member wave-dominated estuaries (Dalrymple et al., 1992). It is likely that a combination of the following factors have led to the boundaries between the central and inner estuarine zones of the Ravenglass Estuary being blurred; i) strong tidal currents pass beyond the low-energy, central basin into the inner parts of the estuary producing extensive tidal bars and tidal dune complexes, and ii) the Ravenglass Estuary is in the later stages of filling (as shown by the presence of the pro-ebb delta) which has been reported to reduce the significance of the energy-minimum in the central part of an estuary (Posamentier and Walker, 2006). Additionally, forced regression, with a gradual relative sea level fall following a minor high-stand (1 m OD) at approximately 6,000 years BP (mid-Holocene) (Lloyd et al., 2013), is reported to have caused the coarsening-upward of central basin tidal flats (Daneshvar and Worden, 2017), further reducing the dissimilarity between the estuarine zones.

Within individual estuarine zones, the relative abundance of chlorite, the dominant illite type (Al-rich vs. Fe-Mg rich), and dominant illite crystallinity (low to high illite crystallinity) appear to be controlled by estuarine-hydrodynamics. In the lower-energy parts at the margins of the inner estuary and central basin, the finest deposits are dominated by the mineral characteristics of the Ravenglass Till (illite-dominated, and relatively Fe-Mg-rich and well-crystalline illite that has low Esquevin and FWHM indices). In contrast, in the higher energy sites, i.e. tidal bars and dunes and channel axis, the coarsest inner and central zone sediment are relatively enriched in chlorite and illite that was derived from the fluvial supply of sediment from the hinterland (chemically-degraded forms of illite with high Esquevin Indices). Within higher-energy, outer estuarine sediment, relative chlorite abundance increases with an increase in grain size ($r = 0.67$) and elevation ($r = 0.49$); this is interpreted to reflect the dominant wave-direction originating from the south-west (Fig. 2.12; Table 2.5). Note that chlorite is most abundant in the coarsest grained sediment fractions (Fig. 17) explaining the strong grain size control on chlorite abundance, at least in the outer estuary zone. Also in the outer estuary, illite is most abundant toward the ebb-channel (Fig. 2.14); this is interpreted to reflect the hydrodynamic connectivity between the southern foreshore, and the illite-enriched central basin. Evidence for this connection comes from: (a) a distinct increase in relative illite abundance upon the southern-foreshore, at the mouth of the ebb-channel (Fig. 2.14), and (b) an enrichment of relatively Fe-Mg-rich illite (low Esquevin

Index) at the mouth of the tidal-inlet, interpreted to be sourced from the Fe-Mg rich illite-dominated inner and central estuarine zone sediments (Fig. 2.16).

Kaolinite is abundant in fluvial sediments (Fig. 2.10; Table 2.4), probably reflecting the drainage of kaolinite-enriched source sediment (specifically the Gosforth Glaciogenic Formation). However, the controls on the distribution of kaolinite at the fluvial-marine interface, and within estuarine sediments of the Ravenglass Estuary are less clear. Three mechanisms have been invoked to explain the distribution of kaolinite in marginal-marine systems: i) kaolinite flocculates at low salinity (Whitehouse et al., 1960); thus sediment at the fluvial-marine interface is likely to be relatively enriched in kaolinite, ii) Edzwald and O'Mella (1975) suggested that illite remains suspended longer than kaolinite (slower aggregation rate), and is thus deposited downstream relative to kaolinite, and iii) kaolinite-enriched fluvial sediment is diluted by an additional source of less kaolinite-rich sediment within the estuary (Feuillet and Fleischer, 1980).

Although there appears to be a slight increase in the relative concentration of kaolinite in the inner and central estuarine zone, there is no evidence for kaolinite enrichment at the head of the estuary. This suggests that clay mineral distribution cannot be explained by differential flocculation or clay mineral stability. Instead, the reduction in kaolinite abundance, as well as chlorite abundance, is probably due to the dilution of the estuarine clay-mineral assemblage by the local erosion of Ravenglass Till.

Both the distribution of clay minerals and depositional environments are strongly controlled by estuarine hydrodynamics. However, a key finding of this study, is that clay mineral distribution patterns are heterogeneous even within a single depositional environment e.g. foreshore deposits (Figs. 2.12 to 2.16); consequently, there is little statistical difference in the relative abundance of specific clay minerals, between different depositional environments (Table 2.7). Thus, the relative abundance of clay minerals (illite, kaolinite and chlorite) are only partly explained by an understanding of depositional environment, and instead knowledge of local specific conditions (e.g. wave-direction) is required.

2.6.4 Early diagenetic control on clay mineral distribution

Sedimentary systems are geochemically active with the possibility of the continuation of weathering that commenced in soils (e.g. feldspar alteration, Fe-Mg-mineral alteration, dissolution) into the realm of sediment accumulation. It is also possible that sites of sediment transport and deposition involve totally new geochemical conditions that lead to a new suite of mineral reactions. Marginal marine settings are especially significant since they involve terrigenous sediment and low salinity, relatively organic- and iron-rich continental waters

meeting marine conditions with their high salinity, high sulphate and locally low oxidation state, low pCO2 waters (Berner and Berner, 2012; Boyle et al., 1974; Boyle et al., 1977; Sholkovitz, 1978; Sholkovitz et al., 1978). Significant diagenetic reactions involving clay synthesis, Fe-reduction and even silica precipitation have been described in marginal marine sediments (Aller and Michalopoulos, 1999; Michalopoulos and Aller, 1995; Michalopoulos and Aller, 2004; Michalopoulos et al., 2000). Some have described physico-chemical processes of mineral alteration in marginal marine settings (Griffin and Ingram, 1955; Grim and Johns, 1954; Nelson, 1960; Powers, 1957). Others have invoked a significant role for macrobenthos in sediment mineral reactions, such as during sediment bioturbation (ingestion and excretion) by the common lugworm (*Arenicola marina*)*;* reported to lead to the formation of new-clay minerals (McIlroy et al., 2003; Needham et al., 2006; Needham et al., 2004; Needham et al., 2005; Worden et al., 2006). In contrast, other studies have suggested that clay minerals undergo negligible transformation in sedimentary environments (Carroll and Starkey, 1958; Chamley, 1989; Rateev et al., 2008).

Based on high-resolution QEMSCAN (SEM-EDS imaging) evidence of a small number of samples from two 1 m cores from the Ravenglass Estuary, Daneshvar and Worden (2017) suggested that detrital K-feldspar grains are preferentially rimmed by neoformed illite, while plagioclase grains may be preferentially rimmed by neoformed kaolinite. It is possible that these host-specific clay mineral rims are the result of continued alteration of the recent sediment with K-feldspar altering to K-rich illite with K-free plagioclase altering to K-free kaolinite. However, it has also been reported that these clay minerals have formed due to intense alteration of feldspars in the hinterland of the Ravenglass Estuary (Moseley, 1978; Quirke et al., 2015; Young et al., 1986) (Table 2.1). It is conceivable that the relationship between feldspars and clay-minerals within the estuary may, alternatively, be due to the transportation and deposition of kaolinized-plagioclase, and illitized-K-feldspars from the hinterland and are thus an inherited feature of the sediment.

In this study the distribution of lugworms have been mapped by counting faecal casts/m^2 (Fig. 2.7D) to test whether lugworm bioturbation may explain clay mineral abundance, as documented in laboratory studies (McIlroy et al., 2003; Needham et al., 2004; Worden et al., 2006). However, there appears to be no spatial relationship between the distribution of the clay minerals and the distribution of lugworms (compare Fig. 2.7D to Fig. 2.11). The statistical analysis of the covariance between lugworm distribution and clay minerals confirms that there is no correlation in the Ravenglass Estuary (Table 2.6). The case for an early diagenetic control on clay mineral distribution patterns (Fig. 2.11) remains unproven with local provenance and hydrodynamic controls potentially sufficient to explain clay distribution patterns.

2.7 SIGNIFICANCE: RESERVOIR QUALITY PREDICTION

Chlorite is relatively enriched in the sediment in both hinterlands; the sediment in the Esk hinterland is dominated by chlorite (Table 2.4). The estuary itself is dominated by illite with subordinate chlorite since local, transient drift deposits, following Holocene glaciations, seem to be locally dominating (diluting) the fluvial-supply of clay minerals. The Holocene drift deposits are actively eroding and will, presumably, be wholly eroded away or blanketed by newly eroded material from the hinterland. Once the influence of the Holocene drift deposits has been lost, the estuary sediment will presumably revert to a more chlorite-rich composition as is currently found in the estuary hinterlands (Table 2.4).

Despite the masking effects of the erosion of Holocene drift it is apparent that chlorite is locally most enriched in the coarsest grain fraction (in whole sediment, Fig. 2.17) and most enriched in estuary zones with the coarsest mean grain size (Fig. 2.12, Table 2.5). Chlorite being present in the coarsest grained sediment suggests that it must be predominantly detrital in origin. The hinterland supplies of chlorite originally come from secondary alteration of altered Fe-Mg minerals such as hornblende, ilmenite and biotite in the Borrowdale Volcanic Group and the Eskdale Granite (Table 2.1). These patterns show that detrital chlorite from the volcanic and igneous rocks are preferentially found in the coarsest grained sands in this marginal marine setting. Hydrodynamic processes in the Ravenglass Estuary have locally concentrated chlorite into the depositional environments with the coarsest sediment so that there is not a simple change of concentration of chlorite traversing from the upper estuary zones (A, B, C) to the inner estuary zones (D, E, F), then into the central estuary zone (G) and finally the outer estuary zone (H). Localised depositional environments, such as bars, sand flats, mud flats, etc., need to be accounted for in any attempt to understand and predict chlorite distribution. Statistical analysis (Table 2.7), and clay mineral maps (Figs. 2.12 to 2.16) show clay mineral distribution patterns are only partly explained by an understanding of depositional environment. For example, within a given zone, such as the outer estuary, chlorite has been locally concentrated by wave energy, dominated by the prevailing SW wind, onto the northern part of the foreshore (Fig. 2.12).

A generalised model of estuarine clay mineral distribution is provided in Figure 2.18. It is important to note, that local-specific conditions (e.g. wave-direction, tidal-range) exert a strong control on clay-mineral distribution patterns in the Ravenglass Estuary; consequently, it is essential that in order to accurately predict clay mineral distribution in the subsurface, local-specific conditions are accounted for. This model should be used carefully, in unison with clay minerals maps (Figures 2.12 to 2.16) and clay-mineral-host-sediment relationships (Table 2.5). Ultimately, to predict the relative distribution of clay minerals, it is advantages

to understand the primary sediment supply by rivers, secondary input from drift deposits, the distribution of depositional environments, and localised hydrodynamic conditions driven by tidal currents and onshore, wind-driven wave energy.

In addition, on a sequence-stratigraphic scale, the current concentration of chlorite is depressed by the transient supply of chlorite-poor sediment from eroding drift deposits but the hydrodynamic processes that have relatively concentrated chlorite will still function once the effect of the drift has been removed. It is thus suggested that the relative values of the chlorite index (Fig. 2.12) will at least double, or maybe even treble, when the dominant sediment supply is, once again, fluvial (e.g. approaching 0.6 as shown in Table 2.4).

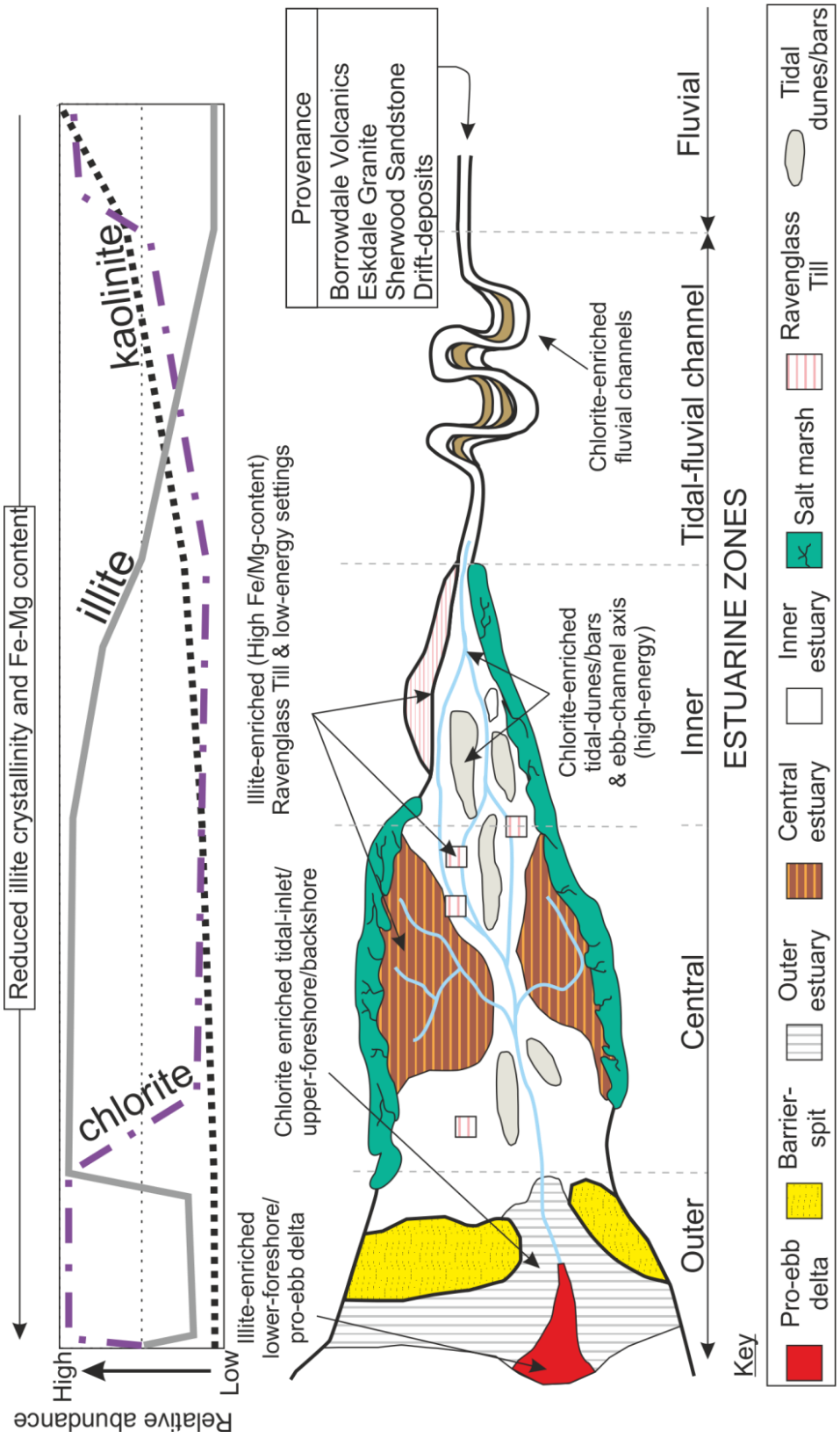

Figure 2-18 – Generalised model depicting the major clay mineral distribution trends observed within the Ravenglass Estuary. Note, in order to make accurate predictions in the subsurface, it is necessary to take into account local specific conditions.

2.8 CONCLUSIONS

1. The Ravenglass Estuary in NW England contains a range of sedimentary environments from mud-flats, to mixed-flats, and sand-flats, to tidal bars and dunes, tidal inlets, gravel beds, backshore and foreshore deposits and a small pro-ebb delta.
2. The Ravenglass sedimentary deposits can be subdivide into fluvial, inner-estuary, central-estuary and outer-estuary zones that merge into littoral sediments. The estuary is fed by two main rivers that drain distinctive hinterland lithologies containing granite (southern Esk arm) and andesite and redbed sandstones (northern Irt arm). Transient Holocene glacial till deposits surround parts of the estuary and occur as a natural clay-rich floor upon which the post-Holocene estuarine succession was deposited.
3. The clay mineralogy of the present day estuary sediment surface has been strongly affected by input from the illite-dominated Holocene glacial till deposits but there are strong heterogeneities in the distribution of the clay minerals.
4. Chlorite is most enriched in the coarsest grain fractions of the estuarine sediment, with kaolinite and illite most enriched in the finest grained fractions.
5. Chlorite is most concentrated in the higher energy sites, i.e. tidal bars and dunes and channel axis; the coarsest inner and central zone sediment are relatively enriched in chlorite and illite that was derived from the fluvial supply of sediment from the hinterland (chemically-degraded forms of illite).
6. The outer estuary is coarse-grain dominated and hosts the greatest abundance of chlorite within the estuarine environment. Chlorite abundance increases with increasing grain size in higher-energy, outer estuarine sediments to the north of the littoral zone, reflecting the dominant wave-direction originating from the south-west since chlorite is most abundant in the coarsest grained sediment fractions.
7. Illite is most abundant toward the ebb-channel in the outer estuarine sediments reflecting the hydrodynamic connection between the southern foreshore, and the central basin. Kaolinite is relatively uniformly distributed in the inner estuary and central basin sediment, whilst outer estuarine sediment is slightly depleted in kaolinite abundance.
8. Sediment supply has played a major role in controlling clay mineralogy in the Ravenglass Estuary although the supply has been dominated by the eroding glacial till around the estuary rather than the chlorite-dominated sediment supply deriving from the hinterland via the river.

9. Despite the difference in sediment supply from the two main rivers feeding the estuary, the inner estuary zones are not diagnostic of the rivers due to hydrodynamic mixing and sorting processes redistributing the sediment.
10. Clay mineral distribution patterns cannot be explained by depositional environment alone. Instead, the relative abundance of specific clay minerals, can be predicted (models should be tailored to an individual marginal marine system), if there is knowledge of the primary sediment supply by rivers, secondary input from drift deposits (if present), the distribution of depositional environments, and localised hydrodynamic conditions driven by tidal currents and onshore, wind-driven wave energy.

3. CLAY COATS, CLAY MINERALS, PYRITE AND ESTUARINE FACIES: MODERN SHALLOW-CORE ANALOGUE FOR ANCIENT DEEPLY-BURIED SANDSTONES

3.1 ABSTRACT

The spatial distribution of clay minerals and clay coated sand grains in ancient and deeply buried petroleum reservoirs, which may enhance or degrade reservoir quality, is poorly-understood. A modern-analogue study (Ravenglass Estuary, UK), integrating lithofacies, clay coat, clay mineral and Fe-sulphide distribution patterns, is here presented to better predict clay coat and clay mineral distribution patterns in petroleum reservoirs. X-ray diffraction determined mineralogy (clay mineralogy and Fe-sulphides) and the extent of detrital clay-coat coverage of sediment in twenty-three one-metre cores was established, at an unprecedented high-resolution. Results of this study show clay mineral distribution patterns are primarily controlled by the physical sorting of clay minerals by grain size. Chlorite is most abundant in coarser-grained sediment (e.g. outer estuary and inner estuary tidal-bars and low-amplitude dunes), whereas illite is most abundant in finer-grained sub-environments (e.g. mud-flats). Kaolinite abundance is relatively homogenous, whereas smectite abundance is negligible in estuarine sediments. Optimum clay coat coverage, which would preserve anomalously high-porosity in deeply-buried sandstone reservoirs, is likely to occur in mixed-flats and low-amplitude dunes in the inner-estuary and central basin. Furthermore, oxidation of sediment, through bioturbation in mixed-flats and low-amplitude dunes, has reduced the growth of Fe-sulphides (e.g. pyrite), which would otherwise sequester iron. As a result, iron remains available for the formation of authigenic Fe-bearing clay minerals, such as chlorite, from precursor clay minerals which may not contain a source of iron, such as kaolinite. This study shows clay mineral and clay coat distribution patterns are controlled by processes active during deposition and bio-sediment interaction in the top few millimetres in the primary deposition environment. In the Ravenglass Estuary, clay mineral and clay coat distribution patterns are not over-printed by the post-depositional processes of sediment bioturbation or mechanical infiltration.

3.2 INTRODUCTION

Clay minerals can significantly impact the petrophysical properties (e.g. porosity, permeability and water saturation) of sandstone reservoirs. For example, pore-filling quartz cement in deeply-buried sandstones (> 80 to 100 °C), can be inhibited by diagenetic chlorite

clay-coats (Ehrenberg, 1993; Skarpeid et al., 2017; Stricker et al., 2016), while some clay minerals (e.g. illite) can plug pore-throats and promote chemical compaction (Worden and Morad, 2003). Diagenetic clay coats in sandstones have been reported to originate from i) the thermally-driven recrystallization of low-temperature, precursor (prior to burial) detrital clay coats, and ii) through *in situ* growth from the authigenic alteration of precursor and early-diagenetic minerals, which interact with pore fluids during burial (Ajdukiewicz and Larese, 2012; Worden and Morad, 2003). The grain coat coverage (i.e. fraction of the sand grain-surface covered by clay minerals), as well as the mineralogy of the clay coat, have been reported to be the dominant controls on the ability of grain coats to inhibit quartz cementation (Ajdukiewicz and Larese, 2012; Billault et al., 2003; Lander et al., 2008). The availability of iron is essential to the creation of porosity-preserving Fe-bearing chlorite during burial-diagenesis. In sediment, if iron is locked up as either pyrite or siderite, then it will be forever unavailable to create chlorite. Pyrite and siderite grow much more quickly than the Fe-silicate clay minerals (such as chlorite) so that, if there is competition at any one time, then pyrite or siderite will preferentially grow at the expense of chlorite (Worden and Morad, 2003).

Clay minerals (including the mineralogy of clay coats) in sandstones are probably not a result of the mass influx of materials into sandstones during burial diagenesis, since many of the main components of clay minerals (for chlorite: Fe-, Mg- Al- and Si-oxides) are effectively water-insoluble, even during the long time-scale over which burial diagenesis occurs (Worden and Morad, 2003). As a result, it has been concluded that the clay mineralogy present in sandstones (both pore-filling and grain-coating) is controlled by the primary depositional composition, i.e. the mineralogy of precursor components in the initial sediment (Worden and Morad, 2003).

The fundamental motivation for this study was to establish how clay coats and clay minerals (chlorite, illite, kaolinite and smectite) are distributed in the near-surface (one metre cores; n = 23) of a modern estuarine setting (Ravenglass Estuary, UK; Fig. 3.1), on a similar scale to many oil and gas fields. This study provides the first integrated near-surface study, which compares the relationship between clay minerals, clay coats, Fe-sulphides and lithofacies in marginal-marine sediments, and may be used by analogy, to better predict reservoir quality.

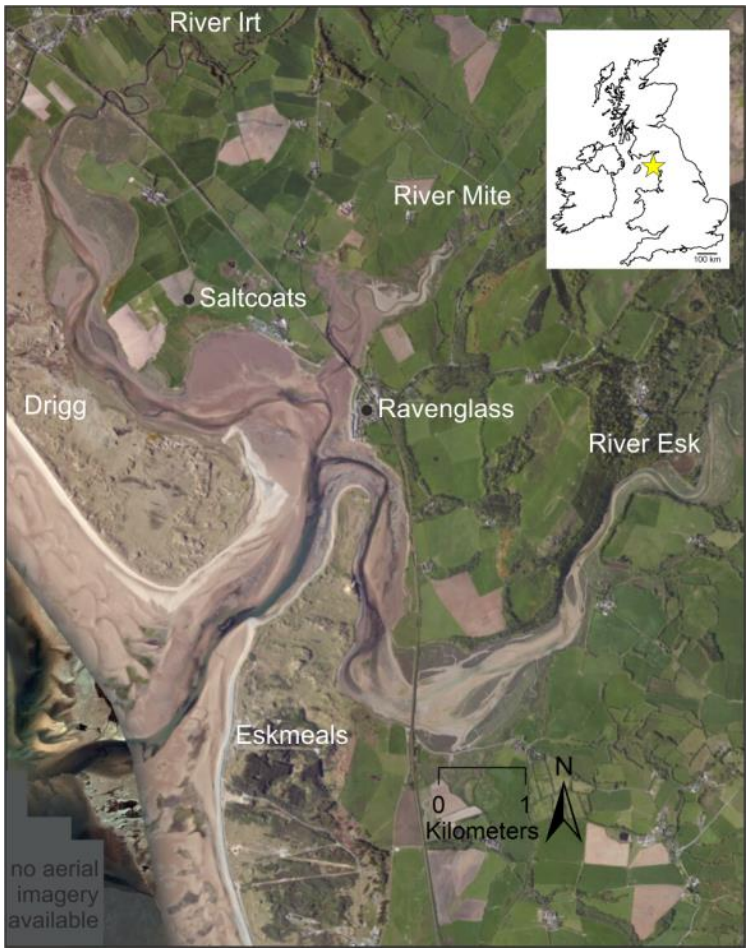

Figure 3-1 - Aerial image of the Ravenglass Estuary, UK.

It has been reported that clay coat distribution patterns in surface sediment (< 2 cm) of the Ravenglass Estuary are controlled by the physical attachment of clay size material to sand grain surfaces by adhesive extracellular polymeric substances (biofilms) excreted by diatoms during locomotion (Wooldridge et al., 2017a). Experiments showed that detrital clay coats may develop through the direct ingestion and excretion of sediment by *Arenicola marina* (lugworms), by creating a sticky mucus membrane that adheres fine-grained sediment to the surface of sand grains (Needham et al., 2005; Worden et al., 2006). In contrast, Wooldridge et al. (2017b) showed that, in the Ravenglass Estuary, there is no spatial correlation between the population density of *Arenicola marina* and the extent of detrital clay coat coverage in surface sediment (< 2 cm). However, as acknowledged by Wooldridge et al. (2017b), it remains unknown whether sediment bioturbation by *Arenicola marina*, or other estuarine macro-fauna, may form clay coats at sediment depths greater than 2 cm. Furthermore, clay coats have been reported to originate from the post-depositional mechanical-infiltration of clay-laden-waters through the pore-spaces of sediments in modern sediments and in ancient sandstones (Buurman et al., 1998; Matlack et al., 1989; Moraes and De Ros, 1990; Wilson,

1992). A primary aim of this study was therefore to establish whether surface (< 2 cm) clay coat distribution patterns in the Ravenglass Estuary (Wooldridge et al., 2017a; Wooldridge et al., 2017b), are transferred to the immediate near-surface (< 1 m), or whether they may be over-printed by post-depositional processes (e.g. bioturbation or mechanical infiltration).

A combination of climate (i.e. chemical and mechanical weathering intensity), relief (i.e. topographic elevation) and provenance (i.e. sediment supplied) has been proposed to control the type and abundance of clay minerals (clay mineral assemblage) found in modern oceanic and marginal-marine settings (Chamley, 1989; Eberl et al., 1984; McKinley et al., 2003; Rateev et al., 2008). It has been suggested that clay mineral distribution patterns in marginal-marine sedimentary systems may be controlled by: the landward displacement of marine sediment (Chamley, 1989; Hathaway, 1972; Meade, 1969; Postma, 1967), differential settling due to salinity or clay mineral stability (Edzwald and O'Mella, 1975; Whitehouse et al., 1960), the physical sorting of clay minerals by size (Gibbs, 1977), local hydrodynamics (Feuillet and Fleischer, 1980), provenance (Biddle and Miles, 1972; Feuillet and Fleischer, 1980; Hathaway, 1972; Rudert and Müller, 1981), mechanical infiltration (Matlack et al., 1989). and both early physicochemical (Griffin and Ingram, 1955; Grim and Johns, 1954; Nelson, 1960; Powers, 1957), biologically-mediated diagenesis via sediment bioturbation (McIlroy et al., 2003; Needham et al., 2006; Needham et al., 2004; Needham et al., 2005; Worden et al., 2006).

In summary, a detailed shallow-core study of the Ravenglass Estuary, UK, has been designed to address the following specific research questions, in order to provide a modern analogue for the prediction of clay mineral, clay coat and Fe-sulphide distribution patterns in marginal-marine sandstone reservoirs.

1. How are clay coats distributed in near-surface (< 1 m) estuarine sediment? How do near-surface clay coat distribution patterns compare to surface (< 2 cm) clay coat distribution patterns reported by Wooldridge et al. (2017b)? What are the fundamental controls on clay coat distribution patterns in near-surface sediment?
2. What clay minerals are found in near-surface sediment of the Ravenglass Estuary? How are clay minerals distributed? What controls clay minerals distribution patterns?
3. What Fe-sulphides are found in near-surface sediment of the Ravenglass Estuary? How are Fe-sulphides distributed? What controls clay Fe-sulphide distribution patterns?
4. Can precursor clay coat, clay mineral and/or Fe-sulphide distribution patterns be predicted as a function of lithofacies?

3.3 STUDY AREA: RAVENGLASS ESTUARY

3.3.1 Geomorphology and estuarine hydrodynamics

The Ravenglass Estuary is located in north-west England on the west coast of Cumbria, and encompasses the tidal-reaches of the westward flowing Rivers Irt, Mite and Esk (Fig. 3.1). The inner-estuary and central-basin are sheltered from wave-action by two coastal spits (Drigg and Eskmeals), but are subject to strong tidal-currents owing to a macro-tidal regime (> 7 m tidal range). The Ravenglass Estuary is here classified as 'dual-funnelled' and mixed-energy system. The Ravenglass Estuary is shallow (Fig. 3.2), and occupies an area of 5.6 km^2 of which ~ 86% is intertidal (Bousher, 1999; Lloyd et al., 2013; Wooldridge et al., 2017b). The shallow bathymetry causes frictional effects that promote strong tidal-asymmetry, meaning the outward ebb tidal-flow is prolonged in comparison to the inward tidal-flow (Kelly et al., 1991). The rivers flowing into the estuary have average flow-rates of 0.4 m^3s^{-1} for the Mite, 3.4 m^3s^{-1} for the Irt, and 4.2 m^3s^{-1} for the Esk and (Bousher, 1999). The short length of the estuary (due to geological-mediated topographic constraints) has been reported to cause quick ebb-drainage, meaning that the maximum discharge measured for the lower-Esk arm of the estuary during the ebb tidal-flow (4.99 m^3 s^{-1}) is only slightly lower than flood tidal-flow (5.41 m^3 s^{-1}) (Kelly et al., 1991). Anthropogenic impact on the estuary is here considered to be minor, with exception of sheltering of the inner-Mite and increased salt marsh development as a consequence of the railway viaduct construction (Fig. 3.1) (Carr and Blackley, 1986).

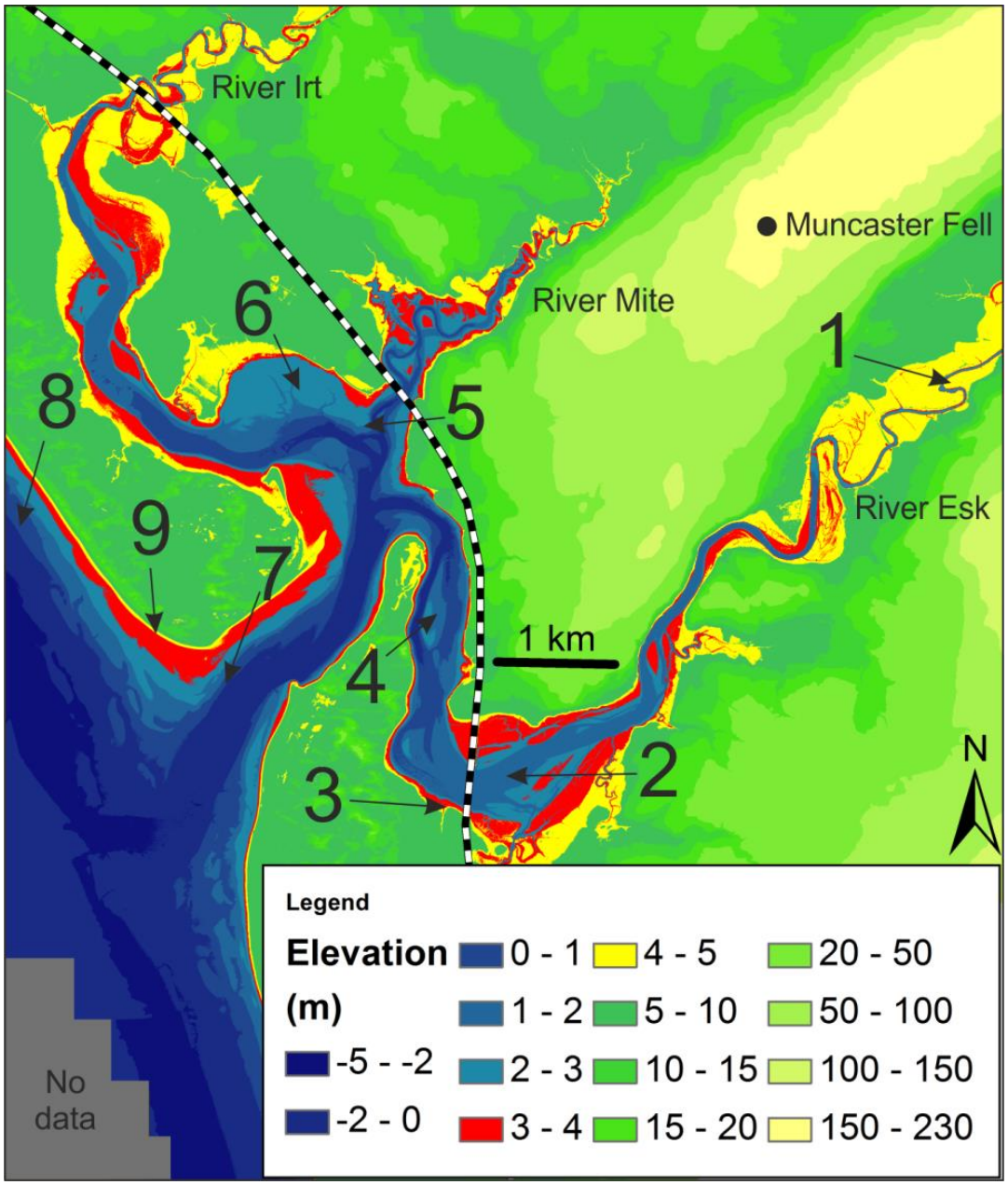

Figure 3-2 – Estuarine bathymetry and hinterland elevation (m OD) derived from Lidar Imagery collected by the UK Environmental Agency (UK Environmental Agency, 2015). The position of nine core regions highlight the location of core samples (n = 23). Shades of blue highlight intertidal regions, whereas salt marsh and backshore, as well as floodplains are highlighted in red and yellow.

3.3.2 Geological setting, hinterland bedrock and quaternary-drift

The Ravenglass Estuary is fed by two river catchments, the northern River Irt and River Mite, and the southern River Esk. The River Irt and River Mite predominantly drain Ordovician Borrowdale Volcanic Group andesites and Triassic Sherwood Sandstone Group sedimentary rocks. The River Esk drains an area dominated by Devonian Eskdale Granite (Fig. 3.3A). The weakly-metamorphosed, fine-grained sedimentary rocks of the Skiddaw

Group (Merritt and Auton, 2000) has marginal exposure at Muncaster Fell (Fig. 3.3A). The Borrowdale Volcanic Group is dominated by subduction-related, K-rich, calc-alkaline andesite, and was subject to regional, sub-greenschist facies metamorphism at about 395 Ma during the Caledonian Orogeny (Quirke et al., 2015). Chlorite is abundant in the Borrowdale Volcanic Group and has been reported to be pseudomorphs after pyroxene (Quirke et al., 2015). The Lower Triassic Sherwood Sandstone Group (locally known as the St Bees sandstone) is predominantly composed of fluviatile sandstones (Quirke et al., 2015). The northern part of the Eskdale Granite is a coarse-grained granite, the southern part is granodioritic (Young et al., 1986). Chloritization of mafic silicates and plagioclase-alteration are widespread in both Eskdale granite types (Moseley, 1978; Quirke et al., 2015; Young et al., 1986).

The northern part of the UK (including Cumbria) is presently undergoing limited isostatic recovery following the last glacial maximum (Bousher, 1999) that occurred in the late Devensian at about 28 to 13 ka (McDougall, 2001; Moseley, 1978). Glacioisostatic rebound following deglaciation, and glacioeustatic sea-level change, led to fluctuations in relative sea-level during the Holocene, which resulted in the deposition of a suite of tills, and glaciofluvial and glaciolacustrine deposits (Fig. 3.3B). Much of the glacial deposit has been removed from the land surface following the last glaciations (Merritt and Auton, 2000). Drift deposits are locally known as the Seascale Glacigenic Formation (the Ravenglass Till member being the dominant unit in the Ravenglass area) and the overlying Gosforth Glacigenic Formation (Lloyd et al., 2013; Merritt and Auton, 2000). Estuarine sediments are therefore underlain by glacial till which is exposed as knolls throughout the estuary. These post-glacial estuarine sediments have a maximum thickness of ~ 10 to 15 meters in this area (Bousher, 1999). Quaternary sediments contain distinctive clasts of the underlying bedrocks which allows detailed lithostratigraphical division as well as revealing complex ice-movement patterns (Merritt and Auton, 2000).

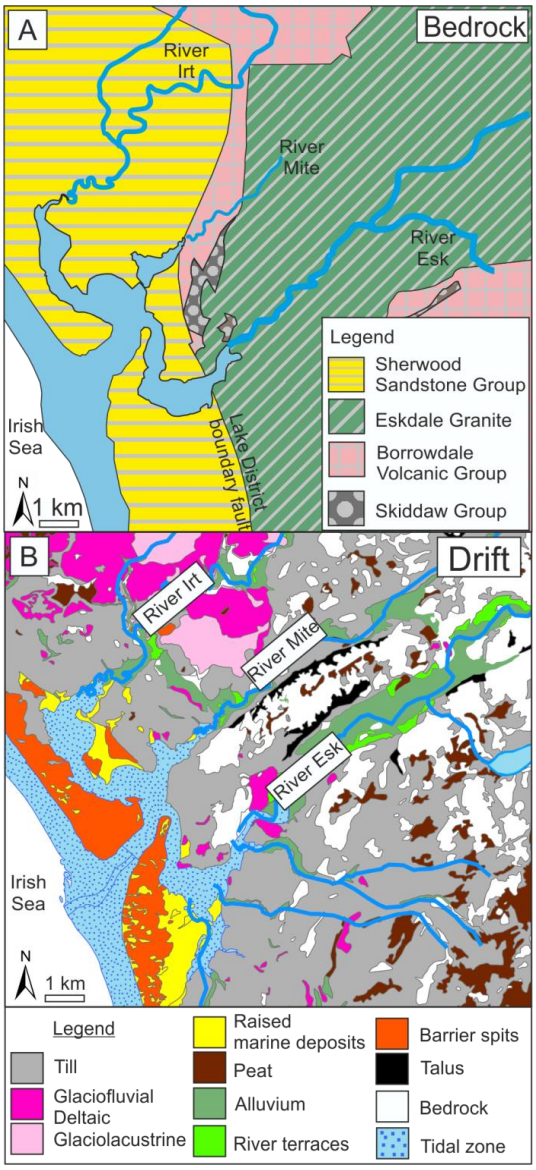

Figure 3-3 – Geological setting of the Ravenglass Estuary, UK, (A) bedrock geology, and (B) Quaternary drift-deposits.

3.4 SAMPLES AND METHODS

3.4.1 Field mapping and core collection

Detailed ground-surveys, aided by aerial imagery (Fig. 3.1) and LIDAR survey (Fig. 3.2)(UK Environmental Agency, 2015) were used to define a suite of estuarine environments. Tidal flats were differentiated based upon sand-abundance, following the tidal-flat classification scheme proposed by Brockamp and Zuther (2004) whereby a sand-flat is > 90 % sand grade material, a mixed-flat has 50 to 90% sand grade material, and a mud-flat has 15 to 50 % sand grade material. Sand abundance was determined for sediment samples using a Beckman Coulter Laser Particle Size Analysis (LPSA) in unison with GRADISTAT (Blott and Pye, 2001).

Twenty-three cores, covering nine regions (Fig. 3.2), were collected along predefined transects (Fig. 3.4) in order to capture surface-sediment heterogeneity (Fig. 3.5). Cores were collected with negligible sample disturbance using a jackhammer-driven window sampler following the method detailed by Dowey et al. (2017). Each core was retrieved in a polythene liner to avoid oxidation and sample degradation, and protected in a rigid plastic tube.

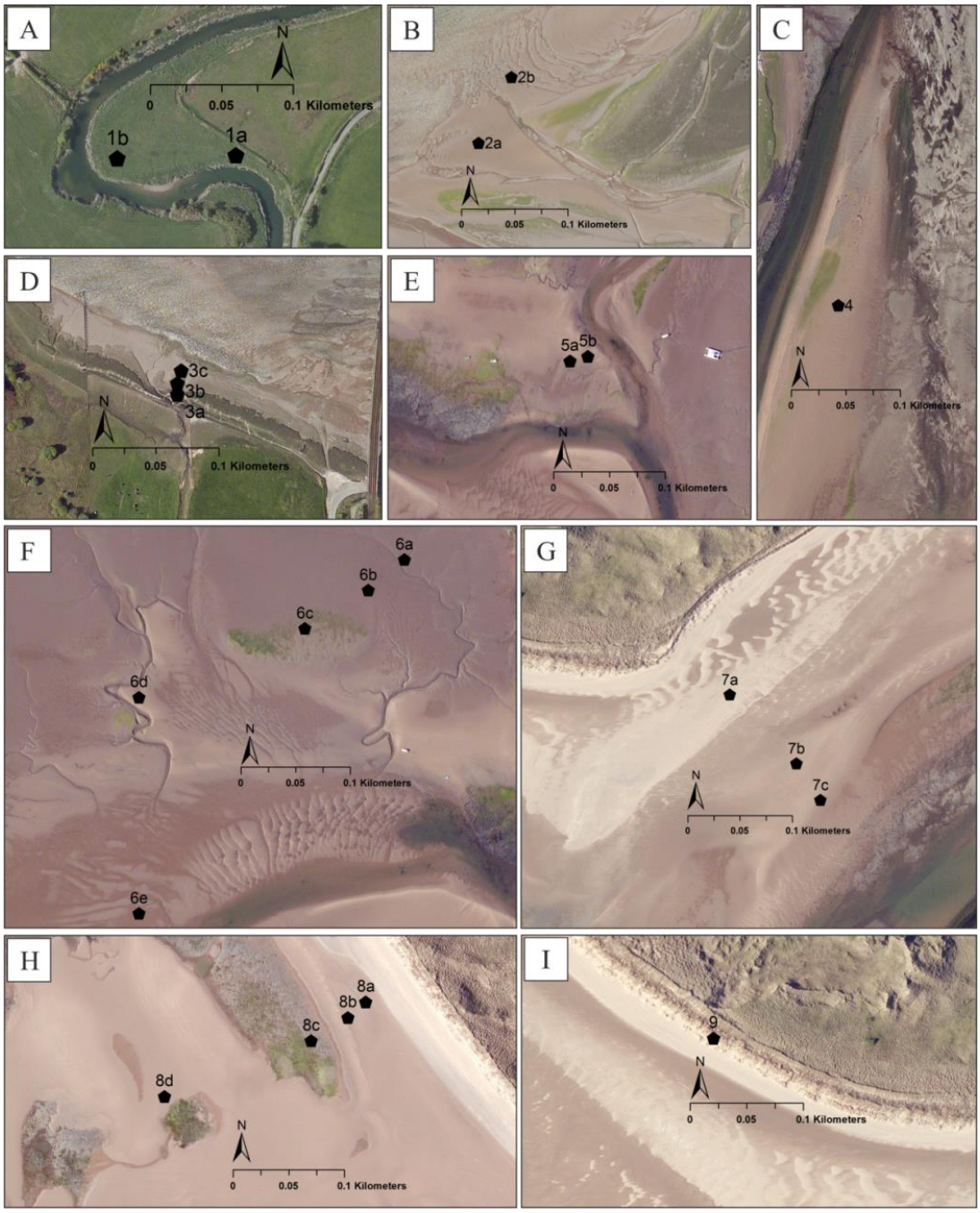

Figure 3-4 – Aerial images of the nine core regions; A, core region 1; B, core region 2; C, core region 4; D, core region 3; E, core region 5; F, core region 6; G, core region 7; H, core region 8; and I, core region 9.

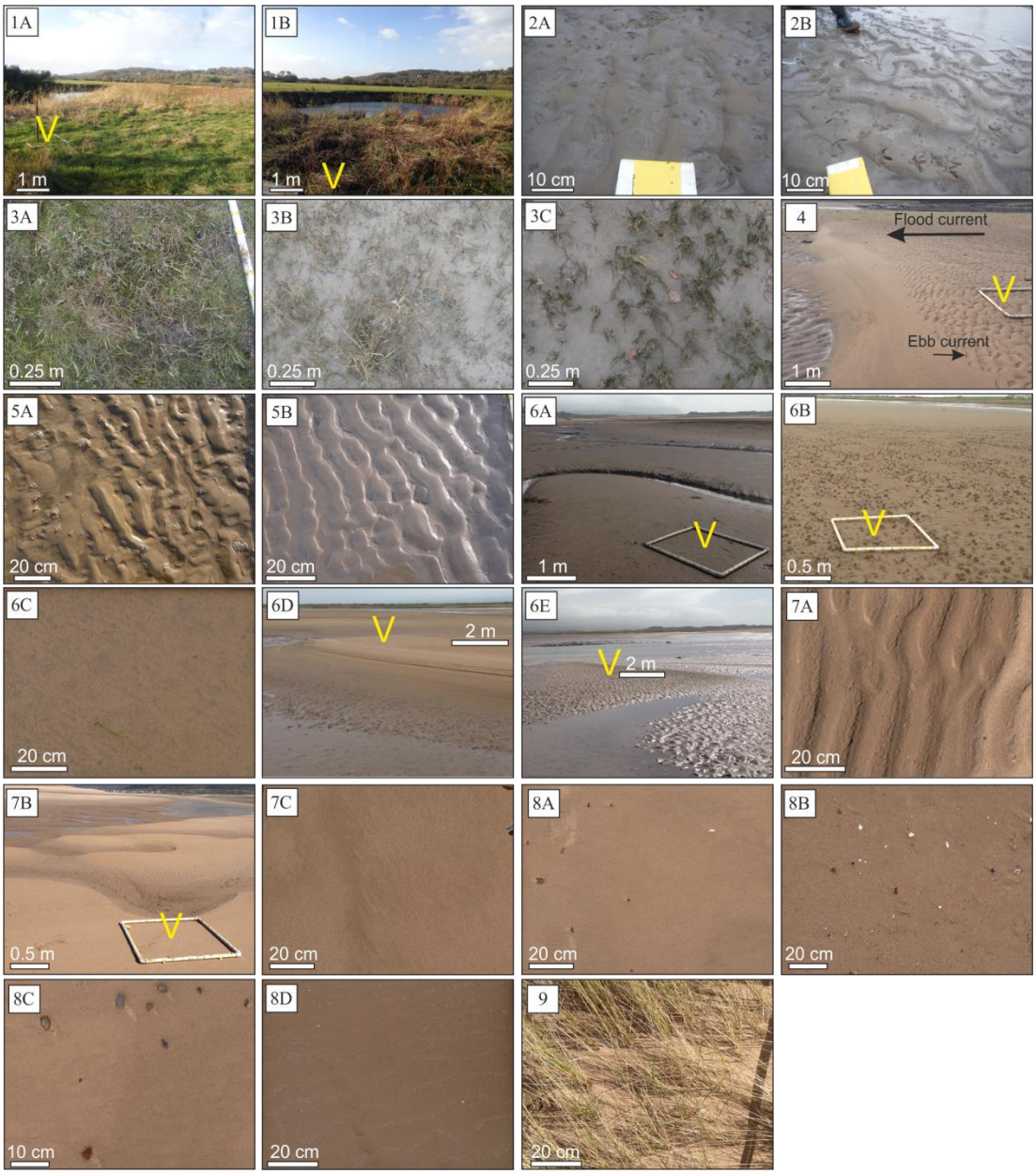

Figure 3-5 – Surface photographs taken at each core site (n = 23). Each photograph is labelled with the corresponding core ID (see figure 3.8). The yellow 'V' symbol represents the location of where individual cores were collected.

3.4.2 Core preparation and description

Sediment cores were dissected and photographed, wet and dry, to capture redox boundaries, ichnofabrics (bioturbation traces) and key sedimentary structures in the laboratory. Core samples collected for X-ray diffraction analysis were extracted and placed in an air-tight, screw-top plastic jar, stored in the dark, and refrigerated (at ~ 2 °C) to avoid degradation prior to analysis. Sediment samples, used to determine detrital clay coat coverage, were collected following the same procedure outlined by Wooldridge et al. (2017b).

Sediment grain-size was measured in the laboratory using a hand-lens and grain-size card every 5 cm in relatively homogenous facies, and at a sub-centimetre scale where necessary e.g. in very thinly-bedded sediment (< 3 cm). In this study, the Campbell (1967) classification to assign bed-thickness was used. Wavy flaser bedding and wavy bedded heterolithics have been defined following Reineck and Wunderlich (1968). Bioturbation Index (BI) was recorded using the classification scheme proposed by Taylor and Goldring (1993) (Table 3.1) to test the strength of the relationship between bioturbation intensity, mineralogy and extent of detrital clay coat coverage.

Table 3.1 - Bioturbation index classification scheme, after Taylor and Goldring (1993), and detrital clay coat coverage classification scheme, after Wooldridge et al. (2017b).

Class	Classification of Bioturbation Index (BI), after Taylor and Goldring (1993)	Classification of detrital clay coat coverage, after Wooldridge et al. (2017b)
0	No bioturbation	x
1	Sparse bioturbation, bedding distinct, few discrete traces and/or escape structures	Complete absence of attached clay
2	Low bioturbation, bedding distinct, low trace density, escape structures often common	1-5 % coverage is observed on < 50 % of the sand grains
3	Moderate bioturbation, bedding boundaries sharp, traces discrete, overlap rare	All grains have at least 5-15% clay coat coverage
4	High bioturbation, bedding boundaries indistinct, high trace density with overlap common	All grains have clay coats, with the majority of grains having 15-30 % clay coat coverage
5	Intense bioturbation, bedding completely disturbed (just visible), limited reworking, later burrows discrete	> 30 % clay coat coverage (extensive) is observed on all grains
6	Complete bioturbation, sediment reworking due to repeated overprinting.	x

3.4.3 Qualitative clay coat coverage analysis

To achieve a direct comparison between detrital clay coat coverage in surface sediment (< 2 cm) and near-surface (< 1 m) sediment, detrital clay coat coverage was determined qualitatively following the methodology proposed by Wooldridge et al. (2017b). A qualitative estimation of clay-coat coverage on individual sand grains (five principle classes; Table 3.1) was achieved by analysing 200 sand grains (per grain-mount sample), imaged using Scanning Electron Microscopy (SEM). Bin classes were defined as; (class 1) complete absence of attached clay coats; (class 2) less than half of the grains have a small (~ 1 to 5 %) surface area of attached clay coats; (class 3) every grain exhibits at least ~ 5 to 15 % surface area of attached clay-coats; (class 4) clay coats on every grain with the majority exhibiting extensive (~ 15 to 30 %) surface-area grain coverage; and (class 5) greater than 30 % surface area covered by clay coats on every grain (Table 3.1) (Wooldridge et al., 2017b).

3.4.4 Clay mineral separation, identification and quantification

The clay fraction (< 2 μm) of, dried and weighed representative core sub-samples and Quaternary glaciogenic drift deposits (sourced from cliff sections in the inner-Esk) were physically separated (isolated from the silt- and sand-fraction) prior to XRD analysis. This was performed using an ultrasonic bath to disaggregate sediment, followed by gravity settling to separate out the sand and silt size fractions, and then centrifuge settling at 5,000 rpm for 10 minutes to collect the clay size fraction. The separated clay fraction was then dried at 60°C for 24 hours and weighed to calculate the percentage of clay-size material. The mineralogy of the clay fraction was determined using a PANalytical X'Pert Pro MPD X-ray Diffractometer (Fig. 3.6). Samples were glycolated for 24 hours and re-scanned over a range of 3.9 to 13.0°2θ to test for the presence of expandable clay minerals (i.e. smectite) following the methodology outlined by Moore and Reynolds (1997). Following the definition of Grim et al. (1937), the term illite in this study is used for all clay-size, mica-like minerals commonly associated with clastic-sediments. To assess relative clay mineral abundance, clay mineral indices were derived as follows; relative abundances of chlorite (chlorite/(chlorite + illite + kaolinite)), kaolinite (kaolinite/(chlorite + illite + kaolinite)), and illite (illite/(chlorite + illite + kaolinite)).

The mineralogy of an array of grain-size separates was achieved using a combination of gravity-settling (as above) and sieving followed by X-ray diffraction analysis. Grain-size classes included, < 0.2 μm (fine clay); 0.2 μm to 2 μm (coarse clay); 2 μm to 32 μm (fine silt); 32 μm to 62 μm (coarse silt); 62 μm to 125 μm (very fine sand); and 125 μm to 250 μm (fine sand).

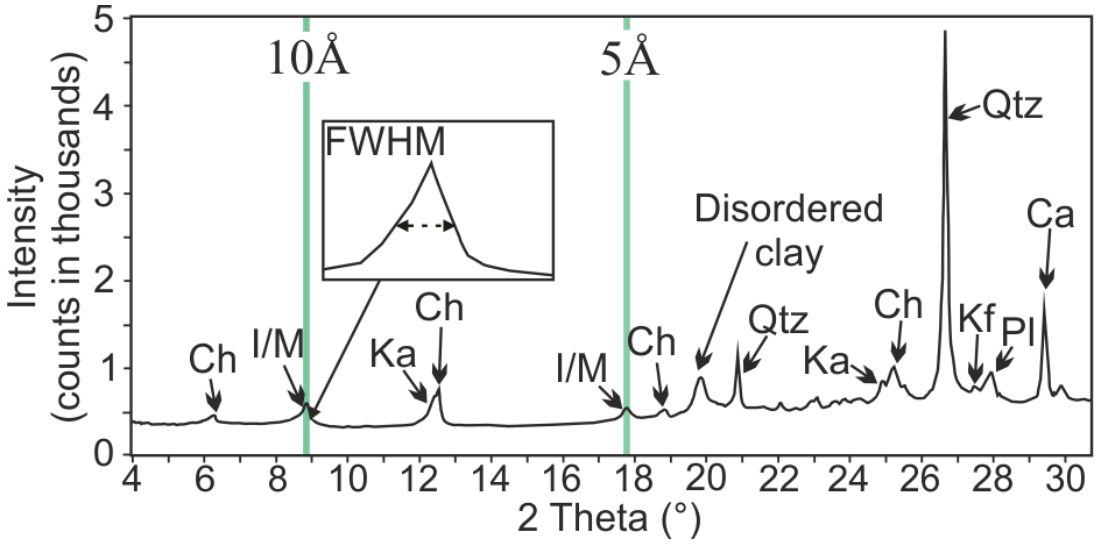

Figure 3-6 – Example of an X-ray diffractogram used to quantity clay mineral abundance. Esquevin Index is derived by comparing the relative peak heights of the 5Å and 10Å illite peaks (highlighted by a green line). Illite crystallinity is measured on the 10Å illite peak, using the full width at half maximum (FWHM).

The Esquevin Index has been calculated to differentiate Al-rich from Fe-Mg-rich illite. The Esquevin Index is calculated by analysing the ratio between the (002) and (001) peak heights (Esquevin, 1969), on X-ray diffractograms i.e. the ratio between the intensity of the 5Å and 10Å peaks (Fig. 3.6). The following classification boundaries are used in this study, after Esquevin (1969); biotite, < 0.15; biotite + muscovite, 0.15 to 0.3; phengite, 0.3 to 0.4; muscovite, > 0.4. Thus, high Esquevin Indices indicate Al-rich illites, whereas, low Esquevin Index values represent relatively Fe-Mg-rich illites. Low Esquevin Indices are characteristic of physically eroded, unweathered rocks (Chamley, 1989). High Esquevin Indices correspond to chemically-weathered rocks that have lost divalent cations (Fe and Mg) from the octahedral sites (Chamley, 1989).

The full width at half-maximum (FWHM) of the 10Å (001) illite peak was measured on X-ray diffractograms in order to establish illite crystallinity index ($2^0\theta$), also known as the *Kübler* Index (Kübler, 1964). Poorly-crystalline illite is reflected by broad basal reflections (high FWHM values), associated with highly-degraded, low growth-temperature, low-structural-order illite (Chamley, 1989; Kübler, 1964). Highly-crystalline illite is reflected by narrow basal-reflections (low FWHM values), associated with relatively unaltered, high growth-temperature, high-structural-order illite (Chamley, 1989; Kübler, 1964). The following boundaries are used, after Kübler (1964); epizone (highest temperature): < 0.25; anchizone: 0.25 to 0.42, diagenesis (lowest temperature): > 0.42.

3.4.5 Statistical analysis

Statistical analysis was performed to test whether lithofacies, sediment depth (proxy for mechanical infiltration) and bioturbation index (intensity) may explain clay mineral, pyrite and/or clay coat distribution patterns in the Ravenglass Estuary. All statistical analyses were performed in R statistical software (R Core Team, 2016), using the following symbols to highlight statistical significance; marginally-significant (+) when $p < 0.1$; significant (*) when $p < 0.05$; very-significant (**) when $p < 0.01$; and extremely significant (***) when $p < 0.001$. Note statistical analyses were not performed on any lithofacies which had a sample number less than 3.

3.4.5.1 Clay coat: lithofacies, infiltration and bioturbation

A Kruskal-Wallis H test was used to test whether there is a statistically significant difference in detrital clay coat coverage as a function of estuarine lithofacies. Following the Kruskal-Wallis H test, a post-hoc Dunn test was employed to highlight where the identified significant differences occurred in detrital clay coat coverage between individual facies. The Benjamini-Hochberg method (False Discovery Rate) (Benjamini and Hochberg, 1995) was applied to correct the *p-values* after performing multiple comparisons.

Pearson's correlation coefficients were calculated to describe the strength of the relationship between clay fraction abundance and core depth, to assess whether there is any evidence for a post-depositional increase in clay content, which may be due to mechanical infiltration. In order to determine whether mechanical infiltration may have led to the post-depositional formation of clay coats, Spearman's correlation coefficients were calculated to describe the strength of the relationship between clay coat coverage and core depth. To assess whether the act of sediment bioturbation may form clay coats, Spearman's correlation coefficients were calculated to test the strength of the relationship between Bioturbation Index (BI) and extent of clay coat coverage.

3.4.5.2 Mineralogy: lithofacies, infiltration and bioturbation

An Analysis Of Variance (ANOVA) test was used to test whether there is a statistically significant difference in clay mineral indices (chlorite, illite, kaolinite and smectite) and pyrite abundance, as a function of estuarine lithofacies. Following ANOVA, a post-hoc Tukey's honestly significant difference (HSD) test was employed to highlight where the identified significant differences in relative abundance of clay minerals and/or pyrite between individual facies could be found.

The strength of the relationship between depth and clay mineral indices were calculated using Pearson's correlation coefficients to test whether vertical mechanical infiltration may have led to the stratification of clay minerals. Pearson's correlation coefficients were calculated to test the strength of relationship between depth and pyrite abundance in order to determine whether pyrite formation is primarily controlled sediment depth (i.e. increasing anoxic conditions with an increase in sediment depth). It is acknowledged that redox-boundary depth is also dependent on other variables, such as sediment properties (e.g. grain size and sorting). To establish whether bioturbation may have led to the early-diagenetic alteration and/or formation of new clay minerals, Spearman's correlation coefficients were used to test the strength of the relationship between Bioturbation Index (BI) and clay mineral indices.

3.5 RESULTS

The surface characterization of the Ravenglass Estuary, as well as sedimentary logs, a detailed lithofacies scheme, mineralogical analyses (clay mineral indices, pyrite abundance, Esquevin index, and illite crystallinity) and clay coat distribution data from twenty-three one-metre cores is here presented.

3.5.1 Surface depositional environments and facies associations

The ten discrete depositional environments in the Ravenglass Estuary are presented in Figure 3.7: gravel-beds (De 1), mud-flats (De2), mixed-flats (De3), sand-flats (De4), tidal bars and low-amplitude dunes (De5), tidal-inlet (De6), backshore (De7), foreshore (De8), pro-ebb delta (De9) and coastal spits (De10). Lidar imagery (Fig. 3.2) reveals the extent of salt marsh and backshore deposits (3 to 4 m OD; coloured in red) and floodplain deposits (4 to 5 m OD; coloured in yellow). The general appearance of depositional environments at each core location is displayed in figures 3.4 and 3.5.

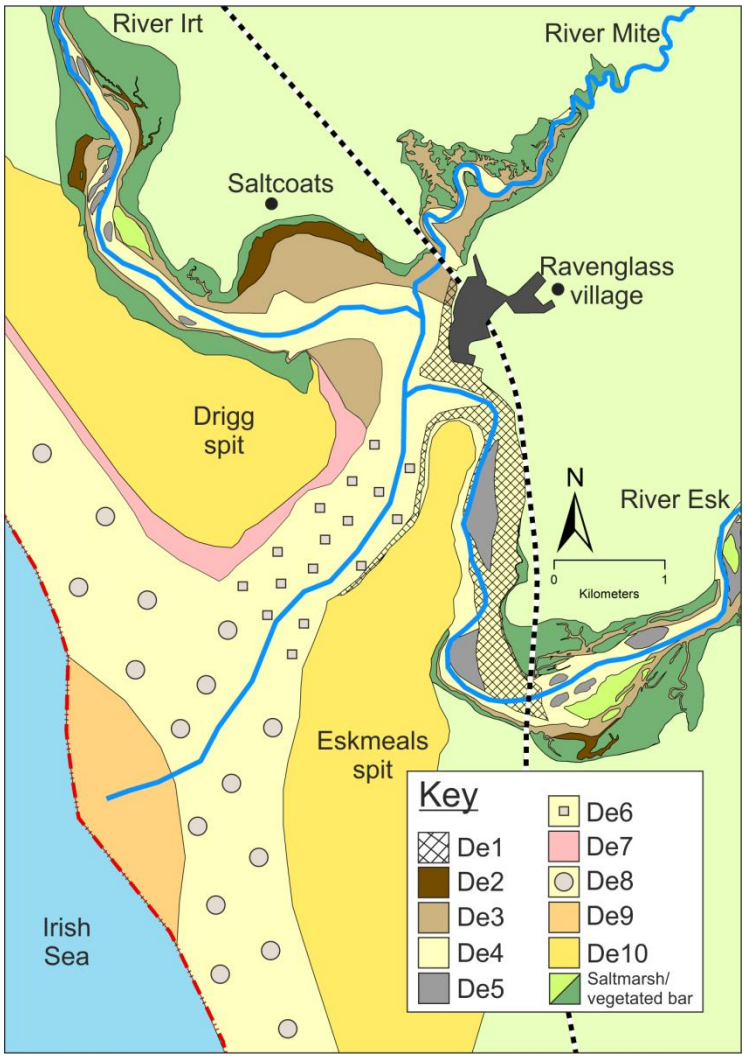

Figure 3-7 – Type and distribution of estuarine depositional environments in the Ravenglass Estuary. Depositional environments are labelled accordingly; De1, gravel-bed; De2, mud-flat; De3, mixed-flat; De4, sand-flat; De5, tidal bars and dunes; De6, tidal-inlet; De7, backshore; De8, foreshore; De9, pro-ebb delta; and De10 coastal spits.

Schematic sedimentary logs (n = 23) showing variation in lithofacies, bioturbation intensity and extent of detrital clay coat coverage in each core are presented in Figure 3.8. The sedimentary facies of the Ravenglass Estuary have been grouped into eight distinct facies associations (Table 3.2). The abundance (%) of each facies in each core is summarised in Figure 3.9. The descriptive characteristics (texture, sedimentary structures, and ichnofabrics) for each lithofacies are summarised in Table 3.2, which may be used to characterise specific depositional environments and sediment transport processes.

Core region 1 (Fig. 3.2) is located in the River Esk floodplain (Figs. 3.2, 3.4A and 3.5.1A-B) and consists of cores 1A and 1B (Fig. 3.8.1A-B).

Core region 2 (Fig. 3.2) is situated in the inner-Esk and consists of cores 2A and 2B (Figs. 3.8.2A and 3.8.2B), both of which were drilled through low-amplitude tidal-dunes (Figs.

3.4B). The low-amplitude tidal dunes are bioturbated primarily by *Arenicola marina* (lugworms), and contain current-ripples (sinuous to sigmoidal) that are draped with mud (Figs. 3.5.2A-B).

Core region 3 (Fig. 3.2) consists of a three-core transect; upper- middle- and lower-tier salt marsh (Fig. 3.4D). Core 3A (Fig. 3.8.3A) was collected in upper-tier, well-vegetated salt marsh (Fig. 3.5.3A). Core 3B (Fig. 3.8.3B) was collected from middle-tier, moderately-vegetated salt marsh (Fig. 3.5.3B). Core 3C (Fig. 3.8.3C) was collected from moderate- to sparsely-vegetated, lower-tier salt marsh (Fig. 3.5.3C). All salt marsh tiers are heavily bioturbated by *Corophium volutator* (sand shrimp) which form densely populated U-shaped burrows (< 5 cm depth).

Core region 4 (Fig. 3.2) consists of core 4A (Fig. 3.8.4A), which is located in the inner-Esk (proximal to glacial-cliffs), and was collected in the axis of an elongate detached tidal-bar (Fig. 3.4C). The crest and trough of the planar tidal-dunes contain current-ripples with isolated mud-drapes (Fig. 3.5.4).

Core region 5 (Fig. 3.2) contains cores 5A and 5B (Figs. 3.8.5A and 3.8.5B), which are located in the central-basin (Fig. 3.4E). Bioturbated (mainly *Arenicola marina*) tidal current-ripples (straight to sinuous) with extensive mud-drapes occur at the surface (Figs. 3.5.5A and 3.5.5B).

Core region 6 (Fig. 3.2) consist of a ~ 450 m five-core transect (Fig. 3.4F) which captures the sediment heterogeneity of the Saltcoats tidal flat (Fig. 3.5.6A-B). Core 6A (Fig. 3.8.6A) was extracted from a mud-flat (commonly fluidised-mud), proximal to a small tidal-creek, which is intensely bioturbated by *Corophium volutator* (Fig. 3.5.6A). Core 6B (Fig. 3.8.6B) is located in an intensely bioturbated (predominantly by *Arenicola marina*) mixed-flat comprised of sinuous current-ripples with isolated mud-drapes (Fig. 3.5.6B). Core 6C (Fig. 3.8.6C) was collected from a mixed-flat, which contains poorly-formed current-ripples with mud-drapes (Fig. 3.6C). Core 6D (Fig. 3.6D) was collected from the crest of a tidal-creek point-bar (Fig. 3.6D), which hosts mud-draped ladder-back current-ripples and sporadic *Arenicola marina* castings. Core 6E (Fig. 3.6E) was cored through a low-amplitude dune (bioturbation is absent) proximal to the main ebb-channel (Fig. 3.6E).

Core region 7 (Fig. 3.2) is comprised of a three-core transect (~ 150 m) which captures the sediment heterogeneity of the tidal-inlet (Fig. 3.4G). The surface environment of core 7A (Fig. 3.8.7A) is proximal to backshore deposits and is characterized by wave-ripples (Fig. 3.5.7A). Core 7B (Fig. 3.8.7B) was collected from the crest of a 3D dune (Fig. 3.5.7B). Core

7C (Fig. 3.8.7C) was drilled through an upper-phase plane bed (Fig. 3.5.7C), proximal to the ebb-channel (Fig. 3.4G).

Core region 8 (Fig. 3.2) consists of a ~ 200 m four-core transect (Fig. 3.4H) which covers the upper- and lower-foreshore (Fig. 3.4H). Cores 8A and 8B (Figs. 3.8.8A and 3.8.8B) were collected from the upper-foreshore, proximal to backshore-deposits, and show no discernible sedimentary structures at the surface (Figs 3.5.8A and 3.5.8B). Cores 8A and 8B are separated by cores 8C and 8D (Figs. 3.8.8C and 3.8.8D) by an approximately 1 m reduction in surface elevation (break in slope) (Fig. 3.2). The surface environment of core 8C contains abundant granules and pebbles deposited in the swash-zone (Fig. 3.5.8C). Core 8D was collected from the lower-foreshore, the surface contained wave-formed ripples which are draped in disarticulated shell-fragments (Fig. 3.5.8D).

Core region 9 (Fig. 3.2) consists of core 9 (Fig. 3.8.9) that was collected in well-vegetated aeolian dunes (Figs 3.4I and 3.5.9) on the fringe of Drigg coastal-spit.

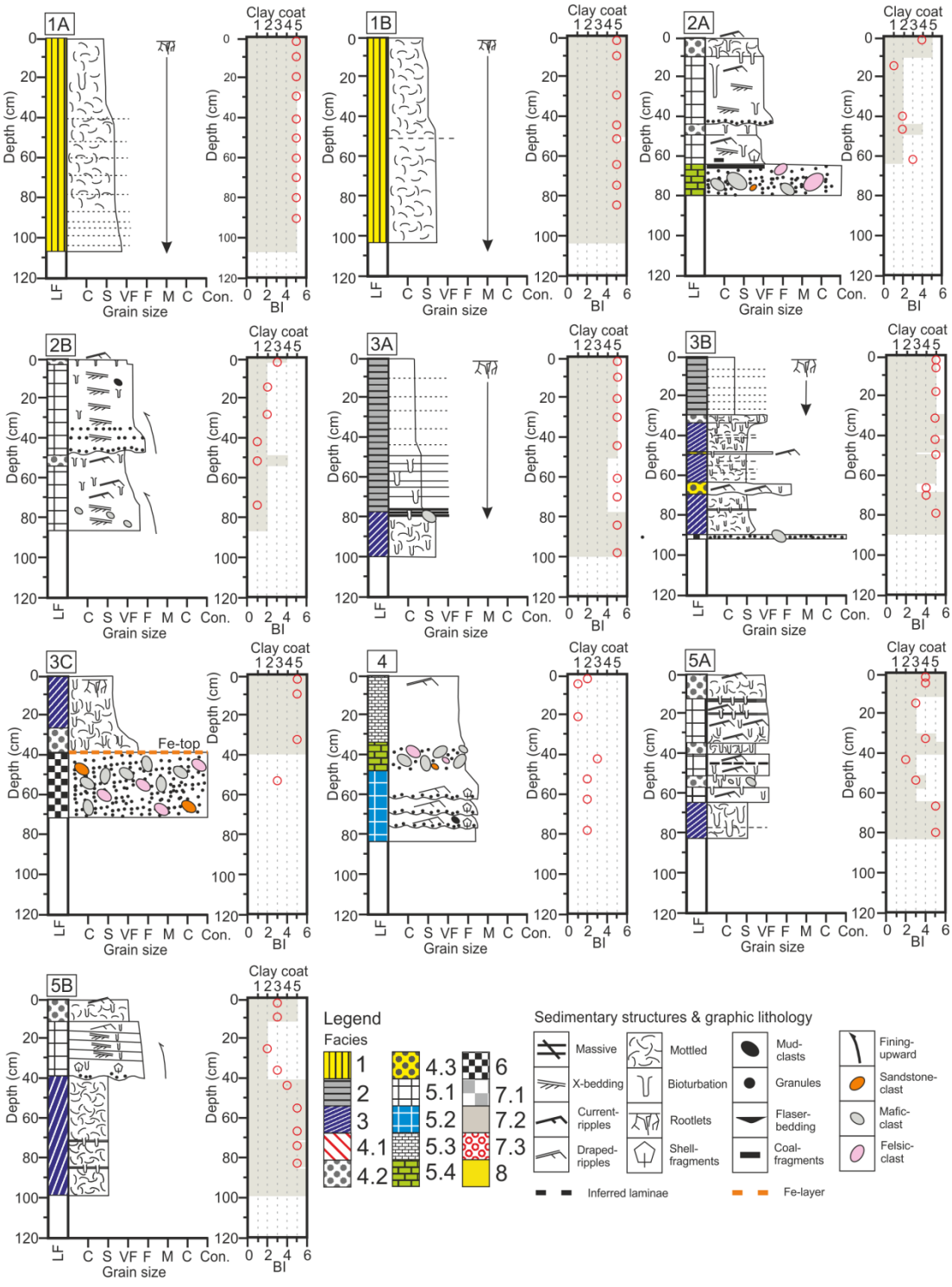

Figure 3-8 – Schematic sedimentary logs alongside the extent of detrital clay coat coverage (red circles) and bioturbation index (BI) (greyed area). Refer to Table 3.2 for explanation of lithofacies codes.

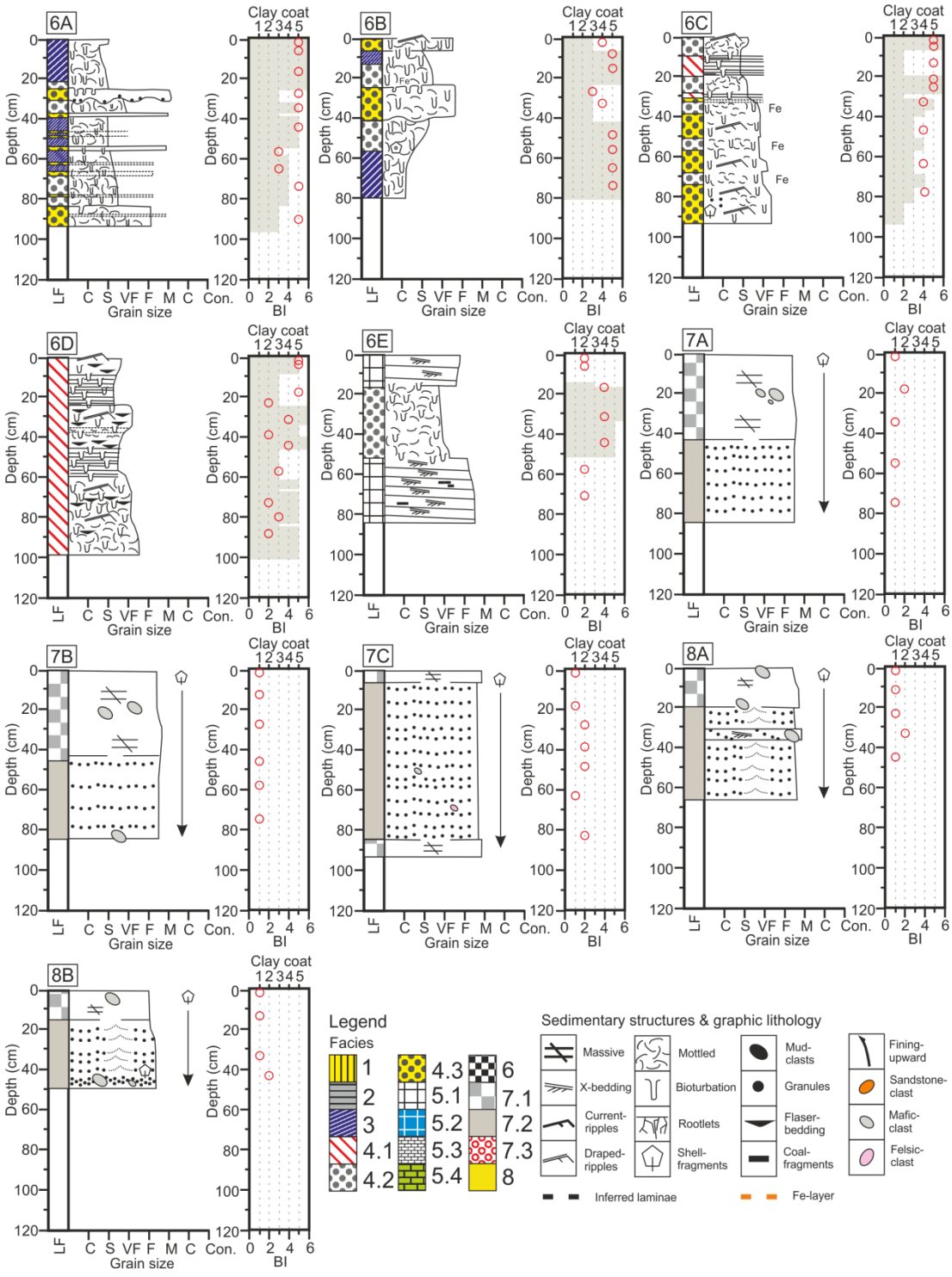

Figure 3.8 continued

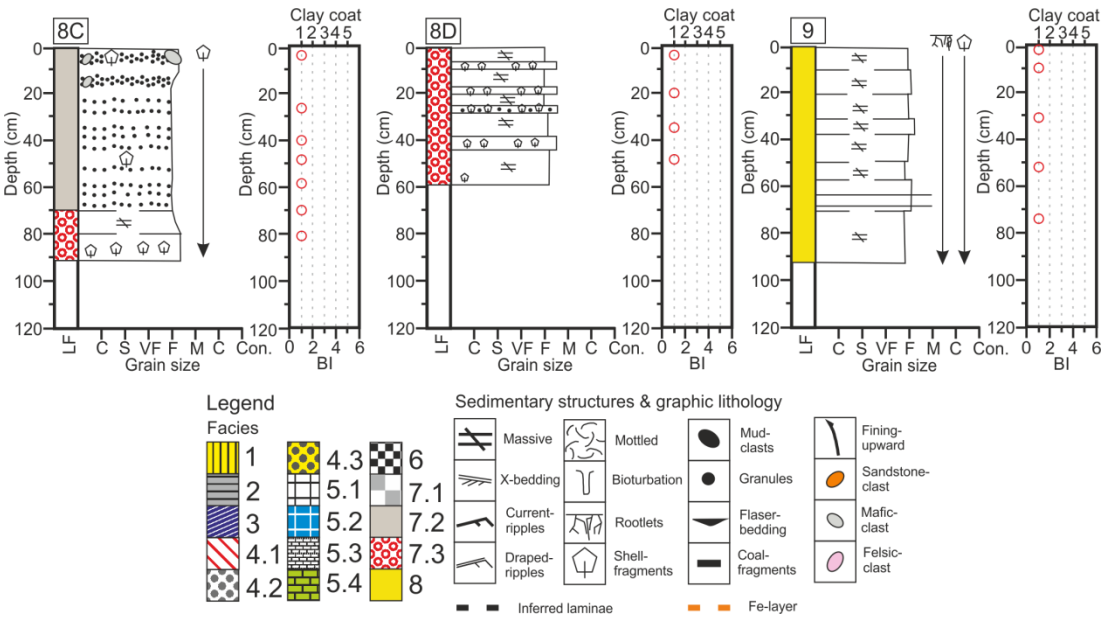

Figure 3.8 continued

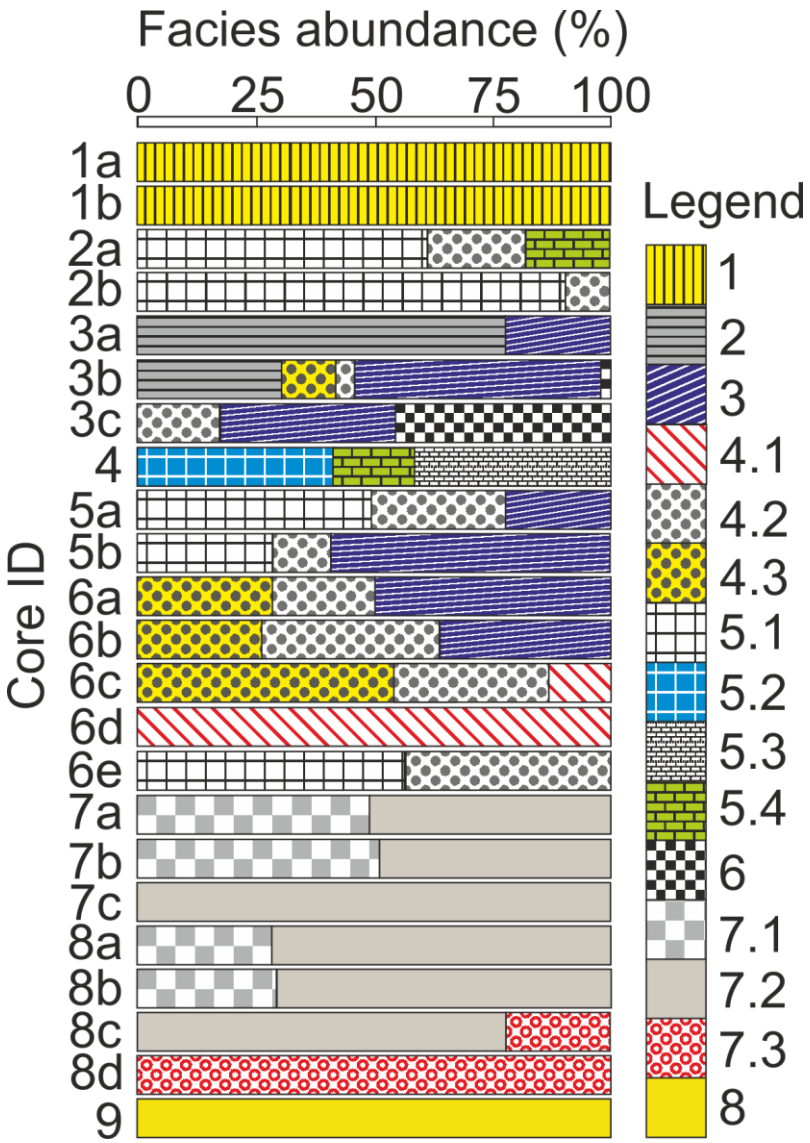

Figure 3-9 – Lithofacies type and abundance in each core. Refer to Table 3.2 for explanation of lithofacies codes.

Table 3.2 - Diagnostic features (dominant texture, sedimentary structures, and ichnofabrics) of facies associations (FA) and lithofacies (LF) encountered in a wide range of depositional environments in the Ravenglass Estuary.

FA	LF	Dominant texture and sedimentary structures	Dominant ichnofabrics	Estuarine-environment & depositional processes	Core
1 (Floodplain)	1	Vegetated, mottled silt to very fine-grained sand with sporadic (obscured) very fine-grained sand lamina.	Common: rootlets & *Lumbricidae* (earthworm)	**Estuarine environment:** fluvial-floodplain **Depositional process:** alluvium aggradation - deposition of clay, silt and sand during periods of overbank flooding (periods of high-fluvial discharge and/or spring-tide).	1A, 1B
2 (Salt marsh)	2	Vegetated, and bioturbated silt-grade sediment with cyclic (cm-scale) very fine-grained lamina.	Common: rootlets & *Corophium volutator* (sand shrimp)	**Estuarine environment:** salt marsh (estuarine fringe) **Depositional process:** marine alluvium aggradation Deposition of clay, silt and sand during high-tide.	3A, 3B
3 (Mud flat)	3	Mottled, clay-and-silt size sediment with very-fine sand filled burrows, and obscured very-fine sand lamina.	Common: *Corophium volutator* & pioneer salt marsh	**Estuarine environment:** mud-flat (estuarine margins) **Depositional process:** Deposition of clay-and-silt sediment through suspension settling during periods of low-energy (e.g. slack water). Fine-grained lamina are deposited during periods of increased energy (e.g. spring-tide, storm-events), and are typically mottled by intense bioturbation.	3A, 3B, 3C, 5A, 5B, 6A, 6B
4 (Mixed-flat and thinly-bedded sediments)	4.1	Very-fine grained wavy flaser bedding and wavy bedded heterolithics, with variable bioturbation intensity.	Common: *Corophium volutator* Rare: *Arenicola marina*	**Estuarine environment:** tidal-creek point bar **Depositional process:** wavy bedding occurs when the mud layers typically fill the ripples trough, and overlay the ripple-crest. In contrast, wavy flaser bedding fail to form continuous layers, and occur when the mud flasers fill only the ripple troughs or only overlie the ripple crest. Deposition of wavy flaser-bedded or wavy-bedded heterolithics is dependent on tidal-conditions and the relative amount of suspended load during deposition.	6C, 6D

	4.2	Mud-rich, very fine-grained sand (~ 4 % clay size fraction), with current-ripples draped in mud.	Common: *Corophium volutator* and *Arenicola marina*	**Estuarine environment:** mixed flat **Depositional process:** migration of tidal-current generated ripples, draped with mud during periods of slack-water (during low-tide). Intense bioturbation (*Corophium volutator* and *Arenicola marina*) often leads to sediment homogenization (mottled texture).	2A, 2B, 3B, 3C, 5A, 5B, 6A, 6B, 6C, 6E.
	4.3	Very-fine to fine-grained thinly-bedded deposits (typically, < 10 cm; ~ 3 % clay fraction). The base-contact of the incursions are typically bioturbated or erosive.	Common: *Corophium volutator* and *Arenicola marina*	**Estuarine environment:** thin-bed incursions in mud flats and mixed flats **Depositional process:** minor incursions (erosive base) are likely to occur during periods of higher-energy within the inner estuary and central basin (e.g. storm-events) and due to the progradation and retrogradation of mixed-flats and mud-flats.	3B, 6A, 6B, 6C.
5 (low-amplitude dunes and tidal bars; inner estuary and central basin)	5.1	Very fine- to medium-grained, cross-bedded and current-rippled sand with an erosive base (< 1 % clay size fraction). Mud-drapes are common.	Common: *Arenicola marina*	**Estuarine environment:** low-amplitude tidal-dunes (inner estuary and central basin) **Depositional process:** migration of low-amplitude tidal-dunes and current-ripples, proximal to the ebb-channel. Mud-drapes are deposited during low-tide.	2A, 2B, 5A, 5B, 6E
	5.2	Fine- to medium-grained and sands with an erosive base, comprised of disarticulated shell fragments and granules.	Very rare: *Arenicola marina*	**Estuarine environment:** inner estuary tidal bar (toe- and bottom-sets) **Depositional process:** Migration of planar dunes, with the deposition of granules and shell fragments within the toe- and bottom-sets of planar dunes.	4
	5.3	Very fine- to fine-grained sand with no discernible bedding structures.	Very rare: *Arenicola marina*	**Estuarine environment:** inner estuary tidal bar (dune crest) **Depositional process:** Deposition of fine to medium grained sand at the crest of migratory tidal dunes.	4
	5.4	Matrix-supported conglomerate (pebble-size).	Absent	**Estuarine environment:** lag-deposit in tidal-bar trough **Depositional process:** Deposition of pebble-size material, (likely derived from neighbouring glacial till deposits) in the trough of migratory tidal-dunes.	2A, 4

6 (Glacial)	6	Fe-stained clast-supported (pebble-size), conglomerate capped by a Fe-cemented layer (1 cm thick).	Absent	**Estuarine environment:** glacial outwash **(**estuarine "basement") **Depositional process:** glacial-outwash of sand and gravels at the end of the last glacial period.	3C
7 (Tidal inlet and foreshore)	7.1	Massive, fine to medium grained, lithic-rich sand. Pebbles are common.	Absent	**Estuarine environment:** tidal inlet, upper foreshore and backshore (typically > 2 m OD, in the Ravenglass Estuary). **Depositional process:** sediment is deposited by wave- and tidal-currents and typically reworked by wind-action. Surface sedimentary structures vary from upper-phase plane beds, 3D dunes, wave-ripples and wind-blown surfaces.	7A, 7B,8A, 8B
	7.2	Medium-grained sand, with granules deposited as lamina-sets, with frequent pebble and shell lag-deposits.	Absent	**Estuarine environment:** tidal inlet and lower foreshore (typically < 2 m OD, in this study). **Depositional process:** granule-rich sediment is primarily deposited during swash- and backwash. Shell-lag deposits are deposited in the trough of migratory 3D dunes.	7A, 7B, 7C, 8A, 8B, 8C
	7.3	Massive, carbonate-rich fine-grained sand.	Absent	**Estuarine environment:** lower foreshore (proximal to the mean low-water line). **Depositional process:** wave action, which generated wave-formed ripples, draped in disarticulated shell-fragments.	8C, 8D
8 (Spits)	8	Very-fine- to fine-grained, massive, well-sorted sands (partly vegetated).	Absent	**Estuarine environment:** coastal-spit **Depositional process:** aeolian dune migration (partly-stabilised by dune-vegetation).	9

3.5.2 Detrital clay coat coverage: lithofacies, bioturbation intensity and core depth

The abundance (average and standard deviation) of clay fraction (< 2 µm) in each lithofacies is summarised in Table 3.3. Average clay fraction for each lithofacies ranges from 0.1 % to 22.6 %, with a weighted estuarine clay fraction average of 5.9 % (Table 3.3). Detrital clay coat abundance in each core is presented in Figure 3.8. The range, upper and lower quartile, and median of clay fraction abundance (%) for each lithofacies and for each core are presented in Figure 3.10.

There is a strong, positive correlation between clay fraction abundance and detrital clay coat coverage ($r = 0.92$, $p < 0.001$). The variability of clay coat coverage (relative abundance of classes 1 to 5) for each lithofacies is presented in Figure 3.11. Kruskal-Wallis H test results show there is a statistical difference ($p < 0.05$) in the extent of detrital clay coat coverage between lithofacies. Post-hoc Dunn test results (Table 3.4) reveal between which lithofacies there are statistical differences in detrital clay coat coverage. There is a strong, positive correlation between detrital clay coat coverage and bioturbation index ($r = 0.84$, $p < 0.001$). Pearson's correlation coefficient test results reveal there is no consistent relationship between depth below the sediment surface and the abundance of clay fraction (Table 3.5). Spearman's correlation coefficient test results reveal there is no consistent relationship between depth below the sediment surface and the extent of detrital clay coat coverage (Table 3.5).

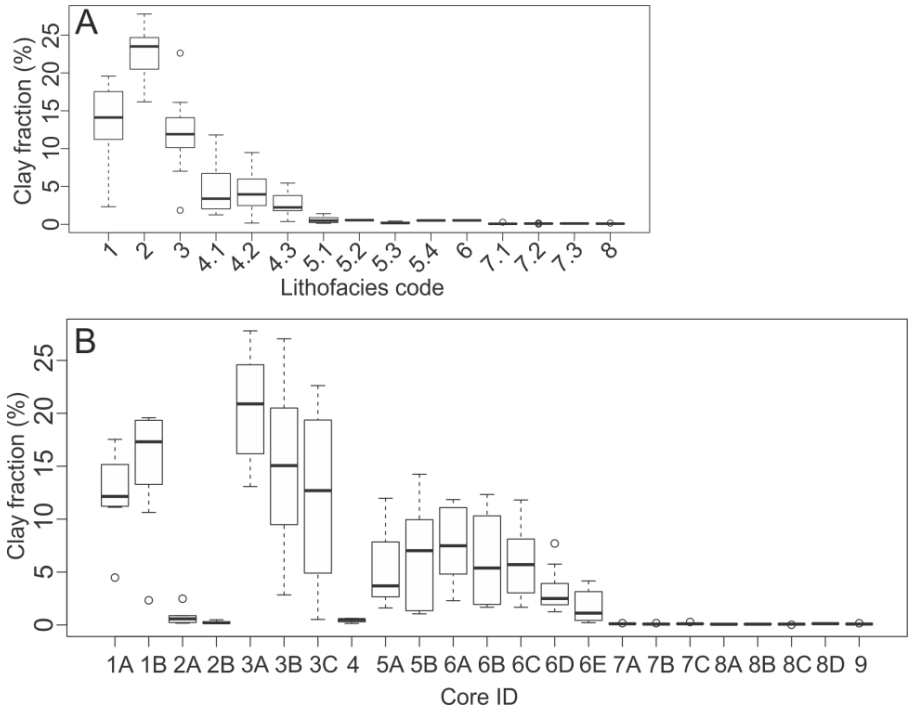

Figure 3-10 – Clay fraction abundance (%) as a function of (A) lithofacies, and (B) core ID (core position). Refer to Table 3.2 for explanation of lithofacies codes.

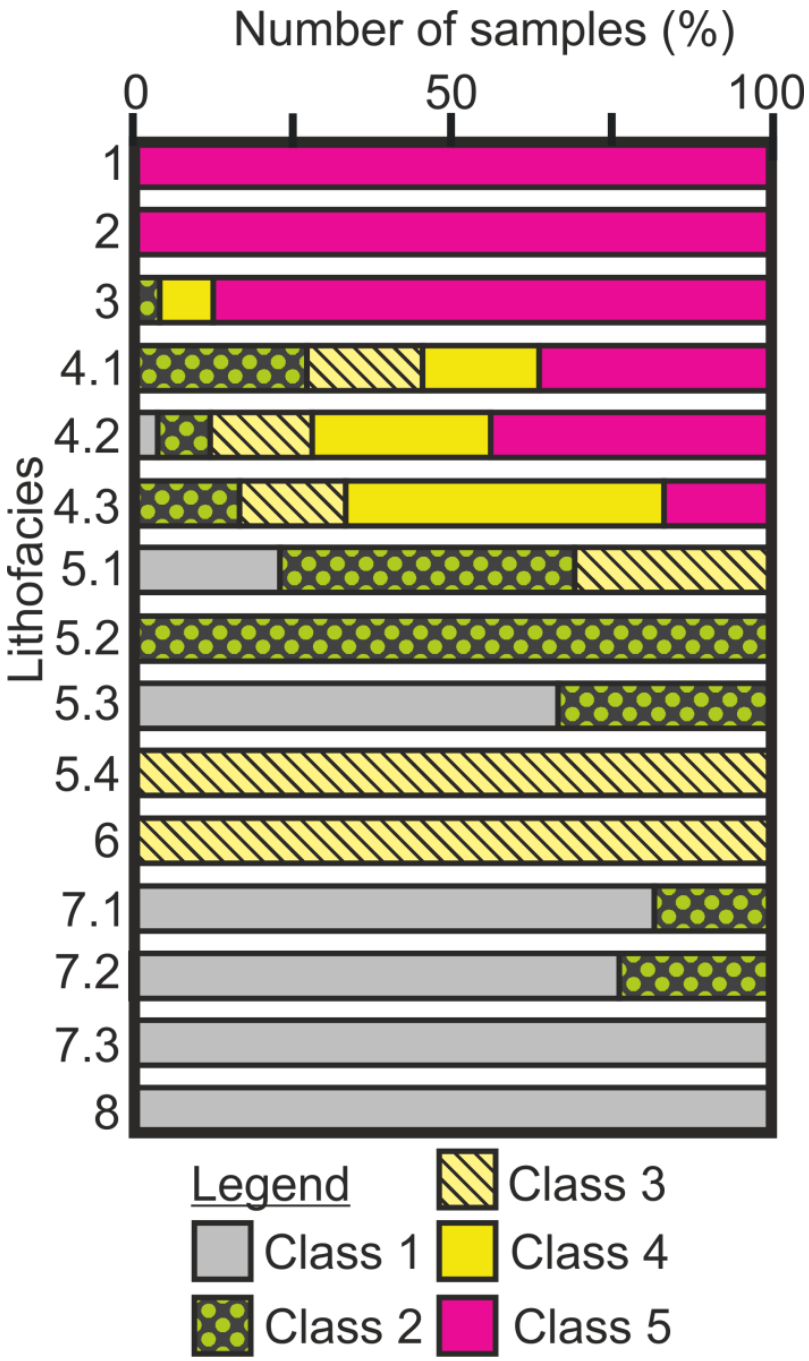

Figure 3-11 – Clay coat class (1-5) abundance in each lithofacies. Clay coat classes are defined as follows: (class 1) complete absence of attached clay coats; (class 2) less than half of the grains have a small (~ 1 to 5 %) surface area of attached clay coats; (class 3) every grain exhibits at least ~ 5 to 15 % surface area of attached clay-coats; (class 4) clay coats on every grain with the majority exhibiting extensive (~ 15 to 30 %) surface-area grain coverage; and (class 5) greater than 30 % surface area covered by clay coats on every grain (Table 3.1), after Wooldridge et al. (2017b). Refer to Table 3.2 for explanation of lithofacies codes.

Table 3.3 - Average clay fraction, clay mineral, Esquevin index, illite crystallinity and pyrite abundance in each lithofacies (standard deviation shown in brackets). As well as the weighted-average (W.av) for clay fraction, clay mineral, Esquevin index, illite crystallinity and pyrite abundance of the entire dataset. Refer to table 3.2 for explanation of lithofacies codes.

Lithofacies code	1	2	3	4.1	4.2	4.3	5.1	5.2	
number of samples (n)	18	10	24	11	25	12	13	3	
Clay fraction (%) (mean (sd))	13.68 (4.84)	22.59 (3.87)	11.97 (3.84)	4.57 (3.38)	4.25 (2.56)	2.69 (1.55)	0.6 (0.47)	0.57 (0.04)	
Chlorite index (mean (sd))	0.187 (0.19)	0.177 (0.004)	0.176 (0.010)	0.174 (0.008)	0.181 (0.013)	0.184 (0.022)	0.197 (0.19)	0.182 (0.017)	
Kaolinite index (mean (sd))	0.213 (0.020)	0.205 (0.012)	0.207 (0.012)	0.211 (0.011)	0.214 (0.010)	0.215 (0.014)	0.225 (0.009)	0.222 (0.015)	
Illite index (mean (sd))	0.562 (0.017)	0.617 (0.014)	0.608 (0.016)	0.613 (0.011)	0.600 (0.020)	0.591 (0.037)	0.577 (0.023)	0.593 (0.032)	
Smectite index (mean (sd))	0.039 (0.036)	0.001 (0.003)	0.009 (0.015)	0.001 (0.001)	0.005 (0.013)	0.01 (0.033)	0.001 (0.003)	0.000	
Esquevin index (mean (sd))	0.293 (0.026)	0.295 (0.022)	0.290 (0.021)	0.310 (0.050)	0.299 (0.024)	0.307 (0.044)	0.330 (0.057)	0.316 (0.039)	
Illite crystallinity (mean (sd))	0.226 (0.016)	0.242 (0.018)	0.246 (0.019)	0.25 (0.017)	0.25 (0.023)	0.252 (0.031)	0.268 (0.031)	0.267 (0.021)	
Pyrite (%) (mean (sd))	0.000	0.000	0.546 (0.637)	0.282 (0.462)	0.756 (1.227)	0.167 (0.389)	0.708 (1.369)	0.000	
Lithofacies code	**5.3**	**5.4**	**6**	**7.1**	**7.2**	**7.3**	**8**		**W. av**
number of samples (n)	3	1	1	11	21	6	5		
Clay fraction (%) (mean (sd))	0.25 (0.016)	0.51 (n/a)	0.52 (n/a)	0.1 (0.07)	0.1 (0.04)	0.11 (0.02)	0.09 (0.04)		5.877
Chlorite index (mean (sd))	0.187 (0.007)	0.205 (n/a)	0.214 (n/a)	0.244 (0.016)	0.238 (0.022)	0.205 (0.018)	0.235 (0.011)		0.196
Kaolinite index (mean (sd))	0.219 (0.017)	0.227 (n/a)	0.190 (n/a)	0.225 (0.020)	0.212 (0.016)	0.219 (0.013)	0.213 (0.019)		0.214
Illite index (mean (sd))	0.594 (0.022)	0.545 (n/a)	0.595 (n/a)	0.531 (0.028)	0.550 (0.028)	0.575 (0.021)	0.553 (0.025)		0.582
Smectite index (mean (sd))	0.001 (0.001)	0.230 (n/a)	0.000	0.000	0.000	0.001 (0.001)	0.000		0.009
Esquevin index (mean (sd))	0.293 (0.014)	0.308 (n/a)	0.228 (n/a)	0.309 (0.033)	0.310 (0.047)	0.328 (0.051)	0.289 (0.046)		0.303
Illite crystallinity (mean (sd))	0.313 (0.006)	0.29 (n/a)	0.26 (n/a)	0.253 (0.040)	0.254 (0.026)	0.257 (0.010)	0.294 (0.021)		0.252
Pyrite (%) (mean (sd))	0.000	0.000	0.000	0.000	0.000	0.000	0.000		0.285

Table 3.4 - Post-hoc Dunn test results (following a Kruskal-Wallis H test) reveal between which lithofacies there is a statistical difference in detrital clay coat coverage. Paired lithofacies which have a statistically significant difference in detrital clay coat coverage have significant values (z values) highlighted in bold. In contrast, pale numbers represent insignificant differences in clay coat coverage between compared lithofacies. Levels of statistical significant are coded as follows; Marginally-significant (+) when p < 0.1, Significant (*) when p < 0.05, very-significant (**) when p< 0.01, extremely significant (***) when p < 0.001. Grey values representing no significant difference when p > 0.1. Refer to Table 3.2 for explanation of lithofacies codes.

Detrital clay coat coverage													
	1	2	3	4.1	4.2	4.3	5.1	5.2	5.3	7.1	7.2	7.3
2	0	x										
3	0.47	0.39	x									
4.1	**2.23+**	1.96	1.95	x								
4.2	**2.23+**	1.84	1.9	-0.46	x							
4.3	**2.54***	**2.21+**	**2.27+**	0.22	0.74	x						
5.1	**4.74*****	**4.1*****	**4.58*****	**2.12+**	**3.03****	1.94	x					
5.2	**2.7***	**2.56***	**2.51***	1.28	1.63	1.14	-0.06	x				
5.3	**3.49****	**3.31****	**3.32****	2.03	**2.44***	1.91	0.71	0.6	x			
7.1	**5.99*****	**5.24*****	**5.89*****	**3.37*****	**4.43*****	**3.22****	1.38	0.93	0.17	x		
7.2	**7*****	**5.85*****	**7.04*****	**3.75*****	**5.27*****	**3.6****	1.49	0.91	0.11	-0.11	x	
7.3	**5.14*****	**4.7*****	**4.99*****	**3.09*****	**3.82****	**2.95***	1.42	1.04	0.35	0.27	0.38	x
8	**4.8*****	**4.43*****	**4.63*****	**2.91*****	**3.54****	**2.77***	1.33	1.01	0.34	0.25	0.35	0

Table 3.5 - Correlation (Spearman's and Pearson's correlation coefficients) between clay mineral indices, pyrite abundance, clay content and clay coat coverage as a function of depth (per core). Bold numbers represent significant correlation coefficients, whereas pale numbers represent insignificant differences, in clay mineral attributes (and pyrite) with depth. "x" represents values that were either absent or uniform with depth. Levels of statistical significant are coded as follows; Marginally-significant (+) when p < 0.1, Significant (*) when p < 0.05, very-significant (**) when p< 0.01, extremely significant (***) when p < 0.001. Grey values representing no significant difference when p > 0.1.

Core	Pearson's					Spearman's
	Chlorite index	**Illite index**	**Kaolinite index**	**Pyrite**	**Clay fraction**	**Clay coat**
1a	**-0.72***	0.20	**-0.86****	x	0.14	x
1b	**-0.95*****	-0.17	**-0.99*****	x	**0.83****	x
2a	0.63	-0.70	0.75	0.66	-0.55	-0.05
2b	0.62	-0.49	0.25	0.69	**-0.91****	**-0.93****
3a	-0.12	-0.11	0.17	x	-0.17	x
3b	-0.11	**-0.64+**	-0.76	x	**-0.63+**	-0.52
3c	0.69	0.21	-0.76	x	-0.88	-0.77
4	0.10	-0.23	0.38	x	**0.71+**	0.36
5a	-0.59	**0.73***	**-0.84****	-0.92	**0.76***	0.32
5b	-0.36	0.57	**-0.74***	-0.38	**0.92*****	**0.86****
6a	0.31	0.14	0.10	**0.81****	-0.52	-0.34
6b	**0.88****	0.13	-0.54	**0.91****	**0.87****	0.11
6c	0.22	0.21	**-0.68***	x	**-0.76***	**-0.87****
6d	-0.27	**-0.57+**	**0.79****	**0.74****	-0.45	**-0.68***
6e	0.42	-0.44	0.43	x	-0.04	0
7a	0.55	-0.59	0.58	x	0.80	-0.35
7b	0.08	0.38	-0.65	x	0.44	x
7c	**0.74+**	**-0.84***	**-0.84***	x	**0.85***	0.43
8a	-0.28	0.44	-0.46	x	**0.89***	0.35
8b	**0.94+**	0.06	-0.67	x	0.83	0.77
8c	0.07	-0.13	0.11	x	0.47	x
8d	0.29	-0.E26	0.13	x	0.50	x
9	-0.33	0.23	-0.11	x	-0.66	x

3.5.3 Mineralogy: lithofacies, bioturbation intensity and core depth

The relative abundance of the three dominant clay minerals (illite, chlorite and kaolinite) as a function of facies association (Table 3.2) is shown in Figure 3.12. All facies associations are illite-dominated (> 50 %). Illite is most abundant in facies associations 2 to 4 (> 60 %).

Facies associations 1, 7 and 8 are relatively enriched in chlorite (> 20 %). Kaolinite is relatively ubiquitous and is typically present in abundances ~ 20 to 25 % (Fig. 3.12).

The relative abundance of chlorite, kaolinite, illite, and smectite, as well as Esquevin Indices, illite crystallinity and the abundance of pyrite in each lithofacies are summarised in Table 3.3. The range, upper and lower quartile, and median for each specific clay mineral indices as a function of lithofacies are presented in Figure 3.13. The range, upper and lower quartile, and median for Esquevin index, illite crystallinity and pyrite, as a function of lithofacies is presented in Figure 3.14.

Analysis Of Variance (ANOVA) test results reveal chlorite, illite, kaolinite and smectite abundance is significantly different ($p < 0.001$) between lithofacies. The multi-comparison, post-hoc Tukey HSD test results reveal between which individual lithofacies there are statistical differences (Table 3.6).

The range, upper and lower quartile, and median of clay mineral and Esquevin indices, as well as illite crystallinity and pyrite abundance as a function of core position are represented in Figures 3.15 and 3.16. Pearson's test results show there is no consistent relationship between core depth and the relative abundance of chlorite, illite and kaolinite (Table 3.5). Pyrite abundance typically increases with depth in central basin estuarine cores (6A, 6B and 6C); Pearson's correlation coefficients range from 0.74 to 0.91 ($p < 0.001$) (Table 3.5).

The relationship between bioturbation index and the relative abundance of chlorite, illite and kaolinite are presented in Figure 3.17. Chlorite typically decreases with an increase in bioturbation intensity ($r = - 0.62$, $p < 0.001$), illite abundance broadly increases with an increase in bioturbation intensity ($r = 0.49$, $p < 0.001$) and kaolinite abundance shows little relationship with bioturbation intensity ($r = -0.18$, $p < 0.05$).

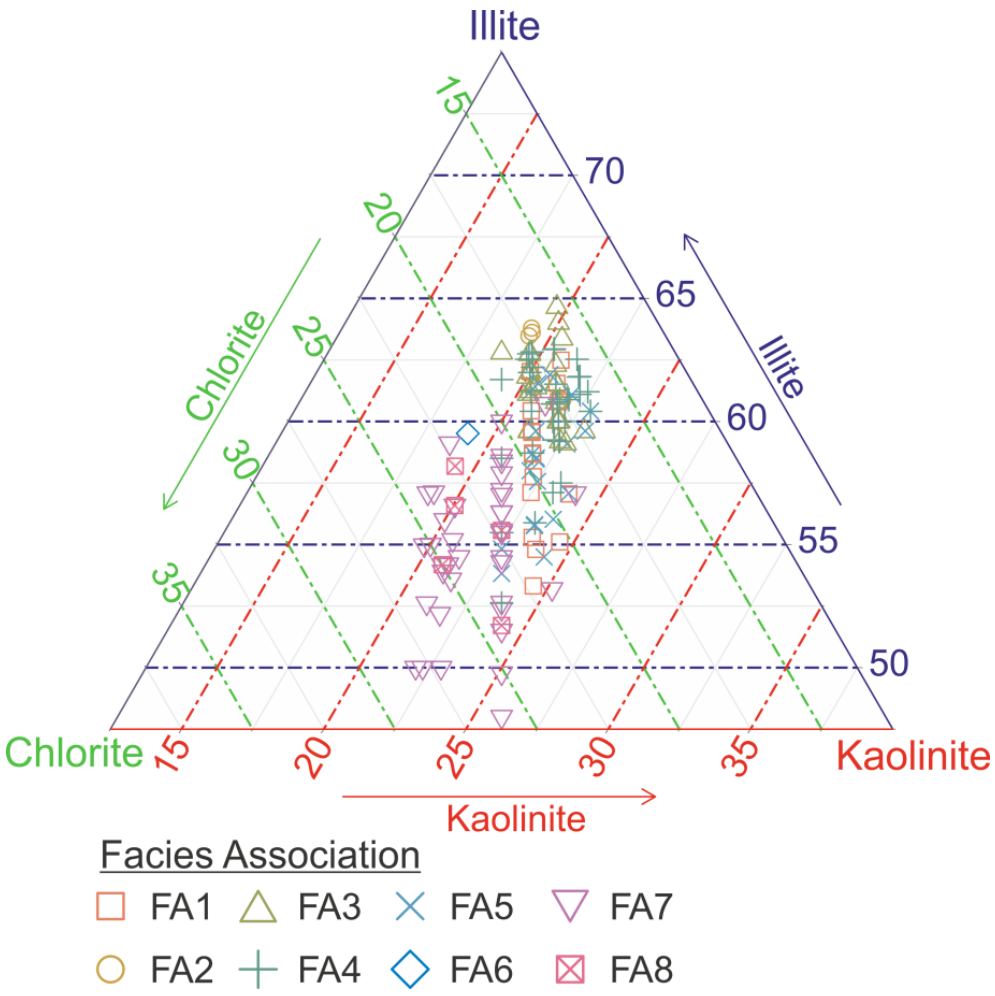

Figure 3-12 – Relative clay mineral abundance (illite, chlorite, kaolinite) as a function of facies association. Facies associations are labelled accordingly: FA1, floodplain; FA2, salt marsh; FA3, mud flat; FA4, mixed-flat and thinly-bedded deposits; FA5, low-amplitude tidal dunes and tidal bars 5; FA6, glacial-outwash; FA7, tidal inlet and foreshore; and FA8, coastal spit.

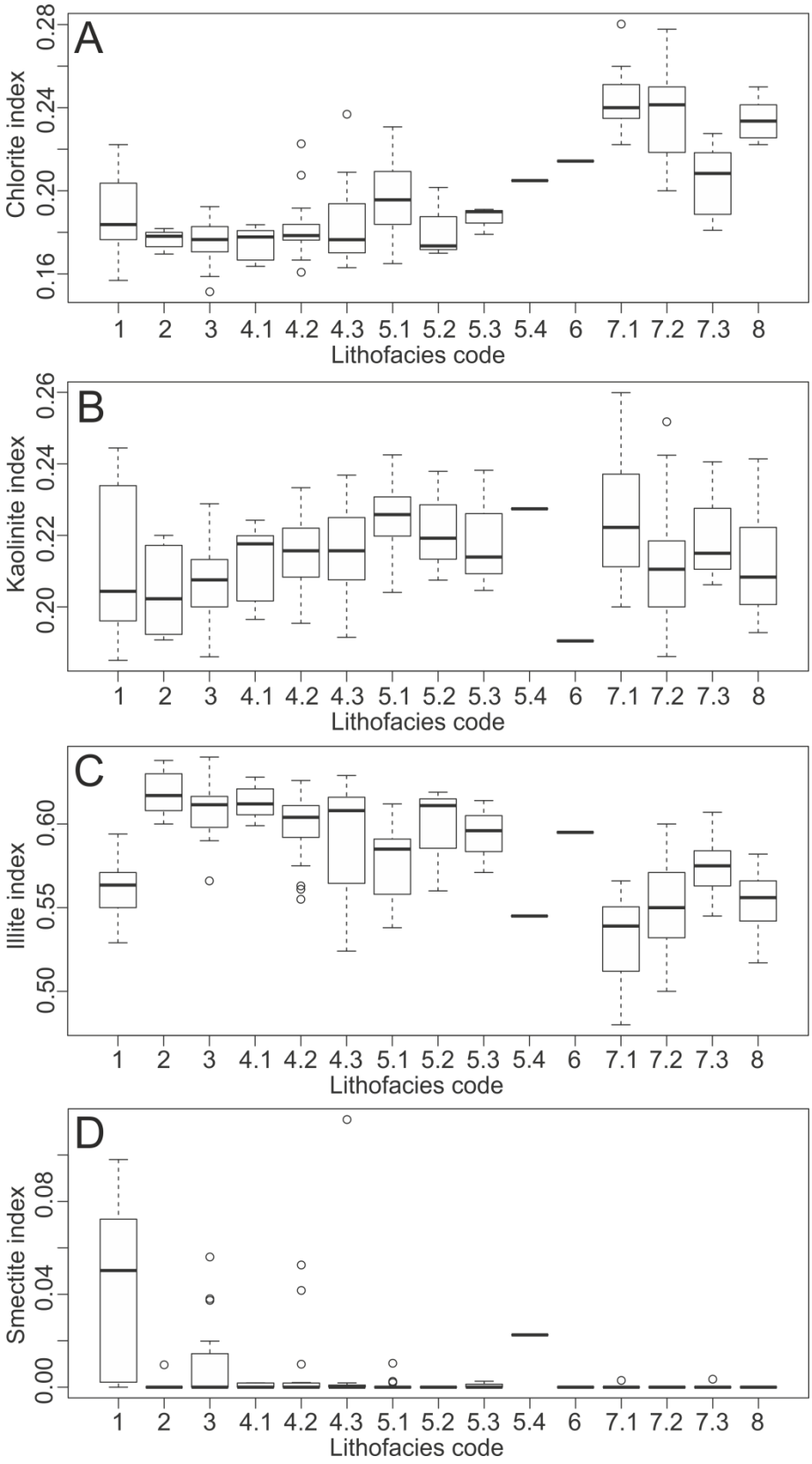

Figure 3-13 – Relative clay mineral abundance as a function of lithofacies (A) chlorite index, (B) kaolinite index, (C) illite index, and (D) smectite index. Refer to Table 3.2 for explanation of lithofacies codes.

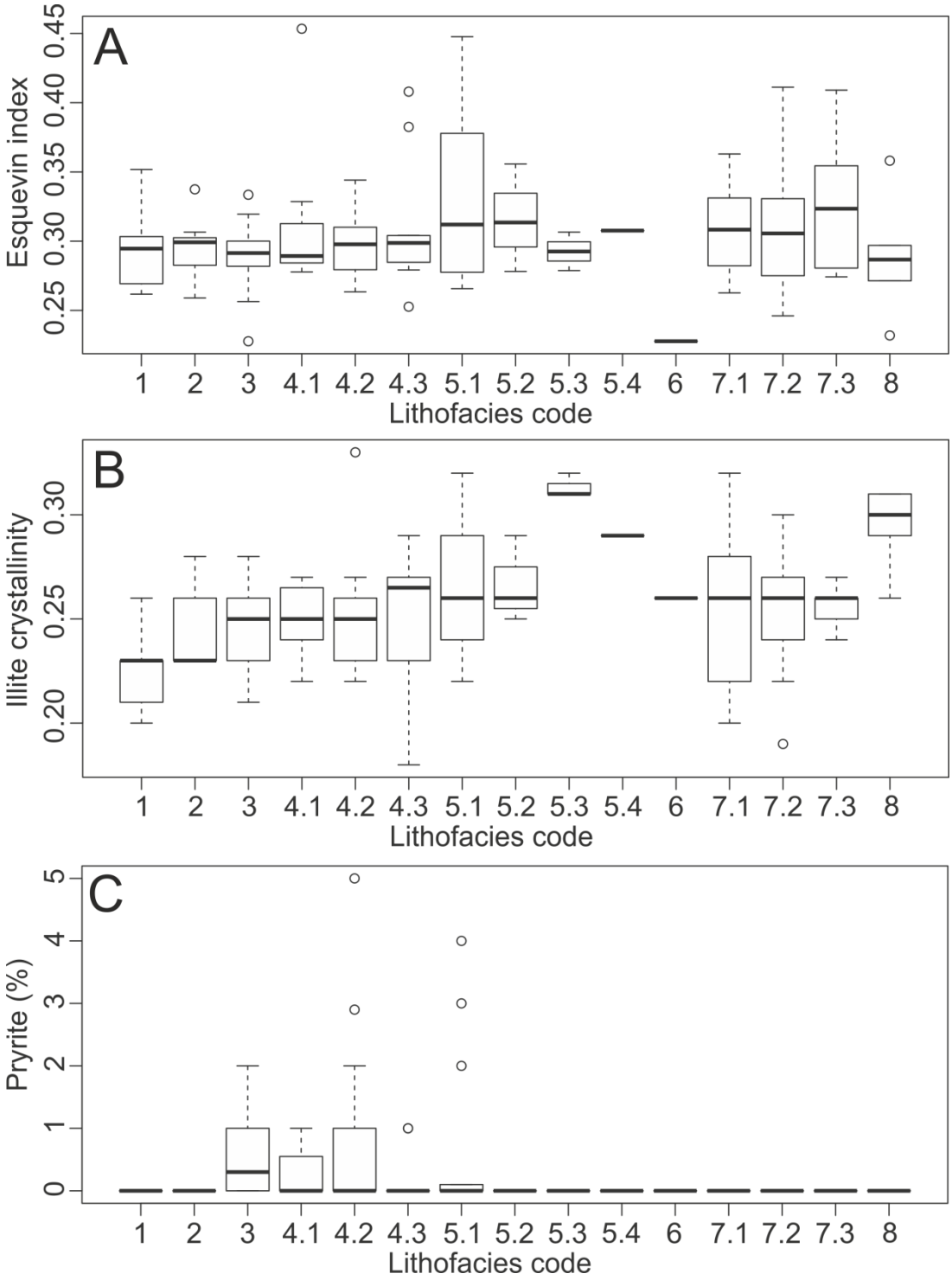

Figure 3-14 – Variation in illite chemistry, crystallinity and pyrite abundance as a function of lithofacies (A) Esquevin index (B), illite crystallinity and (C) pyrite abundance. Refer to Table 3.2 for explanation of lithofacies codes.

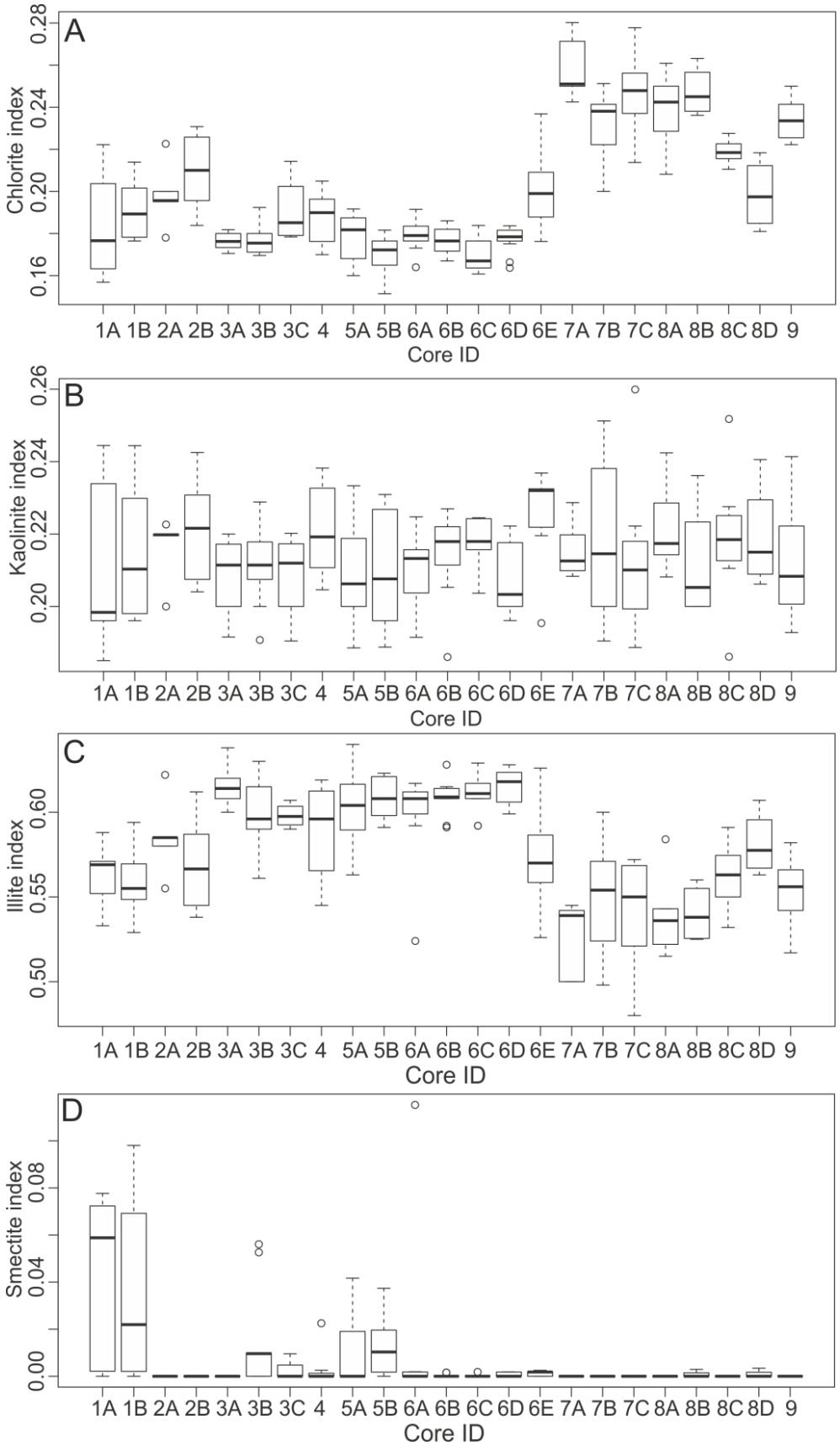

Figure 3-15 – Relative clay mineral abundance as a function of geographic core-position (core ID) (A) chlorite index, (B) kaolinite index, (C) illite index, and (D) smectite index.

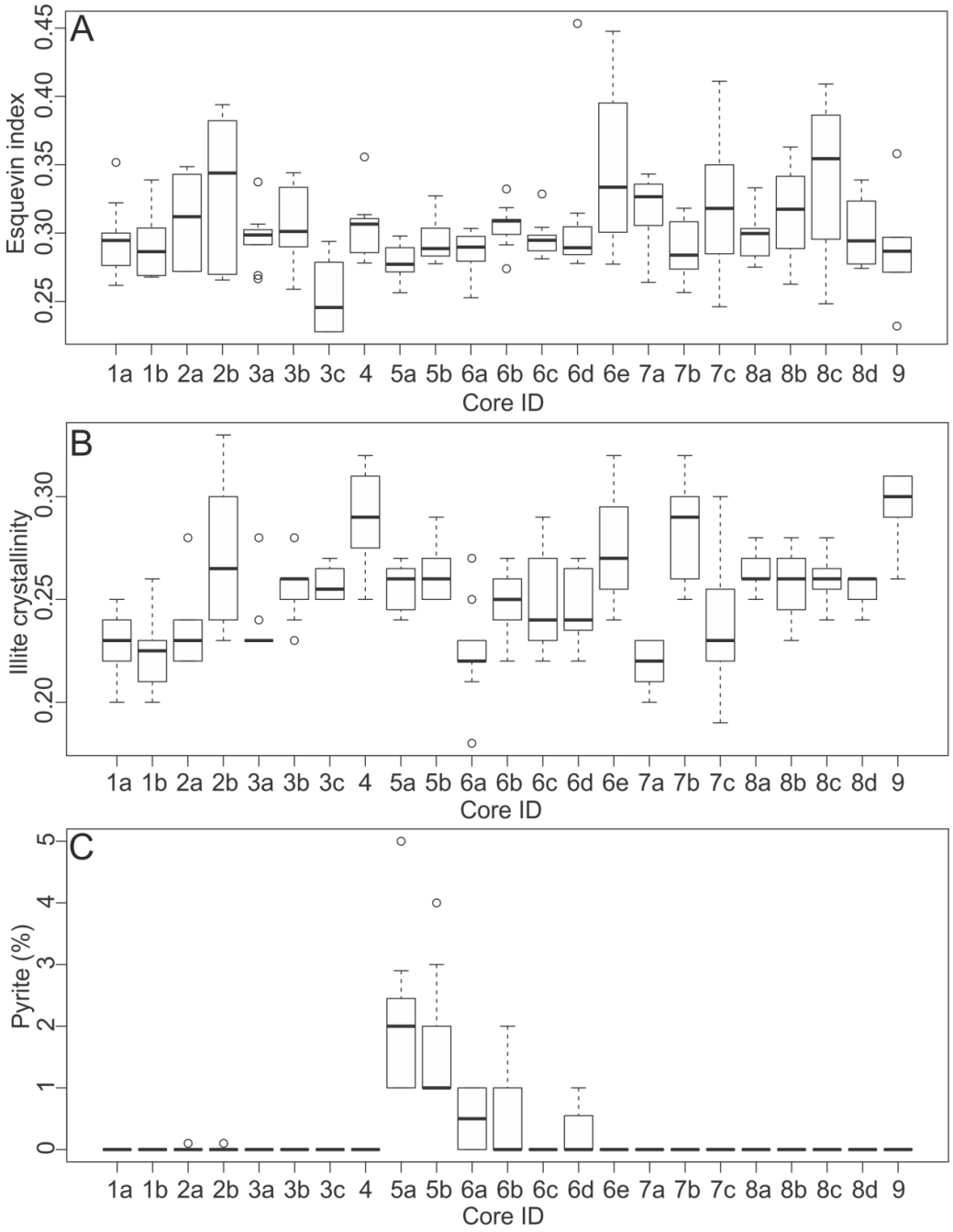

Figure 3-16 – Variation in illite chemistry, crystallinity and pyrite abundance as a function of geographic core-position (core ID) (A) Esquevin index, (B), illite crystallinity and (C) pyrite abundance.

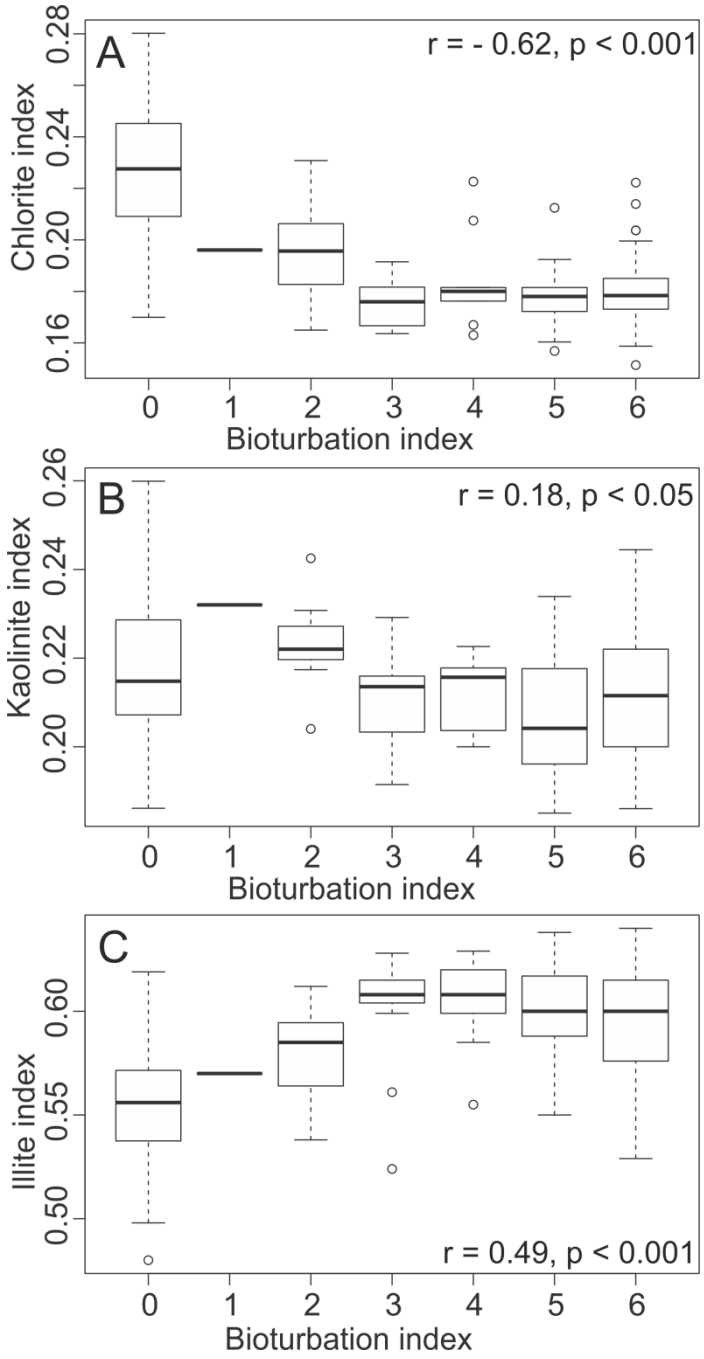

Figure 3-17 – Relationship between bioturbation index, after Taylor and Goldring (1993) and relative clay mineral abundance; (A) chlorite index, (B) kaolinite index, and (C) illite index. Spearman's correlation coefficients (r) between bioturbation index and clay mineral indices are presented, including the level of significance (p).

Table 3.6 - Post-hoc Tukey HSD test results (following an ANOVA test) revealing between which lithofacies there is a statistical difference in chlorite, illite, kaolinite and smectite abundance. Significant values (z values) are highlighted in bold. Bold numbers represent significant differences; pale numbers represent insignificant differences, in clay mineral indices between compared depositional environments. Levels of statistical significant are coded as follows; Marginally-significant (+) when p < 0.1, Significant (*) when p < 0.05, very-significant (**) when p< 0.01, extremely significant (***) when p < 0.001. Grey values representing no significant difference when p > 0.1. Refer to Table 3.2 for explanation of lithofacies codes.

Chlorite index												
	1	2	3	4.1	4.2	4.3	5.1	5.2	5.3	7.1	7.2	7.3
2	-0.01	x										
3	-0.01	0	x									
4.1	-0.01	0	0	x								
4.2	-0.01	0	0.01	0.01	x							
4.3	0	0.01	0.01	0.01	0	x						
5.1	0.01	0.02	0.02	**0.02***	0.02	0.01	x					
5.2	0	0.01	0.01	0.01	0	0	-0.02	x				
5.3	0	0.01	0.01	0.01	0.01	0	-0.01	0	x			
7.1	**0.06*****	**0.07*****	**0.07*****	**0.07*****	**0.06*****	**0.06*****	**0.05*****	**0.06*****	**0.06*****	x		
7.2	**0.05*****	**0.06*****	**0.06*****	**0.06*****	**0.06*****	**0.05*****	**0.04*****	**0.06*****	**0.05*****	-0.01	x	
7.3	0.02	**0.03***	**0.03****	**0.03***	**0.02+**	0.02	0.01	0.02	0.02	**-0.04*****	**-0.03****	x
8	**0.05*****	**0.06*****	**0.06*****	**0.06*****	**0.05*****	**0.05****	**0.04****	**0.05****	**0.05****	-0.01	0	0.03
Illite index												
	1	2	3	4.1	4.2	4.3	5.1	5.2	5.3	7.1	7.2	7.3
2	**0.06*****	x										
3	**0.05*****	-0.01	x									
4.1	**0.05*****	0	0.01	x								
4.2	**0.04*****	-0.02	-0.01	-0.01	x							
4.3	**0.03*****	-0.03	-0.02	-0.02	-0.01	x						
5.1	0.02	**-0.04****	**-0.03****	**-0.04****	-0.02	-0.01	x					
5.2	0.04	-0.02	-0.01	-0.02	0	0.01	0.02	x				
5.3	0.03	-0.02	-0.01	-0.02	-0.01	0	0.02	0	x			
7.1	**-0.03***	**-0.09*****	**-0.08*****	**-0.08*****	**-0.07*****	**-0.06*****	**-0.05*****	**-0.07*****	**-0.06*****	x		
7.2	-0.01	**-0.07*****	**-0.06*****	**-0.06*****	**-0.05*****	**-0.04*****	**-0.03*****	**-0.05+**	-0.04	0.02	x	
7.3	0.01	**-0.04***	**-0.03+**	**-0.04+**	-0.02	-0.02	0	-0.02	-0.02	**0.04***	0.03	x
8	-0.01	**-0.06*****	**-0.06*****	**-0.06*****	**-0.05*****	**-0.04****	**-0.02+**	-0.04	-0.04	0.02	0	-0.02
Kaolinite index												
	1	2	3	4.1	4.2	4.3	5.1	5.2	5.3	7.1	7.2	7.3
2	-0.01	x										
3	-0.01	0	x									
4.1	0	0.01	0	x								
4.2	0	0.01	0.01	0	x							
4.3	0	0.01	0.01	0	0	x						
5.1	0.01	**0.02+**	**0.02***	0.01	0.01	0.01	x					
5.2	0.01	0.02	0.01	0.01	0.01	0.01	0	x				
5.3	0.01	0.01	0.01	0.01	0	0	-0.01	0	x			
7.1	0.01	**0.02+**	**0.02***	0.01	0.01	0.01	0	0	0.01	x		
7.2	0	0.01	0	0	0	0	-0.01	-0.01	-0.01	-0.01	x	
7.3	0.01	0.01	0.01	0.01	0	0	-0.01	0	0	-0.01	0.01	x
8	0	0.01	0.01	0	0	0	-0.01	-0.01	-0.01	-0.01	0	-0.01
Smectite index												
	1	2	3	4.1	4.2	4.3	5.1	5.2	5.3	7.1	7.2	7.3
2	**-0.04*****	x										
3	**-0.03*****	0.01	x									
4.1	**-0.04*****	0	-0.01	x								
4.2	**-0.03*****	0	0	0	x							
4.3	**-0.03****	0.01	0	0.01	0.01	x						
5.1	**-0.04*****	0	-0.01	0	0	-0.01	x					
5.2	**-0.04***	0	-0.01	0	0	-0.01	0	x				
5.3	**-0.04***	0	-0.01	0	0	-0.01	0	0	x			
7.1	**-0.04*****	0	-0.01	0	0	-0.01	0	0	0	x		
7.2	**-0.04*****	0	-0.01	0	0	-0.01	0	0	0	0	x	
7.3	**-0.04*****	0	-0.01	0	0	-0.01	0	0	0	0	0	x
8	**-0.04****	0	-0.01	0	0	-0.01	0	0	0	0	0	0

3.5.4 Clay mineral abundance as a function of grain size fraction

The relative abundance of clay minerals (chlorite, illite, kaolinite and smectite) for each grain size separate is shown in Figure 3.18. Chlorite abundance increases with an increase in grain size (Fig. 3.18). Illite and kaolinite abundances decrease with an increase in grain size (Fig. 3.18). Smectite is typically restricted to sediment fractions < 15 µm.

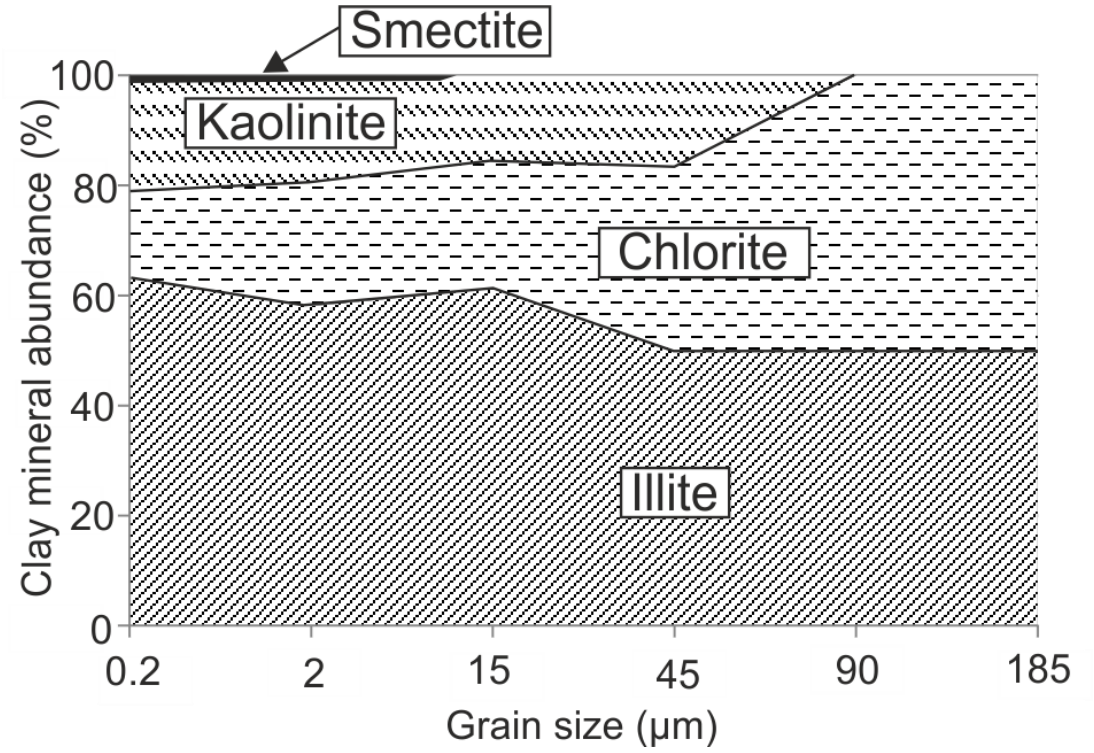

Figure 3-18 – Relative abundance of chlorite, illite, kaolinite and smectite as a function of grain-size separate, derived from a whole surface (< 2 cm) sediment sample from the central basin (Saltcoats).

3.5.5 Mineralogy of quaternary drift-deposits

X-ray diffraction analysis was performed on drift deposits exposed in the cliff sections in the inner-Esk (Gosforth Glaciogenic Formation and Seascale Glaciogenic Formation), and from Ravenglass Till (part of the Seascale Glaciogenic Formation) exposed as knolls throughout the estuary. XRD analyses show the fine fraction (< 2 µm) of the Ravenglass Till (part of the Seascale Glaciogenic Formation) is dominated by well-crystalline, Fe-Mg-enriched illite (illite index, 0.62; Esquevin index 0.28; illite crystallinity, 0.24), and has a low to moderate abundance of kaolinite (kaolinite index, 0.21) and chlorite (chlorite index, 0.17). XRD-analyses show the fine fraction (< 2 µm) of the Fishgarth Wood Till Member (part of the Gosforth Glaciogenic Formation) is dominated by Al-enriched illite (illite index, 0.61; Esquevin index 0.43; illite crystallinity, 0.21), relatively enriched in kaolinite (kaolinite index, 0.31), and depleted in chlorite (chlorite index, 0.08).

3.6 DISCUSSION

3.6.1 Estuarine facies: nature and organization

It is challenging to discriminate between tide-dominated and wave-dominated estuaries based on outcrop and subsurface data, due to the typical paucity of data (i.e. limited spatial resolution) (Davis and Dalrymple, 2011). As a result many reconstructions are likely to adhere too strictly to either wave- or tide-dominated models (Davis and Dalrymple, 2011). Consequently, mixed-energy estuarine systems such as Ravenglass (this study) and Gironde (Allen and Posamentier, 1994) are likely to be under-reported in the stratigraphic record.

The dominant controls on the distribution of lithofacies in the Ravenglass Estuary are in broad agreement with those reported in wave- and tide-dominated end-member estuarine models detailed by Dalrymple et al. (1992). The Drigg and Eskmeals coastal-spits, diagnostic of wave-dominated estuaries (Dalrymple et al., 1992), provide shelter to the inner estuary and central basin from wave-action. As a result the spits have led to a relatively quiescent central-basin and the deposition of mud flats (facies association 3; Table 3.2) and mixed-flats and thinly bedded heterolithic deposits (facies association 4; Table 3.2). Strong tidal-currents, diagnostic of tide-dominated estuaries (Dalrymple et al., 1992), pass beyond the low-energy central basin into the upper estuary leading to the deposition of low-amplitude dunes and tidal bars (facies association 5; Table 3.2). Tidal currents and wave-action have led to the deposition of a suite lithofacies, diagnostic of tidal inlet and outer estuarine sub-environments (facies associations 7 and 8; Table 3.2). The lithofacies scheme presented in this study may be used, by analogy, in mixed-energy estuaries; however, as with previously published facies models, local variability may cause departure from the generalised descriptions.

3.6.2 Detrital clay coats: origin and distribution

Clay coat distribution patterns reported in surface sediment (< 2 cm) (Wooldridge et al., 2017a; Wooldridge et al., 2017b) and near-surface sediment (this study; < 1 m) in the Ravenglass Estuary are consistent with those reported in the Anllóns Estuary, Spain (Dowey et al., 2017) and the Brazos River, Texas, USA (Matlack et al., 1989). The extent of detrital clay coat coverage in the near-surface sediment of the Ravenglass Estuary is directly related to the abundance of clay fraction in the sediment ($r = 0.92$, $p < 0.001$), which is at least partly controlled by estuarine hydrodynamics and thus predictable as a function of lithofacies (Table 3.4; Fig. 3.11). In agreement with Matlack et al. (1989), detrital clay coats coverage is absent or negligible in high-energy, coarser-grained, outer estuarine depositional

environments (e.g. foreshore, tidal inlet and backshore) due to paucity of clay size material (minimum-suspended load). In contrast, detrital clay coat coverage is most extensive in low-energy, finer-grained, inner estuary and central basin depositional environments (e.g. mud-flats and mixed-flats), due to an abundance of clay size material that was deposited during slack-water conditions. Furthermore, diatoms are most abundant in the inner estuary and central basin (Wooldridge et al., 2017a); diatoms have been reported to physically attach clay size material to sand grain surfaces by adhesive extracellular polymeric substances (biofilms) in the top few millimetres of the sediment surface (Wooldridge et al., 2017a).

Clay coats have previously been reported to originate from the mechanical-infiltration or illuviation of clay-laden waters in sediment (Buurman et al., 1998; Matlack et al., 1989; Moraes and De Ros, 1990; Pittman et al., 1992; Wilson, 1992). Infiltration may occur on a centimetre- to metre-scale in marginal marine depositional environments (Santos et al., 2012), and therefore, may lead to the over-printing of surface clay coat distribution patterns in the near-surface. However, the absence of a systematic increase or decrease in clay content with depth (Table 3.5), suggests that mechanical infiltration has not occurred. It is acknowledged that, in landscapes with a strong lateral groundwater movement, transport of clay may be oblique (Buurman et al., 1998), and may thus cross-cut depositional facies (Morad et al., 2010). However, in the Ravenglass Estuary, depositional-environments that are relatively clay-depleted at the surface (< 1 %), and have the same lithofacies association down to 1 m, and remain depleted in clay content throughout (Fig.3.10). The absence of a systematic increase or decrease in clay content with depth (Table 3.5) suggests that mechanical infiltration has not occurred in significant quantities to over-print surface detrital clay coat distribution patterns as reported by Wooldridge et al. (2017a). Furthermore, in an experimental study by Matlack et al. (1989), which showed clay coats may develop through mechanical infiltration, relatively high percolation speeds were achieved for the suspended clays (through the sand-pack columns due to free gravity induced flow) which is unrepresentative of estuarine depositional environments (Buurman et al., 1998). For example, under natural conditions, reduced flow-velocities will lead to minerals flocculating, which are then deposited as mud-drapes, which are seen to clog the upper pore throats of the sediment and inhibit the infiltration of clay-laden water further into the sediment subsurface (e.g. Figures 3.5.2A and 3.5.2B). It is noteworthy that clay flocculation is especially common in marginal-marine systems, due to increased salinity at the fluvial-marine interface (Chamley, 1989). Furthermore, clay-rich layers create impermeable barriers in tidal-flats which form a baffle to mechanical infiltration, often resulting in the formation of fluidised-mud layers at the surface.

Experimental studies have shown that detrital clay coats may develop through the direct ingestion and excretion of sediment by *Arenicola marina* (lugworms) (Needham et al., 2005; Worden et al., 2006). However, *Arenicola marina* are restricted to a limited environmental grain-size niche in the Ravenglass Estuary, typically 88 to 177 µm (Wooldridge et al., 2017b), and are not present in mud-flats, where clay coats are most abundant (Fig. 3.11). Therefore, in agreement with distribution patterns presented by Wooldridge et al. (2017b), clay coat distribution patterns in near-surface sediment also do not appear to be determined exclusively by the bioturbation of *Arenicola marina*. However in contrast to Wooldridge et al. (2017b) , this study measures the bioturbation signal of all fauna, and not just the castings developed by *Arenicola marina*; there is a strong correlation between bioturbation index (signal from all micro- and macro-fauna) and clay coat coverage ($r = 0.84$, $p < 0.001$). As reported by Wooldridge et al. (2017b), it may be possible that other estuarine macro- or micro-organisms may provide a mechanism of clay coat formation. *Corophium volutator* (which create densely spaced U-shaped burrows, up to 5 cm deep) are confined to mud-flats and mixed-flats in the Ravenglass Estuary (Kelly et al., 1991), and thus correspond to high-degrees of clay coat coverage. Previous studies have also reported that *Corophium volutator* can occur in abundance up to 140,000 m^{-3} in estuarine mudflats and salt marsh (Gerdol and Hughes, 1994). However, despite the striking similarity between bioturbation intensity (primarily through *Corophium volutator* activity in mud- and mixed-flats) and detrital clay coat coverage, *Corophium volutator* are unlikely to have formed clay coats. First, *Corophium volutator* are reported to increase the water content of sediment and thus decrease shear strength and promote erosion and winnowing of sediment (Gerdol and Hughes, 1994), which are all likely to remove clay coats. Second, *Corophium volutator* are reported to consume diatoms in marginal-marine sediments (Gerdol and Hughes, 1994; Underwood and Paterson, 1993), which are known to adhere clay-size material to sand grain surfaces via biofilms (Wooldridge et al., 2017a). As a result, despite there being a strong correlation between macro-faunal bioturbation intensity (primarily by *Corophium volutator* in clay-rich depositional environments with the most extensive detrital clay coat coverage) and detrital clay coat coverage, *Corophium volutator* may in fact reduce detrital clay coat coverage, through the reduction of diatom populations. Instead, the strong correlation is more likely driven by (i) the absence of both clay coats and bioturbation in outer estuarine sediment, (ii) a high abundance of *Corophium volutator* and clay coats in mud-flats.

In summary, detrital clay coat distribution patterns in estuarine near-surface (< 1 m) sediment are likely controlled by processes active during deposition and in the top few centimetres of the primary deposition environment; the physical sorting of sediment by grain size via estuarine hydrodynamics, and the adhesion of clay to sand grain surfaces by biofilms

excreted by diatoms (Wooldridge et al., 2017a). Thus, detrital clay coat distribution patterns in surface sediment (< 2 cm) in the Ravenglass Estuary are not over-printed by post-depositional processes.

3.6.3 Clay mineralogy: origin and controls on distribution

To better predict the distributions of clay minerals in sandstones reservoirs, it is necessary to understand the fundamental controls on clay mineral type and occurrence in the primary depositional environment. The distributions of chlorite, illite, kaolinite and smectite are not homogenous in the Ravenglass Estuary (Figs. 3.12 and 3.13). In this section, the primary controls on the clay mineral assemblage and clay mineral distribution patterns in the Ravenglass Estuary are discussed.

3.6.3.1 Origin of clay minerals in the Ravenglass Estuary

The proportions of illite, chlorite and kaolinite in the Ravenglass Estuary are approximately 3:1:1 with a trace quantity of smectite (average smectite index of 0.009; maximum smectite index of 0.09) (Table 3.3; Figs. 3.13 to 3.16). Illite, the dominant clay mineral in the Ravenglass Estuary, has an average Esquevin index of 0.30 and illite crystallinity of 0.25, representing relatively well-crystalline and Fe-Mg-rich illite (Esquevin, 1969; Kübler, 1964).

Potential sources of clay minerals in the Ravenglass Estuary include: i) fluvial drainage of Paleozoic and Triassic bedrock and Quaternary-drift, ii) the landward-displacement of littoral-zone sediment, iii) internal erosion of Ravenglass Till that is exposed as knolls throughout the estuary and in proximal cliff-sections.

The primary source of chlorite is probably the Eskdale Granite and Borrowdale Volcanic Group, because intense chloritization of mafic silicates has been reported in the Eskdale Granite (Moseley, 1978; Quirke et al., 2015; Young et al., 1986) and widespread chloritization of pyroxene has been reported in the Borrowdale Volcanic Group (Quirke et al., 2015).

The provenance of illite in the Ravenglass Estuary has been established using Esquevin Indices. Illite in this estuary is relatively well-crystalline and Fe-Mg-rich (Fig. 3.14A-B and 3.16A-B), this is typical of cold-climatic conditions that favour mechanical weathering allowing the primary white mica to retain its Fe-Mg-rich composition and original high degree of crystallinity (Chamley, 1989). The chemical composition of illite in estuarine sediment (average Esquevin index of 0.30) closely compare to values calculated for the Ravenglass Till (average Esquevin index of 0.28). The evidence therefore suggests that the dominant source of illite in the Ravenglass Estuary is the Ravenglass Till, which is relatively

well exposed throughout the estuary and in the drainage basin. Al-rich illite, which is primarily found in outer estuarine sediment, is characteristic of chemically-weathered rocks that have lost Fe and Mg (Chamley, 1989). Al-rich illite may reflect the widespread alteration of feldspars to fine-grained aluminous clay-minerals (i.e. illite and kaolinite), which has been reported in the Eskdale Granite (Quirke et al., 2015; Simpson, 1934; Young et al., 1986) and the Borrowdale Volcanic Group (Quirke et al., 2015).

Kaolinite may have been derived from the chemical weathering of any silicate minerals in the hinterland or in the Ravenglass Estuary basin. However, it is noteworthy that the glaciofluvial and glaciolacustrine sediments of the Fishgarth Wood Till Member (Fig. 3.3B) are relatively enriched in kaolinite (kaolinite index, 0.31) and so may provide a dominant source of kaolinite in the estuarine sediment.

Smectite, which is of minor abundance in the Ravenglass Estuary (average smectite index of 0.009), is typical of weathering from semi-arid continental sources, that have been subjected to the initial stages of chemical weathering (Salem et al., 2000). In addition, weathering will only result in smectite, rather than other clay minerals, if the excess metal cations and silica cannot be flushed from the aqueous geochemical system, for example, in low-lying topography with poor drainage and stagnant groundwater conditions (McKinley et al., 2003). In contrast, in flowing and active groundwater systems, loss of metal cations is easily achieved, resulting in the possibility of more advanced chemical weathering and reduced preservation potential of smectite minerals (McKinley et al., 2003). As a result, smectite is most abundant, but still of relatively minor significance (smectite index of 0.09), in floodplain sediments of the River Esk (Fig. 3.15D); analogous to the formation of dioctahedral smectite downslope of weathered granitic rocks of the French Armorican Massif (Aoudjit et al., 1995).

3.6.3.2 Clay mineral distribution: estuarine hydrodynamics

Similar to estuaries worldwide (Dalrymple et al., 1992), estuarine hydrodynamics has a profound influence on the nature and organization of lithofacies in the Ravenglass Estuary. Clay minerals may be physically sorted, due to grain size variation, in marine environments during transport, as reported in Atlantic Ocean sediment influenced by the Amazon River (Gibbs, 1977). This study has shown that hydrodynamics processes appear to have exerted a strong control on the distribution of lithofacies and specific clay minerals in the Ravenglass Estuary (Figs. 3.12 and 3.13; Table 3.6).

Chlorite abundance typically increases with an increase in sediment grain size (Fig. 3.18). As a result, chlorite is relatively most abundant in high-energy and the coarser grained depositional environments, i.e., outer estuarine sediment (lithofacies 7.1, 7.2 and 8; Fig.

3.13A) and in some inner estuarine and central basin low-amplitude dune sediments (lithofacies 5.1; Fig. 3.13A). It is noteworthy that chlorite abundance appears to reduce toward the mean low water line in foreshore sediment (in lithofacies 7.3; Fig. 3.13A). Floodplain sediments are some of the finest-grained sediments in the estuary basin and could be expected to be chlorite-depleted (Fig. 3.18). However, floodplain sediments are relatively enriched in chlorite (chlorite index up to 0.25; Fig. 3.13A); this may reflect the fluvial deposition of chlorite-enriched River Esk sediment which drains the chloritized Eskdale Granite.

In the Ravenglass Estuary, illite is most abundant in finer-grained sediment (Fig. 3.18), and therefore illite-enrichment occurs in sediment that is deposited under relatively quiescent conditions at the margin of the inner estuary and central basin (Fig. 3.13C). However, estuarine hydrodynamics does not only appear to control illite abundance, but also segregates illite by chemical composition and crystallinity (Figs. 3.14A and 3.14B). Well-crystalline Fe-Mg-rich illite is most abundant in finer-grained sediment, at the margin of the inner estuary and central basin. In contrast, poorly-crystalline Al-rich illite is most abundant in relatively high-energy inner-estuarine and central basin lithofacies, such as low-amplitude dunes, as well as in outer estuarine sediment. Fe-Mg-rich illite may be finer-grained than Al-rich illite due to Fe-Mg-rich illite being derived from sediment which has undergone extensive sub-glacial-comminution (Ravenglass Till). Therefore, it is here speculated that the transport history of illite (intensity of abrasion and thus grain size) and estuarine hydrodynamics may also govern illite-type distribution in the Ravenglass Estuary.

Kaolinite has been reported to flocculate at low salinity in comparison to other clay minerals, and therefore is suggested to increase in abundance relative to other clay minerals at the fluvial-marine interface (Whitehouse et al., 1960). Kaolinite is also reported to have a faster aggregation rate than illite, and is therefore deposited upstream relative to illite (Edzwald and O'Mella, 1975). However, in the Ravenglass Estuary there is no evidence for enrichment of kaolinite at the head of the estuary (Figs. 3.13B and 3.15B). Instead, kaolinite abundance is relatively homogenous throughout the Ravenglass Estuary. Differential settling therefore does not appear to exert a strong control on kaolinite distribution in the Ravenglass Estuary. The effect of differential settling may be dampened by strong tidal-currents, wind, and a short-estuarine length promoting intense estuarine mixing resulting in a less well-defined fluvial-marine interface.

Smectite is present in the hinterland and in cores in the River Esk floodplain; however smectite is present in negligible abundance in Ravenglass estuarine sediments. There are two possible scenarios which may explain the paucity of smectite in estuarine sediments. First,

smectite is typically present in the finest of all sediment fractions (Fig. 3.18), and is therefore likely to remain in suspension during transport, and so pass through the Ravenglass Estuary and be deposited offshore (Edzwald and O'Mella, 1975; McKinley et al., 2003; Worden and Burley, 2003). Second, ground-water flushing has previously been reported to minimise the development and accumulation of smectite (McKinley et al., 2003). It is here speculated that estuaries may not be sites of preferential smectite accumulation, since metal cations (essential for smectite) can be flushed from estuarine sediment by twice-daily tides and meteoric groundwater flow through estuarine sediment.

3.6.3.3 Clay mineral distribution: early-diagenesis

Both physico-chemical processes (Griffin and Ingram, 1955; Grim and Johns, 1954; Nelson, 1960; Powers, 1957) and biologically-mediated early diagenesis (McIlroy et al., 2003; Needham et al., 2006; Needham et al., 2004; Needham et al., 2005; Worden et al., 2006) have been suggested as potential controls on clay mineral distribution patterns in sedimentary environments.

The direct ingestion and excretion of sediment by *Arenicola Marina* has been shown to lead to clay mineral alteration and formation under laboratory conditions, due to the chemical conditions in their guts (McIlroy et al., 2003; Needham et al., 2004; Worden et al., 2006). This study has specifically focused on whether bioturbation may have affected clay mineral distribution patterns in the Ravenglass Estuary. Bioturbation intensity recorded in this study primarily reflects sediment modification by i) *Arenicola marina*, largely restricted to inner estuary and central basin mixed-tidal flats (Wooldridge et al., 2017b), that ingest particles < 2 mm in diameter (Riisgard and Banta, 1998) and ii) *Corophium volutator*, confined to mud-flats and mixed-flats in the Ravenglass Estuary (Kelly et al., 1991), that ingest particles < 62 μm in diameter (Fenchel et al., 1975).

In the Ravenglass Estuary, there is a negative correlation between chlorite abundance and bioturbation intensity, and a weak positive correlation between illite abundance and bioturbation intensity (Fig. 3.17). There is little relationship between kaolinite abundance and bioturbation intensity (Fig. 3.17). The relationships between chlorite and illite abundance and bioturbation intensity is probably an artefact of grain size, and not early-mineral alteration or formation, since chlorite is most abundant in relatively high-energy, coarser-grained depositional environments barren of bioturbation. In contrast, illite is most abundant in low-energy, finer grained depositional environments, which are intensely bioturbated by *Corophium volutator* and/or *Arenicola marina*.

Daneshvar and Worden (2017) suggested that plagioclase grains are preferentially rimmed by neoformed kaolinite, and detrital K-feldspar grains are preferentially rimmed by

neoformed illite in Ravenglass Estuary sediment, possibly as a result of continued mineral-alteration (early-diagenesis). While early mineral-alteration remains possible, it is reported that clay minerals also formed due to intense alteration of feldspars in the hinterland (Moseley, 1978; Quirke et al., 2015; Young et al., 1986). As a consequence, the relationship between feldspars and clay-minerals in the Ravenglass Estuary plausibly may be an inherited feature from the hinterland, and not due to early-diagenesis in the estuary.

3.6.3.4 Clay mineral distribution: mechanical infiltration

The stratification of specific clay minerals has been reported to result from the mechanical infiltration of clay-laden waters through filtering sand packages in experiments undertaken by Matlack et al. (1989). Experiments undertaken by Matlack et al. (1989) showed illite and smectite pass through the sediment but chlorite is preferentially trapped as clay coats. However, the present results from the Ravenglass Estuary show that, despite mechanical infiltration being likely to occur at a centimetre- to metre-scale in marginal marine depositional environments (Santos et al., 2012), there is no systematic increase or decrease in specific clay minerals with depth (Table 3.5).

The lack of clay mineral stratification in near-surface Ravenglass Estuary sediment brings into question the relevance of experiments undertake by Matlack et al. (1989) to natural estuarine depositional environments. As reported by Buurman et al. (1998), the infiltration experiments undertaken by Matlack et al. (1989) used peptized clay minerals, i.e. clay minerals converted into colloidal suspension, meaning the clay minerals had a minimum tendency to flocculate. As a result, intermediate- to high-surface charge clay minerals, e.g. illite and smectite, are less likely to form floccules and are instead more likely to pass through the filtering sand packages (Buurman et al., 1998). In contrast, chlorite (a low surface charge clay mineral) is more likely to be trapped in the sediment (Buurman et al., 1998). Second, similar to the prevention of clay coat formation via mechanical infiltration (as discussed previously), the formation of clay drapes during flow-deceleration and presence of clay-rich impermeable layers in tidal flats, are likely to clog pore-throats and baffle mechanical infiltration.

3.6.4 Early-diagenetic pyrite: origin and distribution

Fe-sulphides (e.g. pyrite), are common early-diagenetic minerals in marginal marine sediments due to bacterial sulphate reduction that occurs when aqueous sulphate (derived from marine-inundation) is reduced by organic matter (Berner, 1980). In the Ravenglass Estuary, pyrite is most abundant in finer-grained, low-energy, cohesive and anoxic, central-basin tidal flats (Fig. 3.16C; lithofacies 3, 4.1 and 4.2). Pyrite abundance typically increases

with depth in tidal-flat cores (6A, 6B, 6D) due to increasing anoxic conditions and the development of a distinct redox boundary, defined by colour of sediment at depth typically between 6 to 50 cm (Table 3.5; Fig. 3.8). Pyrite is absent throughout the near-surface in relatively high-energy and coarser grained outer estuary sediment and inner estuary and central basin low-amplitude tidal dunes.

The relationship between pyrite abundance and depth is complicated in mixed-flat depositional environments (facies association 4) by sediment bioturbation (Table 3.5). *Arenicola marina*, which live in J-shaped burrows between 10 to 40 cm deep, develop a tail-to-head directed ventilatory water flow system cause an upward flow of oxygenated water in the sediment in front of the head (Riisgard and Banta, 1998). As a result, the irrigation and oxidation of the burrow by *Arenicola marina* exert a localised but strong effect on the geochemical environment in the near-subsurface, in this case, inhibiting the growth of pyrite due to oxidation. In contrast, *Corophium volutator* which live in relatively shallow (< 5 cm deep U-shaped burrows) do not influence pyrite growth, since they do not typically penetrate the redox boundary. It is noteworthy that thinly-bedded sediments (lithofacies 4.3), which primarily occur as minor incursions in tidal-flats, lead to irrigation and oxidation underlying and overlying sediments, and thus, may also inhibit the growth of pyrite.

3.7 SIGNIFICANCE: IMPLICATIONS FOR SANDSTONE RESERVOIR QUALITY

Hydrocarbon exploration, in ancient and deeply buried sandstone reservoirs, typically involves avoiding the cleanest and most clay-free lithofacies. However, note that the cleanest and most clay-free lithofacies tend to become increasingly quartz cemented at burial temperatures > 80 to 100 °C (Worden and Burley, 2003). Anomalously high-porosity in deeply-buried sandstones may be preserved due to the presence of clay coats on sand grains through the inhibition of quartz cement (Ehrenberg, 1993). Examples of porosity-preserving clay coats, in deeply-buried marginal-marine sandstones reservoirs, include the Knarr field, northern Norwegian North Sea (Skarpeid et al., 2017) and the Upper Cape Hay Formation, Australia (Saïag et al., 2016).

The completeness and mineralogy of clay coats have been reported to be the dominant controls on the ability of grain coats to inhibit quartz cementation (Ajdukiewicz and Larese, 2012; Billault et al., 2003; Lander et al., 2008). The optimum grain coat coverage to preserve porosity varies as a function of grain size, since coarser grained sandstones have a smaller surface area and thus require less clay to achieve full surface coverage (Bloch et al., 2002). For example, Pittman et al. (1992) suggested an optimum range of 4 to 7 % sediment volume

of clays for the Berea Sandstone and 5 to 12 % in the Tuscaloosa Formation. In contrast, Bloch et al. (2002) reported that a relatively minor amount of clay (as little as 1 to 2 % of the rock volume) can form extensive coats on individual sand grains. In many reservoir examples, grain coats have mixed-mineralogy, typically containing illite and chlorite (analogous to the Ravenglass Estuary), such as the Egret field (Stricker et al., 2016), the Lower Cretaceous Missinssauga Formation (Gould et al., 2010) and Jurassic Garn formation (Storvoll et al., 2002).

Based upon compositional (clay mineralogy and pyrite abundance) and textural (grain size and detrital clay coat coverage) datasets presented in this study, it is possible to better predict the distribution of reservoir quality, by analogy, in deeply-buried marginal marine sandstones. Clay coats are most extensive at the margins of the inner estuary and central basin in mud-flats (Fig. 3.11; Table 3.2), however, the abundance of clay and fine-grain size of the sediment will likely result in clay minerals blocking pore-throats and drastically reducing permeability. Furthermore, mud-flats also contain the highest abundance of pyrite (Fig. 3.14C), which sequesters iron, and therefore may inhibit the growth of burial-diagenetic Fe-chlorite, since iron is locked up as a sulphide mineral. In contrast, the relatively clean, clay-free, outer estuarine sediments (Fig. 3.10) are likely to host insufficient quantities of clay size material to form extensive clay coats, and would therefore be expected to be heavily quartz cemented during burial diagenesis (at temperatures > 80 to 100 °C). In contrast, mixed-flats and low-amplitude tidal dunes, in the inner-estuary and central basin, may contain sufficient precursor detrital clay coat coverage (Fig. 3.10 and 3.11) in order to form porosity-preserving authigenic grain coats in deeply-buried sandstone reservoirs. Low-amplitude dunes (lithofacies 5.1; Table 3.2) may, in some cases, be relatively enriched in detrital chlorite (Fig. 3.13A and 3.15A) in comparison to other inner estuary and central basin lithofacies. Furthermore, intense bioturbation in mixed-flat and low-amplitude dune depositional environments (facies association 4 and lithofacies 5.1; Table 3.2), leading to oxidation of near-surface sediment and inhibition of pyrite growth (increasing iron availability), is likely to favour the formation of burial-diagenetic Fe-bearing clay minerals such as chlorite.

3.8 CONCLUSIONS

This study has revealed the dominant controls on detrital clay coat and clay mineral distribution patterns, as well as the preferred environments for the growth of Fe-sulphides, in a modern marginal marine setting. The results of this study may be used, by analogy, to aid reservoir quality prediction in deeply-buried sandstone reservoirs. The main conclusions are summarized below.

1. Detrital clay coats are most extensive in mud-flats and mixed-flats at the margins of the inner estuary and central basin, and absent in outer estuarine sediments. Detrital clay coat distribution patterns in near-surface (< 1 m) sediment are governed by estuarine hydrodynamics (supply of clay size material) and processes active in the top few millimetres (biological adhesion of clay to the sand grain surface) in the primarily depositional environment. Surface (< 2 cm) detrital clay coat distribution patterns are not over-printed by post-depositional processes (e.g. mechanical infiltration or sediment bioturbation) in the near-surface (< 1 m).
2. The fine fraction (< 2 μm) of Ravenglass Estuary sediment is dominated by Fe-Mg-rich illite, with subordinate amount of chlorite and kaolinite, with only a minor amount of smectite. The near-surface clay mineral assemblage is controlled by climate, provenance and the geochemical environment at the site of deposition.
3. Chlorite is relatively most abundant in high-energy, coarser-grained depositional environments, such as outer estuarine sediments and inner-estuary low-amplitude dunes. Kaolinite abundance is relatively homogenous throughout the Ravenglass Estuary. Illite is typically Fe-Mg-rich and most abundant in mud-flat and mixed-flat inner-estuary and central basin lithofacies. Relatively high-energy lithofacies in the outer, inner and central basin sediments typically host a mixture of both Fe-Mg-rich illite and Al-rich-illite. Smectite is most abundant in floodplain sediments, and is typically absent in estuarine sediments.
4. Clay mineral distribution patterns are controlled by estuarine hydrodynamics, due to the physical sorting of clay minerals by grain size. Post-depositional processes, e.g. mechanical infiltration and early-diagenetic mineral alteration via continued weathering of silicate-minerals and biodegradation, do not appear to influence clay mineral distribution patterns in near-surface sediment. It may be possible, that ground-water flushing in estuarine sediments may however minimise the development of smectite accumulation.
5. Pyrite growth is largely restricted to mud- and mixed-flats in the central basin, and typically increases in abundance with depth due to increasing anoxic-conditions. Intense bioturbation in mixed-flats by *Arenicola marina* may however inhibit pyrite-growth (reducing Fe sequestration in the sediment), which may favour the formation of burial-diagenetic chlorite.
6. Precursor clay coat, clay mineral and Fe-sulphide (pyrite) distribution patterns may be predicted as a function of lithofacies, with knowledge of provenance, climate, estuarine hydrodynamics and the distribution of macro- and micro-fauna.

4. COMPOSITIONAL VARIATION IN MODERN ESTUARINE SANDS: PREDICTING MAJOR CONTROLS ON SANDSTONE RESERVOIR QUALITY

4.1 ABSTRACT

The spatial and temporal variability of primary depositional mineralogy in sandstones is poorly-understood and consequently empirical models typically fail to accurately predict reservoir quality. To address this challenge the spatial distribution of quartz, feldspar, carbonates and clay minerals (chlorite, illite and kaolinite), in surface sediment of the Ravenglass Estuary, UK, have here been mapped at an unprecedented high-resolution, at a scale similar to many oil and gas reservoirs. Spatial mineralogy patterns (based on X-ray diffraction data) and statistical analyses revealed the following: (i) estuarine composition is primarily controlled by provenance i.e. character of bedrock and sediment in the source area, (ii) the distribution of quartz, feldspar, carbonates and clay minerals are primarily controlled by the grain size of specific minerals (e.g. rigid versus brittle grains) and estuarine hydrodynamics, and (iii) the abundance of quartz, feldspar, carbonates and clay minerals is predictable as a function of depositional environment and critical grain-size thresholds. This study may be used, by analogy, to better predict the spatial distribution of sandstone composition, and thus reservoir quality in ancient and deeply-buried marginal-marine sandstones.

4.2 INTRODUCTION

The composition of sandstone is controlled by the hinterland geology and all the processes active between the sediment source area and the final site of deposition, as well as during lithification. Sandstone composition can be defined in terms of the proportion of quartz, feldspar and lithics (QFL), the specific type of lithic grains, the mineralogy of the matrix and the amount of carbonate inherited from the initial depositional environment. QFL proportions and the amount of carbonate exert strong controls on reservoir quality (Primmer et al., 1997). The initial composition of sandstone may also significantly impact subsurface flow-rates, influence wireline log-responses (e.g. sandstone density, natural radioactivity electrical conductivity, and water saturation) and thus petrophysical properties, as well as control the feasibility of carbon capture and geological storage (CSS).

Available statistical correlations typically fail to accurately predict reservoir quality, at least partly due to the spatial and temporal variability of sandstone composition being poorly-

understood (Ajdukiewicz and Lander, 2010). The aim of this study is to map and analyse the spatial distribution of quartz, feldspar, carbonates and clay minerals (chlorite, illite and kaolinite) on a scale similar to many oil and gas reservoirs, to aid reservoir quality prediction. This study is built upon the initial assumption that sandstone diagenetic systems are largely isochemical with respect to silicate minerals, although it is acknowledged that diagenetic processes that influence carbonate minerals may be somewhat more open-system (Worden and Burley, 2003). The Ravenglass Estuary (Fig. 4.1) was chosen for its accessibility, the varied hinterland geology, and because eogenetic alterations are common in many shallow-marine and tidally-influenced sandstone reservoirs (Morad et al., 2010). In addition, this work builds on the distribution of detrital clay coats, in the Ravenglass Estuary (Wooldridge et al., 2017a; Wooldridge et al., 2017b)

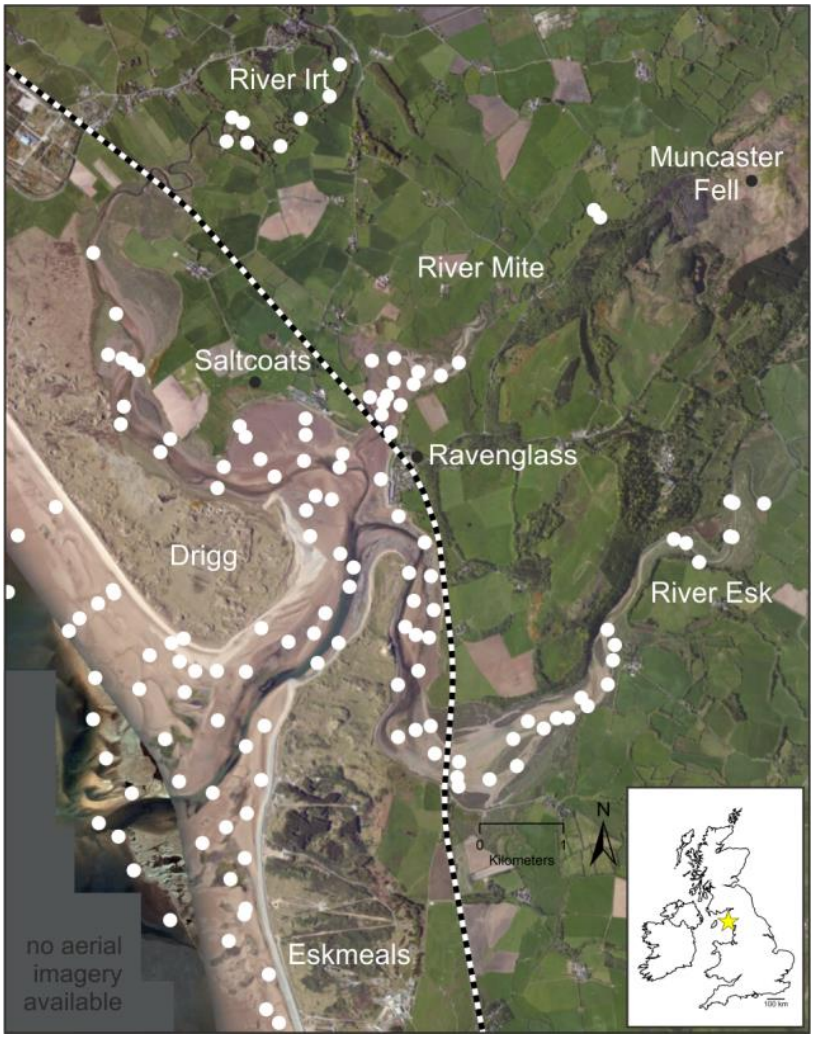

Figure 4-1 – Aerial image of the Ravenglass Estuary, north-west England. Distribution of surface (< 2 cm) sediment samples are highlighted by white circles.

The composition of a sandstone is typically described, by petrographers, in terms of the proportions of quartz, feldspar and lithic grains, hence the use of QFL diagrams (Folk,

1968). QFL diagrams may be used to help define basin evolution, tectonic regime and sediment supply over time (Dickinson and Suczek, 1979; Weltje, 2006), sediment transport routes (Caracciolo et al., 2012), and predict reservoir quality (Dutton and Loucks, 2010). Some petrographic studies recognise that lithics, a bucket term, are important in terms of their behaviour during compaction displaying either ductile or rigid behaviour (Worden et al., 2000; Worden et al., 1997). The ductility of lithic grains is largely down to the proportion of clay minerals present; this led Ramm et al. (1997) to use a clay mineral index, based on X-ray diffraction-defined clay mineral quantities, to predict styles of compaction during sandstone compaction. The quantity of carbonate minerals is also vitally important to reservoir quality in many sandstones (Morad et al., 2010; Morad et al., 1998; Primmer et al., 1997). Carbonate minerals are often inherited from the specific sedimentary environment in which the sediment was deposited, for example bioclasts in marine sediments (Worden, 2006) and calcrete and dolocrete in arid fluvial sediments (Schmid et al., 2006).

Since X-ray diffraction (XRD) analysis has been used, as opposed to petrography (which cannot quantify the mineralogy of clay grade material), in this study of a modern sedimentary analogue to ancient and deeply-buried sediments, the QFL end-members have here been recast. In this study, Q here represents all types of quartz, including mono- and polycrystalline quartz grains and quartz in typically rigid granitic lithic grains and andesitic volcanic lithic grains. F here represents all feldspars including K-feldspar, plagioclase, perthite intergrowths and any feldspar minerals in granitic and andesitic volcanic lithic grains. L is harder to define in terms of XRD data but here L has been chosen to represent the sum total of all clay minerals, independent of grain size, including illite, chlorite, kaolinite and smectite. The term "clay mineral" refers to aluminium-rich sheet silicate minerals; in contrast the term "clay" refers to sediment particles that are smaller than 2 μm in size. The name illite, in this study, is independent of grain size and used for mica-like minerals commonly associated with clastic-sediments (e.g. muscovite) following the definition of Grim et al. (1937). A fourth term (C) representing carbonate minerals has been added since they have a major impact on reservoir quality and are, in many cases, directly attributable to the specific depositional environment; C therefore includes calcite, dolomite, aragonite and siderite. XRD studies of sandstone reservoir quality can therefore be described in terms of QFL-C.

Sandstone composition in terms of QFL-C influences rock properties in different ways at different times; for example during eodiagenesis and mesodiagenesis. The definition of eodiagenesis, during the initial stages of burial and mesodiagenesis, during deeper burial (Choquette and Pray, 1970), is somewhat theoretical but it raises important practical questions about the primary controls on sandstone properties during diagenesis; depth,

temperature, effective stress, fluid composition and mineral composition. Depth of burial is typically treated as the main control although rate of burial, depth-related heating and depth-related effective stress are the extrinsic variables that also need to be taken into account (Worden and Burley, 2003). Fluid composition can be important for sandstones especially if they contain carbonate minerals, simply because carbonate minerals tend to be more soluble and have faster dissolution and precipitation rates than silicate minerals. Eodiagenesis in sandstones has been defined in terms of sediment that is: (i) in the realm of subaerially-influenced water (oxidized and with CO_2 influenced by surface biological activity), (ii) buried to less than about 2000 m or (iii) buried to depths where the sediment is at temperatures less than about 60 or 70°C (Morad et al., 2000; Worden and Morad, 2003). Temperature is probably the most important defining control between eodiagenesis and mesodiagenesis in sandstones, since few mineral reactions happen in sandstones during burial between exiting the realm where microbial processes are dominant and moving to depths/temperatures where a semi-predictable suite of reactions start to occur (e.g., illitization of smectite, feldspar dissolution, quartz cement, dolomite growth). Note that elapsed time also plays a role, given that most mesogenetic reactions are kinetically controlled (Ehrenberg et al., 2009). Thus rocks exposed to lower temperatures for longer periods may have comparable extents of diagenetic alteration with younger, hotter counterparts.

The impacts of QFL-C split between eodiagenesis and mesodiagenesis on rock properties and diagenetic reactivity are now discussed. Porosity and permeability of sandstones are initially controlled by framework mineralogy (content of detrital quartz), matrix content, mean grain size and sorting (Ramm and Bjorlykke, 1994; Scherer, 1987). Primary sediment composition (QFL-C) may influence host-sediment properties (matrix content, mean grain size and sorting) and porosity and permeability in the following ways: (i) Matrix content is typically enriched in clay-minerals due to laws of hydrodynamics (Worden and Morad, 2003). (ii) The proportion of quartz in sand may influence grain size, since quartz grains are relatively resistant to abrasion and are typically coarser than feldspar grains (Odom et al., 1976), (iii) Weak framework grains (e.g. feldspar and clay minerals) are likely to be reduced in size and promote wider grain size distribution (Odom et al., 1976), and (iv) Early framework-strengthening and thus compaction inhibiting carbonate cements such as siderite and calcite (Morris et al., 2006).

Sandstone composition (QFL-C) influences on mesodiagenesis include the following: (i) Clay-rich ductile versus rigid grains, where quartz-rich sediment undergoes rigid compaction and phyllosilicate-lithic- and mica-rich sediment undergoes ductile compaction (Worden et al., 2000). (ii) Weak versus strong grains where feldspar undergoes grain fracturing under

lower tensile stresses than quartz grains (Griffiths et al., 2016). (iii) Reactive versus unreactive grains where quartz is largely unreactive but in contrast feldspar-, phyllosilicate- and carbonate-rich grains as well as matrix or eogenetic phases, tend to be relatively reactive during prolonged burial. For example, influx of CO_2 during burial induces feldspar alteration to clay minerals and carbonates (Barclay and Worden, 2000b; Ehrenberg and Jakobsen, 2001). K-feldspar and kaolinite are unstable together at temperatures greater than about 70 °C (Worden and Burley, 2003), which leads to the formation of illite and quartz (Chuhan et al., 2001). (iv) Quartz grain pressure solution and subsequent quartz cementation can be both promoted by specific clay minerals such as illite (Oelkers et al., 1996) or inhibited by specific grain coating clay minerals such as chlorite (Ehrenberg, 1993), and (v) Wettability where reservoir mineralogy (especially the quantities of kaolinite and carbonate) plays a big role in determining oil-water wetting state of sandstones (Barclay and Worden, 2000a).

Sandstone QFL-C composition also influences a range of anthropogenic activities including: (i) a sandstone's specific geomechanical response to drilling a borehole in terms of thickness of the damaged zone and borehole stability (Plumb, 1994), (ii) the risk of fines migration (typically kaolinite) and formation damage during oil and gas production (Cerda, 1987), and (iii) a sandstone's response to the injection of CO2 during carbon capture and storage (Baines and Worden, 2004).

The ability to predict sandstone composition would help in the subsequent prediction of the petrophysical and geomechanical properties of sandstones; this would of clear benefit during petroleum exploration, appraisal and field development and production as well as during the planning and execution of CCS projects. This study has addressed the following specific questions:

1. What minerals are found in the modern Ravenglass Estuary?
2. How are quartz, plagioclase, K-feldspar, carbonate and clay minerals distributed in this modern marginal marine setting?
3. What controls the whole-sediment mineral assemblage in a modern marginal marine setting?
4. What controls mineral distribution patterns in marginal marine environments?
5. Can the abundance and spatial distribution of sediment composition be predicted as a function of grain size, depositional environment and/or estuarine zone?

4.3 STUDY AREA: RAVENGLASS ESTUARY

4.3.1 Geological setting

Sandstone compositions are largely controlled by character of the sedimentary provenance, sediment processes active in the depositional basin, and sediment transport pathways that link provenance to basin which is ultimately controlled by tectonic regime (Dickinson and Suczek, 1979). As a result, to assess the influence provenance may have on mineral type and distribution patterns in the Ravenglass Estuary, it is first necessary to the identify the potential source of sediment mineral grains in the drainage basin. The type and spatial distribution of bedrock and drift-deposits in the drainage basins of the Rivers Irt, Mite and Esk are presented in Figure 4.2.

The northern River Irt drains Ordovician Borrowdale Volcanic Group andesites and Triassic Sherwood Sandstone Group, whilst the River Esk predominantly drains the Devonian Eskdale Granite (Fig. 4.2A). The Lower Triassic Sherwood Sandstone Group (locally known as the St Bees Sandstone) dominates the low-lying coastal planes and is predominantly composed of fluviatile sandstones (Quirke et al., 2015). The Borrowdale Volcanic Group, dominating to the north of the provenance area, was subject to regional, sub-greenschist facies metamorphism at about 395 Ma during the Caledonian Orogeny; and is comprised of subduction-related, K-rich, calc-alkaline andesite (Quirke et al., 2015). The northern part of the Eskdale Granite, dominating to the east and south of the provenance area, is a coarse-grained granite, and the southern part is granodioritic (Young et al., 1986). Ordovician, Skiddaw Group is comprised of weakly-metamorphosed, fine-grained sedimentary rocks (Merritt and Auton, 2000) and is proximal to the Ravenglass Estuary (Fig. 4.2A).

Quaternary drift-deposits were deposited in response to spatially-variable glacio-isostatic rebound and glacioeustatic sea-level change, following the last glaciation (late Devensian, at about 28 to 13 ka) (McDougall, 2001; Moseley, 1978). However, following the last glaciation, much of the glacial deposit has been removed from the land surface (Merritt and Auton, 2000). The Seascale Glacigenic Formation (wide range of glacial and pro-glacial outwash sediments) is drained by the Rivers Irt, Esk and Mite. The Gosforth Glacigenic Formation is primarily restricted to the northern River Irt and Mite drainage basin (Fig. 4.2B). The Ravenglass Estuary is underlain by the Ravenglass Till (part of the Seascale Glacigenic Formation) which is exposed as knolls throughout the estuary.

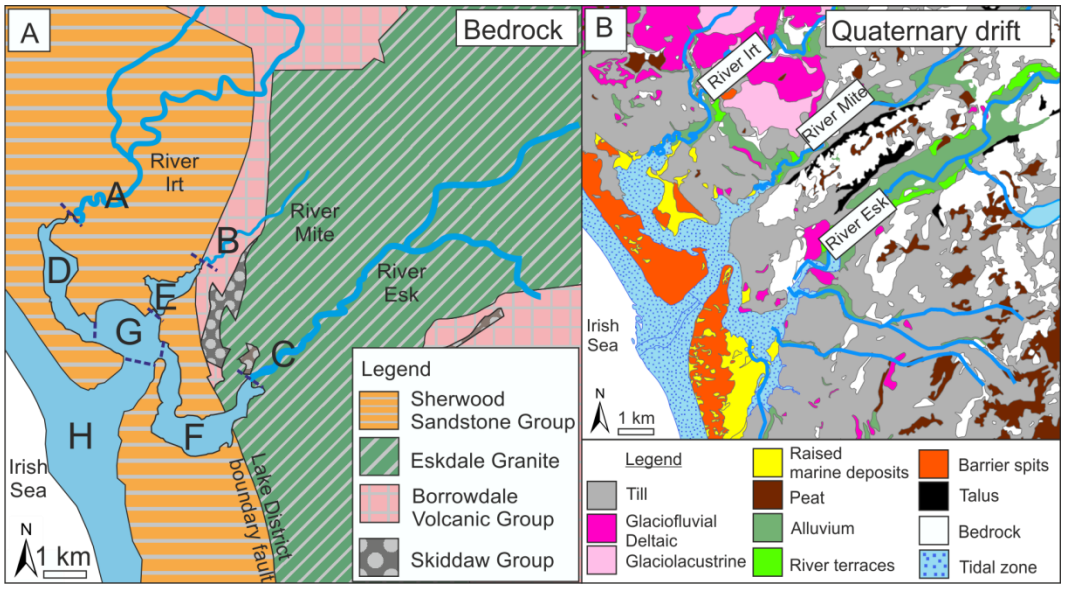

Figure 4-2 – Geological setting of the Ravenglass Estuary, UK. (A) Bedrock geology and division of estuarine-zones; A, lower-Irt; B lower-Mite; C lower-Esk; D, inner-Irt; E, inner-Mite; F, inner, Esk; G, central-basin; and H, outer-estuary, and (B) Quaternary drift-deposits.

4.3.2 Estuarine hydrodynamics and geomorphology

The Ravenglass Estuary is a shallow, mixed-energy and macro-tidal (> 7 m tidal range) estuarine system, which occupies an area of 5.6 km^2 of which ~ 86% is intertidal (Bousher, 1999; Lloyd et al., 2013; Wooldridge et al., 2017b). Shallow estuary bathymetry has led to strong tidal-asymmetry, meaning the outward ebb tidal-flow is prolonged in comparison to the inward tidal-flow (Kelly et al., 1991). Quick ebb drainage resulting from a short estuarine length means that the maximum discharge measured for the lower-Esk arm of the estuary during the ebb tidal-flow (4.99 $m^3 s^{-1}$), is only slightly lower than flood tidal-flow (5.41 $m^3 s^{-1}$) (Kelly et al., 1991). Drigg and Eskmeals coastal spits provide shelter from wave-action to the inner estuarine zones and the central basin (Fig. 4.2A and 4.3); however, strong tidal-currents have resulted in extensive tidal-bars and tidal-dunes landward of the low-energy central minimum. The rivers flowing into the estuary have average flow-rates of 0.4 $m^3 s^{-1}$ for the River Mite, 3.4 $m^3 s^{-1}$ for the River Irt, and 4.2 $m^3 s^{-1}$ for the River Esk (Bousher, 1999). Anthropogenic impact on the estuary is here considered to be minor, excluding the sheltering of the inner-Mite from tidal-currents and increased salt marsh development as a consequence of the railway viaduct construction (Carr and Blackley, 1986).

4.4 SAMPLES AND METHODS

Detailed-ground surveys (aided by aerial imagery) and the collection and analyses of estuarine and drift-deposit samples for grain size and mineralogy was undertaken in order to

assess the relationship between sediment composition, host-sediment properties (e.g. grain size) and depositional environment.

4.4.1 Field mapping and sample collection

Aerial imagery and detailed ground-surveys were used to define a suite of estuarine sub-environments. Sand abundance was used to classify tidal flats following the classification scheme proposed by Brockamp and Zuther (2004); sand-flat is > 90 % sand, a mixed-flat has 50 to 90% sand, and a mud-flat has 15 to 50 % sand. Surface sediment samples (n = 191) were collected at low-tide along pre-defined transects to give an approximately uniform distribution of estuarine and fluvial samples (Fig. 4.1). Quaternary drift-deposits were collected from exposed cliff sections in the inner-Esk, as well as from Ravenglass Till exposed as knolls throughout the estuary. Sediment samples were placed in air-tight plastic-jars in the field and stored in a refrigeration unit at ~ 2°C to prevent sample degradation prior to grain size and mineralogical analyses. Mean grain size (μm), grain-size sorting (σg) and sand abundance (%) were quantified using a Beckman Coulter Laser Particle Size Analyser (LPSA) and GRADISTAT software (Blott and Pye, 2001) for all sediment samples. The grain-size sorting scale presented by Folk and Ward (1957) is here used, where high-values are indicative of poorly-sorted sediment.

4.4.2 Clay mineral separation, identification and quantification

4.4.2.1 X-ray diffraction analysis

To ensure accurate mineralogy identification and quantification (especially for the clay minerals: chlorite, illite and kaolinite) and to analyse illite chemistry and crystallinity, clay fractions (< 2 μm) and silt- and sand-fractions (2 μm to 2 mm) of estuarine sediment and Quaternary-drift samples were physically separated prior to X-ray diffraction (XRD) analysis.

Clay fractions (< 2 μm) were physically separated (isolated from the silt- and sand-fractions) in an ultrasonic bath, followed by gravity-settling, and then centrifuge settling at 5,000 rpm for 10 minutes. The wet-separated clay fractions were then dried at 60°C for 24 hours and weighed to calculate the percentage of clay-size material. Dried clay fractions were crushed using a pestle and mortar prior to back-loading into cavity mounts and XRD analysis.

A representative 5 g subsample was taken from the separated silt- and sand-fractions (2 μm to 2 mm) and placed in an agate McCrone mill with 12 mL of distilled water and finely crushed for 10 minutes. The resultant slurry was washed into a petri dish using distilled water and then dried at 60 °C. The dried material was crushed into a fine loose powder using

an agate pestle and mortar prior to back-loading into cavity mounts and XRD analysis, to quantify the mineralogy of the silt- and sand-fractions (2 µm to 2 mm). A PANalytical X'Pert Pro MPD X-ray Diffractometer was used to quantify the mineralogy of randomly-orientated powders prepared for the fine-fraction (< 2 µm) and silt- and sand-fraction (2 µm to 2 mm). The Relative Intensity Ratio (RIR) method was used to quantify the mineralogy of both size fractions, using PANalytical HighScore Plus software. XRD results of the fine-fraction (< 2 µm) and silt- and sand-fraction (2 µm to 2 mm) were then recombined, factoring in the relative weight percentages of each size fraction, to quantify the mineralogy of the whole sample (all material < 2 mm).

The Esquevin Index has been calculated (using clay fraction XRD-data) to differentiate Al-rich from Fe-Mg-rich illite. Esquevin Index is calculated by analysing the ratio between the 5Å and 10Å peak heights on X-ray diffractograms (Esquevin, 1969). The following classification boundaries are used in this study, after Esquevin (1969); biotite, < 0.15 (most Fe-Mg-rich); biotite + muscovite, 0.15-0.3; phengite, 0.3-0.4; muscovite, >0.4 (most Fe-Mg-depleted). To establish illite crystallinity index ($2^0\theta$), also known as the *Kübler* Index (Kübler, 1964), the full width at half-maximum (FWHM) of the 10Å (001) illite peak was measured on the X-ray diffractogram (using clay fraction XRD-data). The following boundaries are used, after Kübler (1964); epizone (highest temperature): < 0.25; anchizone: 0.25-0.42, diagenesis (lowest temperature): >0.42.

X-ray diffraction determined mineralogy of different size-fractions, separated from a central-basin (mixed-flat) sample, was undertaken by using a combination of gravity-settling (as above) and sieving. The following grain-size classes were analysed; < 0.2 µm (fine clay); 0.2 µm to 2 µm (coarse clay); 2 µm to 32 µm (fine silt); 32 µm to 62 µm (coarse silt); 62 µm to 125 µm (very fine sand); 125 µm to 250 µm (fine sand)..

4.4.2.2 SEM-EDS (QEMSCAN®)

Three polished thin sections were constructed to provide textural and mineralogical information on clay minerals (chlorite, illite and kaolinite) to assess to what extent clay minerals occur as lithics and as part of the fine fraction (< 2 µm). The QEMSCAN® system is comprised of a scanning electron microscope (SEM) coupled with Energy Dispersive Spectrometers (EDS). QEMSCAN® data provide information about the micron-scale texture and chemical and mineralogical composition. Data were collected with a step size of 2 µm to ensure both the fine fraction (< 2 µm) and silt- and sand-fraction (> 2 µm) was analysed.

4.4.3 Spatial mapping

Mineral distribution maps were made in ArcGIS using an inverse distance weighted (IDW) interpolation technique to avoid the creation of ridges or valleys of extreme and unrepresentative values (Watson and Philip, 1985). An interpolation barrier (polyline drawn in ArcGIS) along the long axis of Drigg and Eskmeals spits was used to ensure interpolated values either side of the spits (i.e. in the estuary and on the coast) did not influence one another, despite their relative spatial proximity.

4.4.4 Statistical analysis

An Analysis Of Variance (ANOVA) test was used to assess whether there is a statistically significant difference in abundance of specific minerals as a function of depositional environment (De1 to De9) and estuarine zone (A-H). Following ANOVA, a post-hoc Tukey's honestly significant difference (HSD) test was employed to determine which individual depositional environment or estuarine zones were statistical different from one another as a function of specific mineral abundance (quartz, feldspar, clay minerals and carbonate). The following symbols was used to highlight statistical significance; marginally-significant (+) when $p < 0.1$; significant (*) when $p < 0.05$; very-significant (**) when $p < 0.01$; and extremely significant (***) when $p < 0.001$. All statistical analyses were performed in R statistical software (R Core Team, 2016).

4.5 RESULTS

In this section results are presented from detailed ground surveys (aided by aerial imagery) undertaken to identify the nature and distribution of depositional environment, as well as results from laboratory analyses used to quantify sediment properties (grain size, sorting and mineralogy).

4.5.1 Estuarine sediment characteristics

The estuary has also been subdivided into discrete fluvial, inner, central and outer zones (Fig. 4.2A), based upon the dominant physical processes active in each zone, as well as previously reported salinity data (Assinder et al., 1985; Daneshvar, 2015). Zones A-C represents fluvial (river) regions which are freshwater-dominated; zones D-F (inner) represent brackish, inner river- and tide-dominated regions; zone G (central) is a relatively mixed-energy (fluvial-, tide- and wave-influenced) and heterogeneous central zone with near-seawater salinity that contains extensive mud-flat and mixed-flat (locally named,

Saltcoats tidal flat); and zone H (outer), which is seawater dominated and subject to strong wave and/or tidal currents.

The mapped distribution of nine discrete depositional environments, identified during detailed ground-investigations and aerial image analysis, is presented in Figure 4.3. Depositional environments include: gravel-beds (De1), mud-flats (De-2), mixed-flats (De3), sand-flats (De4), tidal bars and dunes (De5), tidal-inlet (De6), backshore (De7), foreshore (De8) and pro-ebb delta (De9) (Fig. 4.3).

The average grain size and grain size sorting of each depositional environment and estuarine zone are presented in Table 4.1. The mapped distribution of grain size and grain sorting are presented Figure 4.4. Variation in grain size and sorting per estuarine zone and depositional environment are displayed in Figure 4.5.

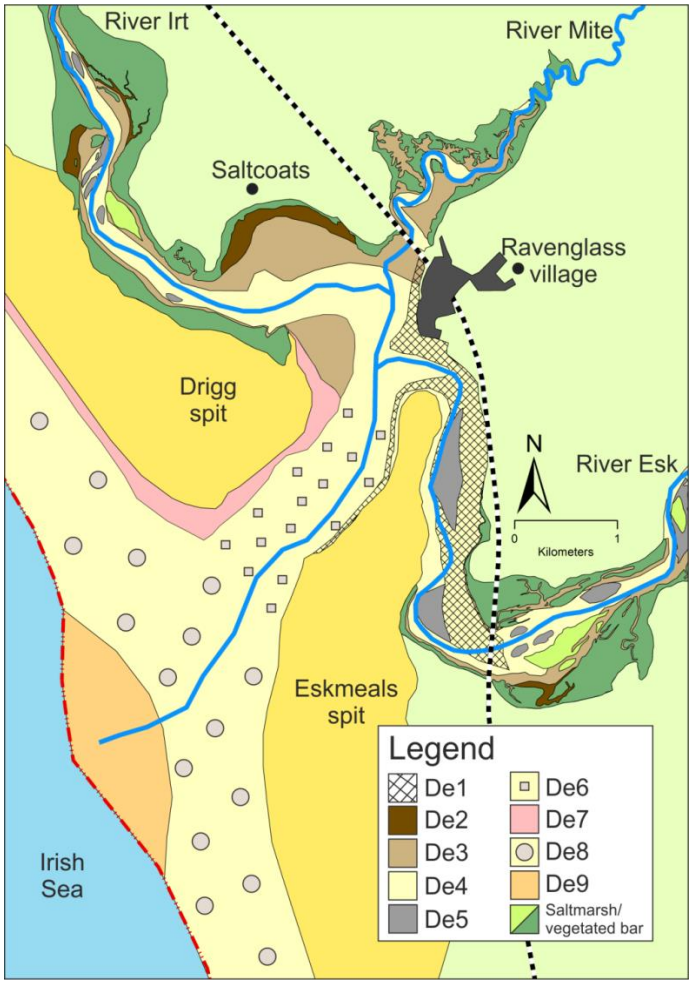

Figure 4-3 – Nature and organization of depositional environments in the Ravenglass Estuary, labelled accordingly; De1, gravel-bed; De2, mud-flat; De3, mixed-flat; De4, sand-flat; De5, tidal bars and dunes; De6, tidal-inlet; De7, backshore; De8, foreshore; and De9, pro-ebb delta.

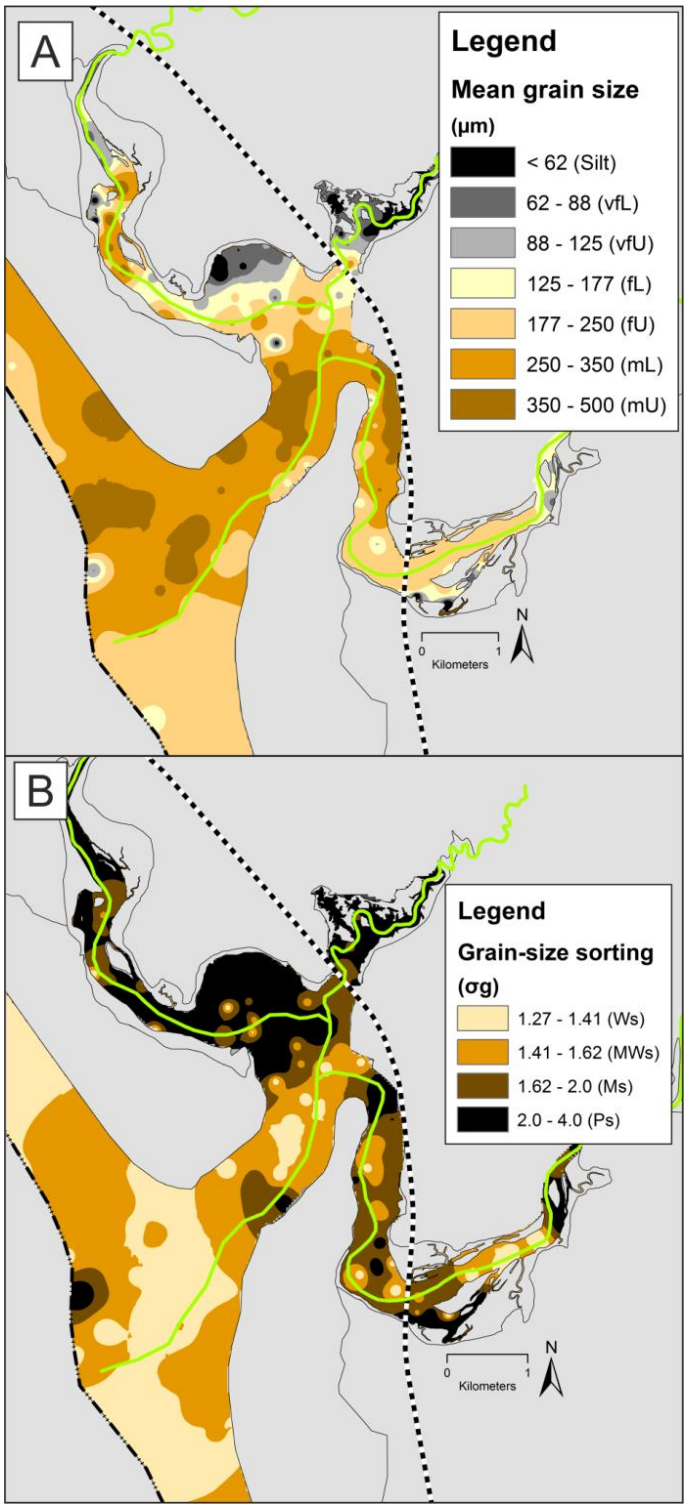

Figure 4-4 – Distribution of host-sediment properties (A) mean grain size, and (B) grain size sorting. Mean grain size classes are labelled accordingly; Silt; vfL, lower very-fine sand; vfU, upper very-fine sand; fL, lower fine sand; fU, upper fine sand; mL, lower medium sand; and mU, upper medium sand. Grain-size sorting classes are labelled accordingly; Ws, well sorted; MWs, moderately well-sorted; Ms, moderately sorted; and Ps, poorly sorted.

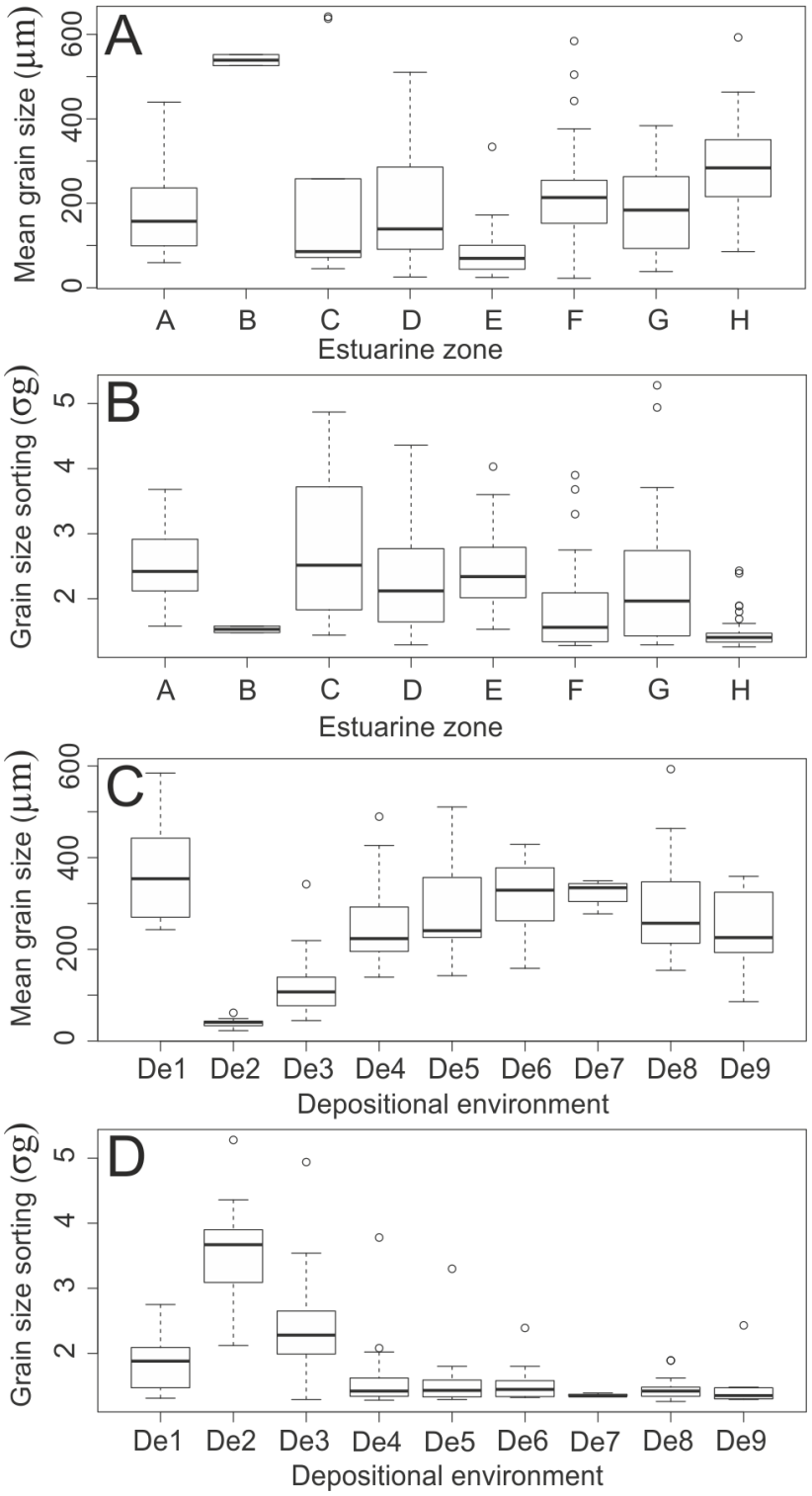

Figure 4-5 – Host-sediment properties as a function of estuarine zone and depositional environment (A) mean grain size, as a function of estuarine zone, (B) grain size sorting, as a function of estuarine zone, (C) mean grain size, as a function of depositional environment, (D) grain size sorting, as a function of depositional environment. Estuarine-zones are labelled accordingly; A, lower-Irt; B lower-Mite; C lower-Esk; D, inner-Irt; E, inner-Mite; F, inner, Esk; G, central-basin; and H, outer-estuary. Depositional environments are labelled accordingly; De1, gravel-bed; De2, mud-flat; De3, mixed-flat; De4, sand-flat; De5, tidal bars and dunes; De6, tidal-inlet; De7, backshore; De8, foreshore; and De9, pro-ebb delta

Table 4.1 - Summary of the mineralogy (mean and standard deviation), and host-sediment properties (mean grain size, and sorting) of the nine depositional environments and eight estuarine zones, including weighted averages (W.Av). Estuarine-zones are labelled accordingly; A, lower-Irt; B lower-Mite; C lower-Esk; D, inner-Irt; E, inner-Mite; F, inner, Esk; G, central-basin; and H, outer-estuary. Depositional environments are labelled accordingly; De1, gravel-bed; De2, mud-flat; De3, mixed-flat; De4, sand-flat; De5, tidal bars and dunes; De6, tidal-inlet; De7, backshore; De8, foreshore; and De9, pro-ebb delta.

Depositional environment	**De1**	**De2**	**De3**	**De4**	**De5**	**De6**	**De7**	**De8**	**De9**	**W.Av**
number of samples (n)	10	13	44	23	14	12	4	41	10	
Quartz (mean (sd))	78.62 (8.48)	71.50 (5.83)	77.78 (6.83)	86.15 (1.33)	85.10 (3.24)	85.40 (2.35)	86.66 (0.02)	85.04 (2.54)	86.32 (0.79)	82.06
Plagioclase (mean (sd))	9.98 (3.47)	11.31 (1.99)	9.45 (2.35)	7.42 (0.98)	8.17 (1.71)	7.29 (0.85)	6.25 (0.57)	7.19 (1.49)	7.35 (0.80)	8.35
K-feldspar (mean (sd))	5.51 (0.55)	5.45 (0.47)	5.84 (0.96)	5.00 (0.79)	4.85 (0.85)	4.73 (1.05)	5.58 (0.57)	5.38 (0.86)	4.66 (0.72)	5.39
Carbonate (mean (sd))	2.00 (1.31)	2.84 (1.12)	2.06 (0.85)	0.88 (0.42)	0.54 (0.51)	1.03 (0.70)	0.50 (0.01)	1.08 (0.72)	0.99 (0.09)	1.43
Chlorite (mean (sd))	1.56 (1.73)	2.33 (1.13)	1.19 (1.23)	0.21 (0.57)	0.67 (1.16)	0.66 (0.60)	0.50 (0.00)	0.54 (0.40)	0.36 (0.37)	0.87
Illite (mean (sd))	2.24 (2.69)	5.50 (3.19)	2.98 (2.68)	0.25 (0.24)	0.55 (0.96)	0.68 (0.69)	0.51 (0.01)	0.62 (0.74)	0.23 (0.27)	1.62
Kaolinite (mean (sd))	0.09 (0.06)	1.06 (0.86)	0.68 (0.64)	0.09 (0.08)	0.12 (0.26)	0.12 (0.18)	0.01 (0.00)	0.06 (0.16)	0.01 (0.00)	0.31
Mean grain size (μm)	370 (110)	39 (11)	115 (56)	253 (90)	283 (109)	312 (88)	324 (32)	291 (101)	239 (84)	225
Grain size sorting (σg)	1.86 (0.44)	3.54 (0.82)	2.37 (0.66)	1.59 (0.53)	1.59 (0.52)	1.53 (0.31)	1.35 (0.02)	1.44 (0.14)	1.48 (0.34)	1.90
Estuarine zone	**A**	**B**	**C**	**D**	**E**	**F**	**G**	**H**	**W.Av**	**Clay index of W.Av**
number of samples (n)	11	2	10	19	19	34	28	68		
Quartz (mean (sd))	75.97 (3.28)	77.88 (1.42)	67.60 (11.11)	78.84 (5.84)	74.44 (7.76)	82.54 (6.00)	81.10 (7.60)	85.36 (2.30)	80.95	
Plagioclase (mean (sd))	11.93 (1.64)	12.01 (0.00)	14.57 (6.81)	10.05 (2.17)	10.53 (2.64)	8.40 (2.21)	8.20 (1.85)	7.21 (1.31)	8.89	
K-feldspar (mean (sd))	6.53 (0.47)	6.50 (0.70)	6.86 (1.85)	5.57 (1.36)	6.01 (0.88)	5.18 (0.65)	5.41 (0.88)	5.17 (0.91)	5.51	
Carbonate (mean (sd))	0.12 (0.35)	0.00 (0.00)	0.22 (0.28)	1.76 (1.20)	2.09 (1.01)	1.34 (1.08)	1.81 (1.01)	1.03 (0.65)	1.27	
Chlorite (mean (sd))	1.50 (0.87)	1.52 (0.71)	3.43 (1.74)	1.20 (1.23)	1.87 (1.42)	0.82 (1.18)	0.78 (1.17)	0.53 (0.42)	1.04	0.31
Illite (mean (sd))	3.46 (1.56)	2.05 (1.41)	5.95 (2.77)	2.15 (2.24)	4.18 (3.00)	1.41 (2.01)	2.22 (3.19)	0.56 (0.67)	1.94	0.58
Kaolinite (mean (sd))	0.46 (0.77)	0.03 (0.00)	1.35 (1.55)	0.40 (0.31)	0.86 (0.77)	0.29 (0.51)	0.49 (0.69)	0.06 (0.15)	0.37	0.11
Mean grain size (μm)	190 (120)	539 (19)	213 (234)	202 (159)	90 (71)	221 (123)	184 (107)	291 (96)	227	x
Grain size sorting (σg)	2.53 (0.69)	1.53 (0.07)	2.79 (1.14)	2.30 (0.87)	2.47 (0.68)	1.86 (0.69)	2.31 (1.10)	1.45 (0.21)	1.97	

4.5.2 Estuarine composition

X-ray diffraction, and not petrographic analysis, has been used to quantify mineralogy; as a result, it is not possible to create traditional QFL ternary diagrams, which are typically used to classify sandstones (Folk, 1954) and in provenance studies (Dickinson and Suczek, 1979). However, SEM-EDS analysis show clay minerals, especially chlorite, occur in the silt- and sand-size fraction as lithic-fragments, as well as the clay fraction of the sediment (Fig. 4.6A). As a result, XRD-QFL plots (Fig. 4.7) therefore closely compare to traditional petrographic-QFL plots and reveal the relative abundance of quartz, feldspar and lithics enriched in clay minerals (typically, chlorite, kaolinite and illite). The relative abundance of QFL varies as a function of estuarine zone (Fig. 4.7).

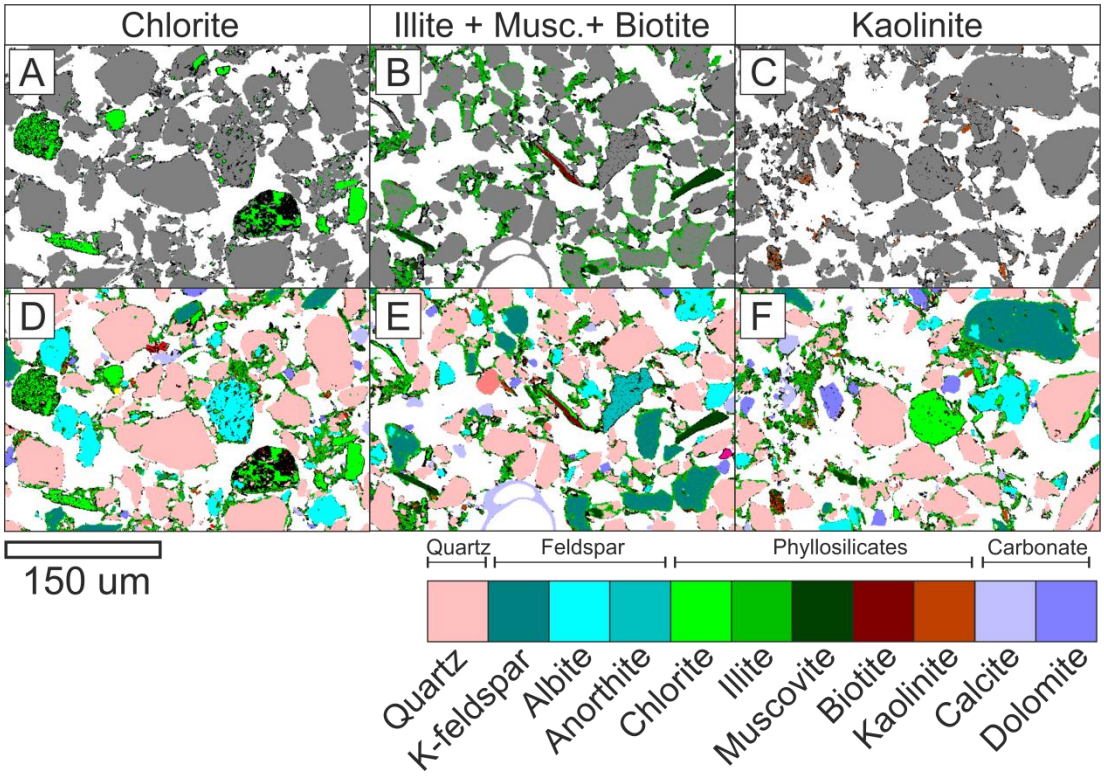

Figure 4-6 – SEM-EDS (QEMSCAN®) analysing the micron-scale (2 µm) texture and chemical and mineralogical composition of a single central-basin sample. (A-C) reveal the textural characteristics of chlorite, illite and biotite and kaolinite, (D-F) reveal the textural characteristics of all framework-grains and matrix minerals.

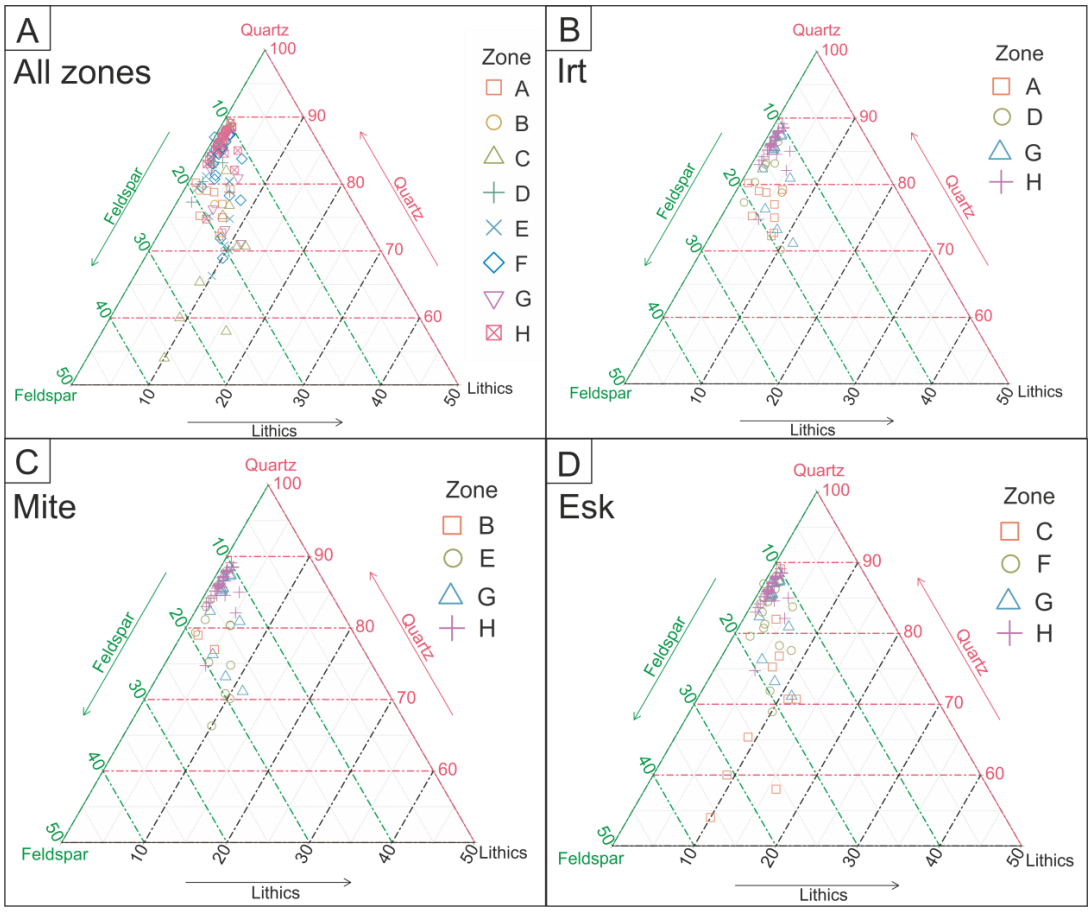

Figure 4-7 – XRD-QFL ternary plots; lithics are here defined as the sum total of clay minerals (chlorite, illite, kaolinite and smectite) in the silt- and sand-fraction. (A) QFL distribution throughout all estuarine zones, (B) River Irt, inner-Irt, central basin, and outer estuarine composition, (C) River Mite, inner-Mite, central basin, and outer estuarine composition, (D) River Esk, inner-Esk, central basin, and outer estuarine composition. Estuarine-zones are labelled accordingly; A, lower-Irt; B lower-Mite; C lower-Esk; D, inner-Irt; E, inner-Mite; F, inner, Esk; G, central-basin; and H, outer-estuary

4.5.3 Composition of drift-deposits

X-ray diffraction data have been produced from; (i) drift-deposits exposed in the cliff sections in the inner-Esk (Gosforth Glaciogenic Formation and Seascale Glaciogenic Formation), and (ii) the Ravenglass Till (part of the Seascale Glaciogenic Formation) that is exposed as knolls throughout the estuary. Ravenglass Till samples (n = 3) have the following mineral assemblage; quartz (65 to 75 %), plagioclase (8 to 14 %), K-feldspar (6 %), chlorite (2 to 3 %), illite (6 to 8 %), and kaolinite (5 %). Ravenglass Till is dominated by well-crystalline, Fe-Mg-enriched illite (Esquevin index 0.28; illite crystallinity, 0.24). The Fishgarth Wood Till Member (part of the Gosforth Glaciogenic Formation) (n = 1) has the following mineral assemblage; quartz (81 %), plagioclase (7 %), K-feldspar (6 %), chlorite (< 0.5 %), illite (5 %) and kaolinite (1 %). The Fishgarth Wood Till Member is dominated by Al-enriched illite (Esquevin index 0.43; illite crystallinity, 0.21).

4.5.4 Mineral abundance and grain size fraction

To determine whether different minerals preferentially fall in different grain size fractions of sediment in the Ravenglass Estuary, a central estuary, whole sediment sample from the Saltcoats mixed-flat was split into different grain size fractions and analysed using X-ray diffraction to quantify mineralogy. The proportion of minerals in each size separate class is shown in Figure 4.8A. Quartz abundance increases with an increase in grain size (Fig. 4.8A). K-feldspar abundance appears to be independent of grain size class (Fig. 4.8A). Plagioclase is most abundant in fine to coarse silt size sediment (~2 µm to ~ 63 µm; Fig. 4.8A). The abundance of clay minerals (chlorite, illite and kaolinite) and carbonate (mostly calcite) decrease with an increase in grain size (Fig. 4.8A).

In order to assess if the relative abundance of specific clay minerals vary in abundance in different grain size fractions, chlorite, illite, kaolinite and smectite abundance has been plotted as a function of grain size fraction (Fig. 4.8B). Relative chlorite abundance typically increases with an increase in grain size, whereas the relative abundance of illite and kaolinite decreases with an increase in grain size (Fig. 4.8B). Smectite abundance is negligible and is largely restricted to size sediment fractions < 15 µm (Fig. 4.8B).

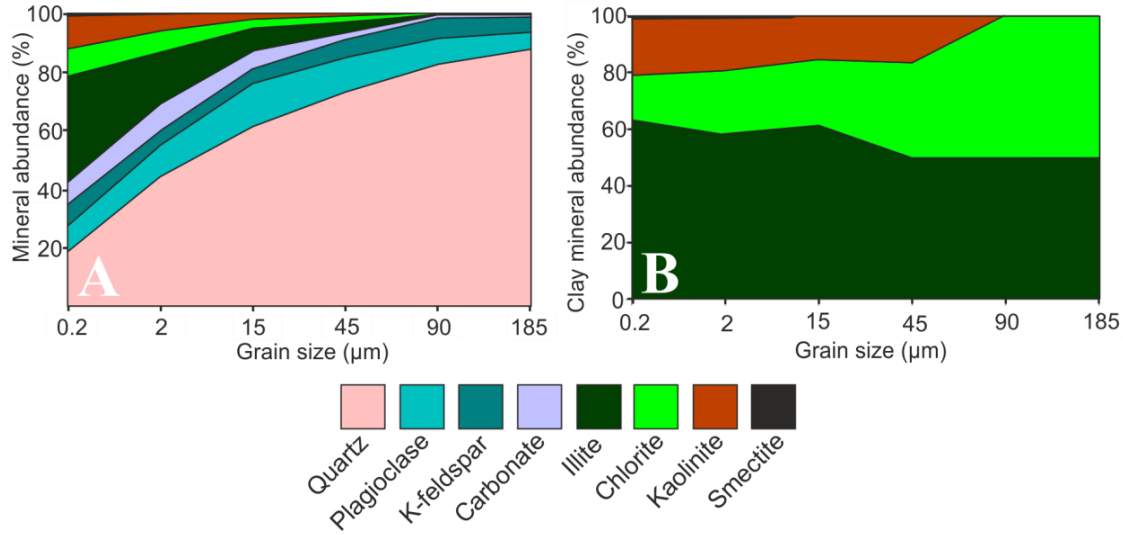

Figure 4-8 – Relative abundance of specific minerals as a function of grain-size class, extracted from a singular central-basin sediment sample, (A) whole mineral assemblage, (B) relative proportions of chlorite, illite, kaolinite and smectite.

4.5.5 Mapped estuarine mineral distribution

The mapped distribution of quartz, plagioclase, K-feldspar and carbonate can be seen in Figure 4.9. Quartz abundance ranges from 64 to 90 % and typically increases in abundance toward the open-sea (Fig. 4.9A). Quartz is most abundant (~ 90 %) in outer estuarine (tidal inlet, foreshore and backshore) sediment and least abundant (~ 64 %) toward the margin of the inner estuary and central basin (Fig. 4.9A). Plagioclase abundance ranges from 6 to 15 % and increases in abundance with proximity to the fluvial-marine interface and toward the margin of the inner-estuary and central basin (Fig. 4.9B).

A minor reduction in K-feldspar abundance is observed in tidal inlet and northern foreshore sediment (Fig. 4.9C); however, variations in K-feldspar abundance (3 to 8 %) is relatively minor throughout the majority of the Ravenglass Estuary. Carbonate abundance ranges from 0 to 5 % (of which > 95 % is calcite, < 5% is aragonite, and < 1 % is dolomite) and increases in abundance toward the margin of the inner estuary and central basin (Fig. 4.9D). Carbonate material is least abundant upon the northern foreshore and in the tidal inlet (Fig. 4.9D).

The mapped distribution of clay fraction abundance as well as specific clay minerals (chlorite, illite and kaolinite) is displayed in Figure 4.10. Clay size material is most abundant toward the estuarine margins in the inner estuary and central basin, and is negligible in the outer estuary (< 0.5 %). Chlorite is most abundant in Saltcoats tidal flat sediment and has a relatively patchy distribution throughout the inner estuary zones (Fig.4.10B). Illite is most abundant in Saltcoats tidal flat and has a relatively patchy distribution throughout the inner estuary zones (Fig. 4.10C). Kaolinite, of minor abundance, is predominantly found in mud-flats (Fig. 4.10D).

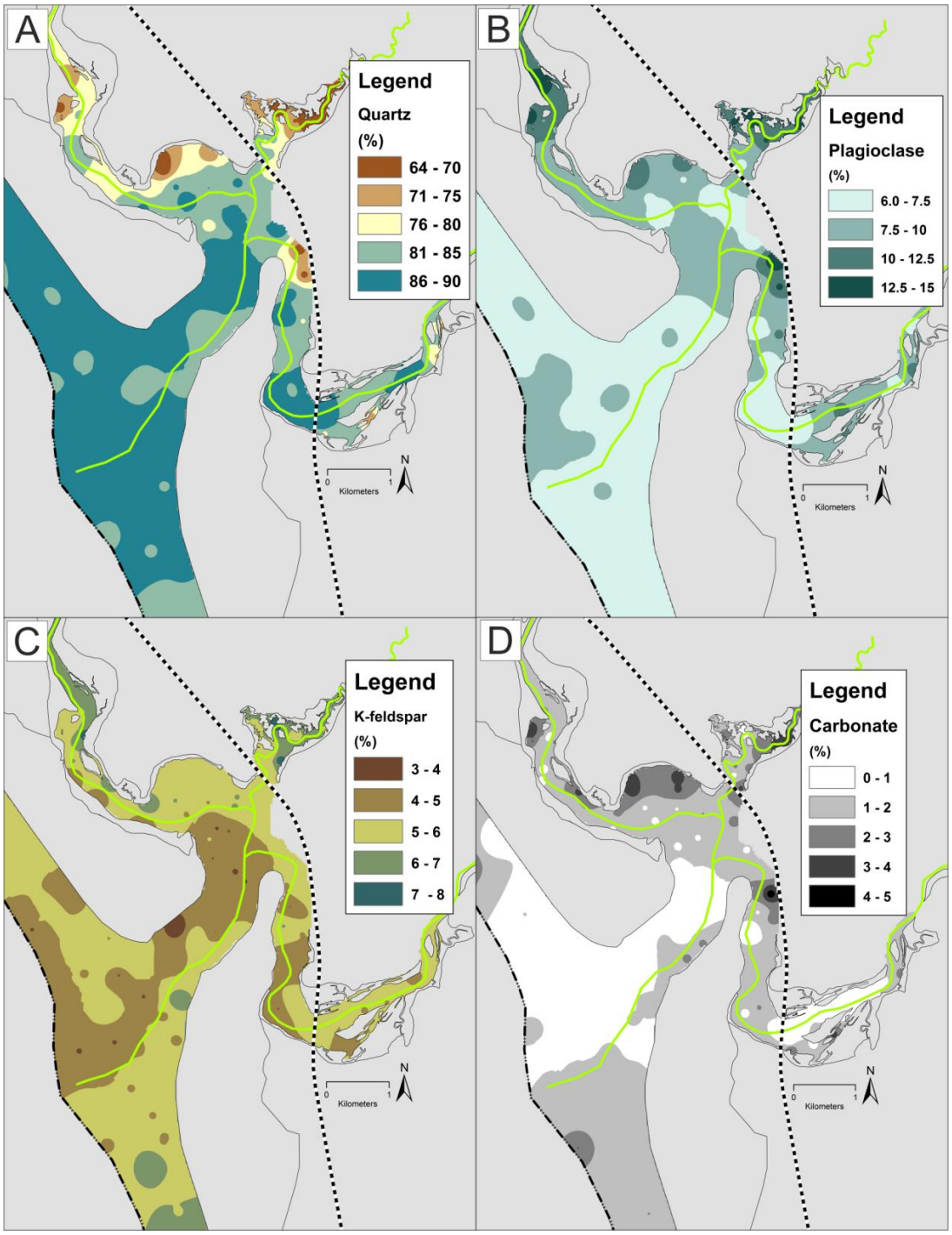

Figure 4-9 – Mapped mineral distribution patterns in the Ravenglass Estuary, UK, (A) quartz, (B) plagioclase, (C) K-feldspar, and (D) carbonate.

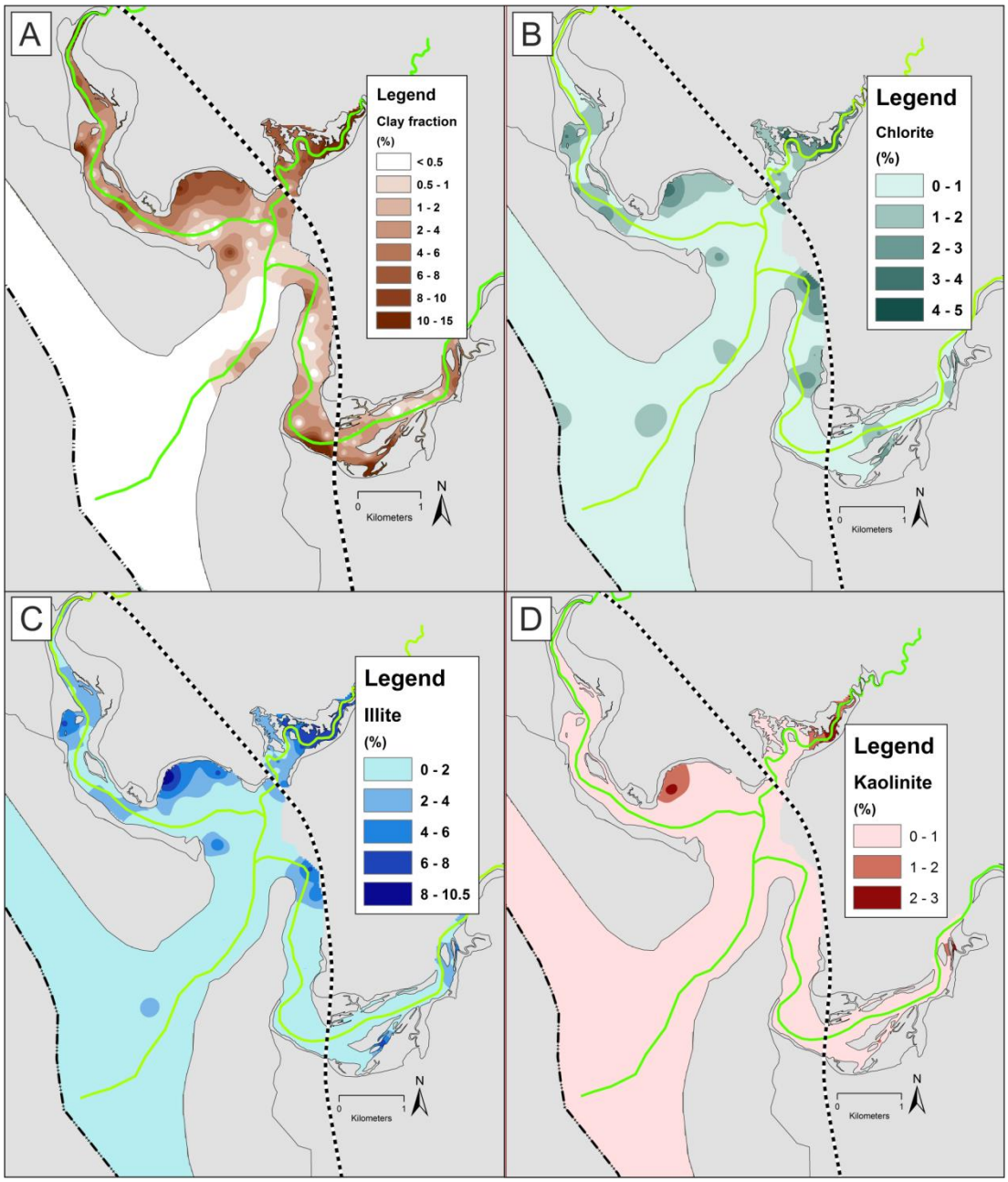

Figure 4-10 – Mapped clay-fraction (< 2µm) and clay mineral distribution patterns in the Ravenglass Estuary, UK, (A) clay fraction, (B) chlorite, (C) illite, and (D) kaolinite.

4.5.6 Mineral abundance versus mean grain size

The relationships between mean grain size and the abundance of quartz, K-feldspar, plagioclase and carbonate, as a function of depositional environment, are presented in Figure 4.11.

Quartz has uniformly high abundance (~ 85 %) in sediment between upper-fine sand (> 177 µm) and medium-upper sand (< 350 µm). Between grain size classes silt to upper-fine sand (62 to 177 µm), in mixed-flat sediments, quartz abundance typically increases with an increase in mean grain size (Fig. 4.11A). Gravel beds have a wide range of quartz abundance (Fig. 4.11A). Note that quartz abundance in mud-flats is relatively low (~ 65 to 80 %), but does not correlate to mean grain size.

Between grain size classes silt to upper very-fine sand (62 to 125 µm) plagioclase abundance typically decreases with an increase in mean grain size (Fig. 4.11B). Plagioclase has lower abundance (~ 6 to 8 %) in sediment between upper-fine sand and medium-upper sand (125 to 350 µm). Gravel beds have a wide range of plagioclase abundance (Fig. 4.11B). Note that plagioclase abundance in mud-flats is relatively high (~ 8 to 14 %), but does not correlate to mean grain size.

There is a subtle reduction in K-feldspar abundance with an increase in mean grain size (Fig. 4.11C); highest abundance in some mixed-flat sediments (7 to 8 %), and lowest abundance in sediment with a grain size greater than 350 µm in tidal-inlet and foreshore (3 to 4 %). However, most depositional environments have a K-feldspar abundance of ~ 5 to 6%.

Between grain size classes silt to upper-fine sand (primarily mixed-flats) carbonate abundance typically increases with a reduction in mean grain size (Fig. 4.11D). Carbonate is most abundant (~ 2 to 4 %) in sediment that has a mean grain size less than upper-fine sand (177 µm) (Fig. 4.11D). Carbonate abundance is relatively uniform (~ 1 %) in sediment which has a grain size greater than upper-fine sand (177 µm). Gravel beds and mud-flats have a wide range of carbonate abundance that show no relationship to grain size (Fig. 4.11D).

The relationships between mean grain size and the abundance of clay fraction in estuarine sediments, as well as the abundance of specific clay minerals (chlorite, illite and kaolinite), as a function of depositional environment, are presented in Figure 4.12.

Clay fraction abundance decreases with mean grain size in sediment up to upper-fine sand (177 µm) (Fig. 4.12A). Clay fraction abundance is uniform (typically < 1 %) in sediment coarser than 177 µm. Clay fraction is most abundant in mud- and mixed-flats; all other

depositional environments (De3 to De9) typically contain low concentrations of clay size material (typically < 1 %).

Chlorite abundance typically decreases with an increase in mean grain size, with a sharp decrease in chlorite abundance in sediment which has a mean grain size greater than lower very-fine sand (88 µm) (Fig. 4.12B). High chlorite concentrations may also occur in some foreshore, tidal inlet, tidal dunes and tidal bars sediments (Fig. 4.12B). Chlorite abundance typically increases in abundance with an increase in grain size in tidal-inlet (De6) and foreshore sediment (De8) (Fig. 4.12B). Gravel beds and mud-flats have a wide range of chlorite abundance that show no relationship to grain size (Fig. 4.12B).

Illite abundance typically decreases with an increase in mean grain size (Fig. 4.12C). A sharp increase in illite abundance is observed in sediment with a mean grain size of less than lower very-fine sand (88 µm) (Fig. 4.12C). Illite abundance is typically low (< 2 %) and shows no relationship with mean grain size in sediment that is coarser than upper-fine sand (177 µm) (Fig. 4.12C). Gravel beds and mud-flats have a wide range of illite abundance which shows no relationship to grain size (Fig. 4.12C).

There is a minor decrease in kaolinite abundance (1 to 3 %) with increasing mean grain size in mud- and mixed-flats (Fig. 4.12C). The majority of depositional environments show kaolinite abundance is minor (< 1 %) and has no relationship with mean grain size.

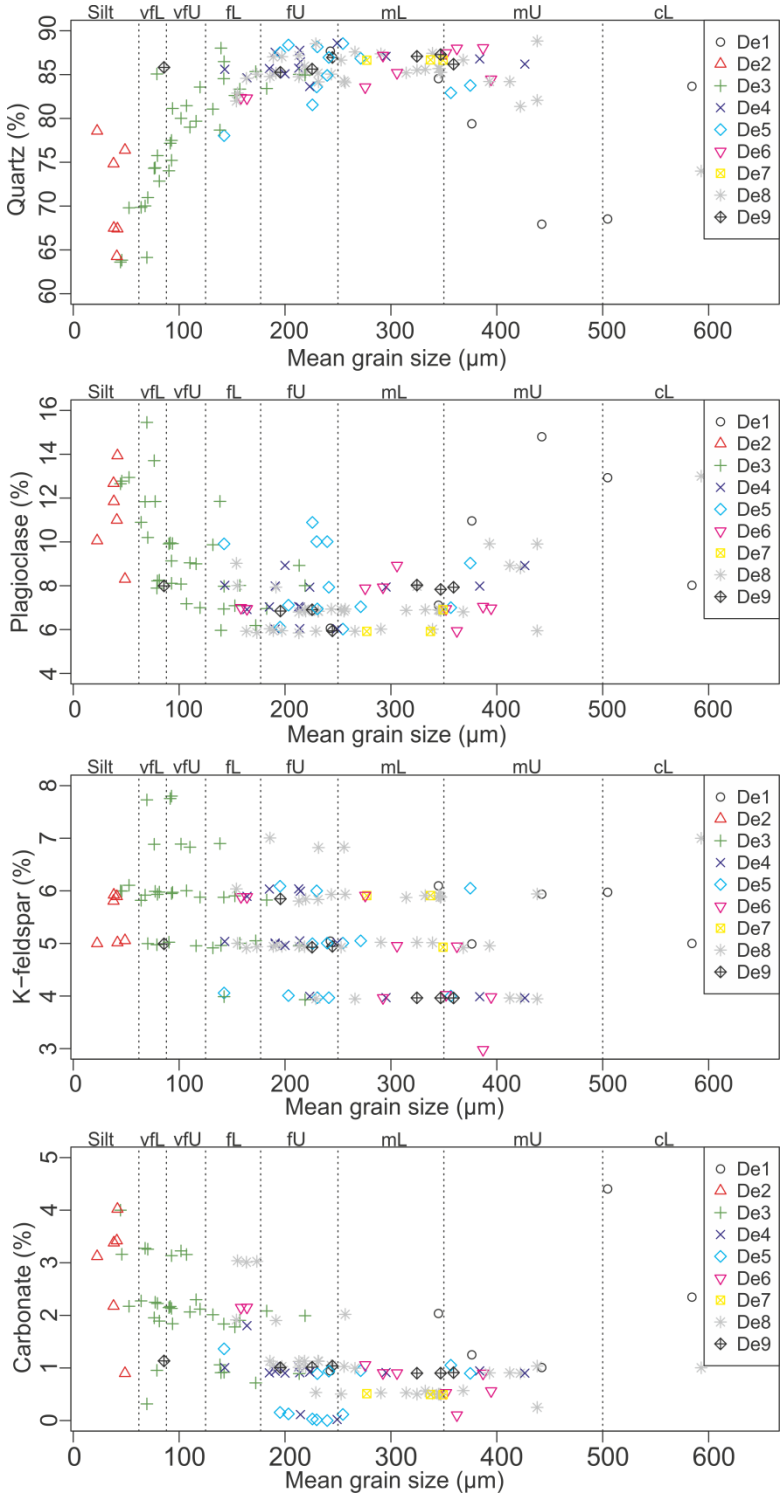

Figure 4-11 – The relationship between specific mineral abundance and mean grain size, coloured as a function of depositional environment, (A) quartz, (B) plagioclase, (C) K-feldspar, and (D) carbonate. Depositional environments are labelled accordingly; De1, gravel-bed; De2, mud-flat; De3, mixed-flat; De4, sand-flat; De5, tidal bars and dunes; De6, tidal-inlet; De7, backshore; De8, foreshore; and De9, pro-ebb delta. Mean grain size classes are labelled accordingly; silt; vfL, lower very-fine sand; vfU, upper very-fine sand; fL, lower fine sand; fU, upper fine sand; mL, lower medium sand; mU, upper medium sand; and cL, lower coarse sand.

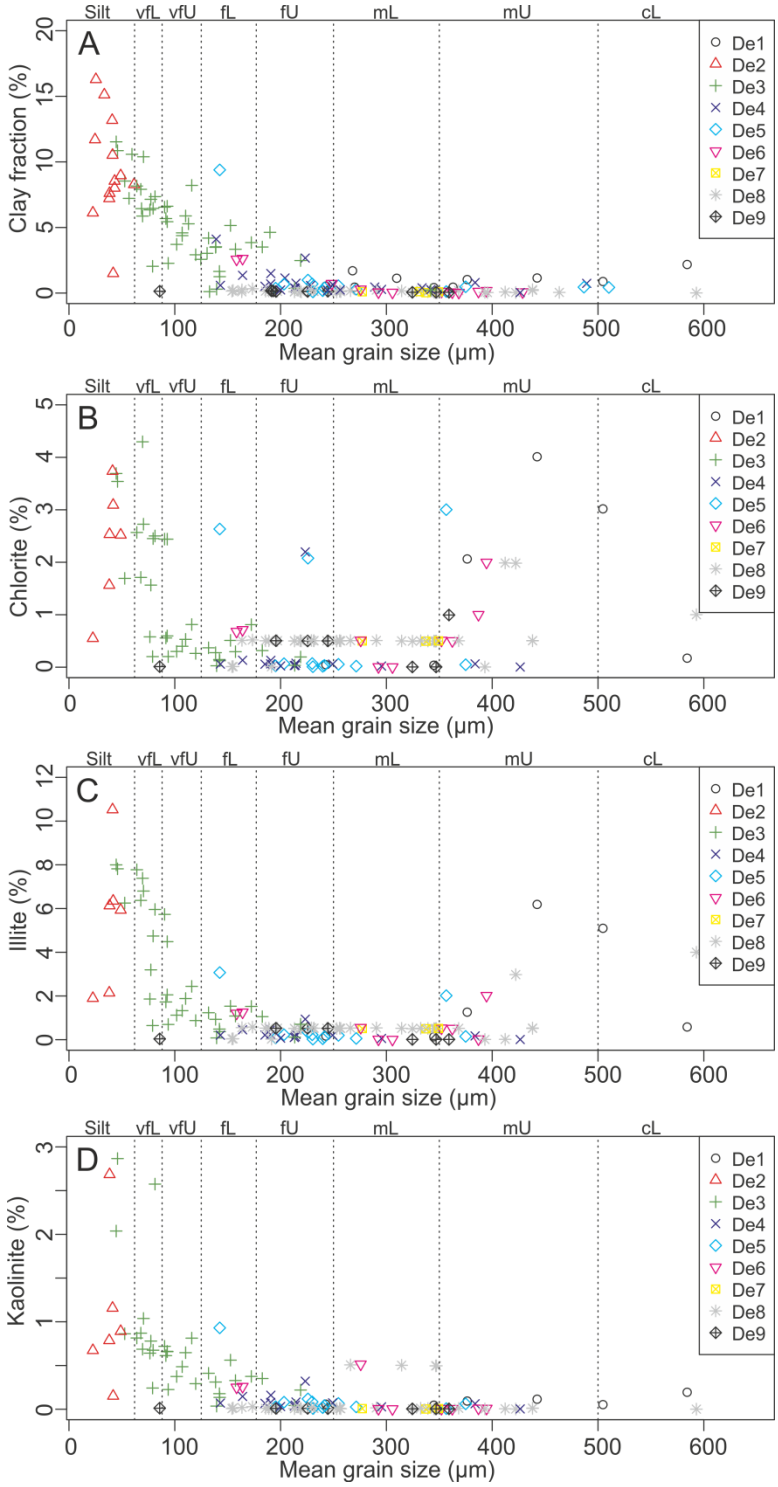

Figure 4-12 – The relationship between clay fraction (< 2 µm) and clay mineral abundance with mean grain size, coloured as a function of depositional environment, (A) clay fraction, (B) chlorite, (C) illite, and (D) kaolinite. Depositional environments are labelled accordingly; De1, gravel-bed; De2, mud-flat; De3, mixed-flat; De4, sand-flat; De5, tidal bars and dunes; De6, tidal-inlet; De7, backshore; De8, foreshore; and De9, pro-ebb delta. Mean grain size classes are labelled accordingly; silt; vfL, lower very-fine sand; vfU, upper very-fine sand; fL, lower fine sand; fU, upper fine sand; mL, lower medium sand; mU, upper medium sand; and cL, lower coarse sand.

4.5.7 Illite composition and crystallinity versus mean grain size

The clay mineral assemblage of the Ravenglass Estuary is dominated by illite (both relatively Fe-Mg-rich illite and relatively Al-rich illite). Illite composition and crystallinity have been plotted against mean grain size as a function of depositional environments in Figures 4.13A and 4.13B respectively.

In sediment with grain size finer than upper-fine sand (177 µm), illite is typically Fe-Mg-rich and relatively well-crystalline. In sediment coarser than upper-fine sand, illite has a wide range of crystallinity values and compositions (Figs. 4.13A-B). Foreshore sediment is primarily composed of poorly-crystalline (illite crystallinity index, > 0.25) and relatively Fe-Mg-depleted (Esquevin index, > 0.30).

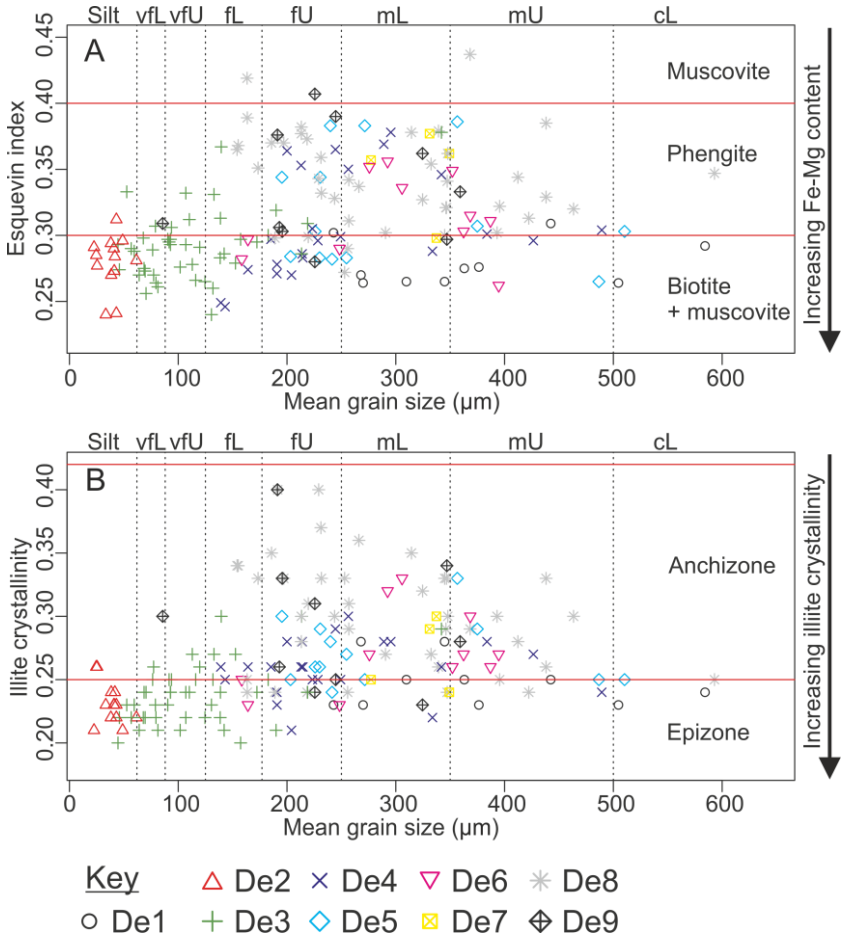

Figure 4-13 – The relationship between (A) illite chemistry (Esquevin index) and (B) illite crystallinity (full width at half-maximum of the 10Å peak) and mean grain size. Depositional environments are labelled accordingly; De1, gravel-bed; De2, mud-flat; De3, mixed-flat; De4, sand-flat; De5, tidal bars and dunes; De6, tidal-inlet; De7, backshore; De8, foreshore; and De9, pro-ebb delta. Mean grain size classes are labelled accordingly; silt; vfL, lower very-fine sand; vfU, upper very-fine sand; fL, lower fine sand; fU, upper fine sand; mL, lower medium sand; mU, upper medium sand; and cL, lower coarse sand.

4.5.8 Mineral abundance, estuarine zones and depositional environments

Average mineral abundances of the nine depositional environments and eight estuary zones are presented in Table 4.1, as well as the relative abundance of each clay mineral (clay mineral indices e.g. chlorite/(chlorite + illite + kaolinite)) for the entire estuary. Box-and-whisker plots display the range and standard deviations as well as the median values for each specific mineral as a function of depositional environment and estuarine zones (Figs. 4.14 and 4.15). Analysis Of Variance (ANOVA) test results show that there is a statistically significant difference ($p < 0.05$) in relative mineral abundance as a function of both estuarine zone, and depositional environment. The multi-comparison, post-hoc Tukey HSD test results show between which estuarine zones and depositional environments there are statistical differences ($p < 0.05$) in the abundance of quartz, plagioclase feldspar, K-feldspar, carbonate (Table 4.2), and clay minerals (Table 4.3).

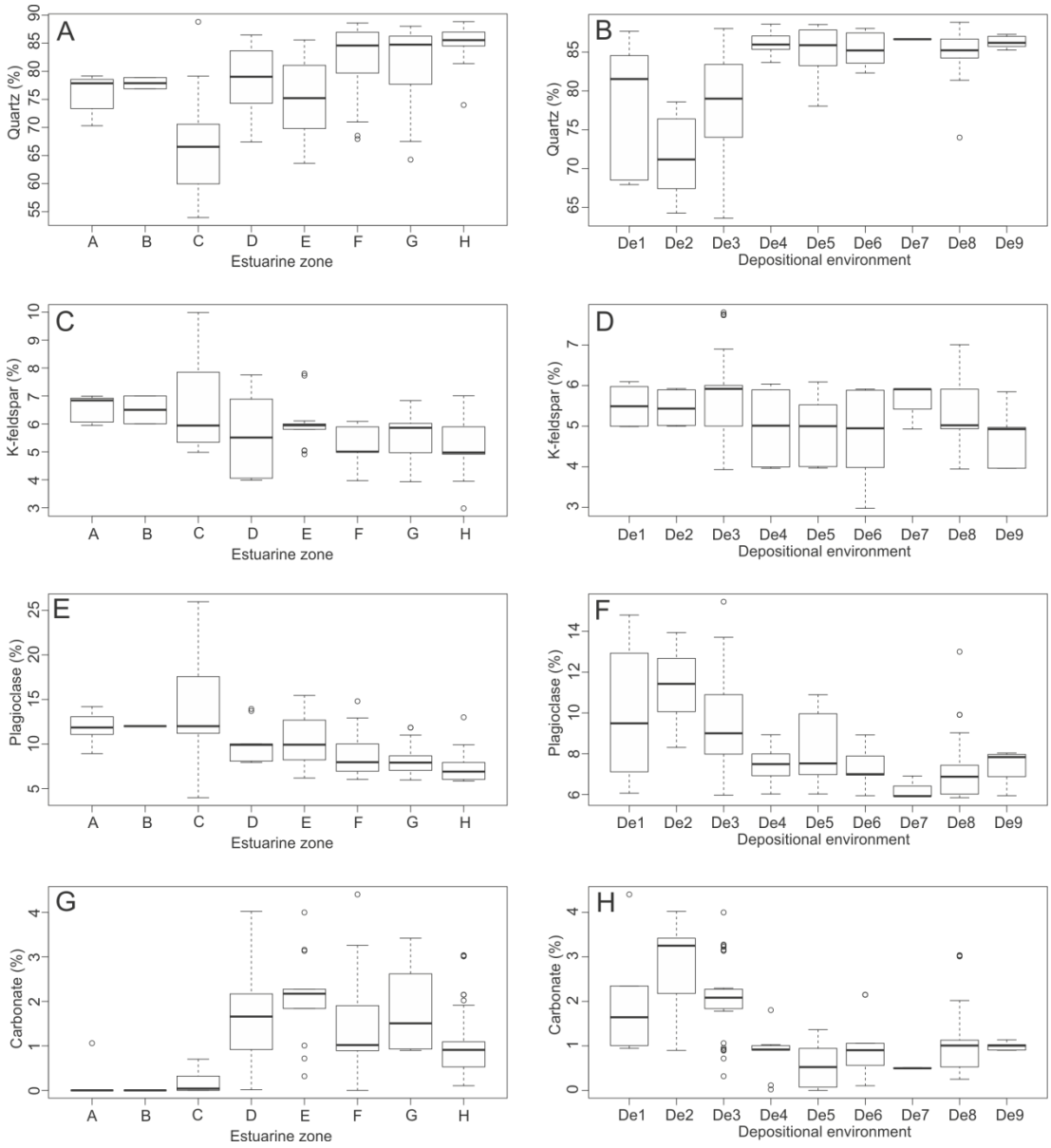

Figure 4-14 – Specific mineral abundance as a function of estuarine zone and depositional environment (A-B) quartz, (C-D) K-feldspar, (E-F) plagioclase, and (G-H) carbonate. Estuarine-zones are labelled accordingly; A, lower-Irt; B lower-Mite; C lower-Esk; D, inner-Irt; E, inner-Mite; F, inner, Esk; G, central-basin; and H, outer-estuary. Depositional environments are labelled accordingly; De1, gravel-bed; De2, mud-flat; De3, mixed-flat; De4, sand-flat; De5, tidal bars and dunes; De6, tidal-inlet; De7, backshore; De8, foreshore; and De9, pro-ebb delta.

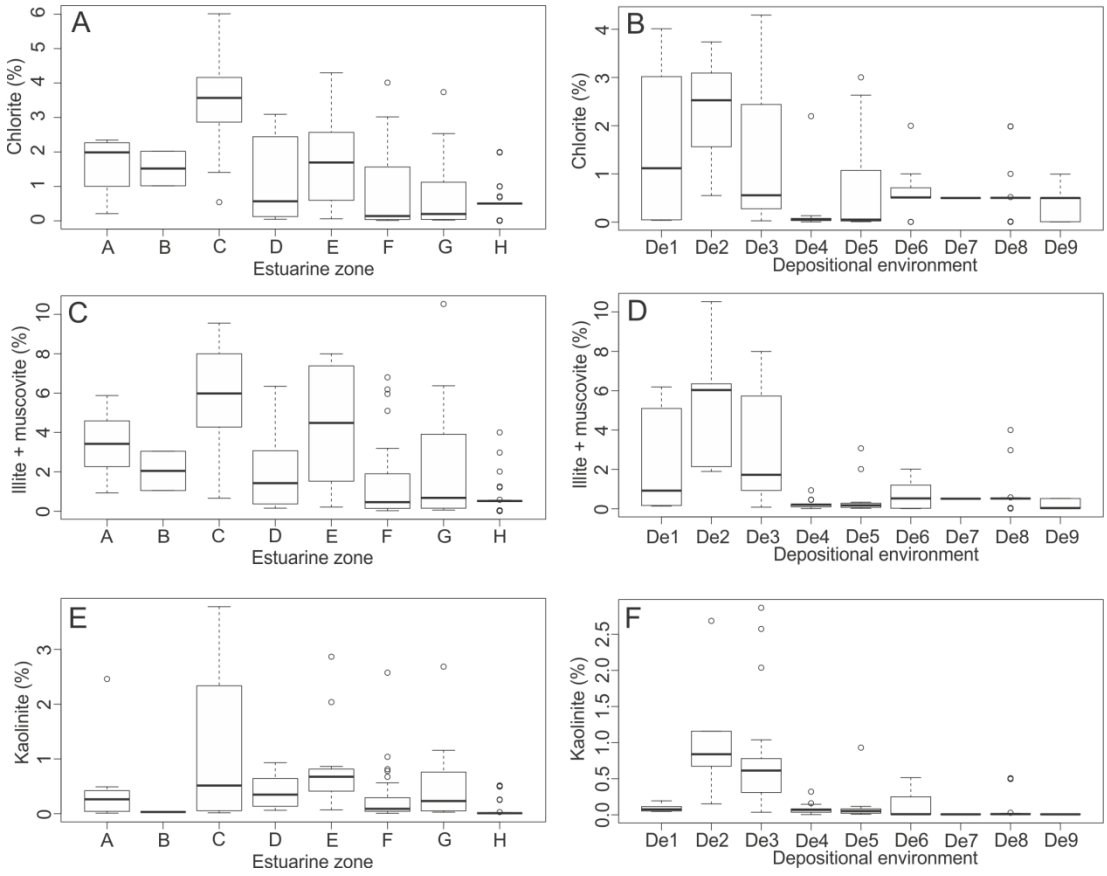

Figure 4-15 – Specific clay mineral abundance as a function of estuarine zone and depositional environment, (A-B) chlorite, (C-D) illite, and (E-F) kaolinite. Estuarine-zones are labelled accordingly; A, lower-Irt; B lower-Mite; C lower-Esk; D, inner-Irt; E, inner-Mite; F, inner, Esk; G, central-basin; and H, outer-estuary. Depositional environments are labelled accordingly; De1, gravel-bed; De2, mud-flat; De3, mixed-flat; De4, sand-flat; De5, tidal bars and dunes; De6, tidal-inlet; De7, backshore; De8, foreshore; and De9, pro-ebb delta.

Table 4.2 - Post-hoc Tukey's HSD test (following analysis of variance) results are presented here as a correlation matrix comparing quartz, K-feldspar, plagioclase and carbonate abundance data between the various estuarine zones and depositional environments from Ravenglass Estuary. Bold values indicate paired zones, or depositional environments are statistically different. Levels of statistical significant are coded as follows; Marginally-significant (+) when p < 0.1, Significant (*) when p < 0.05, very-significant (**) when p< 0.01, extremely significant (***) when p < 0.001. Grey values representing no significant difference when p > 0.1. Estuarine-zones are labelled accordingly; A, lower-Irt; B lower-Mite; C lower-Esk; D, inner-Irt; E, inner-Mite; F, inner, Esk; G, central-basin; and H, outer-estuary. Depositional environments are labelled accordingly; De1, gravel-bed; De2, mud-flat; De3, mixed-flat; De4, sand-flat; De5, tidal bars and dunes; De6, tidal-inlet; De7, backshore; De8, foreshore; and De9, pro-ebb delta.

Depositional environment								
Quartz								
	De1	De2	De3	De4	De5	De6	De7	De8
De2	-7.13							
De3	-0.84	**6.28+**						
De4	**7.5***	**14.66*****	**8.37*****					
De5	6.47	**13.59*****	**7.31*****	-1.05				
De6	6.78	**13.90*****	**7.62*****	-0.75	0.30			
De7	8.04	**15.16*****	**8.88*****	0.51	1.56	1.26		
De8	**6.42***	**13.54*****	**7.26***	-1.11	-0.06	-0.36	-1.62	
De9	**7.69+**	**14.8*****	**8.53*****	0.16	1.22	0.92	-0.34	1.28
K-feldspar								
	De1	De2	De3	De4	De5	De6	De7	De8
De2	-0.06							
De3	0.33	0.39						
De4	-0.51	-0.45	**-0.84+**					
De5	-0.66	-0.60	**-0.99***	-0.15				
De6	-0.78	-0.72	**-1.11***	-0.27	-0.12			
De7	0.08	0.13	-0.26	0.59	0.73	0.86		
De8	-0.13	-0.07	-0.46	0.38	0.53	0.65	-0.21	
De9	-0.85	-0.79	**-1.18***	-0.34	-0.19	-0.07	-0.93	-0.72
Plagioclase								
	De1	De2	De3	De4	De5	De6	De7	De8
De2	1.33							
De3	-0.53	-1.86						
De4	-2.56	**-3.89*****	**-2.03****					
De5	-1.81	**-3.14***	-1.28	0.75				
De6	-2.69	**-4.09****	**-2.16***	-0.13	-0.88			
De7	-3.73	**-5.06****	**-3.2+**	-1.17	-1.92	-1.04		
De8	**-2.79**	**-4.11*****	**-2.26*****	-0.23	-0.98	-0.10	0.94	
De9	-2.63	**-3.95****	-2.09	-0.06	-0.81	0.07	1.11	0.16
Carbonate								
	De1	De2	De3	De4	De5	De6	De7	De8
De2	0.84							
De3	0.07	-0.77						
De4	**-1.12**	**-1.96*****	**-1.18*****					
De5	**-1.45****	**-2.29*****	**-1.52*****	-0.34				
De6	-0.97	**-1.81*****	**-1.03*****	0.15	0.48			
De7	-1.50	**-2.34*****	**-1.56***	-0.38	-0.04	-0.53		
De8	-0.92	**-1.75*****	**-0.98*****	0.20	0.54	0.05	0.58	
De9	-1.01	**-1.85*****	**-1.08***	0.11	0.44	-0.04	0.49	-0.10

Estuarine zone							
Quartz							
	A	B	C	D	E	F	G
B	1.9	X					
C	**-8.4***	-10.3	X				
D	2.9	0.9	**11.2*****	X			
E	-1.5	-3.4	6.8	-4.4	X		
F	**6.6***	4.7	**14.9*****	3.7	**8.1*****	X	
G	5.1	3.2	**13.5*****	2.3	**6.7***	-1.4	X
H	**9.4*****	7.5	**17.8*****	**6.52***	**10.9*****	2.8	4.3
K-feldspar							
	A	B	C	D	E	F	G
B	0.0	X					
C	0.3	0.4	X				
D	-1.0	-0.9	**-1.3+**	X			
E	-0.5	-0.5	-0.9	0.4	X		
F	**-1.3****	-1.3	**-1.7*****	-0.4	-0.8	X	
G	**-1.1+**	-1.1	**-1.5****	-0.2	-0.6	0.2	X
H	**-1.36****	-1.3	**-1.7*****	-0.4	**-0.8+**	0.0	-0.2
Plagioclase							
	A	B	C	D	E	F	G
B	0.1	X					
C	2.6	2.6	X				
D	-1.9	-2.0	**-4.5****	X			
E	-1.4	-1.5	**-4.0****	0.5	X		
F	**-3.5****	-3.6	**-6.2*****	-1.6	-2.1	X	
G	**-3.7****	-3.8	**-6.4*****	-1.8	-2.3	-0.2	X
H	**-4.7*****	-4.8	**-7.4*****	**-2.8***	**-3.3**	-1.2	-1.0
Carbonate							
	A	B	C	D	E	F	G
B	-0.1	X					
C	0.1	0.2	X				
D	**1.6*****	1.8	**1.5****	X			
E	**1.8*****	**2.1***	**1.9*****	0.3	X		
F	**1.2****	1.3	**1.1***	-0.4	-0.7	X	
G	**1.7*****	**1.8+**	**1.6*****	0.0	-0.3	0.5	X
H	**0.9+**	1.0	0.8	-0.7	**-1.1****	-0.3	**-0.8***

Table 4.3 - Post-hoc Tukey's HSD test (following analysis of variance) results are presented here as a correlation matrix comparing chlorite, illite and kaolinite abundance data between the various estuarine zones and depositional environments from Ravenglass Estuary. Bold values indicate paired zones, or depositional environments are statistically different. Levels of statistical significant are coded as follows; Marginally-significant (+) when p < 0.1, Significant (*) when p < 0.05, very-significant (**) when p< 0.01, extremely significant (***) when p < 0.001. Grey values representing no significant difference when p > 0.1. Estuarine-zones are labelled accordingly; A, lower-Irt; B lower-Mite; C lower-Esk; D, inner-Irt; E, inner-Mite; F, inner, Esk; G, central-basin; and H, outer-estuary. Depositional environments are labelled accordingly; De1, gravel-bed; De2, mud-flat; De3, mixed-flat; De4, sand-flat; De5, tidal bars and dunes; De6, tidal-inlet; De7, backshore; De8, foreshore; and De9, pro-ebb delta.

Depositional Environment

Chlorite

	De1	De2	De3	De4	De5	De6	De7	De8
De2	0.77	X						
De3	-0.37	-1.15	X					
De4	**-1.35+**	**-2.12*****	**-0.98****	X				
De5	-0.89	**-1.66***	-0.52	0.46	X			
De6	-0.90	**-1.67***	-0.53	0.45	-0.01	X		
De7	-1.06	-1.83	-0.69	0.29	-0.17	-0.16	X	
De8	-1.01	**-1.79*****	**-0.64+**	0.33	-0.13	-0.11	0.05	X
De9	-1.20	**-1.97****	-0.83	0.15	-0.31	-0.30	-0.14	-0.18

Illite

	De1	De2	De3	De4	De5	De6	De7	De8
De2	**3.26***	X						
De3	0.74	**-2.52***	X					
De4	-1.99	**-5.24*****	**-2.73*****	X				
De5	-1.69	**-4.95*****	**-2.43****	0.30	X			
De6	-1.56	**-4.82*****	**-2.30***	0.43	0.13	X		
De7	-1.73	**-4.99****	**-2.47****	0.26	-0.04	-0.17	X	
De8	-1.62	**-4.88*****	**-2.36*****	0.37	0.07	-0.06	0.11	X
De9	-2.00	**-5.26*****	**-2.74*****	-0.02	-0.31	-0.45	-0.27	-0.38

Kaolinite

	De1	De2	De3	De4	De5	De6	De7	De8
De2	**0.96*****	X						
De3	**0.59****	-0.37	X					
De4	-0.01	**-0.97*****	**-0.59*****	X				
De5	0.03	**-0.93*****	**-0.56*****	0.04	X			
De6	0.03	**-0.94*****	**-0.56*****	0.03	0.00	X		
De7	-0.09	**-1.05*****	**-0.68+**	-0.08	-0.12	-0.11	X	
De8	-0.03	**-0.99*****	**-0.61*****	-0.02	-0.06	-0.05	0.06	X
De9	-0.09	**-1.05*****	**-0.68****	-0.08	-0.12	-0.11	0.00	-0.06

Estuarine Zone

Chlorite

	A	B	C	D	E	F	G
B	0.01	X					
C	**1.92****	1.91	X				
D	-0.30	-0.31	**-2.22*****	X			
E	0.36	0.35	**-1.56****	0.66	X		
F	-0.69	-0.70	**-2.61*****	-0.39	**-1.05***	X	
G	-0.73	-0.74	**-2.65*****	-0.43	**-1.09+**	-0.04	X
H	-0.98	-0.99	**-2.89*****	-0.68	**-1.34*****	-0.29	-0.25

Illite

	A	B	C	D	E	F	G
B	-1.41	X					
C	2.49	3.90	X				
D	-1.30	0.11	**-3.79****	X			
E	0.72	2.13	-1.77	2.02	X		
F	-2.04	-0.63	**-4.53*****	-0.74	**-2.76****	X	
G	-1.24	0.17	**-3.72*****	0.06	-1.96	0.80	X
H	**-2.89****	-1.48	**-5.38*****	-1.59	**-3.61*****	-0.85	**-1.65+**

Kaolinite

	A	B	C	D	E	F	G
B	-0.43	X					
C	**0.89***	**1.31+**	X				
D	-0.06	0.37	**-0.95***	X			
E	0.39	0.83	-0.49	0.45	X		
F	-0.17	0.26	**-1.06*****	-0.11	**-0.56+**	X	
G	0.03	0.46	**-0.86***	0.09	-0.36	0.20	X
H	-0.40	0.03	**-1.29*****	-0.34	**-0.79*****	-0.23	-0.43

4.6 DISCUSSION

Sandstone composition is controlled by the hinterland geology and all the processes between sediment source area, at the final site of deposition and during burial diagenesis. Controls on the composition (mineral assemblage) of the Ravenglass Estuary, as well as the controls on QFL-C distribution patterns are discussed in this section. Influences on mineral distribution patterns that are here discussed include: provenance and sediment transport pathways, estuarine hydrodynamics, and early-diagenesis (both *in situ* diagenesis and continued mineral alteration during sediment transport).

4.6.1 Controls on estuarine sediment composition

There are three potential sources of sediment in the Ravenglass Estuary: (i) fluvial drainage of bedrock in the hinterland (Fig. 4.2A), (ii) fluvial drainage and local erosion of drift and soil deposits in the hinterland, underlying the estuary and exposed in proximal cliff-sections (Fig. 4.2B), and (iii) marine inundation with landward-displacement of littoral-zone sediment into the estuary.

The empirical relationship between composition of sands (QFL; based on sandstone petrology), provenance, and the plate-tectonic setting of the sedimentary basin was first established by Dickinson and Suczek (1979). The 'Dickinson model' was later revised in order to improve predictive capabilities using the additive log-ratio transformation by Weltje (2006). Since whole sediment (QFL-C) mineralogy instead of petrographic QFL data is reported, it is not possible to follow the methodology outlined by Dickinson and Suczek (1979) or Weltje (2006). Moreover, XRD data, unlike petrographic QFL data, can reveal Esquevin indices (Esquevin, 1969) and illite crystallinity (Kübler, 1964) values which may be used to identify possible sediment source areas and transport pathways (Borchers et al., 2011; Bout-Roumazeilles et al., 2013; Du Chatelet et al., 2016; Gingele et al., 2001; Oliveira et al., 2002).

The sediment composition of the Ravenglass Estuary is arkosic to subarkosic (Fig. 4.7), which is likely to reflect the drainage of the Eskdale Granite and Borrowdale Volcanic Group, in agreement with predictive models produced by Dickinson and Suczek (1979). There are no carbonate rocks, or carbonate-rich drift deposits in the hinterland of the Ravenglass Estuary. As a result, carbonate material is likely to have been primarily derived from gravel beds which are partly colonised by shell beds in the inner-Esk (autochthonous) and/or derived from offshore (allochthonous). Detrital chlorite lithics have been reported to be pyroxene pseudomorphs in the Borrowdale Volcanic Group (Quirke et al., 2015), and the result of chloritization of mafic silicates in the Eskdale Granite (Moseley, 1978; Quirke et

al., 2015; Young et al., 1986). As a result, chlorite lithics in the Ravenglass Estuary (Fig. 4.6A) are likely to have been sourced from the Borrowdale Volcanic Group and chloritized areas of the Eskdale Granite; both of which have been reworked, and incorporated into overlying quaternary drift-deposits (Merritt and Auton, 2000).

Fe-Mg-rich and relatively well-crystalline illite (Fig. 4.13), which dominates sediment finer than upper-fine sand (< 177 μm) in the Ravenglass Estuary, is likely sourced from the Ravenglass Estuary; since, such values are typical of physically eroded, unweathered rocks (Chamley, 1989). In contrast, sediment that is coarser than upper-fine sand (> 177 μm), contains illite that have a wide range of crystallinity values and compositions (Figs. 4.13A-B); characteristic of chemically-weathered rocks that have lost divalent cations (Fe and Mg) from the octahedral sites (Chamley, 1989).

XRD results show both rigid framework grains (e.g. quartz) and brittle minerals (e.g. feldspar) are present in high abundance in both the clay- and silt-fraction of drift deposits; likely due to extensive subglacial-comminution. The relatively high concentration of quartz in the clay- and silt-fraction of Ravenglass Estuary sediment is probably in contrast to other non-glacial sedimentary basins that are relatively depleted in quartz in the finest sediments. Furthermore, the Ravenglass Till may also be an important source of plagioclase with abundances up to 14%.

4.6.2 Controls on mineral distribution patterns

4.6.2.1 Provenance controls and sediment transport pathways

Provenance studies, based on sandstone composition, may be undertaken in order to unravel and characterize the complex history that has led to the production and the evolution of sediments, from initial weathering and erosion in the source sediment area, passing through to sediment transport and temporary storages, and finally burial and lithification (Caracciolo et al., 2012). For example, the vertical (stratified) differences in plagioclase content are reported to reflect differences in sediment provenance in the Stratfjord Formation, Gullfaks Field (Dalland et al., 1995).

It is noteworthy, that grain size dependence of sediment composition may lead to environmental bias in provenance studies, as shown by Garzanti et al. (2009). However, despite River Irt and Mite (northern drainage basin) sediment having a comparable mean grain size (Fig. 4.5A), River Esk sediment (southern drainage basin) is relatively chlorite- and feldspar-rich (Fig. 4.15A). The enrichment of feldspar and chlorite may reflect the drainage of chloritized and feldspathic Eskdale Granite bedrock which is primarily restricted to the River Esk drainage basin (south of Muncaster Fell; Fig. 4.1). An important outcome of

this study, is that despite the two major Rivers Irt and Esk having different fluvial compositions, counterpart inner estuarine zones (inner-Irt, zone D; inner-Esk, zone F) show no statistical difference in composition (Tables 4.2 and 4.3). Thus, provenance signals have been removed due to intense estuarine mixing (due to a macro-tidal regime and short estuarine length) and possible dilution by a second estuarine mineral assemblage (e.g. internal erosion of glacial-deposits throughout the estuary).

4.6.2.2 Hydrodynamic controls, mechanical breakdown and physical-sorting of minerals by grain size

Findings of Odom et al. (1976) are often invoked to explain mineral distribution patterns in many sandstone reservoirs. Odom et al. (1976) reported feldspar abundance and distribution in four quartz-rich cratonic sandstones (Cambrian, Ordovician, Pennsylvanian-Permian and Jurassic) was controlled by the degree of sediment abrasion (grain-size), transport processes and depositional environment (Odom et al., 1976). Results presented by Odom et al. (1976) show feldspar tends to be concentrated in the < 125 μm fraction (upper very-fine sand) of the sediment or in some cases that coarse silt fraction in Cambrian to Ordovician sandstones of the upper Mississippi Valley, and Palaeozoic Weber Sandstone. Field and Pilkey (1969) have also shown that feldspar in shelf and beach sands off North Carolina is concentrated in the fine and very fine sand fractions as a result of intense abrasion. In agreement with results from Odom et al. (1976) plagioclase abundance decreases significantly above a critical grain size threshold of 125 μm. However, Odom et al. (1976) hypothesise that 125 μm represents a threshold below which feldspar tends to be less susceptible to further size reduction by abrasion. In contrast, results of this study show plagioclase is susceptible to further size reduction (most likely due to extensive subglacial comminution in this study), and consequently plagioclase abundance typically continues to increase in abundance with a reduction in mean grain size, between grain size classes silt to upper very-fine sand (62 to 125 μm). Glacial comminution, has previously been shown to lead to both quartz and feldspar being concentrated in clay and silt fractions, as reported in glaciomarine deposits e.g. in Gothenburg, Sweden (Stevens, 1991). In contrast, K-feldspar appears to show little relationship with mean grain size, and displays only a minor depletion in sediment upon the northern foreshore, that is typically coarser than upper-fine sand (> 250 μm). The depletion in K-feldspar and carbonate in northern foreshore sediment may reflect the dominant wave-direction originating from the south-west.

Quartz, a rigid-framework grain, is relatively resistant to sediment abrasion and grain-size reduction in comparison to brittle-framework grains such as feldspars, carbonate and clay minerals. Estuarine hydrodynamics cause the physical sorting of grains by size, and consequently has led to a relatively uniform high abundance (~ 85 %) of quartz in

depositional environments comprised of relatively coarse sediment (> 177 to 350 µm). Depositional environments with a mean grain size between 62 to 177 µm typically show a progressive increase in quartz abundance with an increase in mean grain size.

Allochthonous (derived from offshore) carbonate material has likely suffered extensive abrasion due to repeated wave-action, prior to being transported and deposited into the estuarine system. Equally, autochthonous (from gravel beds which are partly colonised by shell beds in the inner-Esk) has likely experienced extensive reworking and abrasion by strong-tidal currents. Consequently, carbonate (> 95 calcite) material is most abundant in low-energy depositional environments, in sediment that has a mean grain size less than upper-fine sand (177 µm) (Fig. 4.11D). In contrast, carbonate material is likely re-suspended, during tidal inundation and due to wave action, in sediment which has a grain size greater than upper-fine sand (177 µm).

Chlorite, illite and kaolinite, as expected, dominate the clay-fraction of estuarine sediment, and are therefore most abundant in relatively low-energy depositional environments (mud- and mixed-flats). However, relatively high-energy tidal-dunes and tidal-bars, foreshore, and tidal inlet depositional environments occasionally contain elevated chlorite concentrations (Fig. 4.12B), which cannot be explain by an increase in clay size material (Fig. 4.12A). As a result, increased chlorite concentrations in such depositional environments are likely to reflect the accumulation of chlorite lithics (Fig. 4.6A).

4.6.2.3 Early mineral alteration and chemical breakdown controls

Early-mineral alteration may be especially significant in marginal marine settings since at the fluvial-marine interface there is a merging of terrigenous sediment transported by low salinity, relatively organic- and iron-rich continental waters, with high salinity, marine conditions, which contain high sulphate and locally low oxidation state, low pCO_2 waters (Berner and Berner, 2012; Boyle et al., 1974; Boyle et al., 1977; Sholkovitz, 1978; Sholkovitz et al., 1978). Early-mineral alteration in the Ravenglass Estuary remains a potential control. Based on high-resolution QEMSCAN® (SEM-EDS imaging), Daneshvar and Worden (2017) report that detrital K-feldspar grains are preferentially rimmed by neoformed illite, while plagioclase grains may be preferentially rimmed by neoformed kaolinite in the Ravenglass Estuary; suggested to be evidence for continued mineral alteration of the estuarine sediment. The concept of early-mineral alteration in the Ravenglass Estuary remains possible, however, it should be noted that intense alteration of feldspars in the hinterland of the Ravenglass Estuary is widely reported (Moseley, 1978; Quirke et al., 2015; Young et al., 1986). As a result, kaolinized-plagioclase, and illitized-K-

feldspars may be an inherited feature of the sediment and not due to continued weathering in the estuary.

4.7 SIGNIFICANCE

4.7.1 Sandstone composition and provenance signals

Many models enable relatively accurate predictions of sandstone composition, during hydrocarbon exploration, field appraisal and development, primarily based upon the hinterland geology (Dickinson and Suczek, 1979; Garzanti et al., 2009; Weltje, 2006). For example, the 'Dickinson Model' (Dickinson and Suczek, 1979) may be used during hydrocarbon exploration to make broad prediction on sediment composition, however, it does not lend itself easily to other applications, such as regional studies of multi-source basin fills (Weltje, 2006). In addition, petrographic-QFL studies may fail to distinguish between glacial and non-glacial derived sediments, unlike Esquevin indices which can be calculated from X-ray Diffractograms; a key proven tool in the Ravenglass Estuary (Fig. 4.13). In this study, it is acknowledged that Esquevin Index and illite crystallinity datasets may not be appropriate when studying sandstones which may have commenced illite-alteration during burial. Fluvial sediment is delivered to the estuary via two main fluvial drainage basins (Fig. 4.1). These rivers drain different bedrock, soil and drift deposits and which therefore have different sediment compositions (Fig. 4.7). However, the relative proportions of minerals in sediment in the counterpart inner-estuarine zones (i.e. inner Esk and inner Irt) are relatively uniform (Table 4.2). The diminution of provenance signals in Ravenglass inner estuarine zones is most likely due to intense mixing promoted by strong tidal currents and a short estuarine length. As a result, provenance signals are likely to be dampened, once sediment has passed through the fluvial-marine interface, at least in macro-tidal estuarine systems with a short estuarine length due to intense sediment mixing.

4.7.2 Mineral distribution patterns: impact on diagenetic processes and anthropogenic activities

The economic viability of sandstone reservoirs can be assessed by prediction of: (i) porosity, which controls petroleum in-place, and (ii) permeability, which controls the rate at which petroleum can be produced. Grain size, sorting, matrix content and sandstone composition are major controls on the porosity and permeability of sandstones reservoirs (Beard and Weyl, 1973; Bloch, 1991; Ramm and Bjorlykke, 1994; Scherer, 1987). Distribution patterns of grain size, grain-size sorting, matrix content and mineral proportions, presented in this study, may therefore be used, by analogy, to better understand the distribution reservoir

quality in marginal-marine sandstones. The impact that primary composition, in terms of quartz, feldspar, clay minerals (as both matrix and lithics) and carbonates (QFL-C), may have on sandstone reservoir quality is best studied as a function of (i) primary porosity and eogenetic processes, (ii) mesogenetic processes; and (iii) anthropogenic activities such as carbon capture and geological storage or injection of water for pressure support.

4.7.2.1 Primary porosity and eodiagenesis: Impact of mineral distribution patterns

Primary porosity and permeability are governed primarily by grain size, grain-size sorting and matrix content (Beard and Weyl, 1973; Bloch, 1991; Ramm and Bjorlykke, 1994; Scherer, 1987). The data from this study show that grain size, sorting and matrix content are highly dependent upon depositional environments and are influenced by composition of the sediment (Figs. 4.4, 4.5C-D, 4.12A). This study may therefore be used, by analogy, to better predict the distribution of grain size, sorting and matrix content in sandstone, and thus predict reservoir quality using empirical relationships (Beard and Weyl, 1973; Bloch, 1991; Ramm and Bjorlykke, 1994). In the Ravenglass Estuary, brittle grains, such as feldspar and clay-mineral-rich-lithics, are noticeably much finer-grained than rigid-grains such as quartz (Figs. 4.8, 4.11, 4.12). Therefore, it is here hypothesized that sediment derived from a hinterland enriched in relatively brittle-minerals e.g. feldspar, may have a wide grain-size distribution through progressive abrasion. As a result, it may be possible to conclude that provenance not only controls sediment composition, but also grain size, sorting and matrix content. It is noteworthy that diatoms are reported to exist in high abundance in mud- and mixed-flats in the Ravenglass Estuary (Wooldridge et al., 2017a). The abundance and distribution of diatoms may be significant since diatoms, which form biofilms, have been reported to increase sediment heterogeneity in tidally-influenced depositional environments (Garwood et al., 2015). As a result, reservoir quality models may need to further consider the influence of bio-sediment interactions on grain size distribution patterns.

In addition to physical processes, chemical reactions during early-burial diagenesis (eodiagenesis) may significantly influence the porosity and permeability of sediment, as well as leading to early-mineral alteration and possible formation of new minerals (typically, clay minerals illite and kaolinite).

It is known that large volumes of early-carbonate cement can obliterate porosity (Kantorowicz et al., 1987). However, early carbonate cement may increase the mechanical strength of sediments (Morris et al., 2006), and may therefore preserve porosity during compaction. As a result, better reservoir quality may be found in estuarine depositional environments that initially contained a small, as yet undefined, amount of carbonate material.

Meteoric water flushing is especially common in estuaries, since marginal marine systems are highly-sensitive to relative sea level changes (Morad et al., 2010). Meteoric water flushing may lead to dissolution and kaolinization of reactive silicate minerals (primarily feldspars and clay minerals) (Glasmann et al., 1989). Kaolinization of feldspar is most likely to occur in fluvial sediment and at the head of the estuary, away from marine-influence, where there is a greatest influence of meteoric water (Worden and Burley, 2003). The greatest abundance of plagioclase is found in fluvial sediment of the River Esk and at the head of the estuary (Figs. 4.7 and 4.9). Therefore, it is here speculated that the replacement of feldspar by kaolinite is most likely to be important in mud- and mixed-flat estuarine sediments and in fluvial sediments.

4.7.2.2 Mesodiagenesis: impact of mineral distribution patterns

Burial diagenesis (mesodiagenesis) of sandstones is controlled by a wide variety of factors such as burial and thermal histories, fluid pressure history, influx of high salinity formation waters causing albitization, influx of CO_2 promoting feldspar-clay reactions, and the influx of petroleum. All of these factors influence mechanical and chemical compaction as well as quartz, clay-mineral, carbonate, sulphate, sulphide and oxide diagenetic reactions. However, primary sediment composition and eodiagenesis together have strong controls on the diagenetic evolution during burial and thus limit the range of likely outcomes during subsequent burial (Primmer et al., 1997). The main compositional controls on reservoir quality during mesogenesis may be summarised as follows: (i) Clay-rich ductile-bearing sediment versus rigid grain-dominated sediment, (ii) Brittle versus rigid grains, (iii) Reactive versus unreactive grains, (iv) Quartz grain pressure solution and subsequent quartz cementation, and (v) Wettability.

Sandstone that is rich in ductiles is likely to experience higher degrees of mechanical compaction than sediment depleted in ductile grains (Worden et al., 2000). Sandstone that is rich in brittle feldspars grains is more likely to undergo grain fracture than sediment rich in rigid grains, such as quartz (Griffiths et al., 2016). Sandstone that is rich in reactive feldspars, clay minerals and carbonates is likely to undergo a rich variety of geochemical reactions but sandstone depleted in reactive grains will probably have a simpler diagenetic history with little other than quartz cement (Primmer et al., 1997). Sediment rich in ductile grains, brittle grains and reactive grains in the Ravenglass Estuary is found in the mud- and mixed-flats in the inner estuary and central basin; these depositional environments would therefore experience greater compaction than outer estuarine zones, e.g. foreshore, where sediment is depleted in ductile and brittle grains. Note that K-feldspar distribution is relatively homogeneous across the Ravenglass Estuary (Fig. 4.9C) and that the variation in

reactive mineral abundance is largely controlled by plagioclase and clay-mineral variations (Fig. 4.9B and 4.10).

The amount of quartz cement in buried sandstones has been directly related to the fraction of quartz grains in a sandstone (Walderhaug, 1994a; Walderhaug, 1994b). In the Ravenglass Estuary, the greatest proportion of quartz grains are found in the outer estuary (Fig. 4.9A), so that that these environments represent sites that would become most extensively quartz cemented if these sediments were buried to > 80 to 100ºC. Quartz-quartz grain pressure solution and quartz cementation has been reported to be exacerbated by the presence of illite (Oelkers et al., 1996). In contrast, quartz cementation has been reported to be inhibited by the presence of chlorite grain coats (Dowey et al., 2012; Ehrenberg, 1993). In the Ravenglass Estuary, mud- and mixed-flats have the greatest quantities of both illite, chlorite and contain the most extensive detrital clay coats (Wooldridge et al., 2017a; Wooldridge et al., 2017b). Whether quartz cementation would be promoted or inhibited is likely to be controlled by the exact proportions of the two minerals, noting that most "chlorite" grain coats have mixed mineralogy (Stricker et al., 2016). It is noteworthy that chlorite-rich lithics may also be found in the highest abundance in the coarser grained sediments throughout the estuary (Fig. 4.10B), typically in low-amplitude dunes and tidal bars, and that these sediments may become chlorite-coated in deeply-buried sandstone reservoirs.

Wettability in sandstones is strongly controlled by the abundance of kaolinite and carbonate minerals (Barclay and Worden, 2000a); greater amounts of kaolinite and carbonate will tend to lead to mixed- and oil-wet rocks. In the Ravenglass sediments, the greatest quantities of carbonate and kaolinite are found in the mud- and mixed-flats (Figs. 4.9D and 4.10D) so that these environments represent sites that would become more oil-wet if the sediments were buried and underwent oil-filling.

4.7.2.3 Anthropogenic activities: impact of mineral distribution patterns on CCS

If carbon capture and geological storage (CCS) requires active sequestering (locking up) of the injected CO_2 as minerals, then clean quartz sandstones are not the ideal rock type (Baines and Worden, 2004). Using the Ravenglass Estuary as an analogue, it is here proposed that CO_2 sequestration will be most effective and safest within mud- and mixed-flats which contain a rich-stew of reactive minerals (Figs. 4.9 and 4.10).

4.8 CONCLUSIONS

This study has revealed the dominant controls on compositional variation in modern estuarine sands. Key findings of this research may be used, by analogy, to better predict the

distribution of primary depositional minerals and burial-diagenetic pathways in sandstone reservoirs. The main conclusions are summarized below.

1. The Ravenglass Estuary is composed of arkosic to subarkosic sediments which reflects the drainage of the major underlying lithologies, namely Eskdale Granite, Borrowdale Volcanic Group and Sherwood Sandstone Group.
2. The clay mineral assemblage of the Ravenglass Estuary is dominated by Fe-Mg-rich and well-crystalline illite, derived primarily from the glacial-till. Chlorite-lithics are relatively abundant in coarser-grained sediment, likely derived from pyroxene pseudomorphs in the Borrowdale Volcanic Group, and chloritized mafic silicates in the Eskdale Granite.
3. Quartz abundance typically increases with increasing grain size up to a critical grain-size threshold of upper-fine sand (177 μm); sediment coarser than 177 μm has relatively high and uniform quartz abundance. Plagioclase and carbonate abundance typically decrease with increasing grain size with a critical grain-size threshold of lower-fine sand (125 μm), sediment that is coarser than 125 μm has a relatively low and uniform abundance of plagioclase and carbonate. K-feldspar abundance is generally uniformly distributed, with a slight depletion in sediment with a grain size coarser than lower-medium sand (350 μm). Clay size fraction and kaolinite abundance decrease with increasing grain size with a critical grain-size threshold of upper-fine sand (177 μm). A sharp decrease in chlorite and illite abundance is observed in sediment that is coarser than lower very-fine sand (88 μm). It is noteworthy that high chlorite concentrations, present as lithic fragments, may also occur in some foreshore, tidal inlet, tidal dunes and tidal bars sediments.
4. Mineral distribution patterns in the Ravenglass Estuary are strongly controlled by the grain size of specific minerals and estuarine hydrodynamics. The grain sizes of specific minerals are controlled by the mineral strength and history of abrasion (e.g. glacial-comminution). Provenance signals present in fluvial sediments (e.g. chlorite- and feldspar-rich River Esk sediments) are dampened by intense estuarine mixing once sediment has been transported past the fluvial-marine interface.
5. This study has shown that the distribution of primary depositional mineralogy (in terms of QFL-C) may be predicted as a function of depositional environment and mean grain size. As a result, findings may be used by analogy, in similar marginal-marine systems to better predict the distribution of burial-diagenetic processes and reservoir quality. Furthermore, Ravenglass Estuary provides an analogue for predicting the best sites based on mineral reactivity, in marginal-marine sandstones, for carbon capture and geological storage (CCS).

5. SYNTHESIS DISCUSSION AND CONCLUSIONS

The aim of this chapter is to provide a summary of key results presented in preceding chapters and to synthesise answers to the seven specific research questions outlined in the introduction of this thesis.

5.1 ESTUARINE COMPOSITION

5.1.1 What is the sediment composition of the Ravenglass Estuary?

The composition of sediments and sandstones can be defined, by petrographers, in terms of the proportion of quartz, feldspar and lithics (QFL) (Folk, 1968). Since X-ray diffraction (XRD) analyses have been used in this study, as opposed to petrography, the term lithics (L) has been recast to include the sum total of all clay minerals (illite, chlorite, kaolinite and smectite). In addition, carbonate material may form an important component of many clastic sediments, and may be autochthonous (formed in its present position) or allochthonous (originated outside of its present location). As a result, the composition of the Ravenglass is here defined by the relative proportions of quartz, feldspar, lithics and carbonates (QFL-C).

The sediment composition of the Ravenglass Estuary sediment (< 2 mm in size) is arkosic to subarkosic (Figs. 4.6 and 4.7). Ravenglass tidally-influenced sediment has average QFL-C proportions as follows: quartz, 62 %; plagioclase, 8 %; K-feldspar, 5%; carbonate, 2%; and lithics, 3 %. Carbonate material is typically composed of, ~ 95 calcite, ~ 5 % aragonite and < 1 % dolomite. The clay mineral assemblage (including clay-mineral-rich lithics) is typically composed of ~ 58 % illite (typically Fe-Mg-rich), ~ 31 % chlorite, ~ 11 % kaolinite, and a minor abundance of smectite (0.009%) (Table 4.1). In near-surface (< 1 m below the sediment surface) sediment pyrite abundance ranges from 0 to 5 % (Fig. 3.16).

5.1.2 What are the fundamental controls on estuarine sediment composition in Ravenglass?

The empirical relationship between composition of sands (quartz, feldspar and lithics), provenance, and the plate-tectonic setting of the sedimentary basin was first established by Dickinson and Suczek (1979). Sediment composition in the Ravenglass Estuary reflects: (i) the fluvial drainage of bedrock in the hinterland (Fig. 1.4A), (ii) fluvial drainage and local erosion of drift deposits in the hinterland (Fig. 1.4B), underlying the estuary and exposed in proximal cliff-sections, (iii) likely the landward-displacement of littoral-zone sediment into

the estuary during marine inundation, and (iv) the geochemical environment at the site of deposition (especially for pyrite and smectite).

The Ravenglass Estuary is composed of arkosic to subarkosic sediments (Fig. 4.7) which reflects the drainage of the major underlying lithologies, namely Eskdale Granite, Borrowdale Volcanic Group and Sherwood Sandstone Group, in agreement with predictive models produced by Dickinson and Suczek (1979). There are no carbonate-rich drift deposits or bedrocks in the hinterland of the Ravenglass Estuary. As a result, carbonate material is likely to have been autochthonous (from gravel beds which are partly colonised by shell beds in the inner-Esk) and allochthonous (derived from both offshore). Pyrite in modern marginal-marine sediments, including the Ravenglass Estuary, originate from bacterial sulphate reduction i.e. aqueous sulphate (derived from marine-inundation) reduced by organic matter.

The type and relative abundance of clay minerals found in modern oceanic and marginal-marine settings have been reported to be governed primarily by a combination the type of sediment supplied (provenance) and climate (weathering intensity) (Chamley, 1989; Eberl et al., 1984; Rateev et al., 2008). In high-latitude marine environments adjacent to land masses, subject to relatively cold climatic-conditions that favour mechanical weathering, chlorite and illite are the dominant clay minerals (Chamley, 1989; Eberl et al., 1984; Rateev et al., 2008; Windom, 1976). In contrast, kaolinite is reported to be most abundant in low-latitude marine environments adjacent to land masses with warm and humid conditions that permit intense chemical weathering (Chamley, 1989; Eberl et al., 1984; Rateev et al., 2008; Windom, 1976). Furthermore, sediment enriched in smectite is generally typical of weathering from semi-arid continental sources, subject to only the early stages of chemical weathering conditions (Salem et al., 2000).

The clay mineral assemblage in the Ravenglass sediment (Fig. 2.17) broadly reflects the global-location of the Ravenglass Estuary (mid-latitude; illite dominated) (Rateev et al., 2008). The mineralogy of clay minerals, present mainly as sediment matrix, is dominated by Fe-Mg-rich illite (Figs. 2.11, 2.15 and 4.13) which reflects the drainage of Ravenglass Till physically eroded, unweathered rocks (Chamley, 1989). Chlorite, present as both sediment matrix (Fig. 2.12) and as lithics (Figs. 4.6), is likely derived from pyroxene pseudomorphs in the Borrowdale Volcanic Group (Quirke et al., 2015), and chloritized mafic silicates in the Eskdale Granite (Moseley, 1978; Quirke et al., 2015; Young et al., 1986) (Fig. 1.4A). Kaolinite is present in relatively minor abundance in the Ravenglass Estuary (Figs. 2.13 and 4.12), and may be sourced from the physical and chemical weathering of most bedrock and drift lithologies in the drainage basin. Smectite is present in negligible abundance in

Ravenglass estuarine sediments, but present in the hinterland and in cores in the River Esk floodplain (Fig. 3.15).

5.2 ESTUARINE MINERAL DISTRIBUTION PATTERNS

5.2.1 How are quartz, feldspar, carbonate, clay minerals and Fe-sulphides distributed in sediment in the Ravenglass Estuary?

Quartz is most abundant in high-energy depositional environments in the outer and inner estuary (pro-ebb delta, foreshore, backshore, tidal inlet, tidal bars and low-amplitude dunes) (Figs. 4.9A). Carbonate, plagioclase and clay minerals are most abundant at the margin of the inner estuary and central basin, in mud- and mixed-flat sediments (Figs. 4.9B and 4.10). K-feldspar is relatively uniformly distributed (Figs. 4.9C). Quartz abundance typically increases with increasing grain size up to a critical grain-size threshold of upper-fine sand (177 μm); depositional environments characterised by sediment that is coarser than 177 μm have relatively high and uniform quartz abundance (Fig. 4.11). Plagioclase and carbonate abundance typically decrease with increasing grain size with a critical grain-size threshold of lower-fine sand (125 μm); depositional environments characterised by sediment that is coarser than 125 μm have a relatively low and uniform abundance of plagioclase and carbonate (Fig. 4.11). K-feldspar abundance is generally uniformly distributed, with a slight depletion in sediment with a grain size coarser than lower-medium sand (350 μm) (Fig. 4.11).

Clay size fraction and kaolinite abundance decrease with increasing grain size with a critical grain-size threshold of upper-fine sand (177 μm) (Fig. 4.12). A sharp decrease in chlorite and illite abundance is observed in sediment that is coarser than lower very-fine sand (88 μm) (Fig. 4.12). It is noteworthy that high chlorite concentrations, present as lithic fragments (Fig. 4.6), may also occur in some foreshore, tidal inlet, tidal dunes and tidal bars sediments (Fig. 4.12). Smectite is primarily restricted to fluvial floodplain sediments (Fig. 3.15). Pyrite formation is largely restricted to mud- and mixed-flats in the central basin and inner-estuary, and typically increases in abundance with an increase in core depth (Fig. 3.14; Table 3.5).

Whether quartz cementation would be inhibited or promoted by mixed-mineralogy clay coats (typically illite and chlorite), likely depends on the relative abundance of chlorite and illite. As a result, using clay mineral index maps it is possible to start to predict the enrichment of one specific clay mineral (e.g. chlorite) relative to other clay minerals e.g. chlorite/(chlorite + illite + kaolinite) (Figs. 2.12 to 2.16). Chlorite and Al-rich illite are relatively most concentrated in the higher energy sites, e.g. foreshore, backshore, tidal bars and dunes and channel axis (Fig. 2.12 and 2.15). In contrast, Fe-Mg-rich illite and kaolinite are relatively

most concentrated in the low-energy sites, at the margins of the inner estuary and central basin i.e. mud- and mixed-flats (Fig. 2.14 and 2.15). Furthermore, this study has established that surface clay mineral distribution patterns (chapter 2) are replicated in the immediate subsurface (chapter 3).

5.2.2 What are the fundamental controls on mineral distribution patterns in the Ravenglass Estuary?

Provenance signals present in fluvial sediments e.g. chlorite- and feldspar-rich River Esk sediments reflecting the drainage of chloritized Eskdale Granite (Fig. 4.7; Table 2.4), are dampened by intense estuarine mixing once sediment has been transported past the fluvial-marine interface.

The distribution of quartz, feldspar, clay minerals and carbonates in the Ravenglass Estuary sediment (Figs. 4.9 and 4.10) are strongly controlled by the grain size of specific minerals (Fig. 4.8) and estuarine hydrodynamics. Extent of abrasion (e.g. glacial-comminution) during sediment transport and the strength of specific minerals control the grain size of each mineral. Further, the geochemical environment at the site of deposition may control smectite distribution, with ground-water flushing metal cations from the estuarine sediment, which are essential for smectite development. Pyrite abundance and distribution in the Ravenglass Estuary is controlled the distribution of organic matter (reducing agent), core depth (redox-conditions) and bioturbation intensity (intense bioturbation in mixed-flats by *Arenicola marina* may appears to have inhibited the formation pyrite-formation, as a result of sediment oxidation).

A significant finding of this study is that post-depositional processes (bioturbation and mechanical infiltration) do not over-print surface clay mineral distribution patterns. Bioturbation intensity, shown to form new clay minerals under laboratory conditions (Needham et al., 2004; Needham et al., 2005), does not appear control clay mineral distribution patterns in the Ravenglass Estuary (Figs. 2.7D and 3.17; Tables 2.5). Furthermore, in contrast to experimental work undertake by Matlack et al. (1989), there is no evidence for a systematic increase or decrease of specific clay mineral abundances as a function of core depth (Table 3.5), suggesting mechanical infiltration does not influence near-surface (< 1 m) clay mineral distribution patterns, at least in the Ravenglass Estuary. It remains possible that continued mineral alteration in the estuary may influence mineral distribution patterns, as previously reported by Daneshvar and Worden (2017); however, it should be noted that intense alteration of feldspars in the hinterland of the Ravenglass Estuary is widely reported (Moseley, 1978; Quirke et al., 2015; Young et al., 1986). As a

result, kaolinized-plagioclase, and illitized-K-feldspars may be an inherited feature of the sediment and not due to continued weathering in the estuary.

5.3 ESTUARINE DETRITAL CLAY COAT DISTRIBUTION

5.3.1 How are detrital clay coats distributed in the Ravenglass Estuary?

Detrital clay coats in near-surface sediment (< 1 m below the sediment surface) are most extensive in mud-flat lithofacies, located at the margins of the inner estuary and central basin (Figs. 3.8 and 3.11; Table 3.2). Detrital clay coat coverage is highly variable in mixed-flat depositional environments, tidal-creek point bars and low-amplitude tidal dunes (Fig. 3.11). Detrital clay coats are typically absent in near-surface sediment deposited in the outer estuary i.e. foreshore, backshore and tidal inlet and high-energy inner estuary and central basin depositional environments i.e. tidal bars (Fig. 3.11). There is no evidence for a systematic increase or decrease in detrital clay coat coverage as a function of core depth (Table 3.5). There is a strong positive correlation between clay fraction abundance ($r = 0.92$, $p < 0.001$) and detrital clay coat coverage in near-surface (< 1 m) sediment in the Ravenglass Estuary. There is a strong positive correlation between bioturbation intensity ($r = 0.84$, $p < 0.001$) and detrital clay coat coverage in near-surface (< 1 m) sediment in the Ravenglass Estuary.

5.3.2 What are the fundamental controls on detrital clay coat distribution patterns in the Ravenglass Estuary?

As reported by Wooldridge et al. (2017a), primary depositional processes tend to lead to physical separation of fine- and coarse-grain materials; however, clay size material is adhered to the surface of sand grains in surface sediments in the Ravenglass Estuary by biofilms, formed by diatoms. Surface detrital clay coat distribution patterns in the Ravenglass estuary, as reported by Wooldridge et al. (2017a), are replicated in the near-surface (Fig. 3.11). Post-depositional processes (e.g. macro-faunal bioturbation and mechanical infiltration) therefore do not appear to over-print surface detrital clay coat distribution patterns in the near-surface (< 1 m). It is therefore concluded, in this study, that detrital clay coat distribution patterns in the near-surface are ultimately controlled by estuarine hydrodynamics (primary control on clay fraction distribution patterns) and processes active in the top few millimetres of the surface sediment i.e. bio-sediment interaction (Wooldridge et al., 2017a), which adhere clay size material to the sand grain surface.

5.4 PREDICTING MINERAL AND DETRITAL CLAY COAT DISTRIBUTION PATTERNS IN DEEPLY-BURIED SANDSTONE RESERVOIRS

5.4.1 Can primary sediment composition and/or detrital clay coat coverage be predicted as a function of host-sediment properties (e.g. grain size, sorting, and bioturbation intensity), depositional environment, and/or estuarine zone?

The distribution of primary depositional mineralogy (in terms of quartz, feldspar, carbonates and clay minerals), of the whole sediment (< 2 mm), is at least partly predictable as a function of depositional environment (lithofacies) (Table 3.6; Fig. 5.1) and mean grain size (Figs. 4.11 and 4.12). The relative abundance of clay minerals appears to be predictable as a function of lithofacies (Table 3.6; Fig. 5.1) in near-surface sediment; however, high-resolution surface sediment clay mineral index maps (chapter 2) reveal that local specific conditions exert a strong control on the relative enrichment of one clay mineral, specific to other clay minerals e.g. the enrichment of chlorite upon the northern foreshore due to wave-direction (Fig. 2.12). As a result, relative clay mineral distribution patterns may not be predicted based solely upon depositional environment alone (Table 2.7). Fe-sulphides (e.g. pyrite) are largely restricted to mud- and mixed-flats in the central basin, and typically increase in abundance with depth, due to increasing anoxic-conditions. Intense bioturbation in mixed-flats by *Arenicola Marina* may however inhibit pyrite-growth, which is likely to favour the formation of burial-diagenetic chlorite.

Detrital clay coat distribution is predictable as a function of lithofacies (Figs. 3.11 and 5.1; Table 3.4), if there is knowledge of estuarine hydrodynamics, which is ultimately controlled by estuarine type (e.g. wave- or tide-dominated, or mixed-energy). Furthermore, understanding the distribution of diatoms, or other biofilms producing organisms, in marginal-marine systems through geological time is critical, since biofilms appear to be the dominant control detrital clay coat distribution patterns (Wooldridge et al., 2017a).

This study may be used, by analogy, to better predict the spatial and temporal distribution of sediment composition and texture in similar marginal-marine systems, and thus sandstone reservoir quality (Figs 5.1 and 5.2). Furthermore, Ravenglass Estuary provides an analogue for predicting the best sites based on mineral reactivity, in marginal-marine sandstones, for carbon capture and geological storage (CCS).

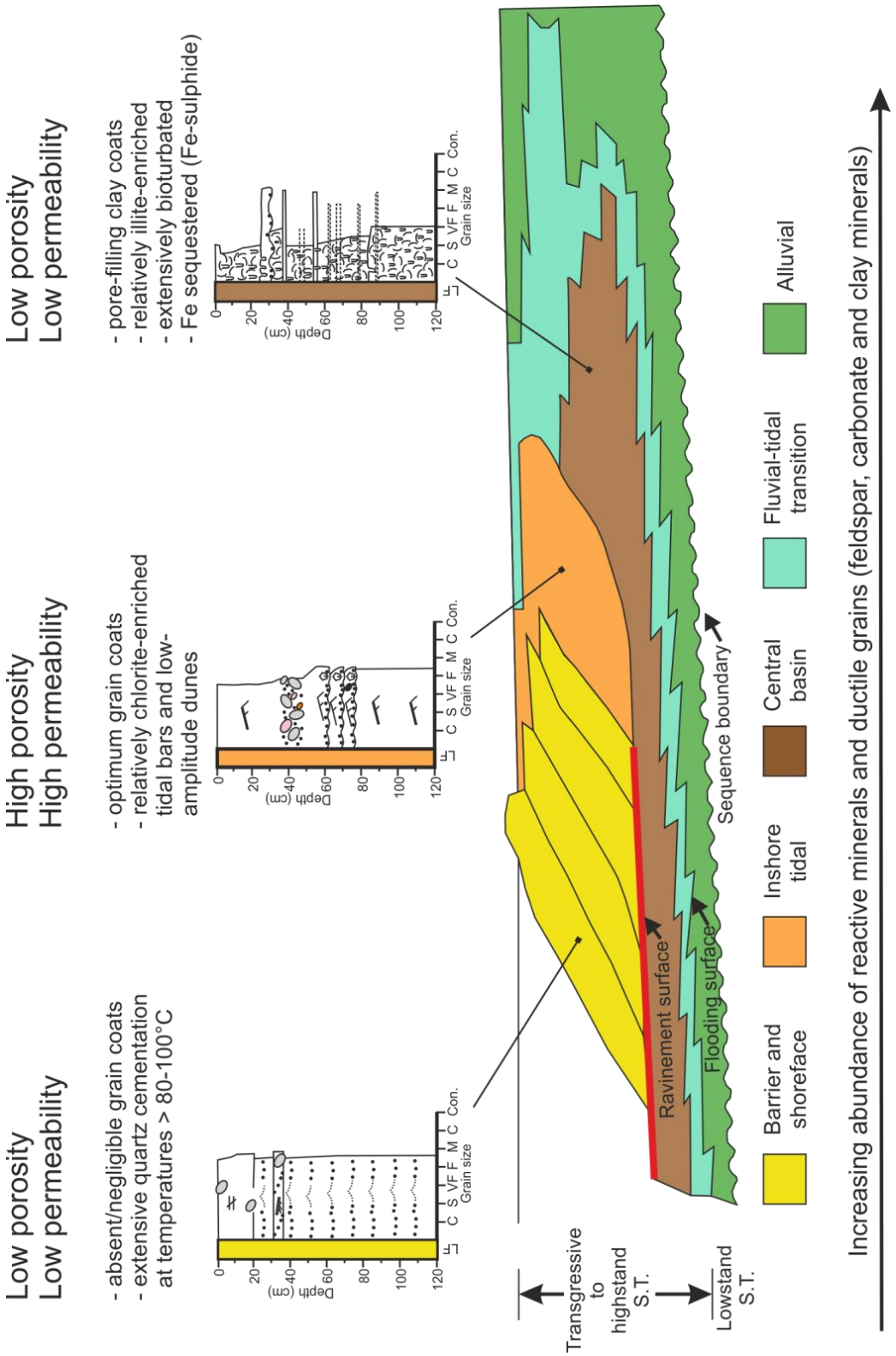

Figure 5-1– Synthesis schematic of textural and compositional variation in modern estuarine sands and predicted resulting reservoir quality in analogous ancient and deeply-buried (> 80-100°C) marginal-marine sandstones. Sequence stratigraphy modified from Dalrymple et al. (1992).

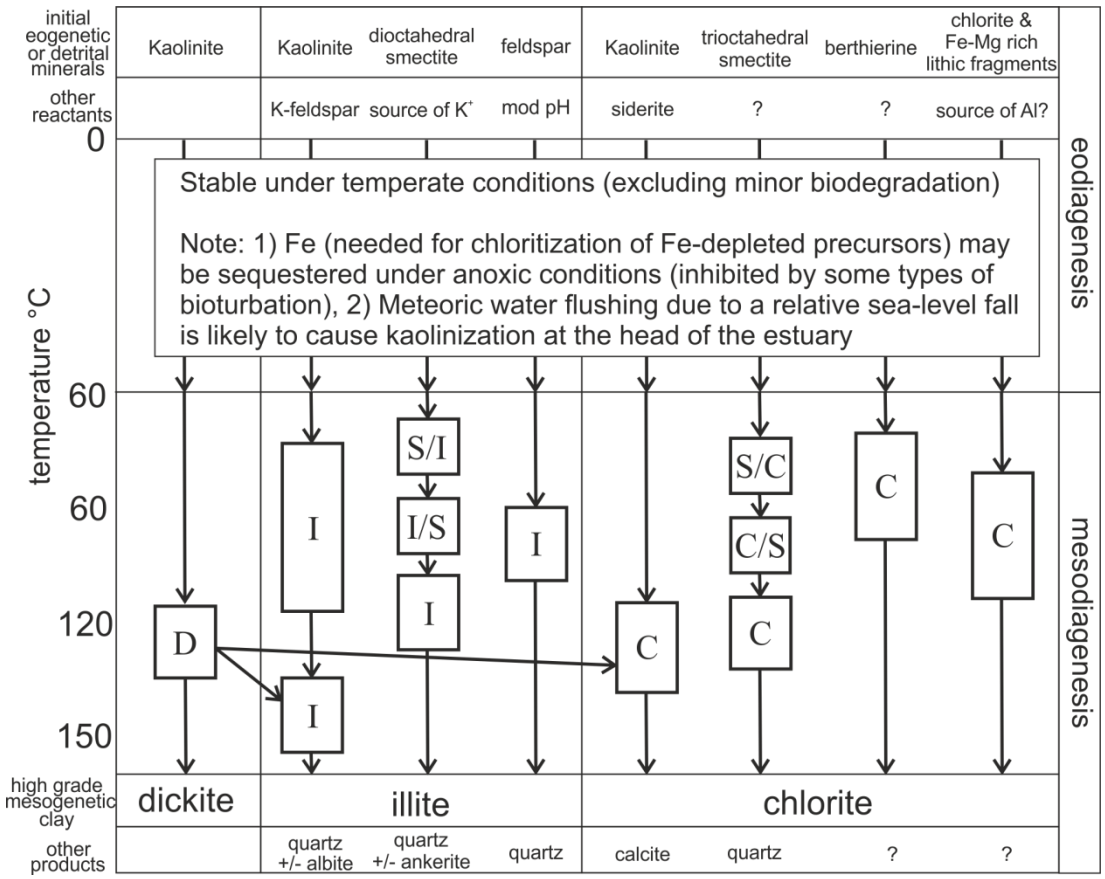

Figure 5-2 - Eogenetic pathways (under temperate conditions in a marginal-marine system, based on the Ravenglass Estuary, this study) and likely mesogenetic pathways for clay minerals in sandstones, adapted from Worden and Morad (2003). Where D is dickite, S is smectite, I is illite and C is chlorite. Randomly stratified mixed-layer clay minerals are named accordingly: S/I is mixed-layer smectite-illite dominated by smectite; I/S is the same mineral mixture dominated by illite.

6. FUTURE WORK

To better understand compositional and textural variability in marginal-marine sandstone reservoirs, the following future work is proposed. Mineralogical and textural alteration is expected in most outcrop localities, and reservoir-studies suffer from poor spatial resolution. As a result, future work suggested here is focused upon continued modern-analogue studies, as well as experimental work, in order to simplify the complexity of natural systems.

6.1 TEXTURAL AND COMPOSITIONAL VARIABILITY THOUGHOUT A HOLOCENE ESTUARINE SUCCESSION

A significant amount of time was dedicated, during this PhD, in planning and collecting deep cores in the Ravenglass Estuary, in order to study the full Holocene estuarine succession. To safely and legally collected high quality cores, a significant amount of permissions was first needed, which included; Natural England, land-owner, Muncaster and Drigg Parish Councils, Lake District National Park, Multiple tenant farmers and other land-stewards, NIREX (Nuclear Inspectorate), Ministry of Defence, SAC (Marine Materials Ordinance) and the Health and Safety Executive.

In November 2015, the company Geotechnical Engineering Ltd (GEL) was appointed as the contracted drillers. Based upon desk studies and predictions of depth of sediment was made, and twenty drill sites were appointed by myself, Luke Wooldridge, James Utley and Richard Worden.

In May 2016 (over a two-month drilling campaign), twenty sedimentary cores were drilled in the Ravenglass Estuary (Fig. 6.1) using P60 rigs and soft track drilling rigs (in environmentally sensitive areas). In addition, Lankelma provided a UXO (unexploded ordnance) survey truck, to ensure there was no unexploded ordnance risk at coring sites. In addition, water installations wells were emplaced at specific borehole locations to study pore-water composition in the subsurface of the Ravenglass Estuary. Twenty cores were collected, with a maximum depth of ~ 15 m.

Future work of the chlorite consortium (Diagenesis Research Group), at the University of Liverpool, will primarily focus upon better understanding the distribution of sediment composition and texture throughout the Holocene succession.

Figure 6-1 – Location of twenty boreholes in the Ravenglass Estuary.

The following work will be undertaken by PhD/MESci/MSc students at the University of Liverpool, who I shall continue to support throughout the duration of the research project. Detailed core descriptions will be undertaken to better understand the evolution of the Ravenglass Estuary, and to test relationships between lithofacies e.g. detrital clay coat coverage versus facies. In addition, peat layers and large shall fragments will be dated using ^{14}C dating in order to understand the spatial and temporal evolution of the estuary. Laser Particle Size Analysis will be undertaken on a high-resolution scale, in order to examine how grain size and sorting in the basin may have evolved through time; a strong control on porosity and permeability. X-Ray Diffraction analysis will be used to better understand the temporal and spatial distribution of sediment composition. SEM-EDS (QEMSCAN®) analyses will be undertaken for quantitative mineralogy and to better understand the extent of detrital clay coat coverage. In addition, X-Ray Florescence and QEMSCAN® will provide information on the distribution of iron throughout the Holocene succession. Water sampling campaigns and isotope and compositional analysis from borehole water installations will be undertaken, and correlated with mineralogy and clay coat datasets.

The study of the Holocene estuarine succession will enable the comparison between trends observed in surface (< 2 cm) and near-surface (< 1 m) sediment, to subsurface (< 15 m) distribution patterns. Subsurface (< 15 m) sediment may have begun grain-reordering (due to compaction) and/or early-diagenesis e.g. kaolinization of feldspars due to meteoric water-flushing and mechanical infiltration. Furthermore, the Ravenglass Estuary has experienced a transition from a tide-dominated estuary, to a mixed-energy system with coastal spits, following the development of Drigg and Eskmeals coastal-spits around 3,000 BP (Bousher, 1999; Lloyd et al., 2013). As a result, it is possible to study how sediment texture and

composition may have evolved throughout a full Holocene succession. Results of this study will allow the population of a detailed sequence stratigraphic model with textural and mineralogical datasets, to better understand both the spatial and temporal distribution of specific minerals and host-sediment properties over an 11,700 year period.

Through analysing pore-water chemistry, it may be possible to better understand the formation and/or alteration of minerals in the Holocene succession, as a result of early-eogenetic processes i.e. Fe-sulphide distribution. In addition, this study may provide a critical insight into the role detrital clay coat formation as a result of mechanical infiltration, for example, clay rich pore waters may be expected above impermeable glacial layers, and thus lead to the post-depositional formation of detrital clay coats, which may cross-cut lithofacies, as reported in fluvial-systems by Morad et al. (2010).

6.2 INFILTRATION AND ILLUVIATION: INFLUENCE ON DETRITAL CLAY COAT FORMATION IN MARGINAL-MARINE SYSTEMS

Clay coats have previously been reported to originate from the mechanical-infiltration of clay-laden waters through the pore-networks of sediment (Buurman et al., 1998; Matlack et al., 1989; Moraes and De Ros, 1990; Pittman et al., 1992; Wilson, 1992). Infiltration and pore water movement may occur on a cm- to metre-scale in marginal marine depositional environments (Santos et al., 2012), and therefore, during falling-tides, clay-laden estuarine waters may transport fine-grained sediment into the underlying sandbody, forming clay coats (Matlack et al., 1989; Moraes and De Ros, 1990; Pittman et al., 1992; Wilson, 1992). Theoretically, mechanical-infiltration could therefore occur in all depositional environments in the Ravenglass Estuary, however, results from this study suggest that mechanical-infiltration, or illuviation, does not appear to over-print primary clay mineral or detrital clay coat distribution patterns in near-surface (< 1 m) sediment. Furthermore, experimental studies undertaken by Matlack et al. (1989), do not account for saline pore-waters, bio-sediment interaction, tidal-cycles, or groundwater-flow which may be oblique to the sediment surface. As a result, the role of mechanical-infiltration or illuviation on clay mineral and clay coat distribution patterns remains poorly-understood in marginal-marine systems at depths greater than < 1 m.

To address this gap in knowledge, three experiments are envisaged (in addition to studying Holocene estuarine core studies, as discussed in section 6.1). First, to better understand how clay size material may be distributed in sand packages in tidally-influenced depositional environments, as a result of mechanical infiltration (tidal-pumping), it would be advantageous to set up an experiment in which clay-laden pore-waters are flushed through

clean sand over multiple tidal-cycles (e.g. simulation of both rising and falling water levels). Second, mechanical infiltration experiments undertaken by Matlack et al. (1989) did not include the use of saline waters, which is known to influence the flocculation of clay minerals (Whitehouse et al., 1960). As a result, mechanical infiltration, using saline waters may lead to a better understanding on how marine-conditions may impact the infiltration of specific clay minerals. Third, as reported by Wooldridge et al. (2017a) and by Arnon et al. (2010), biofilms significantly impact the trapping of clay size material, and consequently, it would be advantageous to test how biofilms may impact the extent of mechanical infiltration in biofilm-rich depositional environments.

6.3 BIOFILMS: IMPACT ON MINERAL DISTRIBUTION PATTERNS IN THE RAVENGLASS ESTUARY

Biofilms are reported to impact sediment transport and bedform stability (Malarkey et al., 2015), grain size heterogeneity (Garwood et al., 2015) and the subsequent diagenesis of sandstones (Jones, 2017). Furthermore, flume experiments undertaken by Arnon et al. (2010) revealed that biofilm formation played a key role in the transport of suspended particles, and that particle retention in the benthic biofilm is grain size specific. As a result, it is hypothesized that biofilms (derived from diatom locomotion) in the Ravenglass Estuary (Wooldridge et al., 2017a), may impact the distribution of specific minerals. By combining field datasets on biofilm abundance in the Ravenglass Estuary, as reported by (Wooldridge et al., 2017a), with XRD datasets presented in this thesis, is may be possible to better understand the potential influence that biofilms may have on mineral distribution patterns in marginal marine systems.

6.4 FE DISTRIBUTION IN THE RAVENGLASS ESTUARY

Iron is critical in the formation of burial-diagenetic Fe-chlorite, which may preserve porosity in deeply-buried sandstones reservoirs. The distribution of iron in the Ravenglass Estuary has been studied by Daneshvar and Worden (2017), however, the study is based on relatively small dataset (two one metre cores). As a result, there remains no high-resolution marginal marine study which reports the distribution of iron that may be used by analogy to better predict the distribution of iron, in deeply-buried sandstones reservoirs, and thus Fe-bearing clay minerals, such as chlorite. It is therefore suggested that using X-Ray Fluorescence and/or SEM-EDS (QEMSCAN®) analyses, Fe-distribution (e.g. in Fe-rich lithics and clay minerals) should be mapped in the Ravenglass Estuary, at a scale similar to many oil and gas reservoirs.

7. REFERENCES

Aase, N.E., Bjorkum, P.A. and Nadeau, P.H. (1996) The effect of grain-coating microquartz on preservation of reservoir porosity. *American Association of Petroleum Geologists Bulletin*, **80,** 1654-1673.

Ajdukiewicz, J.M. and Lander, R.H. (2010) Sandstone reservoir quality prediction: The state of the art. *American Association of Petroleum Geologists Bulletin*, **94,** 1083-1091.

Ajdukiewicz, J.M. and Larese, R.E. (2012) How clay grain coats inhibit quartz cement and preserve porosity in deeply buried sandstones: Observations and experiments. *American Association of Petroleum Geologists Bulletin*, **96,** 2091-2119.

Allen, G.P. and Posamentier, H.W. (1994) Transgressive facies and sequence architecture in mixed tide-and wave-dominated incised valleys: example from the Gironde Estuary, France.

Aller, R.C. and Michalopoulos, P. (1999) *Invited lecture: Tropical, mobile mud belts as global diagenetic reactors*, 289-292 pp.

Aoudjit, H., Robert, M., Elsass, F. and Curmi, P. (1995) Detailed study of smectite genesis in granitic saprolites by analytical electron microsopy. *Clay Minerals*, **30,** 135-147.

Arakel, A.V. (1986) Evolution of calcrete in paleodrainages of the Lake Napperby area, central Australia. *Palaeogeography Palaeoclimatology Palaeoecology*, **54,** 283-303.

Armitage, P.J., Worden, R.H., Faulkner, D.R., Aplin, A.C., Butcher, A.R. and Iliffe, J. (2010) Diagenetic and sedimentary controls on porosity in Lower Carboniferous fine-grained lithologies, Krechba field, Algeria: A petrological study of a caprock to a carbon capture site. *Marine and Petroleum Geology*, **27,** 1395-1410.

Arnon, S., Marx, L.P., Searcy, K.E. and Packman, A.I. (2010) Effects of overlying velocity, particle size, and biofilm growth on stream–subsurface exchange of particles. *Hydrological Processes*, **24,** 108-114.

Assinder, D.J., Kelly, M. and Aston, S.R. (1985) Tidal variations in dissolved and particulate phase radionuclide activities in the Esk Estuary, England, and their distribution coefficients and particulate activity fractions. *Journal of Environmental Radioactivity*, **2,** 1-22.

Baines, S. and Worden, R.H. (Eds)(2004) *Geological Storage of Carbon Dioxide for Emissions Reduction: Technology*. Geological Society Special Publication, 255 pp.

Barclay, S.A. and Worden, R.H. (2000a) Effects of reservoir wettability on quartz cementation in oil fields. *In: Quartz cementation in sandstones (eds. Worden, R.H. and Morad, S.) International Association of Sedimentologists Special Publications*, **29,** 103-118.

Barclay, S.A. and Worden, R.H. (2000b) Geochemical modelling of diagenetic reactions in a sub-arkosic sandstone. *Clay Minerals*, **35,** 57-67.

Beard, D.C. and Weyl, P.K. (1973) Influence of texture on porosity and permeability of unconsolidated sand. *American Association of Petroleum Geologists Bulletin*, **57,** 349-369.

Benjamini, Y. and Hochberg, Y. (1995) Controlling the false discovery rate: a practical and powerful approach to multiple testing. *Journal of the royal statistical society. Series B (Methodological)*, 289-300.

Berner, E.K. and Berner, R.A. (2012) *Global environment: water, air and geochemical cycles. Second edition*. Princeton University Press, Princeton, 444 pp.

Berner, R.A. (1980) *Early diagenesis, a theoretical approach*. Princeton University Press, Princeton.

Biddle, P. and Miles, J. (1972) The nature of contemporary silts in British estuaries. *Sedimentary Geology*, **7,** 23-33.

Billault, V., Beaufort, D., Baronnet, A. and Lacharpagne, J.C. (2003) A nanopetrographic and textural study of grain-coating chlorites in sandstone reservoirs. *Clay Minerals*, **38,** 315-328.

Bjorkum, P.A., Mjos, R., Walderhaug, O. and Hurst, A. (1990) The role of the late Cimmerian unconformity for the distribution of kaolinite in the Gullfaks field, northern North Sea. *Sedimentology*, **37,** 395-406.

Bjorlykke, K. (1998) Clay mineral diagenesis in sedimentary basins - a key to the prediction of rock properties. Examples from the North Sea Basin. *Clay Minerals*, **33,** 15-34.

Bjorlykke, K. (2010) *Petroleum geoscience- from sedimentary environments to rock physics*. Springer, Heidelberg, 508 pp.

Bloch, S. (1991) Empirical prediction of porosity and permeability in sandstones. *American Association of Petroleum Geologists Bulletin*, **75,** 1145-1160.

Bloch, S. and Helmold, K.P. (1995) Approaches to predicting reservoir quality in sandstones. *American Association of Petroleum Geologists Bulletin*, **79,** 97-115.

Bloch, S., Lander, R.H. and Bonnell, L. (2002) Anomalously high porosity and permeability in deeply buried sandstone reservoirs: Origin and predictability. *American Association of Petroleum Geologists Bulletin*, **86,** 301-328.

Blott, S.J. and Pye, K. (2001) GRADISTAT: a grain size distribution and statistics package for the analysis of unconsolidated sediments. *Earth Surface Processes and Landforms*, **26,** 1237-1248.

Boles, J.R. and Franks, S.G. (1979) Clay diagenesis in Wilcox Sandstones of southwest Texas - implications of smectite diagenesis on sandstone cementation. *Journal of Sedimentary Petrology*, **49,** 55-70.

Borchers, A., Voigt, I., Kuhn, G. and Diekmann, B. (2011) Mineralogy of glaciomarine sediments from the Prydz Bay–Kerguelen region: relation to modern depositional environments. *Antarctic Science*, **23,** 164-179.

Bousher, A. 1999. Ravenglass Estuary: Basic characteristics and evaluation of restoration options.

Bout-Roumazeilles, V., Riboulleau, A., Châtelet, E.A., Lorenzoni, L., Tribovillard, N., Murray, R.W., Müller-Karger, F. and Astor, Y.M. (2013) Clay mineralogy of surface sediments as a tool for deciphering river contributions to the Cariaco Basin (Venezuela). *Journal of Geophysical Research: Oceans*, **118,** 750-761.

Boyle, E., Collier, R., Dengler, A.T., Edmond, J.M., Ng, A.C. and Stallard, R.F. (1974) Chemical mass balance in estuaries. *Geochimica et Cosmochimica Acta*, **38,** 1719-1728.

Boyle, E.A., Edmond, J.M. and Sholkovitz, E.R. (1977) Mechanism of iron removal in estuaries. *Geochimica et Cosmochimica Acta*, **41,** 1313-1324.

Brockamp, O. and Zuther, M. (2004) Changes in clay mineral content of tidal flat sediments resulting from dike construction along the Lower Saxony coast of the North Sea, Germany. *Sedimentology*, **51,** 591-600.

Burley, S.D. (1986) The development and destruction of porosity within Upper Jurassic reservoir sandstones of the Piper and Tartan fields, Outer Moray Firth, North Sea. *Clay Minerals*, **21,** 649-694.

Buurman, P., Jongmans, A.G. and PiPujol, M.D. (1998) Clay illuviation and mechanical clay infiltration—Is there a difference? *Quaternary International*, **51,** 66-69.

Campbell, C.V. (1967) Lamina, laminaset, bed and bedset. *Sedimentology*, **8,** 7-26.

Caracciolo, L., Von Eynatten, H., Tolosana-Delgado, R., Critelli, S., Manetti, P. and Marchev, P. (2012) Petrological, geochemical, and statistical analysis of Eocene–Oligocene sandstones of the Western Thrace Basin, Greece and Bulgaria. *Journal of Sedimentary Research*, **82,** 482-498.

Carr, A.P. and Blackley, M.W.L. (1986) Implications of sedimentological and hydrological processes on the distribution of radionuclides: the example of a salt marsh near Ravenglass, Cumbria. *Estuarine, Coastal and Shelf Science*, **22,** 529-543.

Carroll, D. and Starkey, H.C. (1958) Effect of sea-water on clay minerals. In: *Clays and Clay Minerals., 7th Natational conference. Pergamon, Oxford*, pp. 80-101. Elsevier.

Cerda, C.M. (1987) Mobilization of kaolinite fines in porous media. *Colloids and surfaces*, **27,** 219-241.

Chamley, H. (1989) *Clay Sedimentology*. Springer-Verlag.

Choquette, P.W. and Pray, L. (1970) Geologic nomenclature and classification of porosity in sedimentary carbonates. *American Association of Petroleum Geologists Bulletin*, **54,** 207-250.

Chuhan, F.A., Bjorlykke, K. and Lowrey, C.J. (2001) Closed-system burial diagenesis in reservoir sandstones: Examples from the Garn Formation at Haltenbanken area, offshore mid-Norway. *Journal of Sedimentary Research*, **71,** 15-26.

Dalland, A., Mearns, E.W. and McBride, J.J. (1995) The application of samarium-neodymium (Sm-Nd) Provenance ages to correlation of biostratigraphically barren strata: A case study of the Statfjord Formation in the Gullfaks Oilfield, Norwegian North Sea. *Geological Society, London, Special Publications*, **89,** 201-222.

Dalrymple, R.W., Zaitlin, B.A. and Boyd, R. (1992) Estuarine facies models - conceptual models and stratigraphic implications. *Journal of Sedimentary Petrology*, **62,** 1130-1146.

Daneshvar, E. (2015) Dissolved iron behavior in the Ravenglass Estuary waters, an implication on the early diagenesis. *Universal Journal of Geoscience*, **3,** 1-12.

Daneshvar, E. and Worden, R.H. (2017) Feldspar alteration and Fe minerals: origin, distribution and implications for sandstone reservoir quality in estuarine sediments. *Geological Society, London, Special Publications*, **435,** SP435. 17.

Davis, R.A. and Dalrymple, R.W. (2011) *Principles of tidal sedimentology*. Springer Science & Business Media.

Dickinson, W.R. and Suczek, C.A. (1979) Plate tectonics and sandstone compositions. *American Association of Petroleum Geologists Bulletin*, **63,** 2164-2182.

Dowey, P.J., Hodgson, D.M. and Worden, R.H. (2012) Pre-requisites, processes, and prediction of chlorite grain coatings in petroleum reservoirs: A review of subsurface examples. *Marine and Petroleum Geology*, **32,** 63-75.

Dowey, P.J., Worden, R.H., Utley, J. and Hodgson, D.M. (2017) Sedimentary controls on modern sand grain coat formation. *Sedimentary Geology*, **353,** 46-63.

Du Chatelet, E.A., Bout-Roumazeilles, V., Coccioni, R., Frontalini, F., Francescangeli, F., Margaritelli, G., Rettori, R., Spagnoli, F., Semprucci, F. and Trentesaux, A. (2016) Environmental control on a land–sea transitional setting: integrated sedimentological, geochemical and faunal approaches. *Environmental Earth Sciences*, **75,** 123.

Dutton, S.P. and Loucks, R.G. (2010) Diagenetic controls on evolution of porosity and permeability in lower Tertiary Wilcox sandstones from shallow to ultradeep (200-6700 m) burial, Gulf of Mexico Basin, USA. *Marine and Petroleum Geology*, **27,** 69-81.

Eberl, D.D., Farmer, V.C. and Barrer, R.M. (1984) Clay Mineral Formation and Transformation in Rocks and Soils [and Discussion]. *Philosophical Transactions of the Royal Society of London A: Mathematical, Physical and Engineering Sciences*, **311,** 241-257.

Edzwald, J.K. and O'Mella, C.R. (1975) Clay distributions in recent estuarine sediments. *Clays and Clay Minerals*, **23,** 39-44.

Ehrenberg, S.N. (1993) Preservation of anomalously high-porosity in deeply buried sandstones by grain coating chlorite - examples from the Norwegian continental shelf. *American Association of Petroleum Geologists Bulletin*, **77,** 1260-1286.

Ehrenberg, S.N. and Jakobsen, K.G. (2001) Plagioclase dissolution related to biodegradation of oil in Brent Group sandstones (Middle Jurassic) of Gullfaks Field, northern North Sea. *Sedimentology*, **48,** 703-721.

Ehrenberg, S.N., Nadeau, P.H. and Steen, O. (2009) Petroleum reservoir porosity versus depth: Influence of geological age. *American Association of Petroleum Geologists Bulletin*, **93,** 1281-1296.

Esquevin, J. (1969) Influence de la composition chimique des illites sur leur cristallinité. *Bulletin Centre Recherche Elf Pau-SNPA*, **3,** 147-153.

Fenchel, T., Kofoed, L.H. and Lappalainen, A. (1975) Particle size-selection of two deposit feeders: the amphipod Corophium volutator and the prosobranch Hydrobia ulvae. *Marine Biology*, **30,** 119-128.

Feuillet, J.-P. and Fleischer, P. (1980) Estuarine circulation; controlling factor of clay mineral distribution in James River Estuary, Virginia. *Journal of Sedimentary Petrology*, **50,** 267-279.

Field, M.E. and Pilkey, O.H. (1969) Feldspar in Atlantic continental margin sands off the southeastern United States. *Geological Society of America Bulletin*, **80,** 2097-2102.

Folk, R.L. (1954) The distinction between grain size and mineral composition in sedimentary-rock nomenclature. *The Journal of Geology*, **62,** 344-359.

Folk, R.L. (1968) *Petrology of sedimentary rocks*, Austin, Texas: Hemphill.

Folk, R.L. and Ward, W.C. (1957) Brazos river bar. A study in the significance of grain size parameters. *Journal of Sedimentary Petrology*, **27,** 3-26.

Garwood, J.C., Hill, P.S., MacIntyre, H.L. and Law, B.A. (2015) Grain sizes retained by diatom biofilms during erosion on tidal flats linked to bed sediment texture. *Continental Shelf Research*.

Garzanti, E., Andò, S. and Vezzoli, G. (2009) Grain-size dependence of sediment composition and environmental bias in provenance studies. *Earth and Planetary Science Letters*, **277,** 422-432.

Gerdol, V. and Hughes, R.G. (1994) Effect of Corophium volutator on the abundance of benthic diatoms, bacteria and sediment stability in two estuaries in southeastern England. *Marine Ecology Progress Series*, 109-115.

Gibbs, R.J. (1977) Clay mineral segregation in the marine environment. *Journal of Sedimentary Research*, **47**.

Gingele, F.X., De Deckker, P. and Hillenbrand, C.-D. (2001) Clay mineral distribution in surface sediments between Indonesia and NW Australia—source and transport by ocean currents. *Marine Geology*, **179,** 135-146.

Glasmann, J.R., Lundegard, P.D., Clark, R.A., Penny, B.K. and Collins, I.D. (1989) Geochemical evidence for the history of diagenesis and fluid migration - Brent Sandstone, Heather Field, North Sea. *Clay Minerals*, **24,** 255-284.

Gould, K., Pe-Piper, G. and Piper, D.J.W. (2010) Relationship of diagenetic chlorite rims to depositional facies in Lower Cretaceous reservoir sandstones of the Scotian Basin. *Sedimentology*, **57,** 587-610.

Griffin, G.M. and Ingram, R.L. (1955) Clay minerals of the Neuse River estuary. *Journal of Sedimentary Research*, **25**.

Griffiths, J., Faulkner, D.R., Edwards, A.P. and Worden, R.H. (2016) Deformation band development as a function of intrinsic host-rock properties in Triassic Sherwood Sandstone. *Geological Society, London, Special Publications*, **435,** SP435. 11.

Grim, R.E., Bray, R.H. and Bradley, W.F. (1937) The mica in argillaceous sediments. *American Mineralogist*, **22,** 813-829.

Grim, R.E. and Johns, W.D. (1954) Clay mineral investigations of sediments in the northern Gulf of Mexico. *Clays and Clay Minerals*, **2nd National Conference Pergamon, New York,** 81-103.

Gunter, W.D., Bachu, S. and Benson, S. (2004) The role of hydrogeological and geochemical trapping in sedimentary basins for secure geological storage of carbon dioxide. *Geological Society, London, Special Publications*, **233,** 129-145.

Hathaway, J.C. (1972) Regional clay mineral fades in estuaries and continental margin of the United States east coast. *Geological Society of America Memoirs*, **133,** 293-316.

Hendry, J.P., Trewin, N.H. and Fallick, A.E. (1996) Low-Mg calcite marine cement in Cretaceous turbidites: Origin, spatial distribution and relationship to seawater chemistry. *Sedimentology*, **43,** 877-900.

Islam, M.A. (2009) Diagenesis and reservoir quality of Bhuban sandstones (Neogene), Titas Gas Field, Bengal Basin, Bangladesh. *Journal of Asian Earth Sciences*, **35,** 89-100.

Johnsson, M.J. and Meade, R.H. (1990) Chemical weathering of fluvial sediments during alluvial storage: The Macuapanim Island point bar, Solimoes River, Brazil. *Journal of Sedimentary Research*, **60**.

Jones, S.J. (2017) Goo, glue, and grain binding: importance of biofilms for diagenesis in sandstones. *Geology.*, **45,** 959-960.

Kantorowicz, J.D. (1984) The nature, origin and distribution of authigenic clay minerals from Middle Jurassic Ravenscar and Brent Group sandstones. *Clay Minerals*, **19,** 359-375.

Kantorowicz, J.D., Bryant, I.D. and Dawans, J.M. (1987) Controls on the permeability and distribution of carbonate cements in Jurassic sandstones: Bridgeport Sands, southern England, and Viking Group, Troll field, Norway. In: *Diagenesis of Sedimentary Sequences* (Ed J.D. Marshall), pp. 103–118. Blackwell, Oxford.

Kelly, M., Emptage, M., Mudge, S., Bradshaw, K. and Hamilton-Taylor, J. (1991) The relationship between sediment and plutonium budgets in a small macrotidal estuary - Esk Estuary, Cumbria, UK. *Journal of Environmental Radioactivity*, **13,** 55-74.

Khalaf, F.I. and Ala, M. (1980) Mineralogy of the recent intertidal muddy sediments of Kuwait—Arabian Gulf. *Marine geology*, **35,** 331-342.

Krumm, S. and Buggisch, W. (1991) Sample preparation effects on illite crystallinity measurement: grain-size gradation and particle orientation. *Journal of Metamorphic Geology*, **9,** 671-677.

Kübler, B. (1964) Les argiles, indicateurs de métamorphisme. *Review Institute Francais du Pétrole*, **19,** 1093-1112.

Lander, R.H. and Bonnell, L.M. (2010) A model for fibrous illite nucleation and growth in sandstones. *American Association of Petroleum Geologists Bulletin*, **94,** 1161-1187.

Lander, R.H., Larese, R.E. and Bonnell, L.M. (2008) Toward more accurate quartz cement models: The importance of euhedral versus noneuhedral growth rates. *American Association of Petroleum Geologists Bulletin*, **92,** 1537-1563.

Lloyd, J.M., Zong, Y., Fish, P. and Innes, J.B. (2013) Holocene and Late-glacial relative sea-level change in north-west England: implications for glacial isostatic adjustment models. *Journal of Quaternary Science*, **28,** 59-70.

MacKenzie, W.S. and Adams, A.E. (1994) *A Colour Atlas of Rocks and Minerals in Thin Section*. Halsted Press.

Malarkey, J., Baas, J.H., Hope, J.A., Aspden, R.J., Parsons, D.R., Peakall, J., Paterson, D.M., Schindler, R.J., Ye, L. and Lichtman, I.D. (2015) The pervasive role of biological cohesion in bedform development. *Nature communications*, **6**.

Matlack, K.S., Houseknecht, D.W. and Applin, K.R. (1989) Emplacement of clay into sand by infiltration. *Journal of Sedimentary Petrology*, **59,** 77-87.

McBride, E.F., Milliken, K.L., Cavazza, W., Cibin, U., Fontana, D., Picard, M.D. and Zuffa, G.G. (1995) Heterogeneous distribution of calcite cement at the outcrop scale in Tertiary sandstones, Northern Apennines, Italy. *American Association of Petroleum Geologists Bulletin*, **79,** 1044-1063.

McBride, E.F. and Parea, G.C. (2001) Origin of highly elongate, calcite-cemented concretions in some Italian coastal beach and dune sands. *Journal of Sedimentary Research*, **71,** 82-87.

McDougall, D.A. (2001) The geomorphological impact of Loch Lomond (Younger Dryas) Stadial plateau icefields in the central Lake District, northwest England. *Journal of Quaternary Science*, **16,** 531-543.

McIlroy, D., Worden, R.H. and Needham, S.J. (2003) Faeces, clay minerals and reservoir potential. *Journal of the Geological Society*, **160,** 489-493.

McKinley, J.M., Worden, R.H. and Ruffell, A.H. (2003) Smectite in sandstones: A review of the controls on occurrence and behaviour during diagenesis. *In: Clay mineral cements in sandstones (eds. Worden, R.H. and Morad, S.) International Association of Sedimentologists Special Publications*, **34,** 109-128.

Meade, R.H. (1969) Landward transport of bottom sediments in estuaries of the Atlantic coastal plain. *Journal of Sedimentary Research*, **39**.

Merritt, J.W. and Auton, C.A. (2000) An outline of the lithostratigraphy and depositional history of Quaternary deposits in the Sellafield district, west Cumbria. *Proceedings of the Yorkshire Geological Society*, **53,** 129-154.

Michalopoulos, P. and Aller, R.C. (1995) Rapid clay mineral transformation in Amazon Delta sediments - reverse weathering and oceanic element cycles. *Science*, **270,** 614-617.

Michalopoulos, P. and Aller, R.C. (2004) Early diagenesis of biogenic silica in the Amazon delta: Alteration, authigenic clay formation, and storage. *Geochimica et Cosmochimica Acta*, **68,** 1061-1085.

Michalopoulos, P., Aller, R.C. and Reeder, R.J. (2000) Conversion of diatoms to clays during early diagenesis in tropical, continental shelf muds. *Geology*, **28,** 1095-1098.

Moore, D.M. and Reynolds, R.C. (1997) *X-ray Diffraction and the Identification and Analysis of Clay Minerals*. Oxford University Press.

Morad, S., Al-Ramadan, K., Ketzer, J.M. and De Ros, L.F. (2010) The impact of diagenesis on the heterogeneity of sandstone reservoirs: A review of the role of depositional facies and sequence stratigraphy. *American Association of Petroleum Geologists Bulletin*, **94,** 1267-1309.

Morad, S., De Ros, L.F., Nystuen, J.P. and Bergan, M. (1998) Carbonate diagenesis and porosity evolution in sheet-flood sandstones: evidence from the Middle and Lower Members (Triassic) in the Snorre Field, Norwegian North Sea. In: *Carbonate cementation in sandstones. International Association of Sedimentologists Special Publication* (Ed S. Morad), **26**, pp. 53-85. Blackwells, Oxford.

Morad, S., Ketzer, J.M. and De Ros, L.F. (2000) Spatial and temporal distribution of diagenetic alterations in siliciclastic rocks: implications for mass transfer in sedimentary basins. *Sedimentology*, **47,** 95-120.

Moraes, M.A.S. and De Ros, L.F. (1990) Infiltrated clays in fluvial Jurassic sandstones of Recôncavo Basin, northeastern Brazil. *Journal of Sedimentary Petrology*, **60,** 809-819.

Morris, J.E., Hampson, G.J. and Johnson, H.D. (2006) A sequence stratigraphic model for an intensely bioturbated shallow-marine sandstone: the Bridport Sand Formation, Wessex Basin, UK. *Sedimentology*, **53,** 1229-1263.

Moseley, F. (1978) *The geology of the Lake District*. Yorkshire Geological Society.

Needham, S.J., Worden, R.H. and Cuadros, J. (2006) Sediment ingestion by worms and the production of bio-clays: a study of macrobiologically enhanced weathering and early diagenetic processes. *Sedimentology*, **53,** 567-579.

Needham, S.J., Worden, R.H. and McIlroy, D. (2004) Animal-sediment interactions: the effect of ingestion and excretion by worms on mineralogy. *Biogeosciences*, **1,** 113-121.

Needham, S.J., Worden, R.H. and McIlroy, D. (2005) Experimental production of clay rims by macrobiotic sediment ingestion and excretion processes. *Journal of Sedimentary Research*, **75,** 1028-1037.

Neiheisel, J. and Weaver, C.E. (1967) Transport and deposition of clay minerals southeastern United States. *Journal of Sedimentary Research*, **37**.

Nelson, B.W. (1960) Clay mineralogy of the bottom sediments, Rappahannock River, Virginia. In: *Clays and Clay Minerals: Proceedings of the Seventh National Conference on Clays and Clay Minerals*, pp. 135-148.

Odom, I.E., Doe, T.W. and Dott, R.H. (1976) Nature of feldspar-grain size relations in some quartz-rich sandstones. *Journal of Sedimentary Research*, **46**.

Oelkers, E.H., Bjorkum, P.A. and Murphy, W.M. (1996) A petrographic and computational investigation of quartz cementation and porosity reduction in North Sea sandstones. *American Journal of Science*, **296,** 420-452.

Oliveira, A., Rocha, F., Rodrigues, A., Jouanneau, J., Dias, A., Weber, O. and Gomes, C. (2002) Clay minerals from the sedimentary cover from the Northwest Iberian shelf. *Progress in Oceanography*, **52,** 233-247.

Pay, M.D., Astin, T.R. and Parker, A. (2000) Clay mineral distribution in the Devonian-Carboniferous sandstones of the Clair Field, west of Shetland, and its significance for reservoir quality. *Clay Minerals*, **35,** 151-162.

Pittman, E.D., Larese, R.E. and Heald, M.T. (1992) Clay coats: occurrence and relevance to preservation of porosity in sandstones. *In: Origin, diagenesis and petrophysics of clay minerals in sandstones (eds. Houseknecht, D.W. and Pittman, E.D.) SEPM Special Publication*, **47,** 241-255.

Plumb, R. (1994) Influence of composition and texture on the failure properties of clastic rocks. In: *Rock Mechanics in Petroleum Engineering*. Society of Petroleum Engineers.

Posamentier, H.W. and Walker, R.G. (Eds)(2006) *Facies models revisited*. SEPM Special Publication, Oklahoma.

Postma, H. (1967) Sediment transport and sedimentation in the estuarine environment. In: *Estuaries* (Ed G.H. Lauff). American Association for the Advancement of Science,, Washington D.C.

Powers, M.C. (1957) Adjustment of land derived clays to the marine environment. *Journal of Sedimentary Research*, **27**.

Primmer, T.J., Cade, C.A., Evans, J., Gluyas, J., Hopkins, M.S., Oxtoby, N., Smalley, P.C., Warren, E.A. and Worden, R.H. (1997) Global patterns in sandstone diagenesis: their application to reservoir quality prediction for petroleum exploration *In: Reservoir quality prediction in sandstones and carbonates (eds. Kupecz, J.A., Gluyas, J. and Bloch, S.) AAPG Memoir*, **69,** 61-78.

Pye, K. and Blott, S.J. (2014) The geomorphology of UK estuaries: The role of geological controls, antecedent conditions and human activities. *Estuarine, Coastal and Shelf Science*, **150,** 196-214.

Quirke, J., Henderson, C.M.B., Pattrick, R.A.D., Rosso, K.M., Dent, A., Sharples, J.W. and Pearce, C.I. (2015) Characterizing mineralogy and redox reactivity in potential host rocks for a UK geological disposal facility. *Mineralogical Magazine*, **79,** 1353-1367.

R Core Team (2016) R: A language and environment for statistical computing. R Foundation for Statistical Computing, Vienna, Austria.

Ramm, M. (1992) Porosity depth trends in reservoir sandstones - theoretical models related to Jurassic sandstones offshore Norway. *Marine and Petroleum Geology*, **9,** 553-567.

Ramm, M. and Bjorlykke, K. (1994) Porosity depth trends in Norwegain reservoirs - assessing the quantitative effects of varying pore-pressure, temperature history and mineralogy, Norwegian shelf data. *Clay Minerals*, **29,** 475-490.

Ramm, M., Forsberg, A.W. and Jahren, J. (1997) Porosity-depth trends in deeply buried Upper Jurassic Reservoirs in the Norwegian Central Graben: an example of porosity preservation beneath the normal economic basement by grain coating microquartz. *In: Reservoir quality prediction in sandstones and carbonates (eds. Kupecz, J.A., Gluyas, J. and Bloch, S.) AAPG Memoir*, **69,** 177-200.

Rateev, M.A., Sadchikova, T.A. and Shabrova, V.P. (2008) Clay minerals in recent sediments of the World Ocean and their relation to types of lithogenesis. *Lithology and Mineral Resources*, **43,** 125-135.

Reineck, H.-E. and Wunderlich, F. (1968) Classification and origin of flaser and lenticular bedding. *Sedimentology*, **11,** 99-104.

Rezaee, M.R. and Lemon, N.M. (1996) Influence of depositional environment on diagenesis and reservoir quality: Tirrawarra Sandstone Reservoir, Southern Cooper Basin, Australia. *Journal of Petroleum Geology*, **19,** 369-391.

Riisgard, H.U. and Banta, G.T. (1998) Irrigation and deposit feeding by the lugworm Arenicola marina, characteristics and secondary effects on the environment. A review of current knowledge. *Vie et milieu*, **48,** 243-258.

Rudert, M. and Müller, G. (1981) Mineralogy and provenance of suspended solids in estuarine and near-shore areas of the southern North Sea. *Senckenbergiana Maritima*, **13,** 57-64.

Saïag, J., Brigaud, B., Portier, E., Desaubliaux, G., Bucherie, A., Miska, S. and Pagel, M. (2016) Sedimentological control on the diagenesis and reservoir quality of tidal sandstones of the Upper Cape Hay Formation (Permian, Bonaparte Basin, Australia). *Marine and Petroleum Geology*, **77,** 597-624.

Salem, A.M., Morad, S., Mato, L.F. and Al-Aasm, I.S. (2000) Diagenesis and reservoir-quality evolution of fluvial sandstones during progressive burial and uplift: Evidence from the Upper Jurassic Boipeba Member, Reconcavo basin, northeastern Brazil. *American Association of Petroleum Geologists Bulletin*, **84,** 1015-1040.

Santos, I.R., Eyre, B.D. and Huettel, M. (2012) The driving forces of porewater and groundwater flow in permeable coastal sediments: A review. *Estuarine, Coastal and Shelf Science*, **98,** 1-15.

Scherer, M. (1987) Parameters Influencing Porosity in Sandstones - a Model for Sandstone Porosity Prediction. *American Association of Petroleum Geologists Bulletin*, **71,** 485-491.

Schmid, S., Worden, R.H. and Fisher, Q.J. (2006) Sedimentary facies and the context of dolocrete in the Lower Triassic Sherwood Sandstone Group: Corrib field west of Ireland. *Sedimentary Geology*, **187,** 205-227.

Schmidt, V. and McDonald, D.A. (1979) The role of secondary porosity in the course of sandstone diagenesis. In: *Aspects of Diagenesis* (Eds P.A. Scholle and P.R. Schluger), **26**. SEPM Special Publication.

Sholkovitz, E.R. (1978) The floculation of dissolved Fe, Mn, Al, Cu, Ni, Co and Cd during estuarine mixing. *Earth and Planetary Science Letters*, **41,** 77-86.

Sholkovitz, E.R., Boyle, E.A. and Price, N.B. (1978) Removal of dissolved humic acids and iron during estuarine mixing. *Earth and Planetary Science Letters*, **40,** 130-136.

Simpson, B. (1934) The petrology of the Eskdale (Cumberland) granite. *Proceedings of the Geologists' Association*, **45,** 17-34.

Skarpeid, S.S., Churchill, J.M., Hilton, J.P.J., Izatt, C.N. and Poole, M.T. (2017) The Knarr Field: a new development at the northern edge of the North Sea. In: *Geological Society, London, Petroleum Geology Conference series*, **8**, pp. PGC8. 23. Geological Society of London.

Stevens, R.L. (1991) Grain-size distribution of quartz and feldspar extracts and implications for flocculation processes. *Geo-marine letters*, **11,** 162-165.

Stone, P. and Merriman, R.J. (2004) Basin thermal history favours an accretionary origin for the Southern Uplands terrane, Scottish Caledonides. *Journal of the Geological Society*, **161,** 829-836.

Storvoll, V., Bjorlykke, K., Karlsen, D. and Saigal, G. (2002) Porosity preservation in reservoir sandstones due to grain-coating illite: a study of the Jurassic Garn Formation from the Kristin and Lavrans fields, offshore Mid-Norway. *Marine and Petroleum Geology*, **19,** 767-781.

Stricker, S. and Jones, S.J. (2016) Enhanced porosity preservation by pore fluid overpressure and chlorite grain coatings in the Triassic Skagerrak, Central Graben, North Sea, UK. *Geological Society, London, Special Publications*, **435,** SP435. 4.

Stricker, S., Jones, S.J., Sathar, S., Bowen, L. and Oxtoby, N. (2016) Exceptional reservoir quality in HPHT reservoir settings: Examples from the Skagerrak Formation of the Heron Cluster, North Sea, UK. *Marine and Petroleum Geology*, **77,** 198-215.

Strong, G.E., Milodowski, A.E., Pearce, J.M., Kemp, S.J., Prior, S.V. and Morton, A.C. (1994) The petrology and diagenesis of Permo-Triassic rocks of the Sellafield area, Cumbria. In: *Proceedings of the Yorkshire Geological and Polytechnic Society*, **50**, pp. 77-89. Geological Society of London.

Surdam, R.C., Boese, S.W. and Crossey, L.J. (1984) The chemistry of secondary porosity. In: *Clastic diagenesis. American Association of Petroleum Geologists Memoir* (Eds D.A. McDonald and R.C. Surdam), **37**, pp. 127-149.

Taylor, A.M. and Goldring, R. (1993) Description and analysis of bioturbation and ichnofabrics. *Journal of the Geological Society*, **150,** 141-148.

Taylor, T.R., Giles, M.R., Hathon, L.A., Diggs, T.N., Braunsdorf, N.R., Birbiglia, G.V., Kittridge, M.G., Macaulay, C.I. and Espejo, I.S. (2010) Sandstone diagenesis and reservoir quality prediction: Models, myths, and reality. *AAPG bulletin*, **94,** 1093-1132.

UK Environmental Agency (2015) LIDAR Composite DTM

12 August 2015, https://data.gov.uk/dataset/lidar-composite-dtm-1m1.

Underwood, G.J.C. and Paterson, D.M. (1993) Seasonal changes in diatom biomass, sediment stability and biogenic stabilization in the Severn Estuary. *Journal of the Marine Biological Association of the United Kingdom*, **73,** 871-887.

Velde, B. (1985) *Clay Minerals. A Physico-Chemical Explanation of Their Occurrence*. Elsevier, Amsterdam.

Walderhaug, O. (1994a) Precipitation rates for quartz cement in sandstones determined by fluid inclusion microthermometry and temperature history modelling. *Journal of Sedimentary Research Section a-Sedimentary Petrology and Processes*, **64,** 324-333.

Walderhaug, O. (1994b) Temperatures of quartz cementation in Jurassic sandstones from the Norwegian continental shelf - evidence from fluid inclusions. *Journal of Sedimentary Research Section a-Sedimentary Petrology and Processes*, **64,** 311-323.

Watson, D.F. and Philip, G.M. (1985) Comment on “a nonlinear empirical prescription for simultaneously interpolating and smoothing contours over an irregular grid” by F. Duggan. *Computer Methods in Applied Mechanics and eEngineering*, **50,** 195-198.

Weltje, G.J. (2006) Ternary sandstone composition and provenance: an evaluation of the ‘Dickinson model’. *Geological Society, London, Special Publications*, **264,** 79-99.

Whitehouse, U.G., Jeffrey, L.M. and Debbrecht, J.D. (1960) Differential settling tendencies of clay minerals in saline waters. *Clays and Clay Minerals*, **7,** 1-79.

Wilkinson, M. (1991) The concretions of the Bearreraig Sandstone Formation - geometry and geochemistry. *Sedimentology*, **38,** 899-912.

Wilkinson, M., Darby, D., Haszeldine, R.S. and Couples, G.D. (1997) Secondary porosity generation during deep burial associated with overpressure leak-off: Fulmar

Formation, United Kingdom Central Graben. *American Association of Petroleum Geologists Bulletin*, **81,** 803-813.

Wilkinson, M., Milliken, K.L. and Haszeldine, R.S. (2001) Systematic destruction of K-feldspar in deeply buried rift and passive margin sandstones. *Journal of the Geological Society*, **158,** 675-683.

Wilson, M.D. (1992) Inherited grain-rimming clays in sandstones from eolian and shelf environments: their origin and control on reservoir properties. *In: Origin, diagenesis and petrophysics of clay minerals in sandstones (eds. Houseknecht, D.W. and Pittman, E.D.) SEPM Special Publication*, **47,** 209-225.

Windom, H.L. (1976) Lithogenous material in marine sediments. *Chemical Oceanography*, **5,** 103-135.

Wooldridge, L.J., Worden, R.H., Griffiths, J., Thompson, A. and Chung, P. (2017a) Biofilm origin of clay-coated sand grains. *Geology*, **45,** 875-878.

Wooldridge, L.J., Worden, R.H., Griffiths, J. and Utley, J.E.P. (2017b) Clay-coated sand grains in petroleum reservoirs: Understanding their distribution via a modern analogue. *Journal of Sedimentary Research*, **87,** 338-352.

Worden, R.H. (2006) Dawsonite cement in the Triassic Lam Formation, Shabwa Basin, Yemen: A natural analogue for a potential mineral product of subsurface CO2 storage for greenhouse gas reduction. *Marine and Petroleum Geology*, **23,** 61-77.

Worden, R.H., Armitage, P.J., Butcher, A., Churchill, J., Csoma, A., Hollis, C., Lander, R.H. and Omma, J. (in press) Petroleum reservoir quality prediction: overview and contrasting approaches from sandstone and carbonate communities. In: *Reservoir Quality of Clastic and Carbonate Rocks: Analysis, Modelling and Prediction. Special Publication* (Eds P.J. Armitage, A. Butcher, J. Churchill, A. Csoma, C. Hollis, R.H. Lander, J. Omma and R.H. Worden), **435**. Geological Society, London.

Worden, R.H., Bukar, M. and Shell, P. (2017 in press) The effect of oil emplacement on quartz cementation in a deeply buried sandstone reservoir. *American Association of Petroleum Geologists Bulletin*.

Worden, R.H. and Burley, S.D. (2003) Sandstone diagenesis: the evolution from sand to stone. In: *Sandstone diagenesis, recent and ancient. International Association of Sedimentologists Reprint Series* (Eds S.D. Burley and R.H. Worden), **4**, pp. 3-44.

Worden, R.H., Mayall, M. and Evans, I.J. (2000) The effect of ductile-lithic sand grains and quartz cement on porosity and permeability in Oligocene and lower Miocene clastics, South China Sea: Prediction of reservoir quality. *American Association of Petroleum Geologists Bulletin*, **84,** 345-359.

Worden, R.H., Mayall, M.J. and Evans, I.J. (1997) Predicting reservoir quality during exploration: lithic grains, porosity and permeability in Tertiary clastics of the South China Sea basin. In: *Petroleum Geology of S E Asia. Special Publication* (Eds F. A.J., A.J. Matthews and R.W. Murphy), **126**, pp. 107-115. Geological Society, London.

Worden, R.H. and Morad, S. (2003) Clay minerals in sandstones: Controls on formation, distribution and evolution. *In: Clay mineral cements in sandstones (eds. Worden, R.H. and Morad, S.) International Association of Sedimentologists Special Publications*, **34,** 3-41.

Worden, R.H., Needham, S.J. and Cuadros, J. (2006) The worm gut; a natural clay mineral factory and a possible cause of diagenetic grain coats in sandstones. *Journal of Geochemical Exploration*, **89,** 428-431.

Young, B., Fortey, N.J. and Nancarrow, P.H.A. (1986) An occurrence of tungsten mineralisation in the Eskdale Intrusion, West Cumbria. *Proceedings of the Yorkshire Geological Society*, **46,** 15-21.

Yuan, G.H., Gluyas, J., Cao, Y.C., Oxtoby, N.H., Jia, Z., Wang, Y., Xi, K. and Li, X. (2015) Diagenesis and reservoir quality evolution of the Eocene sandstones in the northern Dongying Sag, Bohai Bay Basin, East China. *Marine and Petroleum Geology*, **62,** 77-89.